Applied Optics

August
1963

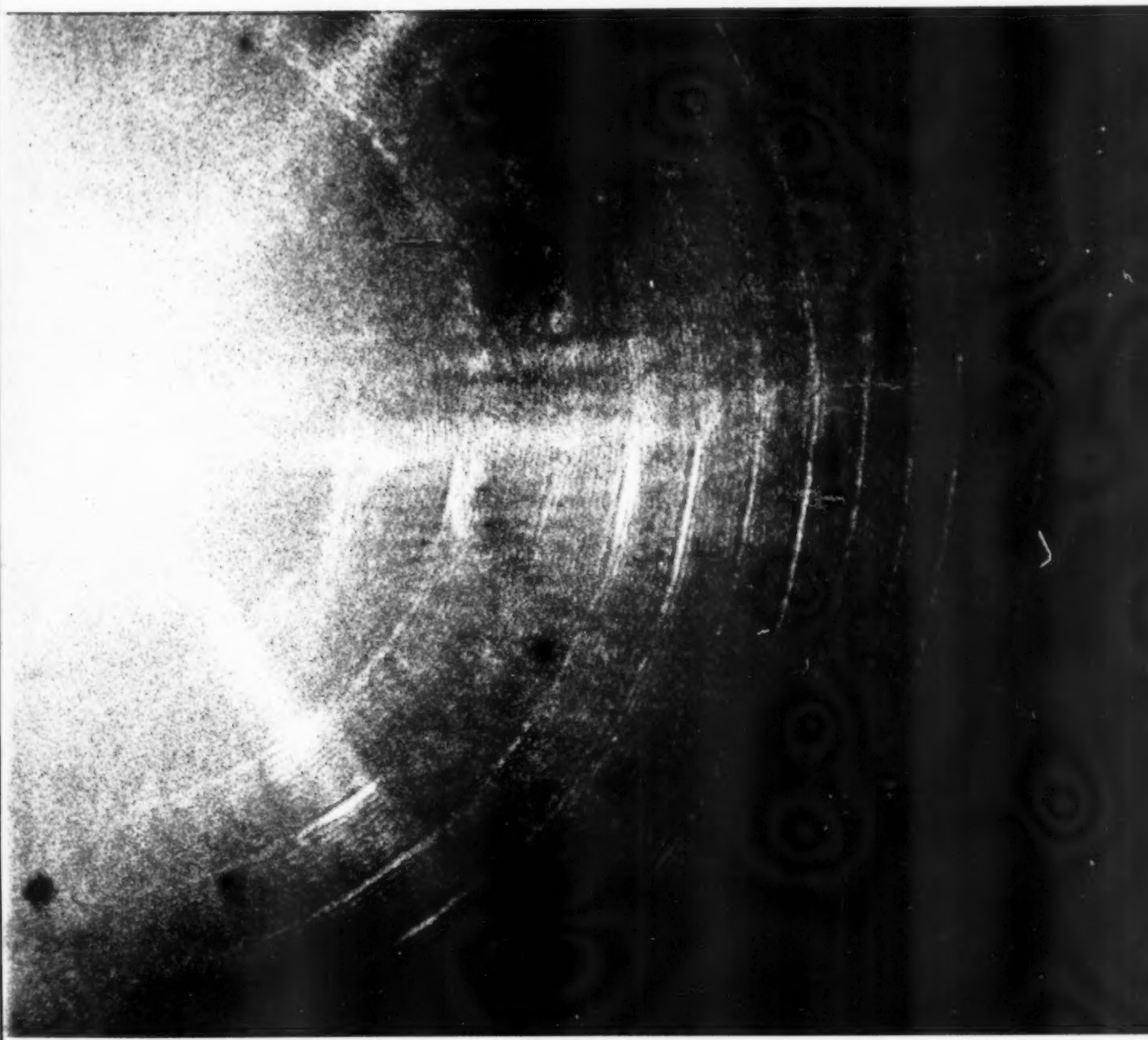

MASERS

Effective Jan. 1, 1965. All back issues and single copies are sold at $3.00 per copy.

Shipped within 48 hours after your order is received!

THERMISTOR INFRARED DETECTORS

TYPICAL SPECIFICATIONS, SOLID-BACKED DETECTORS WITH KRS-5 WINDOWS, NOMINAL VALUES

Code Number	2-101	2-102	2-103	2-104	2-105	2-106	2-107	2-108	2-109	2-110	2-111	2-112
Dimensions of Sensitive Area (millimeters)	0.3x0.3	0.3x0.3	0.5x0.5	0.5x0.5	1.0x1.0	1.0x1.0	1.5x1.5	1.5x1.5	2.0x2.0	2.0x2.0	2.5x2.5	2.5x2.5
Time Constant (milliseconds)	1.1	2.5	1.1	2.5	1.1	2.5	1.1	2.5	1.1	2.5	1.1	2.5
Responsivity (volts/watt)	1065	1600	560	920	220	410	115	230	80	160	40	100
Unit Price	$450.	$450.	$350.	$350.	$350.	$350.	$350.	$350.	$450.	$450.	$450.	$450.

Germanium-immersed thermistor detectors (shown in the photo) have optical gains 3½ times greater than that of equivalent solid-backed detectors. These proven, widely-accepted bolometers are available from stock in the following flake sizes: 0.1 x 0.1 mm, 0.5 x 0.5 mm and 1.0 x 1.0 mm.

FOR COMPLETE DETAILS AND QUANTITY DISCOUNT PRICES, CALL, WRITE OR TWX OUR PRODUCT SALES DEPARTMENT.

Barnes Engineering Company

Defense and Space Division

30 Commerce Road • Stamford, Connecticut

Telephone: 348-5381 (Area Code 203)
TWX: 327-0840 (Area Code 203)

Applied Optics

VOLUME 2
NUMBER 8
AUGUST
1963

A monthly publication of the
Optical Society of America

John N. Howard, Editor

Patricia R. Wakeling, Managing Editor

COVER: The cover photograph is the far-field radiation pattern of a neodymium in glass laser. The central spot was overexposed to show the fine ring structure. The black spots are blemishes in the original negative. The bright rings are the characteristic Fabry-Perot rings as often seen in good optical quality ruby lasers. The fine structure between the rings has an angular separation which is equal to the separation between adjacent maxima in the diffraction pattern of a circular aperture of diameter equal to the diameter of the laser rod. See page 867.

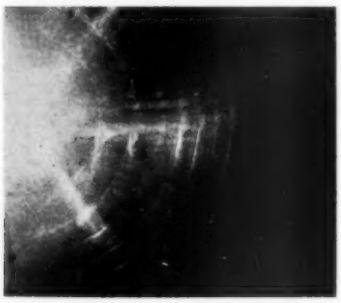

Published monthly by the Optical Society of America, Inc., in cooperation with the American Institute of Physics, at 20th and Northampton Streets, Easton, Pa. Editorial and advertising offices: 1155 16th St. N.W., Washington 36, D.C. 202-Di7-4131 Supported in part by a grant from the National Science Foundation. Subscription rates: $6.00 to OSA members, $8.00 other AIP Societies' members; nonmembers and libraries: $10.00 per year. Single copies $2.00. Second class postage paid at Easton, Pa. © Copyright 1963 by the Optical Society of America.

767 **Investigation of Ruby Optical Maser Characteristics Using Microwave Phototubes**—B. J. McMurtry

787 **Overhauser and Jeffries-Abragam Effect in a Four-Level System**—Mohan Lal Narchal and W. A. Barker

793 **Limiting Parameters and Generalized Characteristics of Xenon Lamps**—I. S. Marshak

801 **Application of the Sénarmont Polariscope to Analysis of Optical Maser Light**—David Hellerstein

807 **Hole-Burning Model of Oscillation of Ruby Laser**—A. J. DeMaria and R. Gagosz

811 **Interference Rings in Ruby Maser Beams**—B. P. Stoicheff and A. Szabo

817 **Tilted-Plate Interferometry with Large Plate Separations**—H. W. Moos, G. F. Imbusch, L. F. Mollenauer, and A. L. Schawlow

823 **Spurious Harmonic Generation in Optical Heterodyning**—H. Z. Cummins, N. Knable, and Y. Yeh

827 **A New Condenser for a Sun-Powered Continuous Laser**—P. H. Keck, J. J. Redmann, C. E. White, and R. E. DeKinder, Jr.

833 **Performance of a Continuous-Wave Neodymium Laser**—P. H. Keck, J. J. Redmann, C. E. White, and D. E. Bowen

839 **Electro-Optic Light Modulation with Cubic Crystals**—C. F. Buhrer, L. R. Bloom, and D. H. Baird

847 **Analysis of Stimulated Raman Scattering of a Giant Laser Pulse**—R. W. Hellwarth

855 **Optical Quality and Radiation Patterns of Ruby Lasers**—C. M. Stickley

DEPARTMENTS

861 **Letters to the Editor**

Influence of Magnetic Fields upon Gas Discharge Lasers—Rudolf G. Buser, J. Kainz, and J. Sullivan

Analysis of Transients and Stability in an Idealized Two-Level Laser System—J. E. Ludman

Improved Cathode for Extreme Ultraviolet Schueler Lamp—R. G. Newburgh

A Technique for Evaluating Half-Wave and Quarter-Wave Plates—A. C. Hall

Spherical-Mirror Oscillating Interferometer—Donald R. Herriott

Far-Field Fabry-Perot Diffraction Patterns of a Neodymium in Glass Laser—C. M. Stickley and R. A. Bradbury

Measurement of the Direct Electro-Optic Effect in Quartz at UHF—D. D. Eden and G. H. Thiess

Power Dip at Line Center of Gaseous Lasers—S. Winsberg

792 **Meeting Reports**

806 **Books**

853 **From the Editor**

Shipped within 48 hours after your order is received!

THERMISTOR INFRARED DETECTORS

TYPICAL SPECIFICATIONS, SOLID-BACKED DETECTORS WITH KRS-5 WINDOWS, NOMINAL VALUES

Code Number	2-101	2-102	2-103	2-104	2-105	2-106	2-107	2-108	2-109	2-110	2-111	2-112
Dimensions of Sensitive Area (millimeters)	0.3x0.3	0.3x0.3	0.5x0.5	0.5x0.5	1.0x1.0	1.0x1.0	1.5x1.5	1.5x1.5	2.0x2.0	2.0x2.0	2.5x2.5	2.5x2.5
Time Constant (milliseconds)	1.1	2.5	1.1	2.5	1.1	2.5	1.1	2.5	1.1	2.5	1.1	2.5
Responsivity (volts/watt)	1065	1600	560	920	220	410	115	230	80	160	40	100
Unit Price	$450.	$450.	$350.	$350.	$350.	$350.	$350.	$350.	$450.	$450.	$450.	$450.

Germanium-immersed thermistor detectors (shown in the photo) have optical gains 3½ times greater than that of equivalent solid-backed detectors. These proven, widely-accepted bolometers are available from stock in the following flake sizes: 0.1 x 0.1 mm, 0.5 x 0.5 mm and 1.0 x 1.0 mm.

FOR COMPLETE DETAILS AND QUANTITY DISCOUNT PRICES, CALL, WRITE OR TWX OUR PRODUCT SALES DEPARTMENT.

Barnes Engineering Company

Defense and Space Division

30 Commerce Road • Stamford, Connecticut

Telephone: 348-5381 (Area Code 203)
TWX: 327-0840 (Area Code 203)

Applied Optics

VOLUME 2
NUMBER 8
AUGUST
1963

A monthly publication of the
Optical Society of America

John N. Howard, Editor

Patricia R. Wakeling, Managing Editor

COVER: The cover photograph is the far-field radiation pattern of a neodymium in glass laser. The central spot was overexposed to show the fine ring structure. The black spots are blemishes in the original negative. The bright rings are the characteristic Fabry-Perot rings as often seen in good optical quality ruby lasers. The fine structure between the rings has an angular separation which is equal to the separation between adjacent maxima in the diffraction pattern of a circular aperture of diameter equal to the diameter of the laser rod. See page 867.

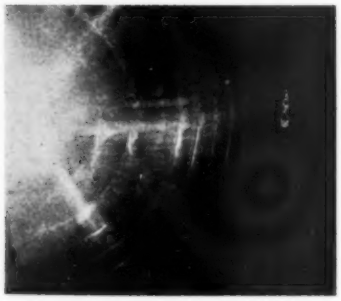

Published monthly by the Optical Society of America, Inc., in cooperation with the American Institute of Physics, at 20th and Northampton Streets, Easton, Pa. Editorial and advertising offices: 1155 16th St. N.W., Washington 36, D.C. 202-Di7-4131 Supported in part by a grant from the National Science Foundation. Subscription rates: $6.00 to OSA members, $8.00 other AIP Societies' members; nonmembers and libraries: $10.00 per year. Single copies $2.00. Second class postage paid at Easton, Pa. © Copyright 1963 by the Optical Society of America.

767 **Investigation of Ruby Optical Maser Characteristics Using Microwave Phototubes**—B. J. McMurtry

787 **Overhauser and Jeffries-Abragam Effect in a Four-Level System**—Mohan Lal Narchal and W. A. Barker

793 **Limiting Parameters and Generalized Characteristics of Xenon Lamps**—I. S. Marshak

801 **Application of the Sénarmont Polariscope to Analysis of Optical Maser Light**—David Hellerstein

807 **Hole-Burning Model of Oscillation of Ruby Laser**—A. J. DeMaria and R. Gagosz

811 **Interference Rings in Ruby Maser Beams**—B. P. Stoicheff and A. Szabo

817 **Tilted-Plate Interferometry with Large Plate Separations**—H. W. Moos, G. F. Imbusch, L. F. Mollenauer, and A. L. Schawlow

823 **Spurious Harmonic Generation in Optical Heterodyning**—H. Z. Cummins, N. Knable, and Y. Yeh

827 **A New Condenser for a Sun-Powered Continuous Laser**—P. H. Keck, J. J. Redmann, C. E. White, and R. E. DeKinder, Jr.

833 **Performance of a Continuous-Wave Neodymium Laser**—P. H. Keck, J. J. Redmann, C. E. White, and D. E. Bowen

839 **Electro-Optic Light Modulation with Cubic Crystals**—C. F. Buhrer, L. R. Bloom, and D. H. Baird

847 **Analysis of Stimulated Raman Scattering of a Giant Laser Pulse**—R. W. Hellwarth

855 **Optical Quality and Radiation Patterns of Ruby Lasers**—C. M. Stickley

DEPARTMENTS

861 **Letters to the Editor**

Influence of Magnetic Fields upon Gas Discharge Lasers—Rudolf G. Buser, J. Kainz, and J. Sullivan

Analysis of Transients and Stability in an Idealized Two-Level Laser System—J. E. Ludman

Improved Cathode for Extreme Ultraviolet Schueler Lamp—R. G. Newburgh

A Technique for Evaluating Half-Wave and Quarter-Wave Plates—A. C. Hall

Spherical-Mirror Oscillating Interferometer—Donald R. Herriott

Far-Field Fabry-Perot Diffraction Patterns of a Neodymium in Glass Laser—C. M. Stickley and R. A. Bradbury

Measurement of the Direct Electro-Optic Effect in Quartz at UHF—D. D. Eden and G. H. Thiess

Power Dip at Line Center of Gaseous Lasers—S. Winsberg

792 **Meeting Reports**

806 **Books**

853 **From the Editor**

LASER MICROPROBE

For analyses of micro-areas without sample preparation

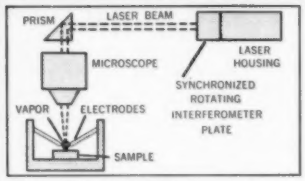

Simplified Diagram of Laser Microprobe

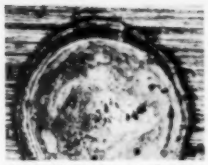

Magnified Laser Crater
Diam. — 50 microns.
Mass — 1 microgram

The new Jarrell-Ash Laser Microprobe heralds an outstanding breakthrough in analytical analysis . . . with almost any Spectrograph, you now can directly analyze micro-areas of any metallic or non-metallic solid sample, without extensive sample preparation.

- 50 Micron Sample Size
- 1 Microgram Sample Mass
- One-shot process in milli-second range
- No physical sample contact
- No sample preparation
- Electrical conductance not required in sample
- No pre-burning for equilibrium
- No Atomic Number restrictions

SOME APPLICATIONS

Metallic impurities in metal matrix . . . analyses of separate phases in phase mixtures . . . identification of micro-inclusions in glass, ceramics, plastics, etc., analyses of segregates . . . analyses of sub-miniaturized semi-conductors . . . rapid analyses of mineral or geological samples.

Ask for Catalog 45-600

Jarrell—Ash

Dedicated to excellence in the research, development and manufacture of precision analytical instrumentation.

For further information . . . clip the coupon, attach to your company letterhead and mail.

JARRELL-ASH COMPANY
26 Farwell Street, Newtonville 60, Mass.

NAME _____

L. M.

NEW HIGH-AVERAGE-POWER LASER FLASH TUBES

FX-65

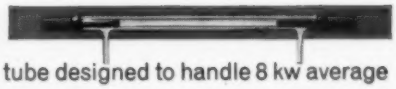

Water-cooled tube designed to handle 8 kw average power input with water flow of 1 gpm. Capable of flash rates up to 50 fps. Arc length is 6½", overall length 12⅞", O.D. 15 mm overall, discharge bore 7 mm. A shorter tube with 3" arc length and 4 kw rating will soon be available. EG&G is in a position to quote on a power supply capable of driving the FX-65.

FX-52

Air-cooled flashtube rated at 600 watts average power input with a minimum air velocity of 40 linear ft/sec. Electrical ratings are similar to those for EG&G FX-42. Arc length is 3", overall length 6 13/16", O.D. 0.945" overall, discharge bore 7 mm.

FX-55

Similar configuration to FX-52 but with 6" arc length, conservatively rated at 1000 watts average power input.

FX-56

Very high energy flashtube designed for operation at up to 3000 joules per inch of arc length with pulse duration of 3 milliseconds. Arc length 6½", overall length 12⅞", O.D. 31 mm, discharge bore 28 mm. Also available on order in arc lengths from 3" to 36".

FX-57

A higher rated version of the popular FX-47. Rating: 13,000 joules @ 3 millisecond pulse duration. Arc length 6½", overall length 12⅞", O.D. 15 mm overall, discharge bore 12 mm. Available on order in any arc length to 36".

EG&G has the widest range of standardized Xenon flashtubes available, plus an unequaled capability for development and manufacture of special tubes. Write or phone Marketing Department for detailed information. Edgerton, Germeshausen & Grier, Inc., 164 Brookline Avenue, Boston 15, Massachusetts.

EG&G

EDGERTON, GERMESHAUSEN & GRIER, INC.

BOSTON • LAS VEGAS • SANTA BARBARA

1005

NO. 26 EPR AT WORK SERIES

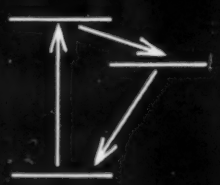

EPR OF TRIPLET STATES

(ELECTRON PARAMAGNETIC RESONANCE)

EPR study of triplet states in organic molecules is of considerable intrinsic interest and has taken on an added importance because these materials are suitable for optical masers. High sensitivity, provision for uv irradiation, and variable temperature equipment make the Varian V-4502 EPR spectrometer particularly useful in this work.

EXAMPLE

Triplet Naphthalene in Durene

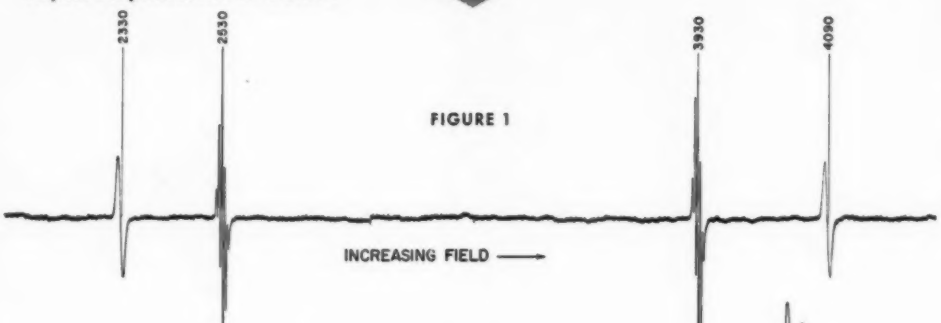

FIGURE 1

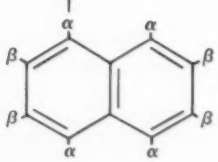

FIGURE 2

FIGURE 3

Observation by EPR of a meta-stable photo excited triplet state in an organic molecule was first reported by Hutchison and Mangum[1]. Success in their work required a dilute suspension of oriented molecules. This was achieved by growing mixed crystals of naphthalene (Fig. 2) in durene. This host substance is transparent to the uv irradiation required to excite the naphthalene triplet state.

The EPR spectrum at 77°K is illustrated in Fig. 1. The Varian F-8 NMR Fluxmeter was used to make the field measurements. There are two molecules per unit cell in durene, at approximately right angles to each other. Naphthalene substitutes isomorphically, and the high and low field lines arise from molecules which have the magnetic field perpendicular to the molecular plane. The lines with structure are associated with molecules in the other site which have the field parallel to the long axis. The difference in heights of the pair of lines from a particular orientation are caused by a difference in the transition probabilities. Zero field splittings from dipole-dipole interaction are comparable to a microwave quantum, resulting in the large anisotropy.

Hyperfine interaction with the protons on the ring positions is anisotropic. With the magnetic field parallel to the long axis of naphthalene, interaction with the 4 equivalent α protons may be resolved, and a 5-line spectrum is observed (Fig. 3). In other orientations, the resolution is poorer, and in no case is the β splitting clearly seen.

Subjects of current interest, under investigation in a number of laboratories are: optical excitation and decay processes, energy transfer mechanisms, and behavior at liquid helium temperatures. In these experiments, the details of the interaction of the naphthalene molecule with the host lattice are being probed. One may expect that the information gained in this work will have immediate practical application in optical masers.

(1) C. A. Hutchison, Jr. and B. W. Mangum, J. Chem. Phys. 29, 952 (1958).

For literature which fully explains the 100 kc EPR Spectrometer and its application to basic and applied research in physics, chemistry, biology and medicine, write the Instrument Division.

VARIAN associates
PALO ALTO 49, CALIFORNIA

HERE'S HELP

from Bausch & Lomb

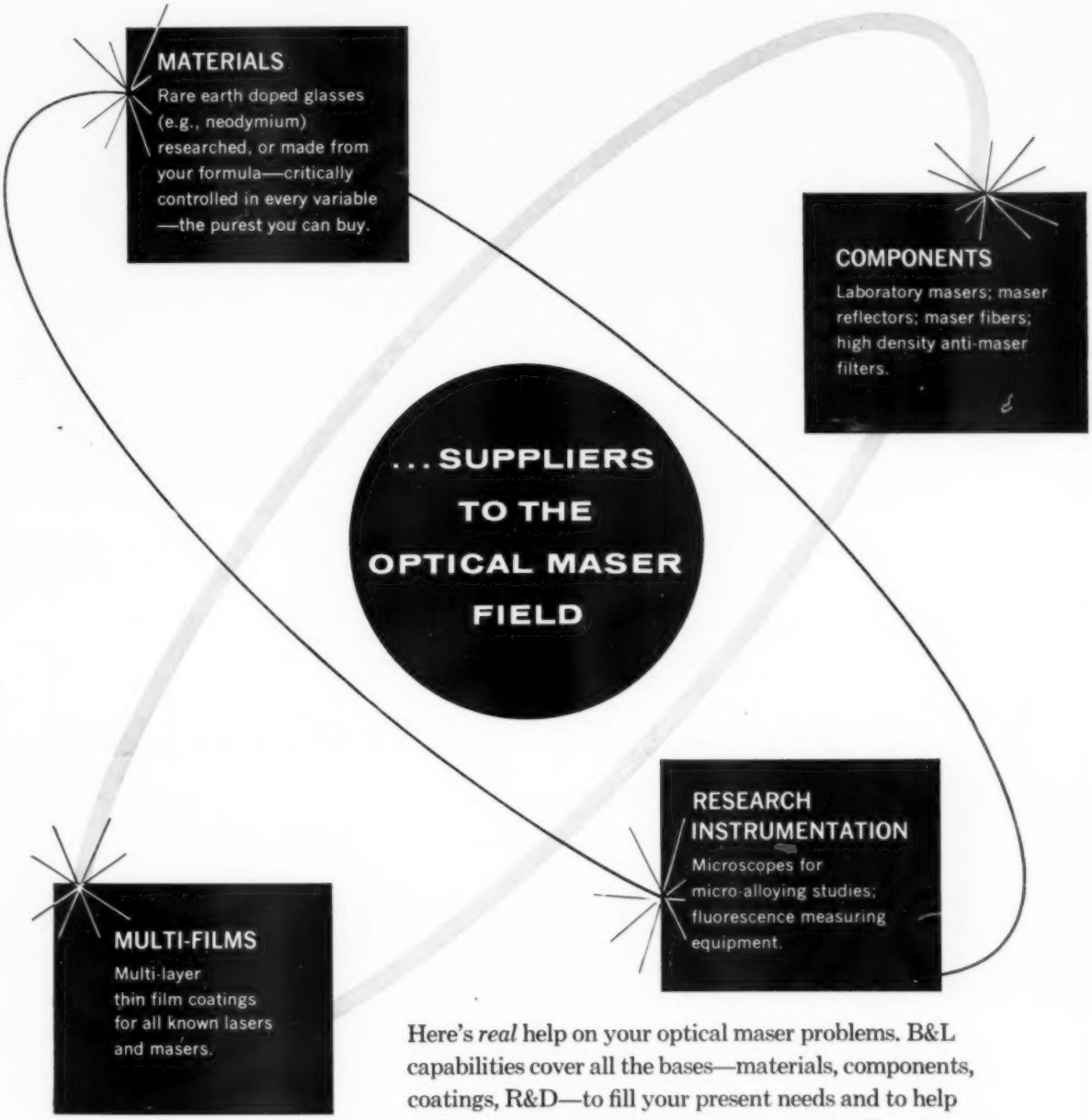
MATERIALS
Rare earth doped glasses (e.g., neodymium) researched, or made from your formula—critically controlled in every variable —the purest you can buy.
COMPONENTS
Laboratory masers; maser reflectors; maser fibers; high density anti-maser filters.
...SUPPLIERS TO THE OPTICAL MASER FIELD
RESEARCH INSTRUMENTATION
Microscopes for micro-alloying studies; fluorescence measuring equipment.
MULTI-FILMS
Multi-layer thin film coatings for all known lasers and masers.

Here's *real* help on your optical maser problems. B&L capabilities cover all the bases—materials, components, coatings, R&D—to fill your present needs and to help with your maser development programs. And you're sure of quality—it's written right into your contract.
For information on your specific problems, write: Commercial Contract Sales Dept., Bausch & Lomb Inc., 77144 Bausch Street, Rochester 2, N. Y.

BAUSCH & LOMB

DOMES....

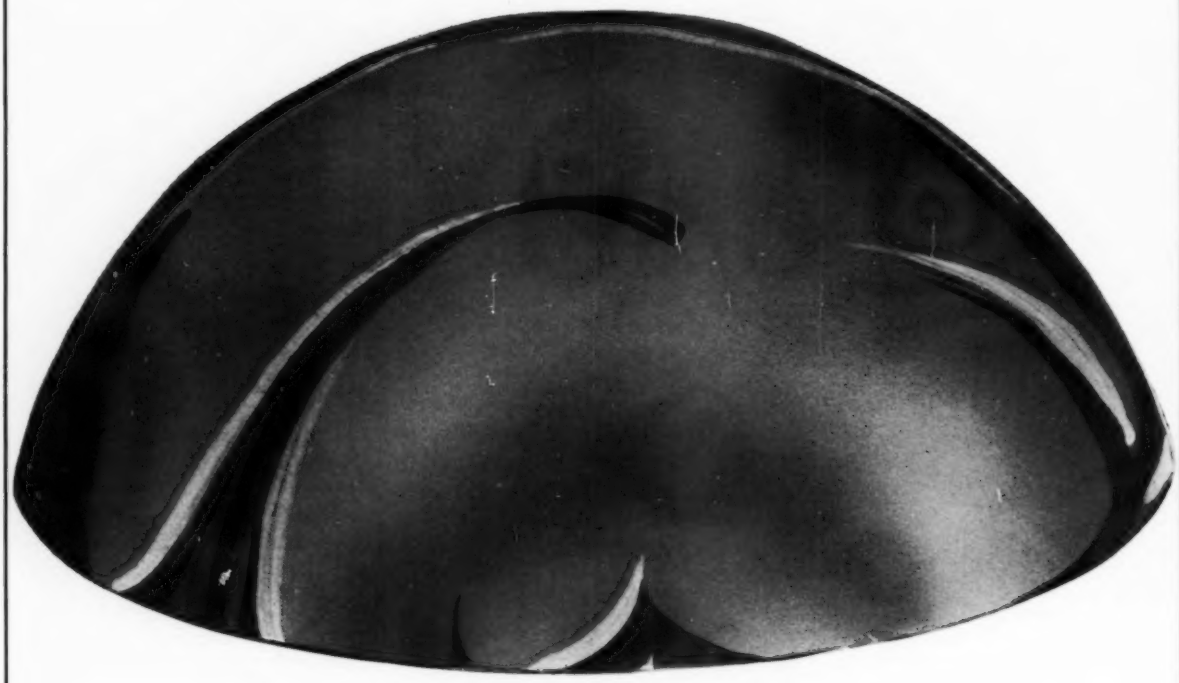

WINDOWS, LENSES OR OTHER SHAPES IN

Silicon and Germanium

- Cast-to-shape in sizes to 24" diameter
- Transmission over a broad range in the infrared
- Hard and durable with excellent thermal conductivity
- High index of refraction

Exotic Materials, Inc.

1534-E EAST CHESTNUT AVE. SANTA ANA, CALIF.
TELEPHONE: (714) 543-8261

Specialists in LARGE optical shapes

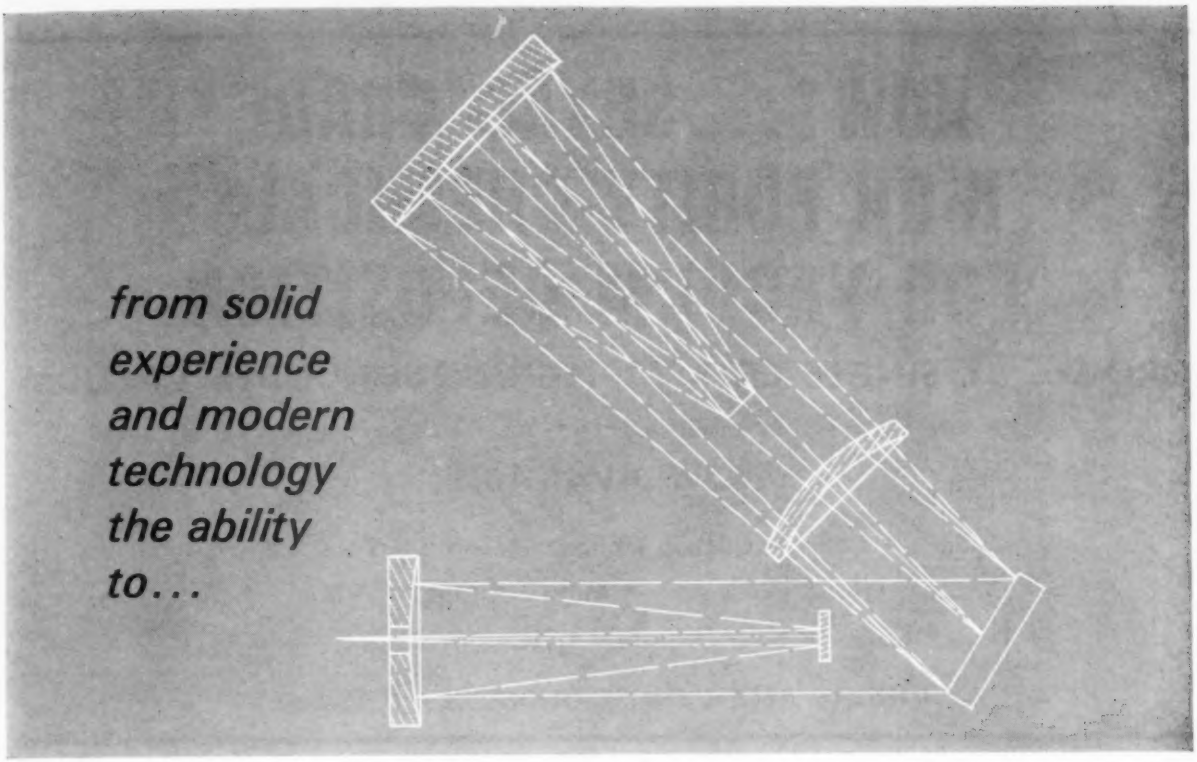

SOLVE YOUR OPTICS PROBLEMS

Modern electronic computer techniques have made it possible to simulate an optical system in every detail. Multiple ray traces produce a spot diagram from which energy distribution for a spot anywhere in the image surface may be derived. Bolometric energy distribution over a wave length region of interest can be calculated and the contribution due to a particular aberration identified. All this (and a great deal more) is accomplished with our IBM 1620, with amazing rapidity and accuracy.

We, also, are currently engaged with several other firms in a co-operative endeavor to develop a program for the 7090 which will automatically optimize the optical parameters for over-all system performance. The first stages of the program have been tested successfully and completion is scheduled for the near future.

Sounds marvelous? It is – but – machines have no imagination, no experience in "working" glass, no knowledge of what makes a practical optical system. Such things are for men.

In the hands of a man with skill and imagination even a desk calculator produced results, slowly to be sure, by modern standards, and with greater approximation. Today's powerful mathematical machines have multiplied his efforts a thousand fold and made possible a degree of accuracy and sophistication unforeseen a few years back.

The attributes peculiar to the man, imagination, skill, experience are now more necessary and valuable than ever.

Perhaps you have need for the talents of our optical design and engineering staff. We will be happy to tackle your systems or instrumentation problem . . . U-V, I-R, or anywhere between.

We can do the whole job from design to a complete prototype instrument, if you like.

The experience, imagination, skill, and talents of our staff are at your service at all times. For consultation or quotation, write, wire or telephone: DIRECTOR OF RESEARCH . . .

FERSON OPTICS, INC.

P. O. BOX 398 / OCEAN SPRINGS, MISSISSIPPI
TELEPHONE 875-5422 (Area Code 601)

OPTIC SYSTEMS FOR AMERICA'S FUTURE

NOW!...SEVAC* GRADE HIGH PURITY CHEMICALS FOR VACUUM DEPOSITION

GROWN BY SINGLE CRYSTAL TECHNIQUES UNDER VACUUM

• No Volatile Impurities • All -10 Mesh Fineness

NOW AVAILABLE

• CaSe • CdS • CdTe • ZnSe • ZnS • ZnTe • GaAs
• GaSb • InSb • InAs • MgF_2 • MgO • PbF • MnF
• LiF • CaF_2 • SrF_2 • BaF_2 • TiO_2 • Al_2O_3 • Si • Ge

INQUIRE ABOUT THOSE UNDER DEVELOPMENT

and!..SINGLE CRYSTALS

MAGNESIUM FLUORIDE—CUPROUS CHLORIDE

for Optical Windows

FROM ULTRAVIOLET
TO INFRARED
11 to .02 Microns

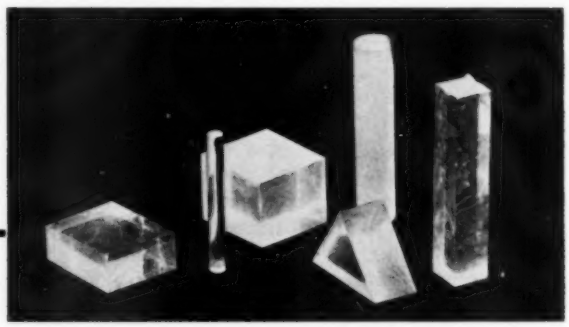

The New MKIA GAS LASER SYSTEM . . . . . COMPLETE $995

MODEL MK KIT
Complete Gas Laser Discharge Tube $495.00

COMPONENTS

Brewster Gas Laser Discharge Tube	$250.00
Confocal Mirrors dielectrically coated - pair	$245.00
R.F. Excitor modified	$250.00
R.F. Coupling	$ 40.00
Mirror Mounts - pair	$150.00

The Worlds Largest Supplier of Single Crystals

Semi-elements, inc.
Saxonburg Boulevard, Saxonburg, Pa.
Phone: 412-352-1548

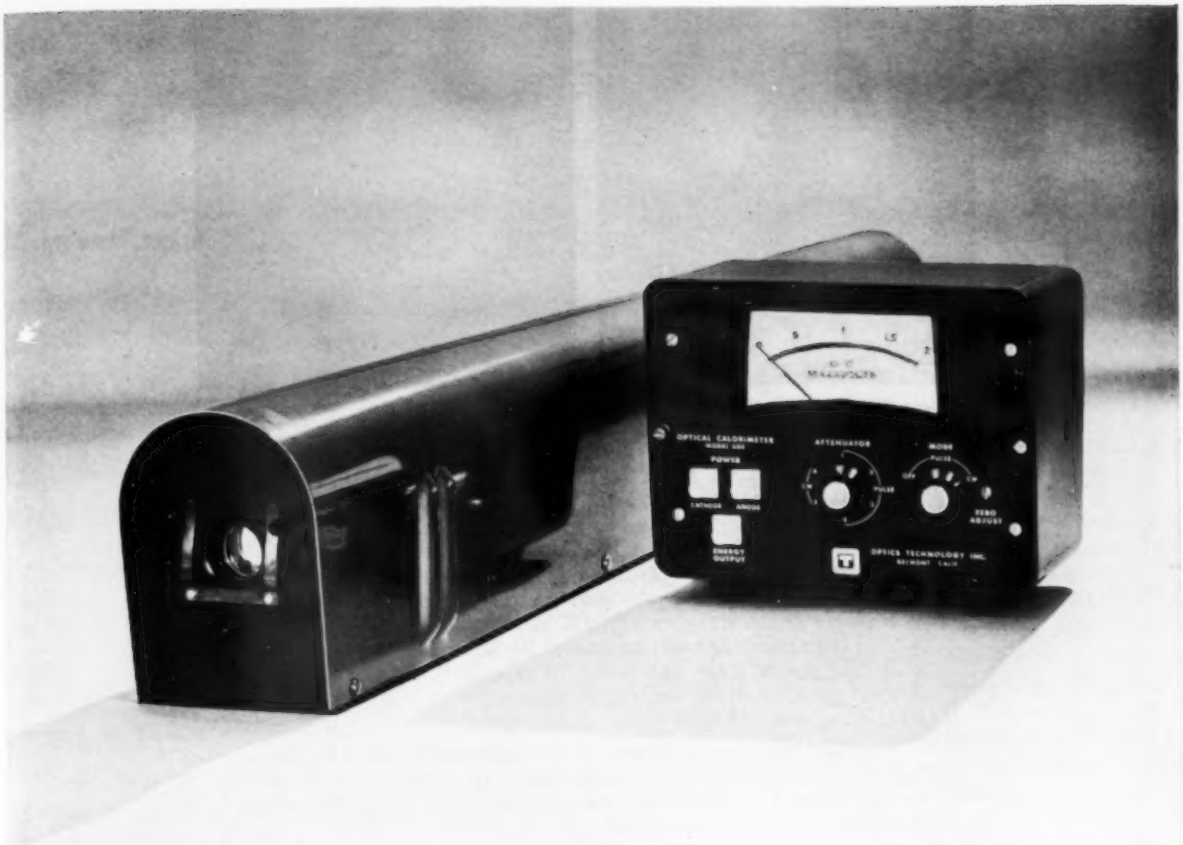

VISIBLE & INFRARED CW LASER

Model 150 is complete with precision multi-layer mirrors in differential thread interferometer assembly and power supply. Gas tube produces continuous coherent output at 6,328 Å and 11,530 Å. Mirrors are available for either wavelength, or for both at once.

Also available:

***Model 120 Pulsed Laboratory LASER**, with power supply, ruby and other LASER crystals, cryogenic cooling and self-contained interferometer accessories.*

***Model 50A Interference Filter Set** provides low absorption attenuators and beam splitters for ruby LASER research.*

OPTICAL CALORIMETER

Model 600 calorimeter measures optical energy, power and peak power. It may be used with either pulsed or CW sources. Range: 312 joules (watts CW) to .037 joules (watts CW). From 20,000 Å to 4,000 Å. Absolute accuracy ±10%. New design eliminates error-producing wedge cavities and simplifies alignment. It incorporates highly sensitive calorimeter cell, phototube, amplifier, meter, and broad band attenuators.

Our high-efficiency multi-layer LASER mirrors can be deposited on your own substrates. Contact us for full details.

OPTICS TECHNOLOGY, INC

248 Harbor Boulevard
Belmont, California
LYtell 1-0358 (Area Code 415)

Research and development positions available for scientists and engineers in Fiber Optics. Contact Personnel Department.

For additional information, write OTI or your nearest OTI representative: New England: H. J. Schuft Co.; New York, Metropolitan: E. C. Smith and Assoc.; New York, Upstate: E. W. Stone Co.; Mid-Atlantic: C. E. Snow Co.; So. California: Abbott Instrument & Engineering; Southwest & Mountain States: Southwestern Engineering & Equipment Co.; Europe: HVL, Brussels; Other export: Henley and Co., New York, N. Y.

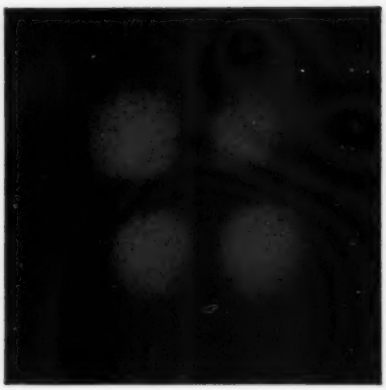

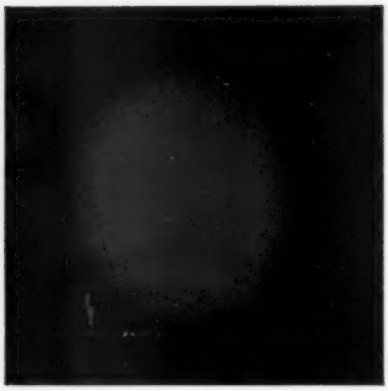

Spectra-Physics LASERS

within a millionth of an inch of perfection

The difference between an ordinary monochromatic gas laser beam (left, above) and one with complete spatial coherence in a single phase wavefront (right) is very largely in the precision of the optics. The reflectors and Brewster's-angle windows in a continuous-wave gas laser, to qualify it as a precision laboratory instrument, require an optical finish of a very small fraction of a wavelength.

You will find this precision in all Spectra-Physics CW gas lasers, a result not only of meticulous care in the preparation of the optics, but also of the practiced skill with which they are integrated into the instrument.

The quality of a Spectra-Physics laser becomes immediately apparent when you turn on the power and observe the uniphase, truly coherent quality of its output. All its power is thus available for insertion into the diffraction limit of an optical system, with the important benefits of better collimation, greater intensity, and sharper focus.

An impressive proportion of all significant laser work now underway is being conducted with equipment produced by Spectra-Physics. Among the many advantages now offered is complete assurance of reliability of operation, backed by a **full year's warranty** which includes even the plasma tube.

Write for information on our Model 115, the higher-powered Model 112, and related accessories. We will also send you Laser Technical Bulletin #2, "Properties of laser resonators giving uniphase wave fronts." Address your inquiry to 1255 Terra Bella Avenue, Mountain View 5, California (or call collect (415) 968-4467).

Spectra-Physics

Investigation of Ruby Optical Maser Characteristics Using Microwave Phototubes

B. J. McMurtry

This paper describes the application of photoelectric mixing techniques to the study of the ruby laser. Following a brief theoretical analysis of laser oscillation frequencies, extensive experiments are described. These experiments permit conclusions concerning: (1) the behavior of the laser's spectral output as a function of pump power and temperature; (2) the validity of applying homogeneous interferometer mode analyses to the case of ruby; and (3) the effects of fluorescence line-shape and stimulated emission in determining oscillation frequencies. In addition, they provide extremely high-resolution measurements of the oscillation line-width.

I. Introduction

In a previous experiment[1] using photomixing techniques with microwave difference-frequencies, it was found that ruby optical masers (lasers)[2,3] generally oscillated at several frequencies simultaneously; the difference between adjacent oscillation frequencies, as determined by the observed microwave beat frequency, corresponded within a few percent to the calculated frequency spacing between adjacent axial modes of the parallel-plane resonator formed by the silvered ends of the rod. In addition the line-width of the individual spectral components in the laser output appeared to be approximately 5 Mc/sec wide, which was an order of magnitude smaller than it had previously been possible to measure using high-resolution spectroscopic methods.[4]

The initial experiment demonstrated the usefulness of microwave phototubes[5-8] for time-resolved, high-resolution examination of ruby laser output. Consequently a detailed investigation was begun in an attempt to answer the following questions:

(a) How do the observed difference frequencies compare with those calculated for the particular resonator?

(b) How does pump power affect the number and frequency of oscillation modes?

(c) How does rod temperature affect the number and frequency of oscillation modes?

(d) What are the relative outputs at the various beat frequencies?

(e) What is the oscillation line-width?

The answers obtained are presented in the remainder of this paper: Section II discusses the theoretical determination of laser oscillation frequencies; Sec. III describes extensive S-band experiments on rods having plane mirrors; Sec. IV describes similar experiments on a confocal rod; and Sec. V describes X-band experiments on plane-mirror rods operated at liquid nitrogen temperature.

II. Theoretical Analysis of Laser Oscillation Frequencies

Detailed analyses of laser oscillation conditions are available in the literature.[1,4,9-11] In general an oscillation frequency is determined by (1) the location and line-width of the resonator modes, (2) the location, shape, and nature of broadening of the fluorescence spectrum, and (3) the frequency and intensity of any previously existing oscillations.

If the fluorescence spectrum is quite broad compared to the cavity-resonance line-width, then the oscillation (or oscillations) will occur at a frequency (or frequencies) corresponding to the centers of the cavity resonances. For such situations a knowledge of the possible modes of the passive resonator should be sufficient to permit the determination of oscillation frequencies. Since these conditions are satisfied in ruby rods near room temperature, passive interferometer analyses[12,13] were used to predict the results of photomixing experiments. The calculated beat frequencies for both plane-mirror and confocal resonators are presented later in this section.

The author is with the Sylvania Microwave Device Division, Mountain View, California.

Received 7 February 1963.

This work was performed at Stanford Electronics Laboratories, Stanford, California, and was supported by the Physical Sciences Division of the Air Force Office of Scientific Research, and by the U.S. Signal Research and Development Laboratories, Fort Monmouth, N.J.

For situations in which the fluorescence line-width is comparable to the interferometer-resonance line-width (e.g., ruby rods at low temperature) the calculations become considerably more complicated.

In order to get an estimate of the shift in oscillation difference-frequencies as a ruby rod is cooled from room temperature to liquid nitrogen temperature, some calculations were performed using a greatly simplified model. The results of those calculations are presented later in this section.

Plane-Parallel Mirrors

By far the most detailed analysis of this type of resonator was carried out by Fox and Li.[12] There are however, two major differences between their model and and a ruby rod. First, they assume that the entire space between the mirrors is filled with the same dielectric material. That is, their analysis does not include any side-wall effects due to reflection at the ruby-air boundary. Second, their analysis assumes that the dielectric medium is lossless and homogeneous. Measurements have shown that even the best available ruby samples are far from being optically homogeneous.[14,15] This fact provides good reasons to doubt the validity of applying the Fox and Li analysis to the case of ruby. A further reason for doubting the validity of the homogeneous dielectric calculations for ruby was that numerous photographs of the ends of ruby rods during laser action had indicated that only certain portions of the rod were active.[16] One of the objectives of this investigation was to determine to what extent their analysis can be applied to the case of ruby.

Fox and Li obtained the result that a parallel-plane resonator many wavelengths long could support a wide variety of steady-state field configurations, each characterized by a certain field distribution. The configuration corresponding to minimum phase shift and diffraction loss had a circularly symmetric field pattern quite similar to that of the dominant TE mode in circular waveguide. Similarly, the configurations with higher phase shift and diffraction loss could be quite easily related to the modes of a circular cylindrical cavity resonator. In fact, they showed that the resonant frequencies can be quite accurately predicted from the theory of circular cylindrical resonators provided only that the Fresnel number $N = a^2/b\lambda$ is large compared to unity (a = mirror radius, b = mirror spacing).

It was also found that the diffraction loss for a particular mode decreased rapidly as N increased. In fact, for normal values of N the diffraction losses for low-order modes were quite small compared to the reflection loss of even the best mirrors that could be produced. In other words, the efficiency of energy storage for a particular mode is generally determined primarily by reflection loss at the mirrors. This is particularly true for cases in which the laser output is obtained through a partially silvered (or perhaps even unsilvered) end of the rod. For example, the power loss due to diffraction is less than 1% for the dominant mode when $N = 10$.

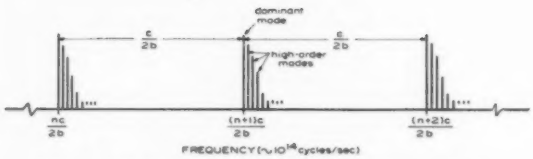

Fig. 1. Mode spectrum of a plane-mirror resonator.

A further result that minimizes the effects of diffraction loss is that even the best ruby crystals have been found to scatter 20–30% of the incident radiation into other modes during one transit through the rod.[14,15] Such an effect completely overwhelms diffraction losses for any reasonable value of N.

Since for maser oscillation the required population inversion depends only on the cavity Q and in no other way upon the resonator shape, this means that the probability of exciting an oscillation in a high-order mode may be essentially the same as that for a dominant mode.

What then should we expect to see in a photomixing experiment if we assume that the fluorescence spectrum is so broad as to have essentially no effect in pulling oscillation frequencies away from cavity resonances? For $N >> 1$ the resonant frequencies are given by[17]

$$f = \frac{c}{2b}\left[n^2 + \left(\frac{bp'_{nl}}{\pi a}\right)^2\right]^{1/2},$$

where a = rod radius; b = rod length; c = velocity of light in ruby; n = distance between mirrors measured in half-wavelengths; p'_{nl} = nth root of the first derivative of the lth order ordinary Bessel function of the first kind.

Note that for an optical maser n is always much larger than $bp'_{nl}/\pi a$. Hence, the optical-mode spectrum for a plane-mirror interferometer is like that shown in Fig. 1, which emphasizes the fact that there are clusters of modes near the dominant or axial modes. The amplitude scale is arbitrary, the dominant ("axial") modes being drawn larger than the high-order modes.

The frequency difference between two modes designated by subscripts 1 and 2 is

$$f = \frac{c}{2b}\left[(n_2 - n_1) + \frac{p_2^2 - p_1^2}{4\pi^2 N}\right].$$

Two adjacent modes (i.e., $n_2 - n_1 = 1$) of the same type (i.e., same p'_{nl}) produce the familiar beat frequency $c/2b$. However, beats between different types of modes (i.e., $p_2 \neq p_1$) will lie some distance away from the "like-mode beat frequency" $(n_2 - n_1)c/2b$.

To obtain the range of frequencies over which the output is spread, we write

$$\Delta f = (c/2b)(n_2 - n_1) + \delta f,$$

where

$$\delta f = (c\lambda/2\pi^2)(p_2^2 - p_1^2)/(2a)^2.$$

Note that δf can be either positive or negative, depending upon the sign of $p_2^2 - p_1^2$. The quantity δf has been computed for all combinations of beats between the first five types of circular-mirror resonator modes, and the results are shown in Fig. 2.

Note that the frequency spread about $(n_2 - n_1)c/2b$ is not large. For example, a 25.4 mm long by 2.54 mm diam ruby rod would contain output at 21 distinct frequencies between about 3333 and 3359 Mc/sec for $n_2 - n_1 = 1$ if all five modes of Fig. 2 were excited about each axial mode. Even though the frequencies are closely spaced, they could be easily resolved in a microwave receiver, provided of course that the linewidths are small compared to the difference frequencies.

Confocal Mirrors

A number of other resonators have been used in addition to the plane-mirror resonator. One of these, the confocal resonator, has certain characteristics which were found to be quite useful for photomixing experiments. In particular, the optical mode spectrum of the confocal resonator is much more degenerate than that of the plane-mirror resonator. This fact, coupled with the particular arrangement of mode frequencies,

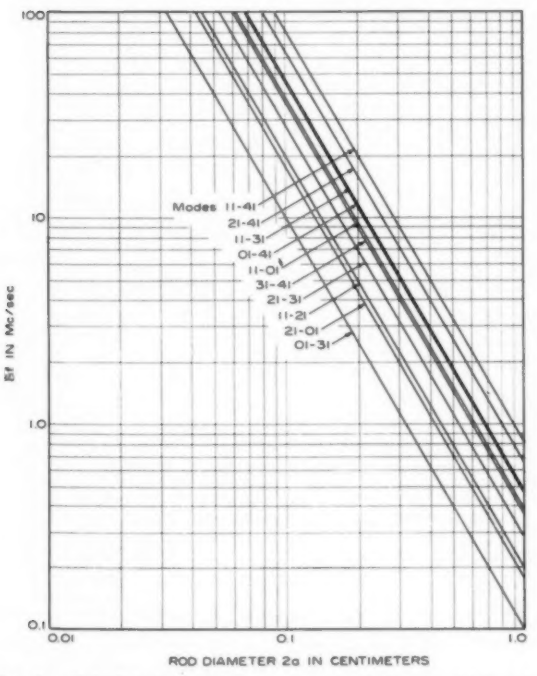

Fig. 2. Calculated beat-frequency spread due to high-order mode excitation in a plane-mirror resonator.

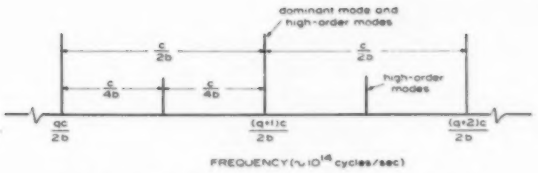

Fig. 3. Mode spectrum of a confocal resonator.

permits an experimental examination of the mode spectrum that is much simpler to interpret than are similar experiments on plane-mirror resonators.

A detailed analysis of the resonator formed by replacing the plane mirrors by concave spherical mirrors was performed by Boyd and Gordon.[13] They found that minimum phase shift and diffraction loss were obtained when the mirrors were separated by a distance equal to their common radius of curvature. Since the focal length of a spherical mirror is one-half its radius of curvature, the mirrors have a common focus at the center of the resonator. This confocal configuration was also examined by Fox and Li, whose results are in good agreement with those of Boyd and Gordon. It was found that diffraction losses are generally considerably lower for the spherical mirrors than for the plane mirrors. An additional advantage of the confocal spherical resonator is that the optical alignment is not extremely critical. A disadvantage of such a resonator is that the divergence angle of the output beam is larger than that for a similar resonator with plane mirrors.

As in the case of plane mirrors the analysis assumed a homogeneous dielectric material between the mirrors and neglected any sidewall effects. Consequently, the same arguments apply concerning the validity of applying the results to the case of ruby.

The field distributions of the various modes are similar in shape to those for the plane-mirror resonator but are generally more nearly concentrated on the axis of the rod. A particularly interesting feature of the mode frequencies is that they are highly degenerate, and the phase shift per transit is independent of the Fresnel number. This highly degenerate mode spectrum leads to a particularly simple beat-frequency spectrum. The resonant frequencies are given by

$$f = (c/2b)[q + (1 + m + n)/2],$$

where q is the length of the rod measured in half-wavelengths; m and n are integers describing the transverse variations; b is the confocal spacing, equal to the radius of curvature; and c is the velocity of light in ruby. Consequently, the predicted beat frequencies are integral multiples of $c/4b$. Odd multiples correspond to beating between dissimilar modes (i.e., $m_2 + n_2 \neq m_1 + n_1$), whereas even multiples can correspond to beating between either similar or dissimilar modes. The optical mode spectrum is shown in Fig. 3, which emphasizes the

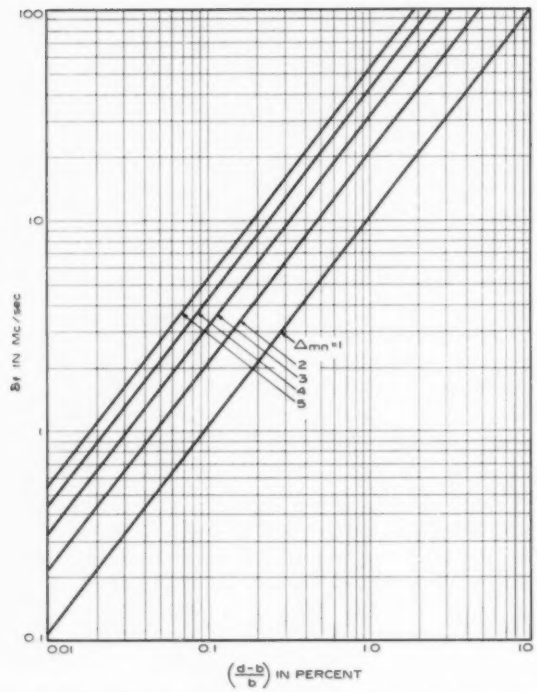

Fig. 4. Calculated beat-frequency spread due to nonconfocal alignment of a spherical-mirror resonator.

simplicity of the confocal spectrum compared to the plane-mirror spectrum of Fig. 1.

Since there are finite tolerances in the construction and alignment of the spherical resonators, one might ask how the resonator characteristics are modified by nonconfocal alignment. Boyd and Gordon have considered the case of spherical mirrors of radius b separated by a distance d. They showed that for $b \simeq d$, the resonant frequencies are given approximately by

$$f = \frac{c}{2d}\left\{q + \frac{1+m+n}{2}\left[1 - \frac{2}{\pi}\left(1 - \frac{d}{b}\right)\right]\right\}.$$

Consequently, the difference-frequencies to be expected are

$$\Delta f = \Delta f_0 + [(c/2d)(1/\pi)(d-b)/b]\Delta mn,$$

where $\Delta mn = m_2 + n_2 - m_1 - n_1$ and Δf_0 is the frequency corresponding to confocal spacing

$$\Delta f_0 = (c/2d)(\Delta q + \Delta mn/2).$$

Figure 4 is a plot of $\delta f = \Delta f - \Delta f_0$ vs $(d/b - 1)$ for values of Δmn between one and five.

This result immediately indicates an important application for photomixing techniques. For situations in which the oscillation frequencies are determined primarily by the location of the cavity resonances, a Fourier analysis of the beat-frequency spectrum can provide an extremely accurate measurement of just how much the resonator alignment differs from the desired confocal condition.

Q Calculations

For the experiments described the reflection and scattering losses are generally quite large compared to the calculated diffraction loss. Consequently, the diffraction losses can be neglected in the Q calculation, and in analogy with the case of a resonant waveguide cavity the optical resonator quality-factor can be written as[12]

$$Q = \frac{|R_1 R_2 e^{-2\alpha b}|}{1 - |R_1 R_2 e^{-2\alpha b}|}\,\frac{2\pi b}{\lambda},$$

where α is the attenuation constant due to scattering by inhomogeneity of the material, R_n = voltage reflection coefficient at nth mirror $= (1 - \delta r_n - \delta d_n)^{1/2}$, and δr and δd are the power losses due to reflection and diffraction, respectively. Since one end of the rod is highly reflecting, and since diffraction losses are small compared to scattering and output-end reflection losses, the Q becomes

$$Q = \frac{(1 - \delta_r)^{1/2} e^{-2\alpha b}}{1 - (1 - \delta_r)^{1/2} e^{-2\alpha b}}\,\frac{2\pi b}{\lambda},$$

where δ_r is the power loss at (and through) the output mirror.

The scattering loss in ruby has been found to vary considerably from sample to sample.[14,15] Since this loss requires individual measurement on each rod, it is convenient to compute the Q in terms of the total

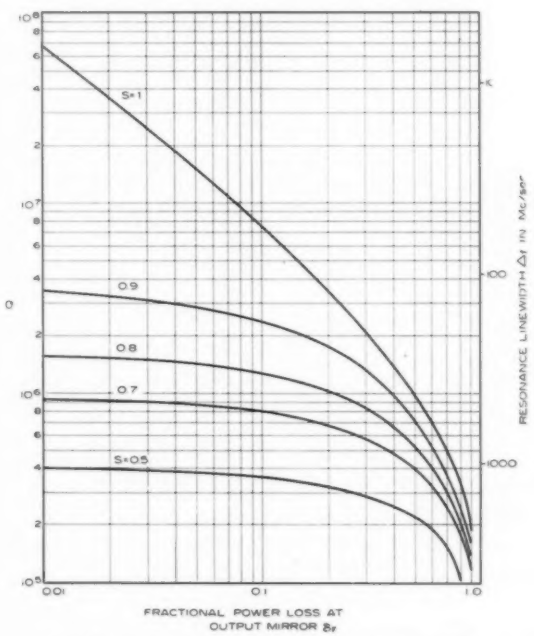

Fig. 5. Calculated Q for a 2.54-cm long ruby rod.

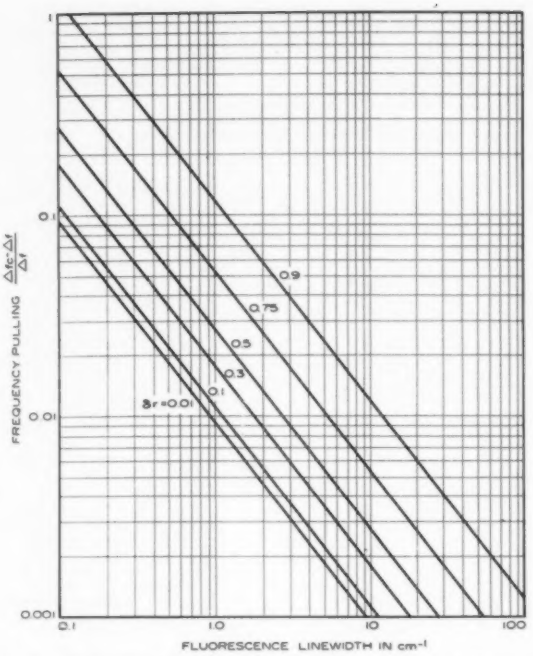

Fig. 6. Calculated frequency-pulling for a 2.54-cm long ruby having 20% scattering loss per pass.

scattering loss per transit $(1 - S)$, where $S = e^{-2\alpha b}$. The quantity Q/b (or Q for a 25.4-mm rod) has been plotted vs δ_r and S in Fig. 5 for pink ruby. Also indicated on the graph is the resonance line-width at the half-power points, Δf, where we have used the relation $Q \cong f/\Delta f$.

Note that these calculations should be valid for the normally large values of the Fresnel number, $N = a^2/b\lambda$. However, since diffraction losses increase rapidly with decreasing N, situations can be achieved in which the diffraction losses are quite large and can no longer be neglected. Hence it is incorrect to assume that the resonator Q can be increased indefinitely by increasing the rod length. This point is more fully discussed by Boyd and Gordon[13] and by Fox and Li.[12]

Effect of Stimulated Emission

Bennett[10] has shown that for most line shapes and broadening mechanisms the oscillation frequency must be obtained by solving a transcendental equation, and that a notable exception to this is provided by the case of a single oscillation occurring in a homogeneously broadened Lorentzian line. For that case the oscillation frequency is[10,18,19]

$$f = \frac{f_c\Delta f_m + f_m\Delta f_c}{\Delta f_m + \Delta f_c},$$

where f_c and f_m are the center frequencies, and Δf_c and Δf_m the line-widths of the cavity resonance and the fluorescence spectrum, respectively. Written in terms of the quality factor of the resonator, Q_c, and the effective quality factor of the fluorescence spectrum, $Q_m = f_m/\Delta f_m$, the oscillation frequency is

$$f = \frac{Q_c + Q_m}{Q_c/f_c + Q_m/f_m}.$$

Thus oscillation occurs at the peak of the cavity resonance when the fluorescence spectrum is broad compared to the cavity resonance. However, as the fluorescence spectrum gets narrower the oscillation frequency is "pulled" toward the center of the fluorescence spectrum.

This is indeed a simple result, and it would be most helpful if it could be used to predict the results of a photomixing experiment. Unfortunately, the assumption of a homogeneously broadened line essentially rules out the possibility of obtaining oscillation in more than a single mode, since gain proportionality is always maintained over a homogeneously broadened line.[10] However, in order to obtain even a crude prediction of what might be observed experimentally, calculations were carried out using the linear frequency-pulling equation derived for a homogeneously broadened Lorentzian line. For $Q_m << Q_c$ the frequency difference between two oscillating modes is given by

$$\Delta f \cong \Delta f_c/(1 + Q_m/Q_c),$$

where Δf_c is the spacing between the centers of the cavity resonances. The fractional frequency-pulling can be defined as

$$(\Delta f_c - \Delta f)/\Delta f \cong Q_m/Q_c.$$

Schawlow[20] found that the line-width of the R_1 fluorescence line in ruby is temperature dependent, varying from about 11 cm^{-1} at room temperature to about 0.2 cm^{-1} at liquid nitrogen temperature. The exact variation of the line-width varies from sample to sample, and it has been demonstrated that low-temperature line-widths are extremely small for crystals having relatively little internal mechanical strain.

These results indicate that the fractional frequency-pulling should increase by roughly a factor of 50 when the rod is cooled from room temperature to liquid nitrogen temperature. Such an effect should be observable in a photomixing experiment, provided of course that the cavity Q is not so high as to produce negligible frequency shifts even at low temperature.

The dependence of the frequency-pulling on the cavity parameters and fluorescence line-width is given by

$$\frac{\Delta f_c - \Delta f}{\Delta f} \cong \frac{Q_m}{Q_c} = 0.0355\,\frac{1 - S(1 - \delta_r)^{1/2}}{S(1 - \delta_r)^{1/2}} \cdot \frac{1}{bL},$$

where L is the R_1 fluorescence line-width in wavenumbers, b is the rod length in inches, and δ_r and $(1 - S)$ are the power losses due to reflection and scattering, respectively. Diffraction losses have been neglected as in the previous calculations of resonator quality factor. Figure 6 shows frequency-pulling as a function of

fluorescence line-width and reflection loss for a 25.4-mm long rod having a 20% scattering loss per pass. These results indicate that the conditions required to permit the observation of linear pulling effects should not be difficult to obtain. For example, a 25.4-mm long rod with 20% scattering loss and 30% power loss at the output reflector might exhibit 0.16% pulling at room temperature and 9% pulling at 77°K; this would correspond to a frequency shift from 3340 Mc/sec to 3040 Mc/sec for the adjacent-axial-mode beat frequency. Such a shift would be easy to observe. Recall, however, that this linear theory may have little validity for the case of ruby. Note also that the expression from which the curves were calculated is valid only for $Q_m << Q_c$.

If the linear frequency-pulling theory did describe the behavior of ruby under certain conditions, then photomixing techniques could provide some very interesting information. For example, by measuring the increase in beat frequency due to rod heating during one pump flash and by knowing the variation of fluorescence line-width with temperature, one could compute the change in rod temperature *during* a single pump flash.

III. S-Band Experiments on Rods with Plane Mirrors

Dependence of Multimoding upon Pump Power

In numerous laser applications, particularly those involving communications, it is imperative that the laser should produce a single, sharp, and stable frequency. In addition, such operation should be obtained at no sacrifice in power output and directionality.

Under what conditions might one hope to obtain single-mode oscillation in a laser? Part of the answer, at least, should be obtainable from the experiments of Javan *et al.* on the He-Ne laser.[21,22] They found that oscillation would occur in a single mode only when the pump power was very close to its value at the threshold of oscillation. For higher values of pump power they found not only oscillations corresponding to other modes of the interferometer, but also oscillations at frequencies corresponding to transitions between other energy levels of the gaseous system.

How might this difficulty be overcome? Ideally one would like to narrow the fluorescence line-width and increase the spacing between interferometer resonances until there was only a single interferometer resonant frequency within the fluorescence spectrum. As pointed out by Boyd and Gordon,[13] a confocal resonator would be desirable because of its high mode degeneracy. That is, although the laser might oscillate in modes with a wide variety of spatial distributions, at least the oscillation frequency would be the same for each mode.

In the 1.153-μ laser the fluorescence line-width will necessarily be as broad as 800 Mc/sec due to Doppler effects. In order to have a single interferometer resonance within this line-width, the mirror separation would have to be about 18 cm. For such a condition the Q would be so low that the gain due to stimulated emission would probably be insufficient to start an oscillation.

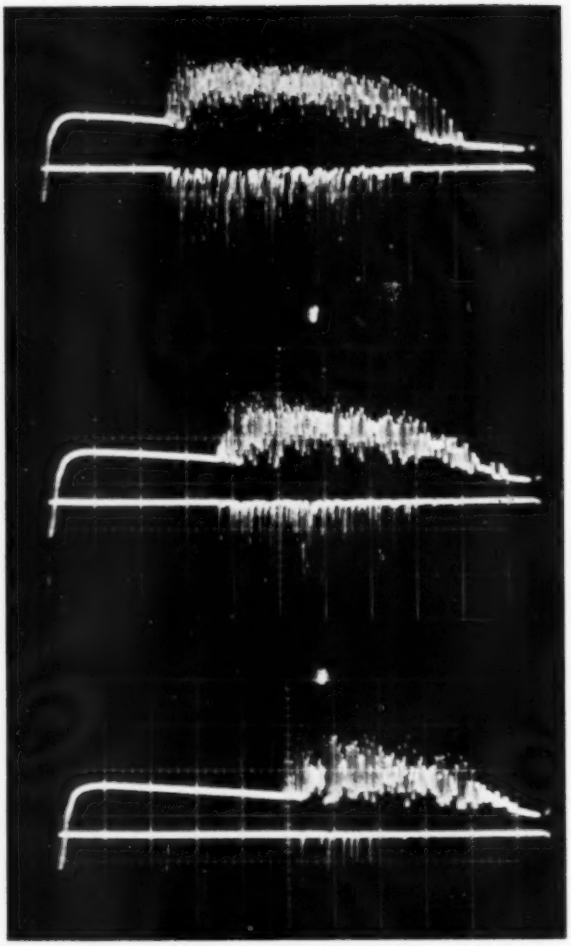

Fig. 7. Photomultiplier output (upper trace) and detected microwave output near 1.48 Gc/sec (lower trace) for values of pump energy 10% (lower photograph), 30 and 60% above threshold. Time scale: 50 μsec/cm.

Many of the conditions that plague single-mode oscillation in the gaseous laser also apply to the ruby laser. However, there are important differences, the most important being that the fluorescence line-width in ruby is a function of both temperature and internal strain (or homogeneity). At liquid nitrogen temperature the line-width can be as small as 5 Gc/sec. In that case a 15-mm long rod with confocal ends could exhibit a single resonant-frequency within the fluorescence line-width, and the gain due to stimulated emission could certainly be sufficient to start an oscillation. However, the fluorescence emission at low temperatures actually consists of *two* lines of com-

parable line-width,[20] separated from one another by about 11.5 Gc/sec. Although one of the lines has a slightly favored transition probability compared to the other, it does not seem unlikely that oscillations could be simultaneously excited in both. The requirement that only a single interferometer resonance be present in *either* fluorescence line leads to rod lengths that are so small as to seem generally impractical.

1. *Description of Experiments*

The initial experiment[1] using a 14.05-cm rod had indicated that the number and amplitude of the detected microwave pulses did indeed depend upon pump power. This result was confirmed by numerous experiments on other rods. Figure 7 shows a typical result for a 5.66 cm long by 3.18 mm-diameter rod. One end of the rod was heavily silvered and the other was silvered uniformly for approximately 15% transmission; the cylindrical surface of the rod was polished to an optical finish. Both the ruby rod and the flashtube were cooled by dry nitrogen gas that had been bubbled through liquid nitrogen. The output of the improvised photo-TWT was passed through a single TWT amplifier and a 20-Mc/sec bandpass filter set at 1480 Mc/sec, corresponding to beats between adjacent axial modes of the resonator. The power output from the photo-TWT was approximately −50 dBm at 1480 Mc/sec for values of pump energy 12% above threshold. This result was essentially the same as that obtained for the gaseous laser, namely, that single-mode oscillation could apparently be obtained only near threshold. These experiments also provided further evidence that there was no obvious connection between the amplitude of a photomultiplier pulse and the presence or amplitude of a pulse of microwave output. Although the first pulse of laser output was usually accompanied by a microwave pulse, there were notable exceptions such as that provided by the lower photograph in Fig. 7.

In order to obtain more detailed information concerning the number of modes excited at a given time and at a particular pump power, several experiments were performed in which the microwave output was examined simultaneously at frequencies corresponding to beats between first through third nearest-neighbor axial modes. The 5.66-cm rod was used and the microwave output was found to be centered at the following frequencies: 1480, 2960, and 4440 Mc/sec. (The actual frequency spread and line-width will be discussed in a subsequent section.) Narrowband superheterodyne receivers were used to select the output near 1480 and 4440 Mc/sec; a TWT amplifier and a narrowband filter were used to select the output near 2960 Mc/sec. As was the case in the early experiments with the 14.05 cm rod, a pulse of microwave output at one beat frequency did not guarantee that there would be a coincident pulse at any other beat frequency, either higher or lower. However, the probability of finding output at a high beat frequency when there is no output at a lower beat frequency was rather small. Based on this result, the following generalization will be used in interpreting the results of this and similar experiments: If no microwave output is observed at the first few possible beat-frequencies, then such an oscillation will be described as "single mode". Although this conclusion is probably valid for the temperatures used in the experiments being described, there is at low temperatures a serious overgeneralization in concluding from S-band measurements that a ruby laser can oscillate in a single mode. Due to the 11.5 Gc/sec splitting of the fluorescence at low temperature, one should really examine frequencies through X-band before generalizing concerning the possibility of single-mode oscillation. This will be discussed further in a subsequent section.

In order to examine the behavior near threshold more carefully, the detected microwave output near 1480 and 2960 Mc/sec was displayed simultaneously with the output of a DuMont 6911 photomultiplier. The two microwave frequencies were selected by using narrowband filters. It was clear from this experiment that the laser under test would oscillate in a single mode only for values of pump voltage *extremely* close to threshold (i.e., within 1% of threshold). In fact, microwave output sometimes accompanied photomultiplier output even when the photomultiplier detected only one or two spikes of laser output.

Similar experiments have been performed on 3.18-mm diam rods of length 14.05, 7.62, and 2.54 cm, and the results have agreed with those described above for the 5.66 cm rod.

2. *Conclusions*

For rod temperatures between approximately 200° and 300°K, the ruby laser generally oscillates at more than one frequency except for values of pump energy within about 1% of the threshold value. In other words, high-power output with a single mode of oscillation does not seem to be achievable in this range of rod temperature.

The power level at the various beat frequencies appears to be a slowly decreasing function of beat frequency. At a given temperature and pump energy, the probability of obtaining output at a low-beat frequency is greater than that of obtaining output at a higher frequency.

Dependence of Multimoding upon Temperature

The most pronounced temperature-dependent effect in ruby is the narrowing of the fluorescence spectrum with decreasing temperature. This narrowing is primarily responsible for the fact that the threshold energy decreases with decreasing temperature. That is, at low temperature the fluorescence is spread over a band of

frequencies containing only a few interferometer resonances; the gain at these resonances is considerably higher than it would be at room temperature, where the fluorescence is distributed among a much larger number of interferometer resonances.

The qualitative interpretation of the dependence of threshold pump-energy on temperature is relatively straightforward, but the determination of the possible number of simultaneously oscillating modes is not so obvious. One might say that, since there are fewer interferometer resonances within the fluorescence linewidth at low temperature, there should be strong oscillations near those resonances. But the nature of the line broadening at low temperature might be somewhat different from that at higher temperatures, so that it may be either more or less likely that more than a single oscillation could be initiated.

There are numerous other temperature-dependent effects that should be noted. First, the center frequency of the fluorescence spectrum shifts toward shorter wavelengths as the rod temperature is decreased[23] from 20–80°C at the rate of approximately 0.065 Å/°C. Second, the whole spectrum of interferometer resonances will shift due to changes in rod length and index of refraction; although the absolute-frequency shift may be large, the difference-frequencies should exhibit negligible changes. Third, if the rod is immersed in different media at different temperatures, part of the difference in threshold energy will result from the fact that certain media provide a better impedance-matching of the pump light into the ruby rod.

There are two additional temperature-dependent effects that will be discussed in subsequent sections. The first is the effect of the "double-peaked" fluorescence spectrum at low temperature, and the second is the effect of stimulated emission in shifting the beat frequencies.

The following paragraphs describe the results of experiments performed in order to determine the number of oscillation frequencies present at various temperatures and pump levels.

1. *Description of Experiments*

In order to permit operation at temperatures ranging from 77°K to room temperature and above, the laser used in the previous experiments was modified to permit immersion of the rod in liquid nitrogen. Experiments were performed using the following rods: 3.18 mm-diam by 5.66 cm-long; 3.18 mm-diam by 7.62 cm-long; and a sapphire-clad rod, 2.54 cm-long with 2 mm-diam ruby and 5 mm over-all diameter.

In every case, *beat-frequency output became very difficult to observe* when the rod was cooled to temperatures close to that of liquid nitrogen. In other words, it appears to be possible to obtain single-mode oscillation (at least within one peak of the fluorescence spectrum) at 77°K, even for power levels considerably above threshold. This was a particularly encouraging result, since the cleaner shape and higher power output at 77°K make it a desirable operating condition.

The fact that the beat-frequency output was generally not visible at rod temperatures near 77°K did not necessarily mean that it was totally absent. That is, higher gain in the microwave receiver might still permit the observation of beat-frequency output. Consequently, several experiments were performed using higher gain in the microwave receiver and greater focusing of the laser output onto the cathode of the photo-TWT. It was found that microwave output could be obtained under these conditions provided the pump voltage was sufficiently far above threshold. Even though the photomultiplier-detected laser output did not exhibit "spikes," still the microwave output consisted of a series of pulses.

2. *Conclusions*

Experiments at rod temperatures between room and liquid-nitrogen temperature produced the result that the amplitude of S-band microwave beat-frequency output decreases drastically as liquid-nitrogen temperature is approached. In other words, single-mode oscillation appears to be possible at liquid-nitrogen temperature for pump voltages farther above threshold than would be possible near room temperature.

Note that, although these experiments provided valuable information concerning the number of S-band beat-frequencies present at various rod temperatures and pump levels, one cannot conclude that the absence of S-band output indicates laser oscillation at a single frequency. Due to the resolved zero-field splitting of the R_1 fluorescence at low temperature, it is rather likely that one oscillation occurs within each of the two peaks even for pump voltages slightly above threshold. Experiments concerned with this phenomenon are discussed in Sec. V.

Comparison with Predicted Cavity-Modes

In the initial experiments it was found that the beat-frequencies obtained were within a few percent of the predicted spacing between resonant modes of the interferometer. That is, for those rod temperatures and pump-power levels, the laser oscillation-frequencies appeared to be determined primarily by the location of the interferometer resonances.

In this section the measured beat frequencies for several rods will be compared with the predicted difference-frequencies for homogeneous, lossless, passive interferometers in which sidewall effects are neglected.

1. *Frequency-Measurement Techniques*

A number of measurement techniques were used in determining the beat frequencies. Beat-frequency out-

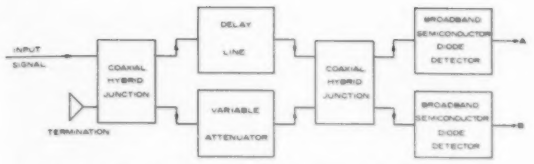

Fig. 8. Block diagram of microwave interferometer.

put was generally first located by the use of either narrowband (10–20 Mc/sec) tunable transmission-cavities or narrowband (7–15 Mc/sec) superheterodyne receivers. More precise frequency-measurements were performed using either of the two methods described in the following paragraphs:

Figure 8 is a schematic diagram of a microwave interferometer that was used in a number of experiments. It can be shown that the ratio of the voltage at A to that at B is given by

$$\frac{V_A}{V_B} = R_d \frac{1 + R_l^2 - 2R_l \cos\beta l}{1 + R_l^2 + 2R_l \cos\beta l},$$

where R_d is the ratio of the sensitivity of the detector at A to that at B, R_l is the ratio of the loss in the delay line to that in the variable attenuator, $\beta = 2\pi/\lambda$, and l is the delay-line length.

If a well-matched pair of detectors is used, and if the loss in the variable attenuator is adjusted to match that in the delay line, the above equation takes the particularly simple form

$$V_A/V_B = (1 - \cos\beta l)/(1 + \cos\beta l).$$

The "nondegenerate bandwidth", defined as the frequency change required to shift V_A/V_B from zero to its maximum value (or vice versa), is given by $\Delta f = c/2l$, where c is the velocity of light in the transmission line. The "center frequency", defined as the frequency for which $\phi = \tan^{-1}(V_A/V_B)$ is half its maximum value, is given by $f_{center} = nc/4l = n\,\Delta f/2$, where n is an odd integer. Both l and f_{center}/n are plotted as a function of Δf in Fig. 9.

Since the interferometer is highly degenerate when the delay-line length is adjusted for high resolution, it is important that initial information should be obtained concerning the upper and lower limits on the frequencies present. Generally, experiments were begun with relatively large bandwidth (i.e., short delay-lines) and then the delay-line length was increased until the frequencies present produced a spread in ϕ from roughly zero to $\pi/2$. That is, the resolution (or permissible nondegenerate bandwidth) was limited by the observed spread in beat frequencies. Of course, the output near other axial-mode beat-frequencies was filtered out before the interferometer was inserted in order to examine the output near a particular axial-mode beat-frequency.

The interferometer can be used in conjunction with either an x-y or a dual-beam oscilloscope. If V_A and V_B are applied to the x and y deflection plates, respectively, of an oscilloscope, the frequency of an incident pulse is "measured" by the angle formed by the pulse and the horizontal (or vertical) direction. If V_A is applied to one and V_B to the other beam of a dual-beam oscilloscope, the frequency is "measured" by the ratio of the pulse amplitudes on the two beams. The x-y presentation has the advantage that the output can be compared directly with a calibration diagram of frequency vs angle, whereas the dual-beam presentation requires subsequent calculations to obtain the frequency. A major disadvantage of the x-y presentation is that all time-information is lost. An even more important disadvantage for these experiments was that it was not possible to photograph the excursions produced by a single 0.5-μsec pulse. Even with oscilloscope intensity modulation and ASA 10,000 speed film, it was impossible to photograph such pulses on a Tektronix 536 oscilloscope, which was the only x-y oscilloscope having sufficient bandwidth (10 Mc/sec) to permit time resolution of the pulses.

Consequently, the interferometer output was generally displayed on a Tektronix 555 dual-beam oscilloscope. The output was photographed and then plotted in x-y form as shown in Fig. 10. The calibration lines in every case are measured, rather than calculated, values.

A second method used for measuring beat frequencies is shown schematically in Fig. 11. The local-oscillator

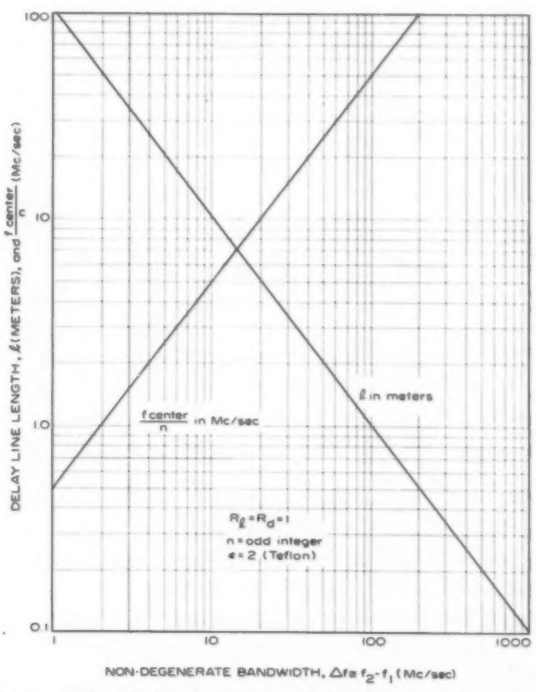

Fig. 9. Delay-line length and center frequency vs nondegenerate bandwidth for the microwave interferometer.

frequency was adjusted until the beat frequency produced in the mixer was visible on the oscilloscope. Generally, the local-oscillator frequency was adjusted until it essentially coincided with the center frequency in the spread of microwave beat-frequency pulses. In that case, pulses at the center frequency would appear in their original shape but with conversion gain, and the difference between that and other frequencies could be measured directly from the other beat-frequencies produced. Figure 12 is a typical result: the lower trace is the output obtained during 100 μsec and the upper trace is an expanded view of the 10-μsec portion of the output beginning at 60 μsec on the lower trace.

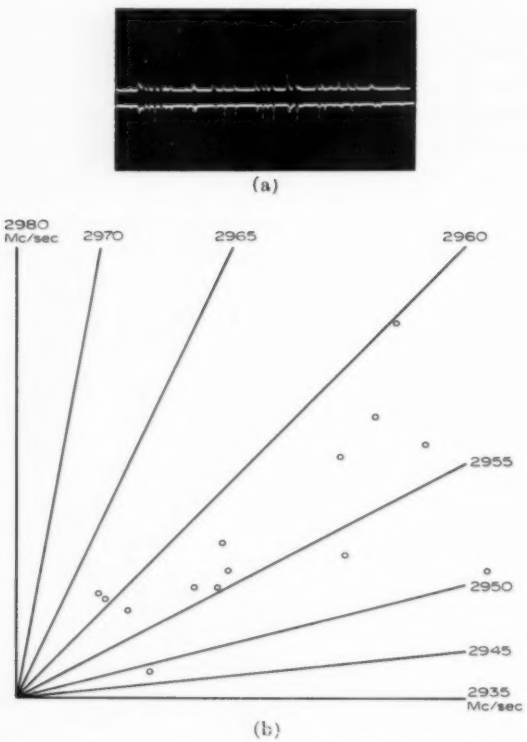

Fig. 10. Frequency measurement using microwave interferometer: (a) photograph of output on dual-beam oscilloscope; (b) x-y plot of data showing frequency as a function of angle (intensity is radial). Time scale: 10 μsec/cm.

The major disadvantage of the microwave-mixing frequency-measurement technique is that accurate frequency-measurements on 0.5-μsec pulses require oscilloscope sweep speeds of at least 0.5 μsec/cm. Hence the examination of all the pulses in a 300-μsec burst of laser output would require some 60 oscilloscope beams with carefully delayed triggering. Consequently, this technique has found major application in line-width measurements for individual pulses.

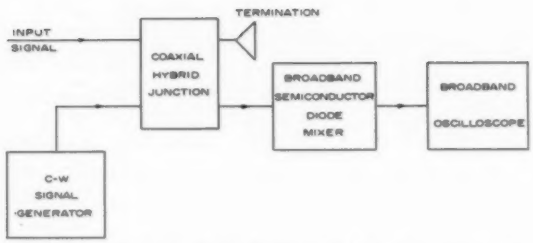

Fig. 11. Block diagram of microwave-mixing frequency measuring technique.

2. Results

In this section we are concerned with the beat frequencies produced in the vicinity of a particular axial-mode beat frequency. For example, in an experiment on a 5.66 cm rod the amplifier gain was adjusted so that signals at 1.5 and 4.5 Gc/sec (corresponding to first and third beats, respectively) were not observable, whereas those at 3 Gc/sec were quite strong. Then, frequency measurements were made using both the interferometer and the microwave-mixing technique.

There were several questions to be answered:

1. How many frequencies near 3 Gc/sec were present during any one 0.5-μsec pulse of laser output?
2. Does the frequency shift from pulse to pulse during the laser output accompanying a single pump flash?
3. How repeatable are the frequencies from flash to flash?
4. How do the frequencies depend upon rod temperature and pump power?
5. Does the frequency spread vary from rod to rod?

Both frequency-measurement techniques were used in an effort to determine whether more than one beat-frequency was present during a 0.5-μsec pulse. It was found that generally a single microwave beat-frequency was present during a 0.5-μsec pulse of laser output. This result was somewhat surprising, since the presence of output at various axial-mode beat frequencies indicated that the output at a particular beat-frequency was composed of beats between a number of different modes. That is, it indicated that the spacing between modes was essentially constant for any two modes within the fluorescence spectrum.

An examination of the frequencies present in a train

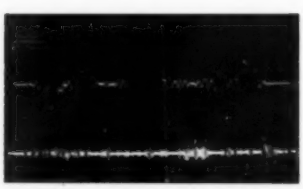

Fig. 12. Frequency measurement using microwave-mixing technique. Time scales: 10 μsec/cm on lower trace; 1 μsec/cm on upper trace, beginning at 60 μsec on lower trace.

of pulses during one pump flash showed that in many instances there were frequency shifts from pulse to pulse. The center frequency of the range of frequencies present was found to be between a fraction of a percent and a few percent lower than the calculated axial-mode beat frequency. Part of this difference can be accounted for by linear frequency-pulling effects. That the linear theory should be applicable is supported by the fact, mentioned above, that a single beat-frequency was generally present during a 0.5-μsec pulse.

The frequencies produced appeared to be fairly reproducible from flash to flash, although the sequence in which the various frequencies appeared was not reproducible.

In many instances the output appeared to "cluster" about certain frequencies separated from one another by a few megacycles. This could readily be interpreted as the result of laser action in high-order interferometer modes since similar results were observed in the He-Ne laser.[22] However, such results were not readily repeatable in the experiments with ruby. The total frequency spread was fairly reproducible, but the output was not always clustered about only a few frequencies. However, when one considers the number of possible modes within the ruby fluorescence linewidth near room temperature, it should come as no surprise that the beat-frequency spectrum is not identically reproducible.

Experiments on the 5.66-cm rod clearly indicated that the frequency spread was a function of pump power and temperature. For temperatures in the vicinity of -100°C the frequency spread was about 3 Mc/sec near threshold and increased to about 20 Mc/sec for pump energy 11% above threshold. For lower temperatures, particularly near liquid-nitrogen temperature, both the center frequency and the frequency spread were observed to change in a manner that will be described later.

The change in frequency spread with pump power could be explained in several ways. If the oscillation frequencies were determined primarily by the interferometer resonances, then the increased frequency-spread could be the result of the excitation of high-order modes. Or there might be some power-dependent frequency-pulling effect which increased the frequency spread as pump power increased. The calculated frequency-spread due to high-order mode excitation was plotted in Fig. 2 for all combinations of the first five modes of the interferometer. (Note that δf represents the frequency shift on *one side* of the axial-mode beat-frequency, so that the frequency spread to be compared with experiment is $2\ \delta f$.) The comparison of theory and experiment is outwardly simple, since one might say that the observed frequency-spread is a measure of the number of types of oscillating modes. However, such a comparison is not particularly meaningful for a number of reasons. First, the possible power-dependent frequency-pulling effects have not been evaluated. Second, there is good reason to doubt the validity of applying the Fox and Li passive interferometer theory to the case of solid materials, which are necessarily quite inhomogeneous. Third, ruby rods have generally been observed to oscillate with spatial distributions that are far from uniform. Although Fox and Li type modes might exist in oscillation in several overlapping regions of the rod, the effective diameter of the waveguide corresponding to the observed spatial-distribution might be different for each mode. In addition, the electrical length of the path between mirrors might be different for oscillations in various parts of the rod. (Even though a focusing lens is used, it is not likely that nonoverlapping oscillations could produce beats since the relatively large solid-angle formed by the converging rays would result in an extremely small coherence-area.)

Table I. Physical Characteristics and Experimental Results for Plane-Mirror Rods

Rod diameter (mm)	Rod length (cm)	$N = a^2/b\lambda$	Mode interval	Calculated axial mode beat frequency (Mc/sec)	Measured center frequency (Mc/sec)	Frequency spread: Near threshold (Mc/sec)	Frequency spread: Above threshold (Mc/sec)
2.00	2.54	101	1	3343	3289	<20	<20
3.18	5.66	113	1	1501	1482	<20	<20
			2	3002	2960	3	20
			3	4503	4439	<20	<20
3.18	7.62	84	2	2231	2208	<20	<20
			3	3346	3280	<20	<20
3.18	14.05	46	3	1815	1800	<20	<20
			4	2420	2410	5	<20
			5	3025	3000	<20	<20
			6	3630	3600	<20	<20
			7	4235	4200	<20	<20

Clearly what was needed was some means of determining conclusively whether or not the existing interferometer-analyses could be applied to the case of ruby: i.e., an experiment in which beat frequencies due to photomixing of oscillations near particular interferometer resonances could be clearly distinguished from possible effects of stimulated emission. A. E. Siegman proposed such an experiment, and it was carried out as described in Sec. IV.

Before proceeding to a discussion of line-width measurements, let us briefly summarize the results of the experiments on rods with plane ends. Table I shows some characteristics of the rods tested. All the results in this table correspond to rod temperatures of approximately -100°C, corresponding to cooling by nitrogen gas that had been bubbled through liquid

nitrogen. The calculated values are based upon an index of refraction of 1.764.

Line-Width

Measurements of the line-width of the beat-frequencies produced in a photomixing experiment can provide valuable information concerning the line-width of the signals producing the beats. Forrester[24] has calculated the results of photomixing experiments involving various line shapes and relative line-widths. Javan *et al.*[21] used this technique to obtain initial estimates of the line-width of the laser oscillation in their helium-neon system.

Before discussing similar experiments on a ruby laser, there is one very important consideration that should be presented. Consider two spectral lines of identical width and shape that are photomixed to produce a beat frequency exhibiting a certain line-width. If the two spectral lines are produced by two distinct sets of radiating atoms so that the phase variations within one line are independent of those within the other line, then the measured line-width of the beat signal provides unique information concerning the line-width of the optical signals. Now consider the case in which there is a distinct relation, or coupling, between the phase variations in one line and those in the other; e.g., sidebands produced by amplitude modulation of an optical signal. In this special case the result of a photomixing experiment can be a sharp signal at the modulating frequency, even though the optical carrier may have a very large line-width. In other words, unique information concerning the line-widths of optical signals can be obtained from photomixing experiments *only* if the spectral lines are known to be uncoupled or if the degree of coupling is precisely known.

This is a consideration that must be borne in mind when one examines the result of a photomixing experiment involving different spectral lines from the same laser. Since the laser oscillations occur on sets of atoms whose radiating frequencies are located near the centers of various interferometer resonances, it seems likely that the oscillations can safely be considered as uncoupled. Only under conditions of very high power and/or relatively narrow fluorescence spectra (e.g., at low temperature) might one expect to see appreciable coupling between the various laser oscillations. Nevertheless, the possibility of coupling between laser oscillations has received relatively little theoretical and experimental investigation, and is consequently not yet well understood.

As a result, the line-width data obtained from photomixing experiments with a single laser cannot be interpreted as decisively as one would desire. The natural step is to confirm (hopefully) the single-laser experiments with an experiment in which optical signals from each of two similar lasers are photomixed. Such an experiment has recently been performed by Javan *et al.*[25] on the gas laser, and the results were found to be in good agreement with line-width data obtained by photomixing using a single laser. A similar experiment involving two ruby lasers and a microwave phototube is being carried out at Stanford University.[26]

In the following paragraphs the results of line-width measurements involving single lasers will be described.

The initial experiment[1] indicated that the beat-frequency line-widths were in every case less than 20 Mc/sec, and in the one case examined carefully, was less than 5 Mc/sec. These measurements were performed using narrowband transmission filters and superheterodyne receivers.

Subsequent line-width measurements were performed on the 14.05- and 5.66-cm rods (each 3.18-mm diam). The technique that proved most valuable was the microwave-mixing circuit shown in Fig. 11. The line-width can be determined by measuring the line-width of the Fourier transform of the beat signal.

The result of all of these experiments was that the line-width was approximately 2 Mc/sec. Since the laser-pulse duration was approximately 0.5 μsec, it appears that the line-width is limited primarily by the pulse duration. That is, longer laser pulses might permit the observation of even smaller line-widths.

Frequency-Pulling Effects

One of the objectives of this investigation was to determine under what conditions the effects of stimulated emission might be sufficient to shift appreciably the laser oscillation frequencies from the passive interferometer resonances. The experiments described earlier indicate that at least the gross structure of the beat-frequency output can be interpreted almost solely on the basis of the passive interferometer resonances. That is, for rod temperatures in the range from approximately -100°C to room temperature, the effect of stimulated emission in determining difference frequencies is relatively small. That this should be the case for these temperatures is in agreement with the linear frequency-pulling theory presented earlier.

But even the linear frequency-pulling theory predicts the possibility of some rather large beat-frequency shifts for conditions in which the effective quality factor of the fluorescence spectrum Q_m becomes appreciable compared to the quality factor of the interferometer resonances Q_c. High Q_m is best obtained in relatively unstrained ruby at low temperature. Low Q_c is obtained in a given rod by using low-reflectivity mirrors.

In experiments using a conventional traveling-wave tube as an improvised microwave phototube, the beat-frequency for a 2.54-cm long rod was found to shift

appreciably as a function of rod temperature. With the rod at room temperature the microwave output was concentrated within a 20-Mc/sec band centered at 3289 Mc/sec. By improving the focusing and receiver sensitivity it was possible to observe weak but distinct output with the rod at liquid nitrogen temperature. The output occurred near both 3242 and 3118 Mc/sec, which represent frequency pulling of 1.4 and 5.2%, respectively, away from the value at room temperature.

The comparison of these results with the linear frequency-pulling theory is somewhat complicated by the fact that the scattering loss was not accurately known. In addition, the silver coating on the output end was not particularly uniform. If the scattering loss were 20% and the reflection loss were 30%, then the predicted pulling would be 0.16% at room temperature and 9% at liquid nitrogen temperature; where it is assumed that the fluorescence line-width changed from 11–0.2 cm^{-1} in going from room temperature to liquid nitrogen temperature. This would correspond to a frequency shift from about 3340 Mc/sec to about 3040 Mc/sec.

Although the only appreciable output was obtained near 3242 and 3118 Mc/sec, the signal levels were so small that firm conclusions could not be drawn concerning the presence or absence of signals at other frequencies. It would be particularly interesting to know whether the beat frequencies shifted in any regular way during the laser output. An effort was made to increase the signal levels and use the microwave interferometer of Fig. 8 but the signal levels could not be made large enough to overcome the insertion loss of the interferometer.

Reasonable signal levels in experiments at liquid nitrogen temperature were first achieved with an improved form of microwave phototube developed by the Sylvania Microwave Device Division at Mountain View, California. Figure 13 is a photograph of the tube, designated as the SY-4302. This tube was used in some experiments on a 3.8-cm sapphire-clad ruby rod operated at liquid nitrogen temperature. The rod was heavily silvered on one end and contained no silver on the other end.

By operating the SY-4302 with about 600 μA of collector current (thermionic), and by focusing the laser output to obtain 20–50 μA of photocurrent, beat-frequency signals were easy to observe. The nature of the beat-frequency output was somewhat different from that observed earlier. The output consisted of rather large spikes superimposed on a slightly raised base line. That is, there was a small amount of microwave output (up to about −55 dBm from the SY-4302) during a large portion of the laser output. Superimposed on this were spikes as large as −35 dBm.

The major purpose of the experiment was to determine the range of frequencies over which the output

Fig. 13. Sylvania SY-4302 traveling-wave microwave phototube (courtesy Sylvania Microwave Device Division).

was spread. The calculated axial-mode beat-frequencies within the band of the SY-4302 were at 2231 and 4462 Mc/sec. The SY-4302 and the amplifier gain were optimized at 2.2 Gc/sec, and the beat-frequency output was then examined using a narrow-band (10 Mc/sec) transmission filter as described earlier. The result was that beat-frequency output occurred over an extremely large band of frequencies; the output through the filter appeared to change rather little (and then not repeatably) as the filter was tuned from 1.9–2.2 Gc/sec. Since it was suspected that some of the output was due to very strong spikes coming through on the skirts of the filter, subsequent experiments were performed using the microwave interferometer.

The delay-line length was initially adjusted so that the interferometer's nondegenerate bandwidth was approximately 140 Mc/sec, and it was found that the frequency shifts were so large that they more than likely exceeded the nondegenerate bandwidth of the interferometer. Subsequent experiments with 250-Mc/sec resolution verified this suspicion, since frequency shifts throughout the whole interferometer range were observed! It appeared that the frequency spread decreased as pump power was decreased, but the results were far from repeatable.

The presence of such a large frequency spread indicated that stimulated emission was extremely important in determining ruby-laser oscillation frequencies at low temperatures. Furthermore, the experiments proved that the laser could be made to

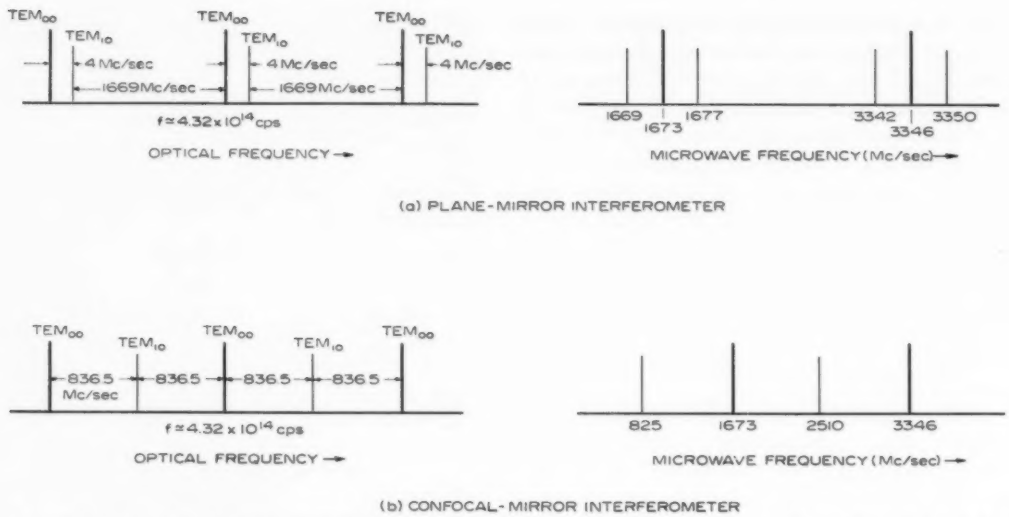

Fig. 14. A portion of the calculated optical and beat-frequency spectra for a 3.18-mm diam, 5.08-cm long ruby rod with (a) plane ends, (b) confocal ends.

oscillate at a number of frequencies simultaneously even at liquid nitrogen temperature.

Nevertheless, it remained to be determined more precisely the extent to which stimulated emission pulled the oscillation frequencies away from the center frequencies of the interferometer resonances. The prospects for accomplishing this with measurements at S-band did not appear to be particularly good. In these particular sapphire-clad rods the zero-field splitting (0.38 cm^{-1}) is clearly resolved at liquid nitrogen temperature. Observed beats at S-band would necessarily correspond to mixing between oscillations within each of the two peaks of the fluorescence spectrum. Since the spacing of the interferometer resonances with respect to the frequencies at the peaks of the fluorescence spectrum is different for resonances within each of the two regions, any pulling effects (other than perfectly linear ones) will lead to different beat frequencies from the two portions of the line. Since the frequency-measuring techniques can lead to ambiguous results for some cases of multiple frequency inputs, it would be desirable to examine the pulling effects in an experiment in which a single beat-frequency at a time might be obtained.

Consequently, it was decided to perform some X-band photomixing experiments using rods at liquid nitrogen temperature. In that case the simultaneous oscillation at two frequencies near the peaks of the fluorescence spectrum could be examined. This would permit the initial measurements of frequency pulling to be performed on a minimum number of oscillating frequencies. The results of such measurements at X-band will be described in Sec. V.

IV. S-Band Experiments on a Rod with Confocal Mirrors

It was pointed out in Sec. II that the spectrum of possible beat-frequencies for a rod having confocal mirrors is different in several important respects from that for a rod having plane mirrors. In each case the highest, Q, or dominant, modes are separated from one another by $f_d = c/2L$, where c is the velocity of light in the rod of length L. However, the distribution of high-order modes is quite different for the two cases. This is illustrated in Fig. 14, which shows the optical and resulting beat-frequency spectra for the particular case of a 3.18-mm diam by 5.08-cm long ruby rod in which several TEM_{00} (dominant) and TEM_{10} modes have been excited. For plane mirrors, beats between a dominant and a high-order mode occur quite close to the frequencies corresponding to beats between adjacent dominant-modes. It was pointed out in Sec. III that this is somewhat of a disadvantage, since beat-frequency shifts due to the pulling effects of stimulated emission can easily be of this order of magnitude or even larger. Hence it was not possible to conclude from the experiments on plane-mirror rods whether or not the predicted high-order modes of Fox and Li could, in fact, be excited in a resonator filled with ruby.

It is in this area that experiments on rods having confocal mirrors could provide some very useful information, since beats between TEM_{00} and TEM_{10} modes occur at frequencies *well separated* from the dominant-mode beat frequency $c/2L$. In fact, those frequencies are odd multiples of one-half the dominant-mode beat-frequency. Hence, the excitation of Fox

and Li-type high-order interferometer resonances could be clearly observable in a confocal rod. In addition, the high degeneracy of the modes of such an interferometer should lead, except for the effects of stimulated emission or nonconfocal alignment, to beat frequencies which do not shift from pulse to pulse during laser action. Therefore, frequency shifts due to stimulated emission could be examined in a truly confocal rod; and frequency shifts due to nonconfocal alignment could be examined in cases for which the effects of stimulated emission were known to be small.

Consequently, a number of experiments were performed on a ruby rod with confocal ends. The 60° orientation rod was 3.18-mm diam by 5.08-cm long. The cylindrical surface was optically polished and multiple-dielectric-layer mirrors were deposited on the confocal ends. One mirror was essentially opaque and the other provided about 3% transmission. The rod was pumped in an elliptic cylinder by an EG and G FX-1 xenon flashtube.

The photomultiplier-detected output for rod temperatures in the range of 200–300°K consisted of pulses that were considerably more distinct and regular than those obtained earlier from plane-mirror rods. The rod exhibited this behavior until a 1.59-mm-diam hole was burned in the output mirror (by operating the rod at liquid nitrogen temperature). Then the photomultiplier output was like that for earlier plane-mirror rods.

The following sections contain a summary of the numerous experiments that were performed on the confocal rod, with particular emphasis on the conclusions that can be drawn concerning the agreement between actual oscillations and theoretically predicted passive interferometer-resonances.

Dependence of Multimoding upon Pump Power

The dependence of multimoding upon pump power was essentially the same as that observed on rods having plane mirrors. As in the case of plane-mirror rods it was found that microwave output at one beat-frequency did not always accompany that at another. Similarly, when output did occur simultaneously at two beat-frequencies, the pulse durations were generally the same; a rare exception to this is shown in Fig. 15.

Further experiments on multimoding as a function of pump power simply verified the results obtained earlier with plane-mirror rods. In particular, single-mode oscillations could be obtained only for pump voltages so close to threshold that the photomultiplier-detected laser-output consisted of only a few pulses.

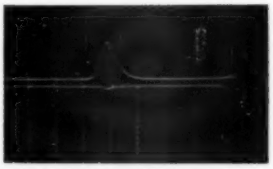

Fig. 15. Detected beat-frequency output near 1.65 Gc/sec (upper trace) and 3.3 Gc/sec (lower trace), illustrating a rare case of different pulse durations for two beat frequencies. Time scale: 0.5 μsec/cm.

Dependence of Multimoding upon Temperature

In many respects the behavior of the confocal rod was like that of the plane-mirror rods described in Sec. III. That is, the threshold pump-energy decreased with decreasing temperature; consequently, the microwave output (for a given pump-power) went through a maximum as the temperature was lowered from room temperature toward that of liquid nitrogen, and microwave output was generally difficult to observe at liquid-nitrogen temperature. However, the detailed behavior at liquid-nitrogen temperature was somewhat different from that observed with plane-mirror rods.

At liquid-nitrogen temperature the photomultiplier-detected output of the confocal rod exhibited some large spikes followed by a few hundred microseconds of "semicontinuous" output (i.e., above the base line) like that observed earlier for plane-mirror rods. Some of the spikes produced microwave beat-frequency output at power levels comparable to those observed for rod temperatures between 200 and 300°K. During other spikes and during all of the "semicontinuous" output, microwave output was not observed.

The general conclusion concerning multimoding at liquid-nitrogen temperature is essentially the same as that for the plane-mirror rods. That is, S-band microwave output is at least several orders of magnitude smaller (if it is present at all) than the output near room temperature, provided the photomultiplier-detected laser-output stays above the base line.

Comparison with Predicted Cavity-Modes

The spectrum of interferometer resonances for a 5.08 cm confocal resonator is given in Fig. 14, along with the corresponding beat-frequency spectrum. Based upon experience with ruby rods having plane mirrors, one would expect that observed beat-frequencies for the confocal rod would surely be close to the dominant-mode beat-frequencies, $mc/2L$, where m is an integer. It was, however, by no means certain that beat-frequency output would be observed at frequencies corresponding to beats between modes calculated for an idealized resonator. Consequently, it was of considerable interest to search for beats at frequencies of $nc/4L$, where n is an odd integer.

1. *Output Near "Dominant-Mode Beat Frequencies"*

Initially, the frequency of the output near 1.65 Gc/sec was measured by using the microwave-mixing technique; the beat frequency during each pulse was apparently so close to that of the local oscillator that the output appeared as detected microwave signals amplified by

Table II. Beat-Frequency Characteristics of Confocal-Mirror Rod

Pump energy (percent above threshold)	6	30	25
Calculated interferometer resonance (Mc/sec)	1673	1673	3346
Measured center frequency (Mc/sec)	1648	1648	3280
Measured frequency spread (Mc/sec)	10	10	2

the conversion gain of the microwave-mixing process. Such apparent frequency-stability had not been observed in any of the previous experiments on plane-mirror rods. Although there were reasons to expect better frequency-stability for confocal rods, it was decided to repeat the experiment and examine the effects of other temperatures and pump-power levels. In four subsequent experiments frequency-shifts from pulse to pulse were observed, even under conditions essentially identical to those of the initial experiment.

Subsequent measurements of frequency and frequency spread were made with the microwave interferometer, and the results are tabulated in Table II. As in the case of the plane-mirror rods, there appeared to be no particular correlation between the order in which the various frequencies appeared, although the total spread of frequencies was fairly reproducible.

2. Output Near "High-Order Mode Beat-Frequencies"

Figure 14 indicates that the frequencies corresponding to beats between TEM_{00} (dominant) modes and TEM_{10} modes in an idealized 5.08 cm confocal resonator would be 837 Mc/sec, 2510 Mc/sec, 4183 Mc/sec, etc. The most convenient region for examination with an SY-4302 microwave phototube was 2510 Mc/sec, since 837 Mc/sec was well below and 4183 Mc/sec was near the upper edge of the usual frequency-band. A low-pass filter was used to remove the 3.3 Gc/sec output, and a high-pass filter was used to remove the 1.65 Gc/sec output. The rest of the receiver consisted of a TWT amplifier and a semiconductor diode detector.

The fact that output was observed provided the first real evidence that the interferometer analyses mentioned earlier could be successfully applied to the case of ruby. That is, in spite of inhomogeneities, sidewall effects, and stimulated emission, the observed beat frequencies for high-order modes agreed with the calculated values.

It is important to note that plane-mirror rods did not exhibit output near $c/4L$. Output at such frequencies was observed only with confocal mirrors, for which its presence is predicted by the interferometer theory.

The behavior of the output as a function of temperature and pump power was similar to that observed earlier at the "dominant-mode beat-frequencies," except for the fact that the amplitude of the beat signals near 2.5 Gc/sec was generally 40 dB lower than that at the dominant-mode beat-frequencies. This can be explained in several ways. First, the quality factor of TEM_{10} modes may be sufficiently less than that of TEM_{00} modes, so that the TEM_{10} modes may be much closer to threshold at a given pump-power. However, it does not seem likely that the difference in Q would be sufficient to produce the observed effects (particularly when one realizes that the Q of the low-order modes is essentially determined by reflection losses rather than by diffraction losses). A second and very likely more important consideration involves the spatial distribution of the modes that are photomixed to produce a beat signal. Some interesting conclusions can be drawn from an examination of the normal mode field configurations.[12] If a pure TEM_{00} mode and a pure TEM_{10} mode are photomixed on a cathode which intercepts essentially all the laser output in these two modes, no net current at the difference frequency will be obtained from the cathode since TEM_{00} modes are symmetric and TEM_{10} modes are antisymmetric. That is, the photocurrent at the difference frquency is proportional to the integral (over the cross-sectional area) of the product of the electric field of the TEM_{00} mode and that of the TEM_{10} mode; this is essentially the basic orthogonality-integral for the two modes. One might argue that the probability of exciting two such pure modes in a ruby is rather small. This is probably true, and in addition, a certain degree of coupling between modes is probably introduced by the aperture through which the laser output is obtained. Nevertheless, the beat-frequency photocurrent for a TEM_{00} and TEM_{10} combination is something like the orthogonality integral for the modes. Hence it is not surprising that the amplitude of beat signals should be larger for modes of the same type than for modes having different spatial-distributions. This suggests some experiments in which beats between dissimilar modes are examined as a function of spatial position and size of the photocathode.

Subsequent frequency measurements using the delay-line interferometer yielded the result that the microwave output was spread over about 40 Mc/sec centered at 2468 Mc/sec (for pump energy up to 22% above threshold).

The problem of trying to correlate frequency spread with nonconfocal alignment is much like the problem of trying to correlate the output of plane-mirror rods with high-order interferometer resonances. That is, the observed spread was small enough to be interpreted on the basis of either interferometer resonances or stimulated emission effects. Most probably the observed frequency spread was the result of both effects.

Line-Width

As in the case of plane-mirror rods, measurements using the microwave-mixing technique indicated that

the line-width was essentially given by the reciprocal of the pulse duration.

Frequency-Pulling Effects

The behavior of the confocal rods at liquid nitrogen temperature was described earlier. A portion of the output mirror was burned away before frequency measurements could be made. This fact, combined with the difficulty of interpreting the S-band results on plane-mirror rods at low temperature, led to the decision that frequency-pulling data could be best obtained in X-band experiments. These experiments are described in the following section.

V. X-Band Experiments on Plane-Mirror Rods at Low Temperature

Introduction

One of the objectives of this research was to perform experiments in which high-order mode excitation could be clearly distinguished from frequency pulling by the fluorescence line. S-band measurements on plane-mirror rods near room temperature were not particularly instructive in this respect since the predicted frequency pulling was of the same order of magnitude as the predicted shift due to high-order mode excitation. However, it was possible to take advantage of the particular mode structure of a confocal resonator, and experiments were performed (Sec. IV) in which the effects of high-order mode-excitation were unmistakably observed.

The next problem was that of performing an experiment in which the effects of frequency pulling could be as clearly observed. Initial S-band experiments on rods at 77°K gave encouraging results, but subsequent experiments with stronger signals showed the beat-frequency output to be spread randomly over a broad band of frequencies. This result is not surprising when one considers that the frequency pulling will be different for lines within each of the two peaks of the low temperature fluorescence-spectrum, and, in order to observe beats at 77°K, it was necessary to pump so far above threshold that oscillations most probably occurred within both fluorescence peaks.

A number of these difficulties might be overcome by performing X-band (8–12 Gc/sec) experiments on relatively short rods. For example, the use of a rod 2.54 cm long would result in the mode spectrum that is shown in Fig. 16 along with the fluorescence spectrum at 77°K. The line-width of the individual fluorescence peaks has been taken as about 6 Gc/sec, corresponding to a relatively unstrained ruby. The widths of the interferometer resonances have been drawn for the case of a rod that is relatively heavily silvered on both ends. In the actual experiment it would be desirable not to silver the output end of the rod. In that case the interferometer-resonance width could be as large or perhaps even larger than that of the fluorescence peaks,

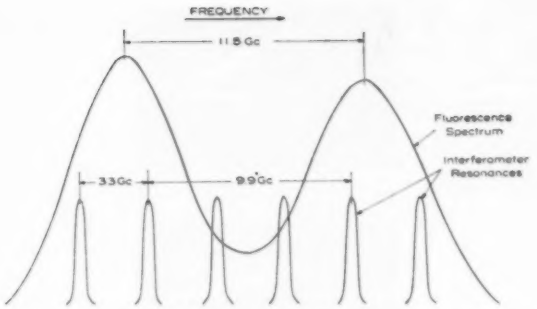

Fig. 16. Fluorescence spectrum at 77°K and axial interferometer resonances for a 2.54-cm long ruby rod.

and hence the frequency pulling could be quite large. In Fig. 16 the location of the resonator modes relative to the fluorescence spectrum has been chosen arbitrarily. In practice, the absolute location of the fluorescence spectrum for a particular rod is determined by the rod temperature, and the absolute location of the resonator modes is determined by the exact length and index of refraction of the rod.

If an oscillation could, in fact, be excited within each of the two fluorescence peaks, and if these two oscillations would photomix in the cathode of a photo-TWT, then some rather conclusive information about frequency pulling might be obtained. As long as the zero-field splitting remains resolved, the frequency pulling of modes lying between the two peaks should result in difference frequencies *larger* than the spacing between interferometer resonances. That is, the oscillation corresponding to a particular resonance would be pulled toward the nearest fluorescence peak, and hence the difference frequency should be increased from 9.9 Gc/sec to some higher value. The limit on this pulling is set by the spacing of the peaks, or 11.5 Gc/sec. Note that this *upward* pulling of the beat frequency should occur only when one of the participating modes is rather close to one fluorescence peak and the other mode is close to the second peak.

If, on the other hand, one mode is half-way between the fluorescence peaks, then it would likely experience negligible pulling; whereas the other mode, lying on the outer skirt of one of the fluorescence curves, would be pulled back toward the fluorescence peaks. In that case the frequency pulling would be *downward;* i.e. the observed beat-frequency would be lower than the 9.9 Gc/sec spacing between interferometer resonances.

Description of Experiments

1. Experimental Arrangement

The need for an X-band photo-TWT was filled by Sylvania's development of the SY-4304, a tube similar in appearance to the S-band SY-4302 shown in Fig. 13. The tube is designed for operation in the 8–12 Gc/sec

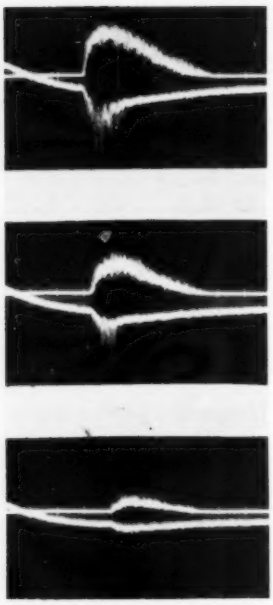

Fig. 17. Photomultiplier output (upper trace) and detected X-band microwave output (lower trace) for values of pump energy 5% (lower photograph), 21 and 39% above threshold. Time scale: 100 μsec/cm.

frequency range. The rod used was the 2.54 cm long sapphire-clad ruby borrowed from A. L. Schawlow. One end of the rod was heavily silvered, and the output end was not silvered. The microwave receiver consisted of a TWT amplifier and a semiconductor diode detector.

2. Results

X-band beat-frequencies were, in fact, observed, and some typical results are shown in Fig. 17. The microwave output appeared as spikes superimposed upon a raised base line. Microwave output was observed for pump voltages very close to threshold, indicating that the threshold level is not very different for oscillations in each fluorescence line.

In some cases very close to threshold there was a time delay between the start of laser oscillation, as detected by the photomultiplier, and the start of the microwave output. The delay was not easily repeatable, and varied from 1–20 μsec. It is likely that the time delay results from the fact that the gain in one peak of the fluorescence spectrum is larger than that in the other. Hence, an oscillation occurs first near the peak with highest gain, followed only slightly later by an oscillation near the other peak.

Frequency measurements were initially performed using the waveguide analog of the microwave interferometer of Fig. 8. The first coaxial hybrid junction was replaced by a 3-dB-waveguide directional coupler, and the second coaxial hybrid was replaced by a hybrid waveguide T ("Magic-T"). The delay-line length was initially adjusted for 100-Mc/sec nondegenerate bandwidth, and it was found that the frequency shifts from spike to spike exceeded this range. In fact, the frequency shifts were larger than the maximum usable nondegenerate-bandwidth of 260 Mc/sec. (The maximum usable bandwidth was limited primarily by the different frequency-response of the detectors.)

Subsequent frequency-measurements were performed using (1) narrowband, tunable transmission filters, (2) the microwave-mixing technique shown in Fig. 11, and (3) a narrowband (10 Mc/sec) superheterodyne receiver.

The most extensive frequency-measurements were performed using the superheterodyne receiver. The local oscillator was tuned in 5 Mc/sec steps from 8.5 Gc/sec to 13 Gc/sec. In the initial experiments, microwave output was observed only in the frequency range from 9.9–10.4 Gc/sec, and it appeared that the frequency decreased during the laser output. This would be consistent with rod heating during the pump flash. However, several subsequent experiments indicated that there was no particular order in which the output frequencies appeared. The latter result compares favorably with recent high-resolution Fabry-Perot investigations by A. L. Schawlow.

In subsequent experiments in which the laser was operated 60% above threshold energy, microwave output was observed in the frequency range from 9.5–10.5 Gc/sec. Again there appeared to be no particular order in which the beat frequencies appeared.

Let us now compare the experimental results with the simple theory presented in Sec. II. If we assume a scattering loss of 20% per pass and power "loss" of 90% through the output end, we find from Fig. 5 that the resonator quality factor, Q_c, is approximately 1.5×10^5 corresponding to a half-power resonance width of about 3 Gc/sec. Since the width of the individual fluorescence lines is approximately 6 Gc/sec, the ratio of fluorescence quality factor to interferometer quality factor, Q_m/Q_c, is 0.5. If we neglect the pulling effect of one fluorescence peak on the oscillation within the other fluorescence peak, we obtain $\Delta f \simeq {}^1/_3\,\Delta f_m + {}^2/_3\,\Delta f_c$, where Δf is the difference between oscillation frequencies, Δf_m is the ground-state splitting, and Δf_c is the spacing between axial interferometer resonances.

In this experiment $\Delta f_m = 11.5$ Gc/sec and $\Delta f_c = 9.9$ Gc/sec, so that $\Delta f = 10.4$ Gc/sec, which is quite close to the highest beat-frequency observed.

In order to get some idea of the minimum beat-frequency that might be expected, we can assume that one mode is about half-way between the fluorescence peaks, and therefore experiences negligible pulling. The other mode would then have to lie some 4 Gc/sec away from a fluorescence peak and would be pulled an amount given

by $f_{osc} - f_c \cong {}^1/_3(f_m - f_c) \cong 1.3$ Gc/sec, resulting a beat frequency of 8.6 Gc/sec, which is about 1 Gc/sec less than the lowest frequency observed. There are at least two reasons for the fact such low-beat frequencies were not observed: (1) it is unlikely that oscillations could occur at frequencies for which the fluorescence is so weak compared to its maximum value; and (2) the heating of the rod during the pump flash broadens the fluorescence lines and hence decreases the effects of frequency pulling in general.

Conclusions

The observations of microwave output at frequencies considerably greater than the spacing between interferometer resonances clearly indicates the presence of frequency pulling by the two peaks of the zero-field split fluorescence spectrum. Although the mechanism by which the frequency shifts by hundreds of megacycles during the laser output is not explained, the upper frequency at which output was observed is in good agreement with the linear frequency-pulling theory presented in Sec. II.

In addition, the presence of microwave output even for pump voltages close to threshold indicates that transitions within one fluorescence peak are not strongly favored over those within the other peak (at least for rods having no silver on one end, i.e., low Q_c).

VI. Conclusions

A considerable amount of hitherto unavailable information about the spectral output of the ruby laser has been obtained. It was found that a ruby laser can oscillate at a number of different frequencies simultaneously and that near room temperature these frequencies are closely related to the calculated interferometer-resonances. For a given rod, the number of frequencies and their locations depend upon both pump power and temperature. For a rod near room temperature, single-mode oscillation can be obtained only for values of pump voltage very close to threshold (within about 1%). At liquid-nitrogen temperature, single-mode oscillation can be obtained for values of pump voltage up to about 10% above threshold. At such low temperatures the oscillation frequencies are pulled away from the interferometer resonances and toward the nearest peak of the zero-field split fluorescence spectrum. Beat-frequency line-width measurements at various temperatures and pump-power levels indicate that the oscillation line-widths are about 2 Mc/sec; that is, the line-width is determined primarily by the 0.5-μsec duration of the pulses.

There are a number of areas in which microwave phototubes can be of further use in examining the characteristics of lasers. The experiments described here provide the basis for both new theoretical analyses and more detailed experiments. In addition to the more straightforward spectroscopic uses of microwave phototubes, they could have specialized applications such as the alignment of interferometer mirrors to produce the optimum spectral output. By combining photomixing techniques with conventional photographic and high-resolution spectroscopic techniques, it should be possible to obtain extremely high resolution, time resolved spectroscopic information. In general, photoelectric mixing is likely to play an important role in the developing technology of communications and spectroscopy involving coherent light.

I would like to thank A. E. Siegman for his guidance throughout every phase of the work; the Sylvania Microwave Device Division, particularly R. G. E. Hutter and J. S. Needle, for support and for the use of their facilities; A. L. Schawlow for stimulating discussions and for the use of ruby rods and other equipment; W. W. Anderson, R. J. Morris, S. E. Harris, and F. T. Arecchi for numerous suggestions; L. E. Wilson for valuable help in performing many of the experiments; L. W. Dague and D. A. McLaren for skilled assistance in constructing the lasers; R. L. Kost, Mrs. Alice Cotich, and Mrs. Alice Lescalleet for help in preparing the manuscript. In addition, I would like to thank the Raytheon Company for their support through the Raytheon Fellowship.

References

1. B. J. McMurtry and A. E. Siegman, Appl. Opt. **1**, 51 (1962).
2. A. L. Schawlow and C. H. Townes, Phys. Rev. **112**, 1940 (1958).
3. T. H. Maiman, Nature **187**, 498 (1960).
4. T. H. Maiman, Phys. Rev. **123**, 1151 (1961).
5. A. E. Siegman and B. J. McMurtry, Electron Device Res. Conf., Troy, New York, June 1961.
6. A. E. Siegman, *NEREM Record*, Boston, Massachusetts, Nov. 1961 (invited paper).
7. A. E. Siegman, B. J. McMurtry, and S. E. Harris, NAECON Proceedings, Dayton, Ohio, May 1962.
8. B. J. McMurtry, Tech. Rept. No. 177-3, Stanford Electronics Labs., Stanford, California, July 1962.
9. W. G. Wagner and G. Birnbaum, J. Appl. Phys. **32**, 1185 (1961).
10. W. R. Bennett, Jr., Phys. Rev. **126**, 580 (1962).
11. Y. H. Pao, J. Opt. Soc. Am. **52**, 871 (1962).
12. A. G. Fox and T. Li, Bell System Tech. J. **40**, 453 (1961).
13. G. D. Boyd and J. P. Gordon, Bell System Tech. J. **40**, 489 (1961).
14. R. J. Collins and D. F. Nelson, Proc. Intern. Comm. for Optics Meeting, London, 1961.
15. W. Kaiser and M. J. Keck, J. Appl. Phys. **33**, 762 (1962).
16. R. J. Collins and D. F. Nelson, paper TB15, Spring Meeting, Opt. Soc. Am., Pittsburgh, Pennsylvania, March 1961.
17. S. Ramo and J. R. Whinnery, *Fields and Waves in Modern Radio* (Wiley, New York, 1953), 2nd ed.
18. J. P. Gordon, H. J. Zeiger, and C. H. Townes, Phys. Rev. **99**, 1264 (1955).
19. C. H. Townes, in *Quantum Electronics*, J. R. Singer, ed. (Columbia Univ. Press, New York, 1961), p. 3.

20. A. L. Schawlow, in *Quantum Electronics*, J. R. Singer, ed. (Columbia Univ. Press, New York, 1961), p. 50.
21. A. Javan, W. R. Bennett, Jr., and D. R. Herriott, Phys. Rev. Letters **6**, 106 (1961).
22. D. R. Herriott, J. Opt. Soc. Am. **52**, 31 (1962).
23. I. D. Abella and H. Z. Cummins, J. Appl. Phys. **32**, 1177 (1961).
24. A. T. Forrester, J. Opt. Soc. Am. **51**, 253 (1961).
25. A. Javan, E. A. Ballik, and W. L. Bond, J. Opt. Soc. Am. **52**, 96 (1962).
26. A. E. Siegman and R. J. Morris (private communication).

Meetings Calendar

August

1–2 Boston Lasers Conf., Northeastern U. *R. Seed, Elect. Eng., Northeastern U., Boston, Mass.*

4–9 Internatl. Conf. and Exhibit on Aerospace Support, Wash., D.C. *Box 6635, Wash., D.C.*

5–9 Optical Masers—Theory, Technology, and Applications, summer course, U. of Mich. *Engr. Summer Confs., W. Engr. Bldg., U. of Mich., Ann Arbor, Mich.*

5–9 Soc. of Photographic Instrumentation Engrs., Ambassador Hotel, Los Angeles *J. A. Clemente, Pacific Missile Range, Pt. Mugu, Calif.*

5–16 Radiation Thermometry Course, UCLA *Engr. Ext., Engr. Bldg., U. of Calif., Los Angeles 24, Calif.*

12–16 Fundamentals of Infrared Technology, summer course, U. of Mich. *Engr. Summer Confs., W. Engr. Bldg., U. of Mich., Ann Arbor, Mich.*

12–16 Gordon Conf. on Instrumentation, Colby Jr. Col., New London, N.H.

12–16 Gordon Conf. on Chemistry and Physics of Solids, Kimball Union Acad., Meriden, N.H.

13–17 5th Ann. Gas Chromatography Session, Fisk U. *N. Fuson, Fisk Infrared Inst., Fisk U., Nashville 8, Tenn.*

13–23 14th Ann. Infrared Spectroscopy Inst., Fisk U. *N. Fuson, Fisk Infrared Inst., Fisk U., Nashville 8, Tenn.*

15–30 Internatl. Assoc. of Meteorology and Atmospheric Physics, Berkeley, Calif. *W. L. Godson, Meteorological Office, 315 Bloor St. W., Toronto 5, Ont., Canada*

19–23 Special Topics in Optics, summer course, U. of Mich. *Engr. Summer Confs., W. Engr. Bldg., U. of Mich., Ann Arbor, Mich.*

19–23 Infrared Spectroscopy Inst., Canisius Col. *H. A. Szymanski, Canisius Col., Buffalo 8, N.Y.*

19–29 Summer Seminar on Pictorial Data Processing and Pattern Recognition, Yeshiva U., NYC *A. Rosenfeld, Belfer Grad. School of Science, Yeshiva U., New York 33, N.Y.*

19–30 Thermal and Luminous Radiative Transfer Course, UCLA *Engr. Ext., Engr. Bldg., U. of Calif., Los Angeles 24, Calif.*

19–30 Advanced Crystallography, McCrone Res. Inst. *J. A. Reffner, McCrone Res. Inst., 451 E. 31 St., Chicago 16, Ill.*

20–23 Australian Spectroscopy Conf., Canberra *E. Spinner, Australian Natl. U., Canberra, Australia*

26–30 Masers-Lasers Course, UCLA *Engr. Ext., Engr. Bldg., U. of Calif., Los Angeles 24, Calif.*

26–30 Gordon Conf. on Glass, Tilton School, Tilton, N.H.

26–30 Internatl. Symp. on the Solar Spectrum, Utrecht *C. de Jager, Theoretical Dept., Sterrewacht, Servaasbolwerk 13, Utrecht, Netherlands*

27–31 Hungarian Soc. of Optics, Acoustics and Film Techniques, Conf. on Scientific and Appl. Photography, Budapest *Optikai, Akusztikai és Filmtechnikai Egyesület, Szabadság tér 17, Budapest V, Hungary*

28–31 APS, Edmonton, Alta., Canada *W. A. Nierenberg, U. of Calif., Berkeley 4, Calif.*

29–30 Solvation Symp., U. of Alberta *P. J. Krueger, Chemistry, U. of Alberta, Calgary, Alba., Canada*

September

— Internatl. Commission on Glass, 14th Ann. Mtg., Lausanne *R. Günther, Bockheimer Landstr. 126, Frankfurt am Main, Germany*

— British Assoc. for the Advancement of Science, 125th Ann. Mtg., Aberdeen, Scotland *G. Allen, Burlington House, London, W. 1, England*

2–7 Internatl. Symp. on Space Technology and Science, Tokyo *I. Tani, Japanese Rocket Soc., Yomiura Newspaper Bldg., 1–3 Ginza-Nishi, Tokyo, Japan*

4–6 Internatl. Conf. on Information Theory, Sendai, Japan *G. L. Turin, U. of Calif., Berkeley, Calif.*

5–6 Symp. on the Ellipsometer and its Use in the Measurement of Surfaces and Thin Films, Sheraton-Park Hotel, Wash., D.C. *E. Passaglia, NBS, Wash. 25, D.C.*

8–13 Illuminating Engin. Soc., Natl. Technical Conf., Detroit, Mich. *W. P. Lowell, Jr., Sylvania Electric Prod., Inc., 60 Boston St., Salem, Mass.*

8–13 ACS Natl. Mtg., New York City *ACS, 1155 16th St. N.W., Wash. 6, D.C.*

8–15 Thin Film Optics Colloq., Marseilles *P. Rouard, Faculte des Sciences de Marseilles, Pl. Victor Hugo, Marseilles 3, France*

9–14 Union of German Physical Societies, Fall Mtg., Hamburg *Verband Deutscher Physikalischer Gesells., Bundesalle 100, Braunschweig, Germany (Fed. Rep.)*

9–18 IUCr, Gen. Assembly and Internatl. Cong., Rome, Italy *D. W. Smits, c/o Math. Inst., U. of Groningen, Reitdiepskada 4, Groningen, Netherlands*

9–20 Microscopic Fusion Methods, McCrone Res. Inst. *J. A. Reffner, McCrone Res. Inst., 451 E. 31 St., Chicago 16, Ill.*

16–18 10th Ottawa Symp. on Applied Spectroscopy, Ottawa *J. Kelly, The Steel Co. of Canada Ltd., Wilcox St., Hamilton, Ont., Canada*

15–19 Internatl. Scientific Radio Union, 14th Gen. Assembly, Tokyo, Japan

23–27 ISA Instrument-Automation Conf. and Exhibit, Philadelphia *W. H. Kushnick, 313 6th Ave., Pittsburgh 22, Pa.*

23–Oct. 5 Photomicrography, McCrone Res. Inst. *J. A. Reffner, McCrone Res. Inst., 451 E. 31 St., Chicago 16, Ill.*

24–28 Photoluminescence of Solids and Liquids Mtg., Toruń *M. Frackowiak, Physics, Nicholas Copernicus U. of Toruń, Grudziadzka 5, Toruń, Poland*

30–Oct. 4 11th Internatl. Conf. on Spectroscopy, Belgrade *Sekretarijat, Prirodno-matematički fakultet, Fizičko-hemijski zavod, Beograd, Studentski trg 16, Blok C, Yugoslavia*

October

— Internatl. Conf. on the Science of Photography, Turin, Italy

— 4th Internatl. Color Conf., Budapest *M. K. Egyesülete, Szabadság-tér 17, Budapest 5, Hungary*

— IAU, 23rd Exec. Comm. Mtg., Erevan, Armenia, U.S.S.R. *D. H. Sadler, c/o Royal Greenwich Observatory, Herstmonceux Castle, Hailsham, Sussex, England*

— IUPAP, 11th Gen. Assembly, Warsaw, Poland

1–6 Internatl. Soc. of Photogrammetry, Commissions 1–4 Mtg., Milan *A. L. Nowicki, c/o Army Map Service, 6009 Mass. Ave. N.W., Wash., D.C.*

9–12 Am. Ceramic Soc. Glass Div., Bedford Springs, Pa. *J. Rood, Bausch & Lomb, Rochester 2, N.Y.*

11–12 Elementary Particles and the Nucleus, Symp. & Fall Mtg. APS N.Y. State Sect., Olean, N.Y. *J. M. Geiger, Physics, St. Bonaventure U., St. Bonaventure P.O., Allegany, N.Y.*

13–18 SMPTE, 94th Semiann. Conv., Boston, Mass. *SMPTE, 55 W. 42 St., New York 36, N.Y.*

Overhauser and Jeffries-Abragam Effect in a Four-Level System

Mohan Lal Narchal and W. A. Barker

The method of partial distributions is used to compute the normalized population distribution in an electron-nuclear coupled spin system in which $I = S = 1/2$. The expressions obtained are more general than those reported previously in that they include the effects of competitive relaxation and competitive radiative induced transition probabilities. It is clear that positive and negative enhancement may be obtained either by the Overhauser or the Jeffries-Abragam effect irrespective of the relative magnitudes of the nuclear Zeeman and hyperfine interaction energies. A small enhancement is not necessarily due to incomplete saturation, but may well be the result of compensating emission and absorption.

I. Introduction

The production of positive and negative nuclear magnetic resonance enhancement is of interest in several practical applications: a low noise amplifier,[1] an oscillator,[2] a magnetometer,[3] or as a sensitive means of detection of nuclei with low natural abundance or small gyromagnetic ratio.[4] NMR enhancement may be achieved by saturating allowed[5] or first-order forbidden[6] EPR transitions in a coupled electron-nuclear spin system placed in a static magnetic field.

Enhancement calculations have been made assuming the dominance of certain types of relaxation.[7] The purpose of this paper is to generalize the earlier treatment to include the effect of all types of competitive thermal relaxations. The calculations are restricted to a four-level system ($S = {}^1/_2, I = {}^1/_2$). The solution of the relevant rate equations is obtained by using the method of partial distributions.[8]

In most of the dynamic nuclear polarization experiments reported in the literature, it is the enhancement, ε, of the nuclear magnetic resonance signal, rather than the nuclear polarization, P_N, which has been detected.[7] Except at very low temperatures, P_N is generally very small (10^{-4} or less) and hard to detect directly whereas ε is appreciable (1 or greater) and readily observable at all temperatures. Disappointingly small values of ε, however, are often reported. These are not necessarily due to incomplete saturation but may well be the result of competitive pumping or unfavorable relaxations.

The authors are with the Physics Department, Saint Louis University, St. Louis, Missouri.

Received 10 January 1962.

This work was supported by a U.S. AFOSR contract.

In Sec. II we use the method of partial distributions. We treat two important cases in which expressions for the normalized population distribution and the enhancement of the NMR are developed. In Sec. III a number of limiting cases of physical interest are studied in detail for which the expressions for ε and P_N are tabulated. Inasmuch as we are primarily interested in ε at $T = 77°\text{K}$ and $300°\text{K}$ for a pump frequency of about 10 Gc/sec, we do make the linear approximation to the Boltzmann factor.[9]

II. Normalized Populations by the Method of Partial Distributions

We consider two types of situations as depicted in Figs. (1a) and (1b). These two four-level diagrams represent an electron-nuclear coupled spin system in which $S = I = {}^1/_2$. The magnetic quantum numbers of electron and nucleus, respectively, are $M = \pm {}^1/_2$ and $m = \pm {}^1/_2$. The precise labeling of the four states depends on the relative strength of the nuclear Zeeman term and the hyperfine term and also on the algebraic sign of the nuclear magnetic moment and the hyperfine interaction constant. In each situation treated the coupled system makes transitions from one level to another through eight different mechanisms of which six are thermal (w_{ij}) and two are radiative induced (W_{ij}). These two cases are distinct from one another in that two different pumping schemes are shown. In Fig. 1(a) two simultaneous pumping fields of the same frequency are applied between levels (1,3) and (2,4). In Fig. 1(b) two simultaneous pumps of different frequency are applied between levels (1,4) and (2,3).

Tables I and II summarize the results obtained by an

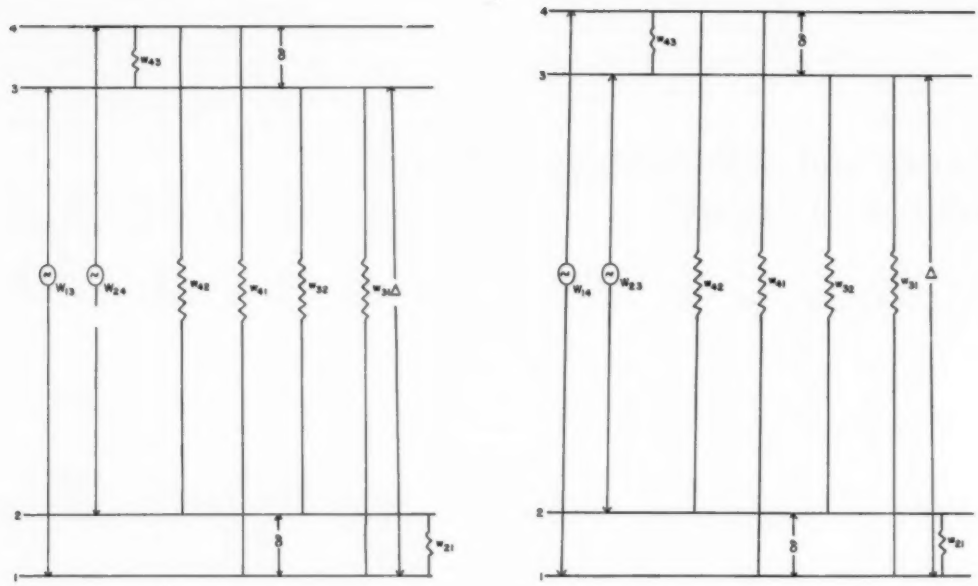

(a) (b)

Fig. 1. Energy level diagrams of an electron-nuclear coupled spin system in which $S = I = 1/2$. Two different pumping schemes (a) and (b) are shown. All possible thermal relaxations are indicated. $M, m = \pm 1/2$ are the magnetic quantum numbers of the electron and nucleus, respectively. The m values are not explicitly labeled inasmuch as they depend on the relative size of the nuclear Zeeman interaction and the hyperfine interaction and on the algebraic sign of γ_n or A. The W_{ij} denote radiative induced transition probabilities, the w_{ij} denote thermal relaxation transition probabilities.

examination of all allowed partial distributions associated with Figs. 1(a) and 1(b). The partial unweighted values for the n_i $(i = 1,2,3,4)$ are given in terms of N and two dimensionless parameters: $\Delta = (E_3 - E_1)/kT = (E_4 - E_2)/kT$, $\delta = (E_4 - E_3)/kT = (E_2 - E_1)/kT$. The weighting factors a_k, a_k' of the kth partial distribution are given by

$$a_k = \frac{C_k}{\sum_{k=1}^{10} C_k}, \quad \text{(Fig. 1a)} \tag{1a}$$

$$a_k' = \frac{C_k'}{\sum_{k=1}^{12} C_k'}, \quad \text{(Fig. 1b)} \tag{1b}$$

where C_k and C_k' are the following trilinear combinations of the w_{ij} and W_{ij}:

$$\begin{aligned}
C_1 &= W_{13}W_{24}(w_{43} + w_{21}) + (W_{24} + W_{13})w_{43}w_{21},\\
C_2 &= W_{13}W_{24}w_{41},\\
C_3 &= W_{13}W_{24}w_{32},\\
C_4 &= W_{13}(w_{43}w_{42} + w_{43}w_{32}) + W_{13}w_{42}w_{32},\\
C_5 &= W_{13}(w_{42}w_{41} + w_{42}w_{21} + w_{41}w_{21}),\\
C_6 &= W_{13}w_{41}w_{32},\\
C_7 &= W_{24}(w_{43}w_{41} + w_{43}w_{31} + w_{41}w_{31}),\\
C_8 &= W_{24}w_{41}w_{32},\\
C_9 &= W_{24}(w_{32}w_{31} + w_{32}w_{21} + w_{31}w_{21}),\\
C_{10} &= w_{43}(w_{42}w_{41} + w_{42}w_{31} + w_{42}w_{21} + w_{41}w_{32} + w_{41}w_{21}\\
&\quad + w_{32}w_{31} + w_{32}w_{21} + w_{31}w_{21}) + w_{42}(w_{41}w_{32}\\
&\quad + w_{41}w_{31} + w_{32}w_{31} + w_{32}w_{21} + w_{31}w_{21})\\
&\quad + w_{41}(w_{32}w_{31} + w_{32}w_{21} + w_{31}w_{21}).
\end{aligned} \tag{2}$$

$$\begin{aligned}
C_1' &= W_{14}W_{23}(w_{43} + w_{21}),\\
C_2' &= W_{14}W_{23}w_{42},\\
C_3' &= W_{14}W_{23}w_{31},\\
C_4' &= W_{14}(w_{43}w_{42} + w_{43}w_{32} + w_{42}w_{32}),\\
C_5' &= W_{14}w_{43}w_{21},\\
C_6' &= W_{14}w_{42}w_{31},\\
C_7' &= W_{14}(w_{32}w_{31} + w_{32}w_{21} + w_{31}w_{21}),\\
C_8' &= W_{23}(w_{43}w_{41} + w_{43}w_{31} + w_{41}w_{31}),\\
C_9' &= W_{23}w_{43}w_{21},\\
C_{10}' &= W_{23}(w_{42}w_{41} + w_{42}w_{21} + w_{41}w_{21}),\\
C_{11}' &= W_{23}w_{42}w_{31},\\
C_{12}' &= C_{10}.
\end{aligned} \tag{3}$$

The normalized populations N_i, N_i' $(i = 1,2,3,4)$ corresponding to Figs. 1(a) and (b) may now be written in terms of the a_k, a_k'.

$$N_1 = \frac{N}{4}\left[1 + \left(\frac{a_2}{2} - \frac{a_3}{2} - \frac{a_4}{4} + \frac{a_5}{4} + \frac{3a_7}{4} + a_8 + \frac{a_9}{4} + \frac{a_{10}}{2}\right)\Delta + \frac{\delta}{2}\right],$$

$$N_2 = \frac{N}{4}\left[1 + \left(-\frac{a_2}{2} + \frac{a_3}{2} + \frac{3a_4}{4} + \frac{a_5}{4} + a_6 - \frac{a_7}{4} + \frac{a_9}{4} + \frac{a_{10}}{2}\right)\Delta - \frac{\delta}{2}\right],$$

$$N_3 = \frac{N}{4}\left[1 + \left(\frac{a_2}{2} - \frac{a_3}{2} - \frac{a_4}{4} + \frac{a_5}{4} - \frac{a_7}{4} - a_8 - \frac{3a_9}{4} - \frac{a_{10}}{2}\right)\Delta + \frac{\delta}{2}\right],$$

Table I. Partial Normalized Population Distributions Associated with Fig. 1(a)

k	n_1	n_2	n_3	n_4	Number of times the distribution occurs
1	$\frac{N}{4}\left(1+\frac{\delta}{2}\right)$	$\frac{N}{4}\left(1-\frac{\delta}{2}\right)$	$\frac{N}{4}\left(1+\frac{\delta}{2}\right)$	$\frac{N}{4}\left(1-\frac{\delta}{2}\right)$	4
2	$\frac{N}{4}\left(1+\frac{\Delta}{2}+\frac{\delta}{2}\right)$	$\frac{N}{4}\left(1-\frac{\Delta}{2}-\frac{\delta}{2}\right)$	$\frac{N}{4}\left(1+\frac{\Delta}{2}+\frac{\delta}{2}\right)$	$\frac{N}{4}\left(1-\frac{\Delta}{2}-\frac{\delta}{2}\right)$	1
3	$\frac{N}{4}\left(1-\frac{\Delta}{2}+\frac{\delta}{2}\right)$	$\frac{N}{4}\left(1+\frac{\Delta}{2}-\frac{\delta}{2}\right)$	$\frac{N}{4}\left(1-\frac{\Delta}{2}+\frac{\delta}{2}\right)$	$\frac{N}{4}\left(1+\frac{\Delta}{2}-\frac{\delta}{2}\right)$	1
4	$\frac{N}{4}\left(1-\frac{\Delta}{4}+\frac{\delta}{2}\right)$	$\frac{N}{4}\left(1+\frac{3\Delta}{4}-\frac{\delta}{2}\right)$	$\frac{N}{4}\left(1-\frac{\Delta}{4}+\frac{\delta}{2}\right)$	$\frac{N}{4}\left(1-\frac{\Delta}{2}-\frac{\delta}{2}\right)$	3
5	$\frac{N}{4}\left(1+\frac{\Delta}{4}+\frac{\delta}{2}\right)$	$\frac{N}{4}\left(1+\frac{\Delta}{4}-\frac{\delta}{2}\right)$	$\frac{N}{4}\left(1+\frac{\Delta}{4}+\frac{\delta}{2}\right)$	$\frac{N}{4}\left(1-\frac{3\Delta}{4}-\frac{\delta}{2}\right)$	3
6	$\frac{N}{4}\left(1+\frac{\delta}{2}\right)$	$\frac{N}{4}\left(1+\Delta-\frac{\delta}{2}\right)$	$\frac{N}{4}\left(1+\frac{\delta}{2}\right)$	$\frac{N}{4}\left(1-\Delta-\frac{\delta}{2}\right)$	1
7	$\frac{N}{4}\left(1+\frac{3\Delta}{4}+\frac{\delta}{2}\right)$	$\frac{N}{4}\left(1-\frac{\Delta}{4}-\frac{\delta}{2}\right)$	$\frac{N}{4}\left(1-\frac{\Delta}{4}+\frac{\delta}{2}\right)$	$\frac{N}{4}\left(1-\frac{\Delta}{4}-\frac{\delta}{2}\right)$	3
8	$\frac{N}{4}\left(1+\Delta+\frac{\delta}{2}\right)$	$\frac{N}{4}\left(1-\frac{\delta}{2}\right)$	$\frac{N}{4}\left(1-\Delta+\frac{\delta}{2}\right)$	$\frac{N}{4}\left(1-\frac{\delta}{2}\right)$	1
9	$\frac{N}{4}\left(1+\frac{\Delta}{4}+\frac{\delta}{2}\right)$	$\frac{N}{4}\left(1+\frac{\Delta}{4}-\frac{\delta}{2}\right)$	$\frac{N}{4}\left(1-\frac{3\Delta}{4}+\frac{\delta}{2}\right)$	$\frac{N}{4}\left(1+\frac{\Delta}{4}-\frac{\delta}{2}\right)$	3
10	$\frac{N}{4}\left(1+\frac{\Delta}{2}+\frac{\delta}{2}\right)$	$\frac{N}{4}\left(1+\frac{\Delta}{2}-\frac{\delta}{2}\right)$	$\frac{N}{4}\left(1-\frac{\Delta}{4}+\frac{\delta}{2}\right)$	$\frac{N}{4}\left(1-\frac{\Delta}{2}-\frac{\delta}{2}\right)$	16

Table II. Partial Normalized Population Distributions Associated with Fig. 1(b)

k	n_1	n_2	n_3	n_4	Number of times the distribution occurs
1	$\frac{N}{4}\left(1+\frac{\delta}{2}\right)$	$\frac{N}{4}\left(1-\frac{\delta}{2}\right)$	$\frac{N}{4}\left(1-\frac{\delta}{2}\right)$	$\frac{N}{4}\left(1+\frac{\delta}{2}\right)$	2
2	$\frac{N}{4}\left(1-\frac{\Delta}{2}\right)$	$\frac{N}{4}\left(1+\frac{\Delta}{2}\right)$	$\frac{N}{4}\left(1+\frac{\Delta}{2}\right)$	$\frac{N}{4}\left(1-\frac{\Delta}{2}\right)$	1
3	$\frac{N}{4}\left(1+\frac{\Delta}{2}\right)$	$\frac{N}{4}\left(1-\frac{\Delta}{2}\right)$	$\frac{N}{4}\left(1-\frac{\Delta}{2}\right)$	$\frac{N}{4}\left(1+\frac{\Delta}{2}\right)$	1
4	$\frac{N}{4}\left(1-\frac{\Delta}{4}-\frac{\delta}{4}\right)$	$\frac{N}{4}\left(1+\frac{3\Delta}{4}-\frac{\delta}{4}\right)$	$\frac{N}{4}\left(1-\frac{\Delta}{4}+\frac{3\delta}{4}\right)$	$\frac{N}{4}\left(1-\frac{\Delta}{4}-\frac{\delta}{4}\right)$	3
5	$\frac{N}{4}$	$\frac{N}{4}(1-\delta)$	$\frac{N}{4}(1+\delta)$	$\frac{N}{4}$	1
6	$\frac{N}{4}$	$\frac{N}{4}(1+\Delta)$	$\frac{N}{4}(1-\Delta)$	$\frac{N}{4}$	1
7	$\frac{N}{4}\left(1+\frac{\Delta}{4}+\frac{\delta}{4}\right)$	$\frac{N}{4}\left(1+\frac{\Delta}{4}-\frac{3\delta}{4}\right)$	$\frac{N}{4}\left(1-\frac{3\Delta}{4}+\frac{\delta}{4}\right)$	$\frac{N}{4}\left(1+\frac{\Delta}{4}+\frac{\delta}{4}\right)$	3
8	$\frac{N}{4}\left(1+\frac{3\Delta}{4}+\frac{\delta}{4}\right)$	$\frac{N}{4}\left(1-\frac{\Delta}{4}+\frac{\delta}{4}\right)$	$\frac{N}{4}\left(1-\frac{\Delta}{4}+\frac{\delta}{4}\right)$	$\frac{N}{4}\left(1-\frac{\Delta}{4}-\frac{3\delta}{4}\right)$	3
9	$\frac{N}{4}(1+\delta)$	$\frac{N}{4}$	$\frac{N}{4}$	$\frac{N}{4}(1-\delta)$	1
10	$\frac{N}{4}\left(1+\frac{\Delta}{4}+\frac{3\delta}{4}\right)$	$\frac{N}{4}\left(1+\frac{\Delta}{4}-\frac{\delta}{4}\right)$	$\frac{N}{4}\left(1+\frac{\Delta}{4}-\frac{\delta}{4}\right)$	$\frac{N}{4}\left(1-\frac{3\Delta}{4}-\frac{\delta}{4}\right)$	3
11	$\frac{N}{4}(1+\Delta)$	$\frac{N}{4}$	$\frac{N}{4}$	$\frac{N}{4}(1-\Delta)$	1
12	$\frac{N}{4}\left(1+\frac{\Delta}{2}+\frac{\delta}{2}\right)$	$\frac{N}{4}\left(1+\frac{\Delta}{2}-\frac{\delta}{2}\right)$	$\frac{N}{4}\left(1-\frac{\Delta}{2}+\frac{\delta}{2}\right)$	$\frac{N}{4}\left(1-\frac{\Delta}{2}-\frac{\delta}{2}\right)$	16

$$N_4 = \frac{N}{4}\left[1 + \left(-\frac{a_2}{2} + \frac{a_3}{2} - \frac{a_4}{4} - \frac{3a_5}{4} - a_6 - \frac{a_7}{4} + \frac{a_9}{4} - \frac{a_{10}}{2}\right)\Delta - \frac{\delta}{2}\right]. \quad (4)$$

$$N_1' = \frac{N}{4}\left[1 + \left(-\frac{a_2'}{2} + \frac{a_3'}{2} - \frac{a_4'}{4} + \frac{a_7'}{4} + \frac{3a_8'}{4} + \frac{a_{10}'}{4} + a_{11}' + \frac{a_{12}'}{2}\right)\Delta + \left(\frac{a_1'}{2} - \frac{a_4'}{4} + \frac{a_7'}{4} + \frac{a_8'}{4} + a_9' + \frac{3a_{10}'}{4} + \frac{a_{12}'}{2}\right)\delta\right],$$

$$N_2' = \frac{N}{4}\left[1 + \left(\frac{a_2'}{2} - \frac{a_3'}{2} + \frac{3a_4'}{4} + a_6' + \frac{a_7'}{4} - \frac{a_8'}{4} + \frac{a_{10}'}{4} + \frac{a_{12}'}{2}\right)\Delta + \left(-\frac{a_1'}{2} - \frac{a_4'}{4} - a_5' - \frac{3a_7'}{4} + \frac{a_8'}{4} - \frac{a_{10}'}{4} - \frac{a_{12}'}{2}\right)\delta\right],$$

$$N_3' = \frac{N}{4}\left[1 + \left(\frac{a_2'}{2} - \frac{a_3'}{2} - \frac{a_4'}{4} - a_6' - \frac{3a_7'}{4} - \frac{a_8'}{4} + \frac{a_{10}'}{4} - \frac{a_{12}'}{2}\right)\Delta + \left(-\frac{a_1'}{2} + \frac{3a_4'}{4} + a_5' + \frac{a_7'}{4} + \frac{a_8'}{4} - \frac{a_{10}'}{4} + \frac{a_{12}'}{2}\right)\delta\right],$$

$$N_4' = \frac{N}{4}\left[1 + \left(-\frac{a_2'}{2} + \frac{a_3'}{2} - \frac{a_4'}{4} + \frac{a_7'}{4} - \frac{a_8'}{4} - \frac{3a_{10}'}{4} - a_{11}' - \frac{a_{12}'}{2}\right)\Delta + \left(\frac{a_1'}{2} - \frac{a_4'}{4} + \frac{a_7'}{4} - 3\frac{a_8'}{4} - a_9' - \frac{a_{10}'}{4} - \frac{a_{12}'}{2}\right)\delta\right]. \quad (5)$$

It is easily seen from Eqs. (4) and (5) that the normalization condition is satisfied:

$$\sum_{i=1}^{4} N_i = \sum_{i=1}^{4} N_i' = N. \quad (6)$$

The nuclear spin population differences for each electron spin state may now be written.

$$(N_2 - N_1) = \frac{N}{4}\left[(-a_2 + a_3 + a_4 + a_6 - a_7 - a_8)\Delta - \delta\right], \quad M = -1/2, \quad (7a)$$

$$(N_4 - N_3) = \frac{N}{4}\left[(-a_2 + a_3 - a_5 - a_6 + a_8 + a_9)\Delta - \delta\right], \quad M = +1/2, \quad (7b)$$

$$(N_2' - N_1') = \frac{N}{4}\left[(a_2' - a_2' + a_4' + a_6' - a_8' - a_9')\Delta + (-a_1' - a_5' - a_7' - a_9' - a_{10}' - a_{12}')\delta\right], \quad M = -1/2. \quad (8a)$$

$$(N_4' - N_3') = \frac{N}{4}\left[(-a_2' + a_3' + a_6' + a_7' - a_{10}' - a_{11}')\Delta + (-a_1' - a_4' - a_5' - a_8' - a_9' - a_{12}')\delta\right], \quad M = +1/2. \quad (8b)$$

The enhancement of the nuclear magnetic resonance is defined as the power absorbed by the nuclear spin system in the presence of microwave pumping radiation divided by the power absorbed by the nuclear spin system in the absence of an EPR pump. Thus the enhancement for Fig. 1(a) is

$$\varepsilon = \frac{(N_1 - N_2)h\nu_{12}W_{12} + (N_3 - N_4)h\nu_{34}W_{34}}{(N_1^0 - N_2^0)h\nu_{12}W_{12}^0 + (N_3^0 - N_4^0)h\nu_{34}W_{34}^0} \quad (9)$$

with a similar expression for ε' for Fig. 1(b). The nuclear polarization is defined by the well-known expression

$$P_N \equiv \frac{\sum_{i=1}^{4} M_i N_i}{I\sum_{i=1}^{4} N_i}, \quad (10)$$

The zero superscripts which appear in the denominator of Eq. (9) refer to the population distribution of the system in the absence of a microwave pump. The radiative induced transition probabilities W_{12}, W_{34}, W_{12}^0, W_{34}^0 are associated with nuclear transitions ($\Delta m = \pm 1$, $\Delta M = 0$). It is assumed in this treatment that these signal transition probabilities are small in comparison with all w_{ij} and the microwave pump transition probabilities. If this assumption were not made, it is clear of course that all the N_i and N_i' would be influenced by the signal field as well as by the pumping field. In double resonance experiments it has been observed that the nuclear spin-spin relaxation times are not influenced by the saturating radiation. Since the NMR W_{ij}'s are all proportional to the nuclear T_2 values, we set $W_{ij} = W_{ij}^0$. Further since we are considering situations in which either the nuclear Zeeman energy is large or small with respect to the hyperfine interaction energy it follows that $\nu_{21} = \nu_{43}$ and $W_{12} = W_{34}$. Using these assumptions together with Eqs. (8) and (9) we may now write general results for ε and ε'.

Table III. Enhancement Corresponding to Cases Treated in Sec. III

Case	Enhancement ε
A.1	$1 + \dfrac{w_{41} - w_{32}}{w_{41} + w_{32} + 2w_1}\dfrac{\Delta}{\delta}$
A.2	1
B.1	≈ 0
B.2	$\dfrac{2w_1}{w_{42} + w_{31} + 2w_1}$ ($\ll 1$)
B.3	$\dfrac{w_1 + w_{32}}{w_1 + w_2 + 2w_{32}} - \dfrac{w_2 + w_{32}}{w_1 + w_2 + 2w_{32}}\dfrac{\Delta}{\delta}$
B.4	$\dfrac{1}{2}\left[\dfrac{(w_1 + w_2)(2w_1 + w_{31} + w_{42})}{(w_1 + w_2)(w_1 + w_{31} + w_{42}) + w_1w_2 + w_{31}w_{42}} - \dfrac{2w_1w_2 + 2w_{31}w_{42} + (w_1 + w_2)(w_{31} + w_{42})}{(w_1 + w_2)(w_1 + w_{31} + w_{42}) + w_1w_2 + w_{31}w_{42}}\dfrac{\Delta}{\delta}\right]$.
B.5	$\dfrac{w_1 + w_{41}}{w_1 + w_2 + 2w_{41}} + \dfrac{w_2 + w_{41}}{w_1 + w_2 + 2w_{41}}\dfrac{\Delta}{\delta}$
B.6	$\dfrac{1}{2}\left[\dfrac{(w_1 + w_2)(2w_1 + w_{31} + w_{42})}{(w_1 + w_2)(w_1 + w_{31} + w_{42}) + w_1w_2 + w_{31}w_{42}} + \dfrac{2w_1w_2 + 2w_{31}w_{42} + (w_1 + w_2)(w_{31} + w_{42})}{(w_1 + w_2)(w_1 + w_{31} + w_{42}) + w_1w_2 + w_{31}w_{42}}\dfrac{\Delta}{\delta}\right]$

Table IV. Nuclear Polarization Corresponding to the Cases Treated in Sec. III

Case	Nuclear polarization P_N
A.1	$-\frac{1}{2}\frac{\gamma_n}{\lvert\gamma_n\rvert}\left[\frac{w_{32}-w_{41}}{w_{32}+w_{41}+2w_1}\Delta-\delta\right]$
A.2	$-\frac{1}{2}\frac{a}{\lvert a\rvert}\left[\frac{w_2(w_1-w_2)+(w_1w_{42}-W_2w_{21})}{2W_1W_2}\Delta\right]$ $(W_1, W_2) \gg w_{ij}$
	$-\frac{1}{2}\frac{a}{\lvert a\rvert}\left[\frac{w_2+w_{42}}{w_1+w_2+2w_{42}}\right]\Delta$ $(W_2 \ll w_{ij} \ll W_1)$
	$\frac{1}{2}\frac{a}{\lvert a\rvert}\left[\frac{w_2+w_{31}}{w_1+w_2+2w_{31}}\right]\Delta$ $(W_1 \ll w_{ij} \ll W_2)$
B.1	$-\frac{1}{4}\frac{\gamma_n}{\lvert\gamma_n\rvert}\left[\frac{w_2(W_1-W_2)+(W_1w_{32}-W_2w_{41})}{W_1W_2}\Delta - \left(\frac{w_1(W_1+W_2)+(W_1w_{32}+W_2w_{41})}{W_1W_2}\right)\delta\right]$
B.2	$\frac{1}{2}\frac{a}{\lvert a\rvert}\left[\left\{-\frac{w_{42}-w_{31}}{w_{42}+w_{31}+2w_1}-\frac{(w_1+w_2)(w_{42}-w_{31})}{W(w_{42}+w_{31}+2w_1)}\right\}\Delta+\frac{w_1+w_2}{W}\delta\right]$
B.3	$-\frac{1}{2}\frac{\gamma_n}{\lvert\gamma_n\rvert}\left[\frac{w_1+w_{32}}{w_1+w_2+2w_{32}}\Delta-\frac{w_1+w_{32}}{w_1+w_2+2w_{32}}\delta\right]$
B.4	$\frac{1}{4}\frac{a}{\lvert a\rvert}\left[\frac{(w_1+w_2)(w_{31}-w_{42})}{(w_1+w_2)(w_1+w_{31}+w_{42})+w_1w_2+w_{31}w_{42}}(\Delta+\delta)\right]$
B.5	$-\frac{1}{2}\frac{\gamma_n}{\lvert\gamma_n\rvert}\left[-\frac{w_2+w_{41}}{w_1+w_2+2w_{41}}\Delta-\frac{w_1+w_{41}}{w_1+w_2+2w_{41}}\delta\right]$
B.6	$\frac{1}{4}\frac{a}{\lvert a\rvert}\left[\frac{(w_1+w_2)(w_{31}-w_{42})}{w_1w_2+(w_1+w_{31})(w_1+w_2+w_{42})+w_2w_{42}}(\Delta-\delta)\right]$

$$\varepsilon = \frac{\Delta}{\delta}\left\{(a_2-a_3)+\frac{1}{2}(a_5-a_1)+\frac{1}{2}(a_1-a_9)\right\}+1, \quad (11)$$

$$\varepsilon' = \frac{\Delta}{2\delta}\left\{a_8'+a_{10}'+2a_{11}'-a_1'-2a_6'-a_7'\right\} + \frac{1}{2}\left\{2a_1'+a_4'+2a_5'+a_7'+a_9'+2a_9'+a_{10}'+2a_{12}'\right\}. \quad (12)$$

III. Reduction to Special Cases of Interest

In Tables III and IV the enhancement, ε, and the nuclear polarization P_N of eight cases of physical interest are tabulated. The physical features of these cases are summarized below:

A. Figure 1(a)

1. Nuclear Zeeman energy $\gg$ hyperfine interaction energy. The states $E(M,m)$ may now be labeled: $E_1(-1/2,\pm 1/2)$, $E_2(-1/2,\mp 1/2)$, $E_3(1/2,\pm 1/2)$, and $E_4(1/2,\mp 1/2)$. The nuclear substates alternate in sign with the $+(-)$ sign first for γ_n positive (negative). Clearly $w_{43} = w_{21} = w_1$ ($\Delta M = 0$, $\Delta m = \pm 1$), $w_{31} = w_{42} = w_2$ ($\Delta M = \pm 1$, $\Delta m = 0$). $W_{13} = W_{24} = W$ are paramagnetic pumps ($\Delta M = \pm 1$, $\Delta m = 0$). Assume that $W \gg w_{ij}$.

2. Hyperfine interaction energy $\gg$ nuclear Zeeman energy. The states $E(M,m)$ are now relabeled: $E_1(-1/2,\ \pm 1/2)$, $E_2(-1/2,\ \mp 1/2)$, $E_3(1/2,\ \mp 1/2)$, and $E_4(1/2,\ \pm 1/2)$. The nuclear substates are now $+--+$ or $-++-$ according to whether the hyperfine constant $A > 0$ or $A < 0$. Clearly $w_{43} = w_{21} = w_1$ ($\Delta M = 0$, $\Delta m = \pm 1$) and $w_{41} = w_{32} = w_2$ ($\Delta M = \pm 1$, $\Delta m = 0$). W_{13} and W_{24} correspond, respectively, to flip-flop (flip-flip) radiative induced transitions if $A > 0$ ($A < 0$). Let $W_1 = W_{13}$, $W_2 = W_{24}$.

B. Figure 1(b)

1. Nuclear Zeeman energy $\gg$ hyperfine interaction energy. The spin states and thermal relaxations are the same as in A.1. $W_{14} = W_1$ is a flip-flop (flip-flip) pump for $\gamma_n > 0$ ($\gamma_n < 0$) and $W_{23} = W_2$ is a flip-flip (flip-flop) pump for $\gamma_n > 0$ ($\gamma_n < 0$). Assume W_1, $W_2 \gg w_i$.

2. Hyperfine interaction $\gg$ nuclear Zeeman energy. The spin states and thermal relaxations have the same meaning as in A.2. $W_{14} = W_{23} = W$ are paramagnetic pumps ($\Delta M = \pm 1$, $\Delta m = 0$).

3. $W_{23} = 0$. Nuclear Zeeman energy $\gg$ hyperfine interaction energy. The spin states and thermal relaxation are the same as in case A.1. The pump W_{14} is flip-flop (flip-flip) for $\gamma_n > 0$ ($\gamma_n < 0$).

4. $W_{23} = 0$. Hyperfine interaction $\gg$ nuclear Zeeman energy. The spin states and thermal relaxations are the same as in case A.2. The pump W_{14} is paramagnetic ($\Delta M = \pm 1$, $\Delta m = 0$).

5. $W_{14} = 0$. Nuclear Zeeman energy $\gg$ hyperfine interaction energy. The spin states and thermal relaxations have the same meaning as in A.1. W_{23} is a flip-flip (flip-flop) pump for $\gamma_n > 0$ ($\gamma_n < 0$) pump.

6. $W_{14} = 0$. The hyperfine interaction energy $\gg$ nuclear Zeeman energy. The spin states and thermal

relaxation have the same meaning as in A.2. W_{23} is a paramagnetic pump ($\Delta M = \pm 1$, $\Delta m = 0$).

Note that P_N may be significant for ε smaller or vice versa as mentioned in Sec. I.

IV. Conclusion

The treatment outlined in this paper exhibits a number of features of a pumped electron spin-nuclear spin system for $S = I = {}^1/_2$ when no restriction is imposed on the relaxation processes. It is evident that both positive and negative enhancement of the NMR are attainable when either the nuclear Zeeman interaction or the hyperfine interaction is dominant. This is possible either by saturation of single flip or double flip transitions. It is also evident that a small enhancement may well be due to competing relaxations or competing pumps as well as to incomplete saturation. A small enhancement may be accompanied by sizable nuclear polarization or vice versa. The exact solution for the normalized populations of the four levels in Figs. 1(a) and 1(b) given in Sec. II enables one to calculate enhancement, pump power absorbed, polarization, and other quantities of physical interest for cases not covered by the limiting cases treated in Sec. III.

References

1. W. A. Barker and E. A. Desloge, Bull. Am. Phys. Soc. **2,** 226 (1957); L. Bennett and H. C. Torrey, Phys. Rev. **108,** 499 (1957).
2. E. Allais, Compt. Rend. **246,** 2123 (1958); I. Solomon, J. Phys. Radium **19,** 837 (1958); A. Ganssen and E. L. Sloan, III, Bull. Am. Phys. Soc. **7,** 15 (1962).
3. E. Allais, ref. 2.
4. See, for example, D. J. Parker, G. A. McClaren, and J. J. Conradi, J. Chem. Phys. **33,** 629 (1960). Also J. Krebs (private communication).
5. A. W. Overhauser, Phys. Rev. **89,** 689 (1953); **92,** 411 (1953).
6. C. D. Jeffries, Phys. Rev. **106,** 164 (1957); A. Abragam and W. G. Procter, Compt. Rend. **246,** 2253 (1958).
7. W. A. Barker, Rev. Mod. Phys. **34,** 173 (1962).
8. W. A. Barker and J. D. Keating, Appl. Opt. **1,** 335 (1962); J. D. Keating, W. A. Barker, and L. E. Follis, Bull. Am. Phys. Soc. **6,** 68 (1961).
9. It is not necessary to make this approximation. See, for example, references and J. D. Keating and W. A. Barker, J. Franklin Inst. **274,** 253 (1962) in which the exact solution for a three-level maser system is obtained by the "inspection method," another rapid computational technique.

Meeting Reports

IRE Millimeter and Submillimeter Conference, Orlando, Florida, 7–10 January 1963

Reported by M. W. P. Strandberg, MIT

A conference, sponsored by the Orlando Section of the then Institute of Radio Engineers and the Orlando Chapter of the Professional Group on Microwave Theory and Techniques, was held in Orlando, Florida and had as its subject millimeter and submillimeter technology. The response to the meeting was large: in the audience were more than 300 participants and 80 authors and co-authors of the papers presented at the conference. The hospitality offered by the local committee and companies with interests in this field, including The Martin Company, Orlando, was warm, although the weather was not.

From attempts to bridge the gap in the usable spectroscopic technology between the far-infrared and the millimeter-wave regions, a problem has arisen about whether it is better to make this region accessible by taking optically trained technicians and making them proficient in radio-frequency techniques or by taking radio-frequency technicians and teaching them optical tricks. Since this meeting was an engineering show, it would seem to indicate that at least the professional radio engineers consider that the best approach is the latter, and the substance of many papers indicated that millimeter-wave engineers are indeed familiarizing themselves with optical techniques and even becoming virtuosi in their use. The central problem presented by the millimeter- and submillimeter-frequency spectrum (the region of wavelengths from 3 cm to 0.3 mm) is that created by the attenuation in conventional fundamental-mode waveguide transmission lines. Although these microwave components become quite minuscule, they can, nevertheless, be made by one means or another simply by scaling the components developed at longer wavelengths. This would be an acceptable procedure if it were not for the fact that the attenuation becomes as great or greater than 1 dB per foot, and this loss is unacceptably large. For example, at 2 mm, a power divider made with a conventional microwave Tee technique, a so-called 3-dB divider, becomes a 4.2-dB coupler, because of the additional 1.2-dB loss in the transmission-line structure itself. Since free-space losses in the millimeter region, because of atmospheric oxygen and water vapor, are of the order of ${}^1/_{10}$ or ${}^1/_{100}$ of this amount, the so-called quasi-optical transmission lines may be used. These are transmission lines formed from waveguides that are very large compared with the wavelengths and through which the energy may be transmitted with very little interaction with the transmission-line defining surfaces. In this case, power dividers are formed by using plastic prisms with a variable separation to control the reflected and transmitted power by frustrating the total internal reflection. This means that Schafer and Gross's paper in the *Annalen der Physik* **32,** 648 (1910) is a popular reference. Waveguide resonant structures become Fabry-Perot interferometers, and so forth.

Echelette gratings for spectrum analysis were also described and investigated in several papers. There were several discussions of interference spectrometers, especially for the region 0.1–1 mm wavelength. Conventional or unconventional radio-frequency oscillators used as sources of coherent electromagnetic radiation were discussed, together with other incoherent sources, such as the radiation from accelerated electrons, and Čerenkov radiation. In fact, the sources of millimeter and submillimeter power appear to be in such good shape that it seems that the first piece of equipment that a researcher would need is a 20-dB attenuator in order to get the power down to a level that is usable.

In nine sessions, 79 papers were presented or discussed; therefore it is quite impossible to consider the material in any detail. It seemed to this observer that it was usual to assume unconsciously or to consider consciously the electromagnetic properties of technical materials that are being used—in particular, the dielectric—as being given by a simple linear extrapolation from

continued on page 800

Limiting Parameters and Generalized Characteristics of Xenon Lamps

I. S. Marshak

The development of any optical pumping system depends on the knowledge of the possibilities of lamps offered for use. This paper contains generalized data on the maximum load of lamp seals and tube walls (both flash and continuous light), single-flash or repeated operation, at different cooling conditions. Voltage limits of these lamps and the dependence of their efficiency, radiance, and other characteristics on feeding parameters and construction are described. These generalized relations allow one to estimate easily the optical-pumping intensity for each given pumping-time schedule.

The development of any optical pumping system depends on the knowledge of the possible types of lamps available. At present xenon lamps are the most suitable light sources for optical pumping. The accumulated experimental data allow one to form a sufficiently generalized picture of possible parameter variations of these lamps.

I. Modification Limits of Feeding Parameters

In the case of a low power dissipation in the lamp the feeding voltage is limited in low values by the "ignition voltage" U_i and in high values by the "spontaneous-breakdown voltage" U_s.

The feeding voltage $U \geqslant U_i$ guarantees the onset of a heavy current discharge by means of a nominal starting impulse from an auxiliary source (mostly a peak transformer: in lamps with an inner igniting electrode the starting pulse sometimes occurs as a result of a static breakdown of the "ignition electrode-cathode" gas gap and a discharge of the auxiliary condenser). The deterioration of the starting pulse (lowering of amplitude, power, and frequency) may greatly increase U_i. But, as a rule, it is difficult to secure a considerable decrease of U_i by forcing the starting pulse as compared with the nominal owing to the rational matching of the latter in the course of lamp development. This general rule is violated only in the case of a change in the ignition principle: instead of directing the starting pulse to the auxiliary (third) electrode, as recommended for most lamps, it may be directed to the basic gas gap of the lamp by switching into the heavy current discharge circuit either the secondary thick-wire winding of a pulse transformer or an induction coil parallel to the latter. Such a formation of the ionized path may decrease U_i by almost one-half. This method of ignition has a disadvantage—the igniting device dimensions are somewhat enlarged. The method, however, has also its advantages in (a) the decrease of U_i and (b) the possibility of using the lamp in electrically unreliable media (e.g., rarefied air, water) or potentially explosive media. The latter is assured by hermetically sealing the high-voltage wire. The influence on U_i of the lamp construction data is described elsewhere.[1-3]

The condition $U \leqslant U_s$ guarantees an absence of spontaneous, noncontrolled discharges, provided that there are no casual voltage pulses on the lamp electrodes. Generally speaking, the value U_s depends on the arrangement of the surrounding wires and their potential. By removing all outer wires from the lamp bulb (including the external ignition electrode) U_s may be almost doubled.

In connection with the modification limits of feeding voltages two more values should be mentioned: the extinction voltage U_e of a discharge in a flash lamp and the reliable breakdown voltage U_{st} of the lamp's basic gas gap without an auxiliary ionization. The value of U_e may influence the energy dissipated in the lamp which is equal in the absence of a ballast to $(C/2)\cdot(U^2 - U_e^2)$. The value of U_{se} is most significant at a minimum value of U, i.e., for U close to U_i. The difference between ignition and extinction voltages rapidly increases with the increase in the disparity

The author is at the Electric Lamp Works, Moscow, U.S.S.R.
Received 9 April 1962.
This paper was presented at the Spring Meeting of the Optical Society of America in Washington, D. C., March 1962.

between the diameters of the ionizing and high-current channels.[1,2] Consequently, $U_e^2 << U_i^2$, and the value U_e need not be taken into account in lamps with a wide discharge tube at flash energies sufficient for filling its cross section by a heavy current discharge. On the contrary, in capillary lamps with inner diameters less than 1 mm, and in other lamps fed by small condensers (the heavy current channel has no time to widen enough before the exhaustion of the condenser), U_e may be very near to U_i. Thus, for instance, in lamps 70 mm in length and 0.5-mm i.d., U_e at a nominal feeding regime is equal to ~250 V (about half the actual value of U_i). U_e increases similarly to U_i linearly with the lamp length.

The U_{st} voltage is usually 2 or 3 times greater than the U_s value, and, as in the case of U_s, depends on the arrangement of the surrounding wires. U_s and U_{st} increase linearly with the lamp length and the gas pressure but decrease somewhat with the diameter increase of the discharge tube.

The limitation of the feeding condenser and flash frequency is connected with the possibility of destroying the electrodes (usually metal seals in the glass) or the lamp bulb in the case of overloading by a single flash or by a mean dissipated power. It is also connected with the violation of the gas-gap deionization.

The disintegration of the seals, which is of special importance to quartz lamps with 0.02–0.05-mm thick molybdenum foil seals, depends either on an instantaneous discharge of critical energy (similar to a thin-wire explosion) in a metal volume unit or on long-duration overheating and oxidation of exposed-to-the-air metal parts in the course of operating at critical mean power.

The critical-energy data show the following dependence between the maximum rated energy of a single flash $CU^2/2$ (in joules), the cross section S (in cm²) of the molybdenum seal, and the effective resistance of discharge R (determined by the lamp dimension) in ohms:

$$S = \sqrt{\frac{CU^2/2}{2 \times 10^7 R} + \frac{\rho_m^2 l_m^2}{4R^2}} - \frac{\rho_m l_m}{2R};$$

$$R = \frac{\rho l}{\pi r^2}$$

for tubular lamps with discharge channel filling the tube and

$$R = \frac{500\, l^{3/2}}{\sqrt{U} \cdot (CU^2/2)^{0.8}}$$

for spherical lamps. Here l is the distance between the lamp electrodes in cm, r is the internal radius of the discharge tube in cm, ρ is the specific resistance of the discharge plasma equal to ~0.02 ohm·cm for tubular lamps, l_m is the total seal length in cm, and ρ_m is the effective specific resistance of molybdenum close to the point of deterioration for which the oversized estimate 1.7×10^{-4} ohm·cm is known beforehand.

The second and third terms in the first expression for S take into account the part of the energy which is dissipated in the seals but not in the gas-discharge channel. By using the above-mentioned overestimation ρ_m, it is possible in almost all practical cases to appraise the items as totally insignificant in comparison with the first term. The expression for R in the spherical lamp (U feeding voltage is expressed in volts) is based on the experimental data on plasma specific resistance at high electric fields and on channel widening,[2] and also on experimental data on the connection between these values and the seal deterioration.

The data on the critical mean power show a dependence between the maximum rated power P in watts and the cross section of the molybdenum seal S: $S = 1.4 \times 10^{-5} \sqrt{P/R}$, where the channel resistance R has a value according to the above formulas.

The deterioration of the bulb as a result of a single flash action in spherical glass and quartz lamps of the same dimensions occurs approximately at similar flash energies and bears a semblance of an explosion which takes place after a shock-wave impact. Given an almost spherical form, a 3-atm gas pressure, a 2- to 3-mm wall thickness of the bulb, and bulb external diameters of 30, 45, and 60 mm, the maximum energies are approximately equal to 70, 150, and 300 J. If the gas pressure is doubled, the reduction of the wall thickness to 1–1.5 mm, or a substantial departure from the spheric form, cuts down the maximum energy by half. In tubular lamps the bulb deterioration which occurs after an overloading single-flash action results in cracking of the tube, its explosion, or a considerable evaporation of the wall substance which, in its turn, causes an increase of U_i (the latter two forms of destruction are typical for quartz lamps). All these three forms of destruction occur at a roughly similar critical energy. For $l \geq$ 10-cm lamps, in the course of a flash of short duration (less than 0.01 sec), and the absence of an essential external impedance in the discharge circuit (inductivity up to a few μH, active resistance up to centesimal parts of an ohm), this critical energy may be estimated for the selected U from the convenient equation $CU^4/l^3 = K = \text{const}$.

This equation shows that a decrease of U results in an increase in C causing $CU^2/2$ (flash energy) to increase substantially, which evidently depends on lowering the instantaneous loading on the bulb in the case of an appropriate protraction of the flash duration.

The K constant for the single flashes and constructive data (pressure and kind of gas, wall thickness, tube form) of normally used lamps is determined by the diagram presented in Fig. 1. This diagram shows that K for glass lamps is virtually independent of the tube diameter, but for quartz lamps K rises essentially with the

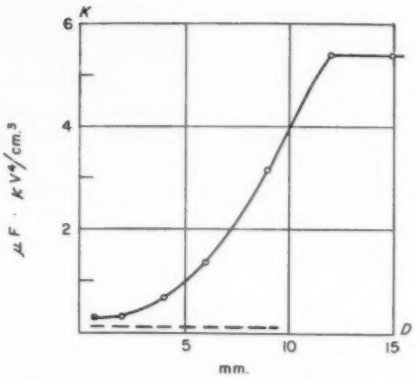

Fig. 1. Dependence of quantity K on the internal diameter of the discharge tube. Solid line—quartz; dashed line—borosilicate glass.

increase of D from 2 to 12 mm. For lamps with a given electrode separation, the maximum permissible energy is estimated from the maximum value of quantity CU^4, which is usually called the "load factor." With the decrease of l to about 1 cm the quantity K increases threefold. This quantity also essentially increases in the presence of a substantial impedance of the discharge circuit. Apart from a partial energy dissipation on an active external resistance, the presence of an impedance prolongs the flash and thus softens the instantaneous loading on the bulb, similar in effect to increasing the feeding condenser capacity with a simultaneous decrease of the feeding voltage.

The load limit on the bulb, in accordance with the mean power, is usually associated with an increase of the glass temperature up to a sharp increase of its electric conductivity or the onset of a chemical reaction between the glass and the getter used in the lamp (alkaline or alkaline-earth metal). Both these effects lead to a convertible or a nonconvertible irregularity in the lamp control. The permissibile temperature of the tubular lamp bulb surfaces is ~200°C for the majority of glasses, and ~800°C for quartz. For spherical glass lamps, the momentary temperature of which does not greatly depart from the mean values, the permissible surface temperature is 300–400°C. The respective values of the mean power dissipated in the lamp relative to the external surface of the bulb's operating part are: 0.5–1 W/cm², 10–15 W/cm², 1.5–3 W/cm². By applying compulsory cooling these limits may be considerably extended. Thus, for instance, the permissible load on 1 cm² for water-cooled, tubular, quartz lamps may be extended up to 150–300 W/cm². Lamps with electrode separations of the same order as the spaces beyond the electrodes permit a medium load approximately twice as great as long lamps.

Apart from overloading the seals or the bulb walls, an increase of the mean dissipated power may be limited by gas deionization irregularities in the intervals between flashes. The quicker the voltage increase on the lamp electrodes after the flash, the sooner this limitation shows its effect. That is why it depends on the nature of the feeding circuit.

A unified approach in estimating frequency limits connected with a deionization for all kinds of feeding circuits may be effected with the aid of a diagram of the recovery of the gas-gap insulation strength. In fact, if by superimposing this diagram on a voltage–time curve these diagrams intersect, then it proves that there is a possibility of noncontrollable discharges in the lamp, i.e., irregularities in its normal operation. The absence of the diagrams' intersection is consequently a requirement which defines the frequency limit of flashes in this circuit.

At present the insulation-strength-recovery diagram has been investigated only for two extreme lamp types: those with capillary and with spherical bulbs.[3,4]

The last limiting characteristic of the lamp is its lifetime. At present there are only partial data about the dependence of lamp life T on its feeding parameters, mainly related to lamps with alkaline-coated cathodes. According to these data in the case where there is a constant mean dissipated power, T slowly grows with the increase of the frequency of flashes (a reduction in flash energy) and is markedly reduced with the increase of the feeding voltage U. In tubular lamps with a 7-cm electrode separation, the respective dependencies take the form (T in hours, f in cps) of:

$$T = 7 \log f + T_{f=1}; \quad U^2 \cdot T = \text{const.}$$

With a constant flash energy, the life expressed by the number of flashes is somewhat lower if the interval between the flashes increases (probably because of a respective diminution of the cathode emissivity).

The substitution of an alkaline-coated cathode by a volume-activated cathode ("tungsten-nickel-barium" alloy, highly thoriated tungsten) leads to a multiply-increased life, whereas the use of pure metal cathodes reduces it considerably.

II. Operating Characteristics

When flash lamps are fed by a condenser with a circuit inductivity differing from the critical $L_{cr} = R^2C/4$ (R = lamp resistance), the light–time diagram approaches the triangle with a steep front and a sloping fall. This takes place both with tubular lamps for which $L << L_{cr}$ usually and with spherical lamps for which L is substantially greater than L_{cr} (in the latter case the fall sometimes shows several waves which correspond to current oscillations in the discharge). The switching into the tubular lamp circuit of an inductivity which is close to L_{cr} allows one to obtain a flash with a nearly symmetric front and fall. The use of an artificial line with a wave impedance close

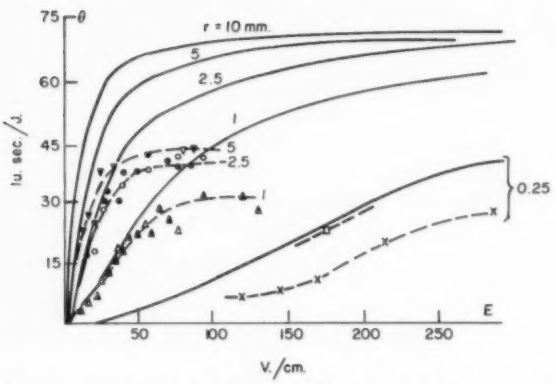

Fig. 2. Dependence of efficiency on initial electric field strength (E) for long, straight, tubular, flash lamps with various internal radii (r in mm) at sufficiently great feeding-condenser capacities.

to R for lamp feeding allows one to obtain a π-form flash. The following relationship between all flash lighting characteristics—the candle-power amplitude J_a, the integral $\int_0^\infty J dt$ ("Lichtsumme") and the duration τ at a 0.35 J_a level (a usually accepted estimate)—suffices for all lamps with an adequate accuracy[5]:

$$\int_0^\infty J dt = K J_a \cdot \tau,$$

where the factor K lies within the limits of 0.85 (condenser fed tubular lamps) and 1 (spherical lamps and lamps with a π-form flash). So it is sufficient to describe the dependence of feeding parameters on the lamp-construction data of only two values, for instance, τ and the radiant efficiency

$$\theta = \frac{M \int_0^\infty J dt}{CU^2/2}$$

(M—the relation of the radiant flux to the radiant intensity in a direction perpendicular to the lamp axis—is equal to ~11.3* for straight tubular lamps and to 10.5 for spiral lamps.)

Detailed data on the efficiency of tubular lamps show that, with a sufficient feeding-condenser capacity C (which ensures the filling by plasma of the channel of the tube cross section), the dependence of θ on the feeding voltage U and the inner tube radius r is described by a family of diagrams shown in Fig. 2. As may be seen, θ depends considerably on the quantities mentioned at their low values but reaches a fairly constant value for all lamps at high U. With low C's a reduction of θ is possible for larger diameter lamps, which is due to the nonfilling of the tube by the discharge channel and to a considerable loss on the widening of the channel. The relative divergence of θ from the maximum quantity, corresponding to the U and r data, may be actually expressed for all lamps by a unified diagram (Fig. 3) of dependence of θ/θ_{max} on $CU^2/2\pi rl$ (this quantity, equal to the energy dissipated in 1 cm³ multiplied by tube radius, may be considered as a measure of the optical thickness of the radiating layer). The reduction of θ begins at $CU^2/2\pi rl \cong 2$ J/cm² and corresponds to an approximate analytical dependence:

$$\frac{\theta}{\theta_{max}} = \frac{CU^{2\ 0.72}}{4\pi rl}$$

(C in μF, l and r in cm, U in V). In cases of short electrode separations the θ is somewhat reduced because of electrode losses which correspond to the effective reduction of feeding voltages at an average of 40–150 V (at respective values of the true initial electric field of 30–145 V/cm). Switching an additional inductivity (with a low active resistance) into the discharge circuit has little influence on θ. Thus, for instance, for lamps with a resistance $R = 40\ \Omega$ at $C = 0.25$ μF, $U = 1.2$ kV, the increase L up to 100 μH does not influence θ, but the increase L up to 2500 μH reduces θ by 20%. In lamps with $R = 0.5\ \Omega$ at $C = 800$ μF, $U = 1$ kV, the increase L up to 1000 μH (active resistance less than 0.05 Ω) does not actually influence θ.

The dependence of flash duration τ of tubular lamps on C is described by the family of curves shown in Fig. 4. In the region of $\tau \gtrsim 1000$ μsec the diagrams correspond to the values of τ calculated from the equation $\tau = RC/2$ (τ being the time constant for the discharge power when the condenser C is discharged through the constant active resistance R calculated from the plasma specific resistance $\rho = 1.25 \times 10^{-2}$ ohm·cm corresponding to $E = 100$ V/cm). At $\tau < 1000$ μsec the dependence of τ on C gradually slows down (because of the relatively increased time of the channel widening and the afterglow as well as the increased dependence of θ on parameters) and finally approaches the

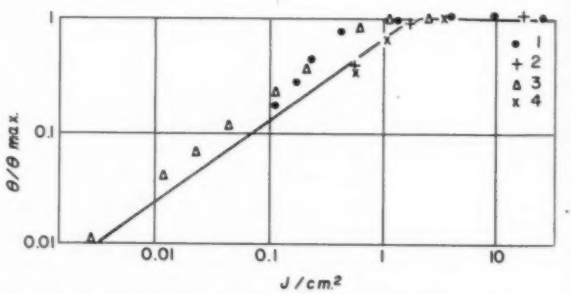

Fig. 3. Dependence of θ/θ_{max} on feeding condenser capacitance at various r and l. —r = 0.25 mm, l = 7 cm; +—r = 0.6 mm, l = 0.6 cm; Δ—r = 2.5 mm, l = 7 cm; x—r = 6.5 mm, l = 50 cm (xenon, p = 100–700 mm of mercury, E_0 = 50–3000 V/cm).

* Values from 11.1 to 11.5 at l = 50 cm and feeding voltages from 6.3 to 2.1 kV were obtained for M. These M values correspond to the integral factor of absorption by the plasma of its own radiation from 1.2 to 2.1 cm⁻¹.[6]

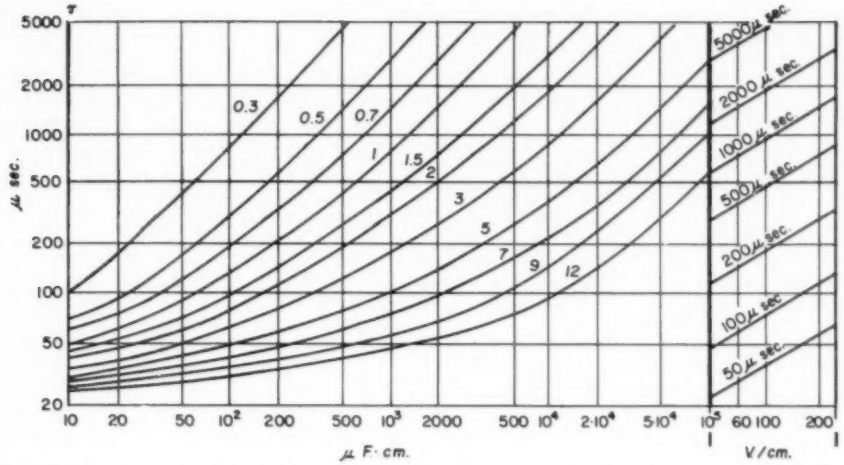

Fig. 4. At left is the family of τ dependencies on Cl for lamps with different tube diameters (shown in figure in mm) at initial electric field strength $E = 100$ V/cm (xenon, 150–600 mm of mercury, l from 2 to 130 cm). At right is the ordinates scale displacement at E_0 modification.

proportionality τ and $\sqrt{C}$. The dependence of τ on E is expressed for tubular lamps by proportion τ and $E^{-0.6}$. Taking as a basis the approximate equality $\tau = RC/2$ it may be expected that, with a discharge circuit inductivity less than the critical $L_{cr} = R^2C/4$ and a ballast resistance $R_b << R$, the flash duration ought not to depend on L and R_b. This is confirmed, for instance, for capillary lamps ($R = 40\ \Omega$, $L_{cr} = 100\ \mu$H) by the fact that introducing $L \sim 100\ \mu$H into the circuit does not in practice influence τ. The introduction of $L = 2500\ \mu$H increases τ by $\sim$2.2 times. Similarly, to double τ in lamps with $R = 0.5\ \Omega$, it is necessary to introduce $L = 1000\ \mu$H, which is $\sim$30 times greater than L_{cr}. It may be considered that τ is approximately proportional to $(L/L_{cr})^{0.2}$. The ballast resistance, which exceeds the estimated resistance of the lamp, has a similar influence on τ.

For large τ, at which the channel widening may be disregarded, it may be considered that the tube cross section is totally filled by plasma and the brightness characteristics of tubular lamps are simply calculated from the data on θ and τ. The comparison of these data with the data on maximum loading (Fig. 1) shows that the maximum brightness integral $\int B\,dt$ for straight quartz lamps with an inner tube radius of from 2 to 6 mm, providing there are equal Cl, has a similar quantity which is expressed by the empirical formula:

$$\int Bdt = 7(Cl)^{0.4}$$

($\int Bdt$—in stilb. sec, C—in μF, l—in cm). In lamps of borosilicate glass at $r = 1$ mm the maximum quantity $\int Bdt$ is almost the same, but if r increases it decreases in proportion to $1/r$. With the limitation of a flash duration (by limiting Cl, the smaller the quantity the smaller r becomes) the maximum brightness integral of straight quartz lamps is approximately expressed by an empirical formula:

$$\int Bdt = 3000\, r \left(\frac{\tau}{10}\right)^{0.4}$$

(τ—in msec, r—in cm). Radiance characteristics of tubular lamps may be defined by a division of horizontal radiant intensity on the channel area $l \cdot r$ with the condition: $CU^2/2\pi rl > 2$ J/cm², which characterizes a satisfactory filling of the tube by the discharge channel. It is then evident that the brightness amplitude B_a with greatly differing lamp construction data is approximately the only function of the longitudinal electric field strength shown in Fig. 5. The same function may be used to estimate the radiance amplitude even if the above-mentioned condition is not fulfilled (the nonfilling of tube). On such occasions B_a is equal to the product of the given function and the square of θ/θ_{max}, the dependence of which on the parameters is shown in Fig. 3).* The analytical expression of the diagram in Fig. 5 has the following form:

$$\frac{B_a}{(\theta/\theta_{max})^2} = \frac{E^{0.9}}{300}$$

(B_a—in megastilb, E—in V/cm).

The efficiency data on spherical lamps show that they depend but little on the feeding voltage, the frequency of flashes, dimensions of the bulb, the discharge circuit inductivity and, within certain limits, on the active circuit resistance. The increase of gas pressure from 1 to 3 atm and the distance between the electrodes

* At present there are insufficient data on the function of θ/θ_{max} for light gases. It may be supposed that for these gases the value $CU^2/2\pi rl$ (below which this function begins to diminish) exceeds the quantity 2 J/cm² found for xenon and krypton.

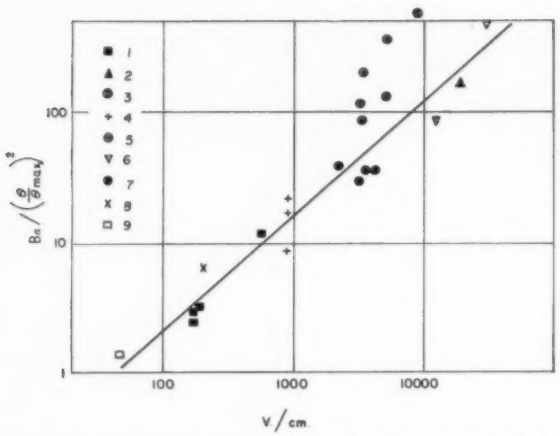

Fig. 5. Dependence on the electric field strength (E) of the brightness amplitude (B_a) of the capillary pulse discharge divided by the factor $(\theta/\theta_{max})^2$, which takes into account the insufficient optic depth of the radiating channel. r varies from 0.2 to 2 mm, l from 1 to 7 cm, p from 100 to 3000 mm of mercury, for xenon, argon, and air.

from 3 to 8 mm lead to an increase of θ by $\sim$1.5 times. The influence on θ of the gas atomic weight (in the practically used region of the other parameters) is shown in Fig. 6. The dependence of θ on C is not great at $C > 0.1$ μF and shows a rapid decrease of θ with C at $C < 0.01$ μF.

The flash duration in spherical lamps is different from that of tubular lamps and does not decrease but rather increases with the higher feeding voltages (proportional to the first power of U). It is also proportional to $\sqrt{C}$, and thus, within wide limits, is proportional to the square root of the flash energy. The influence on it of the kind of gas is seen in Fig. 6. The other factors do not influence τ greatly: a fivefold increase of pressure increases τ not more than twice, and a threefold increase in electrode separation diminishes τ by less than one-half. With an increase in inductivity τ increases proportionately to $\sim L^{1/6}$, and the switching-in of a 0.5-Ω ballast resistance decreases τ (because of a damping of current oscillations) to approximately one-half.

The approximate proportionality of θ and τ to the atomic weight of the gas, and the roughly similar dependence of θ and τ on p, means that, with all other conditions equal, the amplitude of radiant intensity J_a in different gases and at different p ought to be practically the same.*

Because of the independence of θ on U and C and the direct proportionality between τ and the square root of the flash energy, J_a is steady at a constant $CU^2/2$ and different C and U, and is also directly proportional to either $\sqrt{C}$ or U separately (at small C the dependence of J_a on C may be seen more clearly). A reverse course of weak dependencies of θ and τ on L and l shows more clearly that J_a increases with a decrease in L and an increase in l. The slope of the flash front substantially increases as L decreases, especially so in light gases. It also increases as the atomic weight of the gas decreases.

The modern literature contains a great deal of experimental data on the radiance amplitude of short-period flashes and allows one to form the following general opinion of the dependence of radiance on various parameters:

(a) In the open (not limited by walls) spark gap the radiance amplitude B for a certain gas increases up to certain limit (gets "saturated") with an increase in pressure; it also increases with an energy-concentration increase in space and time in lieu of a feeding-voltage increase and a diminishing of the discharge-circuit inductivity and the electrode separation. At pressures of several atm the saturation value B_{sat} (p) attained at a certain energy concentration increases with the pressure, but at still greater p ceases to depend on p. Similarly, the saturation value B_{sat} (E) attained at a certain pressure at first increases with the higher energy concentration, and then ceases to depend on the latter. Thus, each gas has its own characteristic absolute brightness limit of the discharge B_{abs}.

(b) For gases with a lower atomic weight, at lower pressures and energy concentrations B is less than for heavier gases. Attaining B_{abs} in the latter occurs at lower p and energy concentrations than with light gases. A further increase of p and of the concentration leads to an effect where the discharge radiance in light gases exceeds the discharge radiance in heavy gases, which does not increase further. The absolute limit of the

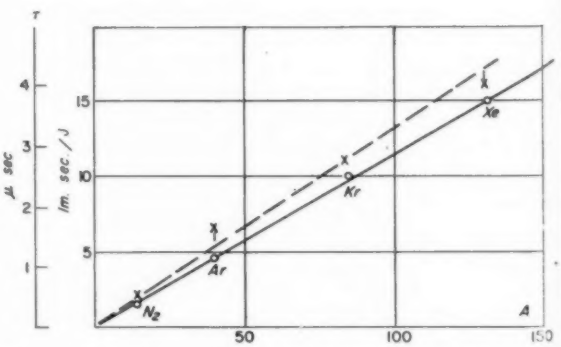

Fig. 6. Dependence of light output (solid line) and flash duration (dotted line) of spherical lamps on the gas atomic weight (A). $C = 0.5$ μF, $U = 5$ kW, $L = 0.12$ μH, $l = 5$ mm, $p = 3$ atm (dots for nitrogen were obtained at 1 atm and recalculated to 3 atm).

* A similar insignificant dependence of the radiant intensity amplitude on the kind of radiating atoms is observed in the discharges in the vapor of an exploding thin wire.[7]

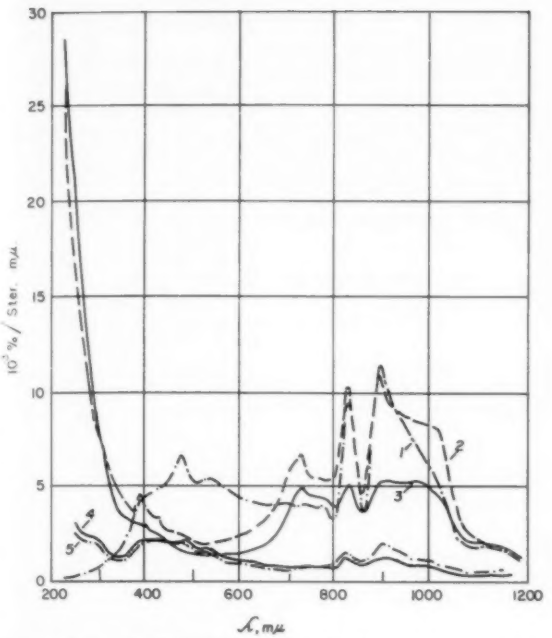

Fig. 7. Spectral efficiency η_λ for tubular (r = 2.5 mm, l = 7 cm; curve 1—C = 2500 μF, U = 0.3 kV; curve 2—8 μF, U = 1.6 kV) and spherical xenon lamps (l = 2.5 mm; curve 3—3 μF, 3 kV; curve 4—0.27 μF, 3 kV; curve 5—0.025 μF, 3 kV).

discharge radiance increases inversely as the gas atomic weight: roughly in proportion to $A^{-1/3}$.

(c) The feeding voltage $U_{0.9}$ of a discharge, the radiance of which is equal to 90% B_{abs}, is approximately proportional to the following parameter degrees: $L^{1/4}$, $C^{-1/4}$, $p^{-1/4}$, A^{-1}.

(d) The discharge spectral radiance in the long wavelength region gets saturated much earlier than in the short wavelength region.

Spectral efficiency diagrams (Fig. 7) give a good idea of tubular and spherical flash-lamp spectral characteristics (the energy radiated in the course of a flash duration in the spectral interval 1 mμ, in a solid angle of 1 sterad, in relation to the energy fed to the lamp from the condenser). As is shown in Fig. 7, at flash energies $\gtrsim$ 10 J even greater parameter changes do not substantially modify the η_λ course in the $\lambda > 400$ mμ region. Only in the short ultraviolet region does the relative spectral intensity increase with an energy concentration increase. A flash energy cut down to 0.1 J substantially reduces the long wavelength radiation of the lamp.

As has been shown,[8,9] high-intensity tubular xenon lamps can operate not only in the short flash regime, but also in the greatly prolonged or even in the continuous regimes. They retain the basic features characterizing the flash lamps: a high active resistance (which allows lamp switching into a circuit without a ballast), a great light output, and the spectral distribution. When applying an intensive compulsory cooling these lamps are able to work continuously up to 10 V/cm (only slightly lower than the usual field strengths in the pulse regime).

Respective radiation intensities differ by not more than one or two orders. So it is possible that in the future the intensities at continuous or quasi-continuous operation may prove to be sufficient for optical pumping purposes.

The study of xenon lamps in the continuous regimes shows that their basic characteristics may be approximately calculated from the following equations:

$$\frac{\rho}{\vartheta^2} = 0.065\,(p_0/rE^2)^{1/2};\quad \theta = 19.3 \log \frac{P}{l} - 12.$$

Here ρ is the discharge plasma specific resistance in ohm·cm, ϑ is the ratio of the discharge channel radius to the inner radius r of the discharge tube (in cm), l is the distance (in cm) between the electrodes (the quantities mentioned depend upon the discharge column resistance $R = l(\rho/\vartheta^2)/\pi r^2$, which determines the current in the lamp), p_0 is the xenon "cold" pressure in mm of mercury, E is the electric field strength (equal to U/l, where U is the feeding voltage in volts), θ is the lamp efficiency in lumen/watts, and P is the power (in watts) dissipated in the lamp.

The formulas cited are true for l not less than a few dozen cm at a very wide variation of other parameters. At short l the electrode energy losses begin to be of significance; this considerably increases R and decreases θ. Special attention is drawn to the simplicity of the last formula. It follows that the efficiency of the lamp depends only on the power dissipated in the tube-length unit and does not depend on the tube radius, gas pressure, gas purity, etc.

References

1. I. S. Marshak, *Proceedings of the Third International Congress on High-Speed Photography* (Butterworth, London, 1957), p. 30.
2. I. S. Marshak, Soviet Phys.–Uspekhi **3,** 624 (1961).
3. I. S. Marshak and L. I. Shchoukin, J. Soc. Motion Picture Television Engrs. **70,** 169 (1961).
4. I. S. Marshak, V. P. Jiltzov, and L. I. Shchoukin, Svetotechnica, No. 11, 13 (1961).
5. N. I. Vassilyev, M. S. Levtshook, and I. S. Marshak, Opt. i Spektr. **11,** 118 (1961), Optics and Spectroscopy **11,** 61 (1961).
6. I. S. Marshak, Svetotechnica No. 6, 17 (1959).
7. I. S. Marshak, Opt. i Spektr. **10,** 801 (1961), Optics and Spectroscopy **10,** 424 (1961).
8. I. S. Marshak, V. I. Vassilyev, I. T. Tokhadze, and N. V. Rogateen, Svetotechnica No. 4, 8 (1961).
9. I. S. Marshak, V. I. Vassilyev, and A. L. Vasserman, Svetotechnica No. 3, 7 (1962).

Meeting Reports *continued from page 792*

their radio-frequency characteristics. This is a dangerous position to take, since this millimeter and submillimeter region is the very region in which the dielectric constants of the radio frequency change mysteriously into the indexes of refraction in the infrared region. We know that, although the junction of these two constants is continuous through this region, their characteristics in this region are not only probably exotic but also, for the most part, unmeasured. It would seem that someone in a position to measure the dielectric properties of materials in this region with an interferometer spectrometer, for example, would earn the undying gratitude of a large group of radio engineers and physicists if he would simply measure these dielectric properties and present them as tables or charts for use by the people interested in designing and using equipment in this region.

Most of the papers presented will be published in a future issue of the *IRE Transactions of the Professional Group on Microwave Theory and Techniques* and will be of interest to both the far-infrared spectroscopist and the millimeter-wave engineer.

Third International Symposium on Quantum Electronics, Paris, France, 11–15 February 1963

Reported by O. S. Heavens, University of London

The usual charms of Paris, rendezvous of this meeting, were somewhat obscured by cold, dreary weather. Compensating excitement was provided (although how many delegates knew at the time?) by certain political activities around the establishment next door—the École Militaire. Although this scene of political unrest is in fact overlooked by the building that housed the conference, it appears that no quantum electronicians were actually involved.

The Palais l'Unesco housed us efficiently, albeit in a slightly clinical atmosphere. The organization proved effective once it started, although at least a timetable could have been provided *before* the conference commenced. Our hosts happily overcame language barriers in most cases; simultaneous translation was provided in French, German, and English, through the truly heroic efforts of the translators. In those cases in which they were forced to concede defeat, it must be said in all fairness that the poor diction of the few guilty speakers generally defeated their compatriots.

One's first over-all reaction to the meeting was that, although 150 papers were covered in two parallel sessions, there were few dramatic developments. Perhaps this is an unfair but natural reaction in a field whose rate of growth, in the brief spell since the arrival of the first optical maser, has been so great that one's threshold for excitement has been raised. Certainly, a considerable amount of consolidation has been achieved in the past year; a glance at the proceedings of the previous two quantum electronics meetings, however, reminds one of the many new developments in the field.

Introductory papers were given by Lamb and Kastler. One feels that the answers to many questions, both present and future, will be found in the details of Lamb's comprehensive attack on the general problems of resonance in maser systems; it is hoped that a detailed account will be available soon. Kastler discussed questions of coherence, which still remains a somewhat vexed question, in spite of the experts who continue to assert that there is no problem while at the same time disagreeing loudly one with another. We can only agree with Glauber's comment that "there is no substitute for quantum theory for dealing with quanta".

Classical descriptions remain useful within their sphere of influence, and of interest in this connection is the result given by Wolf, showing that the coherence of a wave traveling through many apertures tends to increase, regardless of whether stimulated emission occurs.

Perhaps the most exciting of the many results discussed at this meeting was the report by Franken on second harmonic generation at the fantastic efficiency of 22%. We may well recall the act of faith that was required to convince ourselves that the spectrum published originally in *Physical Review Letters* announcing this effect did, in fact, show a line at all. The present figure of 200 kW of second harmonic generation serves to allay any doubts that we might have had. Furthermore, results for *third* harmonic generation were presented as was a suggestion of an orientation dependence. In the realms of solid-state lasers, the remarkably high efficiency of the gallium-arsenide system (75%) would seem to suggest considerable promise for lasers of this type. (There are, however, no signs as yet that people working on what we may now describe as conventional lasers are packing up.) The prospects of gas lasers as length standards were discussed by Javan, who entertained us with a tape recording of the beat note obtained from two helium–neon lasers, which kept within the audio range for a minute or two. The stability observed was of the order 10 cps over a period of approximately 1 sec—a truly remarkable achievement when one thinks of the million times greater bandwidth of the previously sharpest spectral line. At the microwave end of the spectrum, noise figures show an improvement of two orders of magnitude over those attainable 10 years ago. Among the considerable range of results given by the Bell Telephone Laboratories group is the attainment of maser action at wavelengths out as far as 28 μ. Although this is the longest wavelength recorded to date, there seems to be no reason to believe that this represents the limit. At the opposite end of the optical region, maser action in the ultraviolet at a wavelength of 3125 Å is reported by the Naval Research Laboratory from a glass containing gadolinium. Although the power level reported is very low, this result forms a promising break into the ultraviolet region. Speculative comments on the possibilities of maser action in the x-ray and gamma-ray regions were offered, although it seems unlikely that working devices will be offered within the near future. In the realms of high-power crystal lasers, neodymium-doped glass appears to be catching up rapidly with ruby. Snitzer reported powers of the order 30 MW from a 20-cm rod and thus offered indirectly, by a combination with Franken's second harmonic generation, a possible source of substantial power slap in the middle of the visible spectrum.

From the First Quantum Electronics Meeting, attended by less than 100 people, we have now reached the level of 1000 delegates and a 5-day meeting. It seems inevitable that some division will be in order for future meetings—perhaps on the basis of microwave/optical regions. We may expect to see, at the next such meeting, results of the applications of masers to the many fields into which they are spreading.

Quantum Electronics—Masers and Optical Maser Techniques, Tenth Annual Solid State Circuits Conference, Philadelphia, 20-22 February 1963

Reported by Enos E. Witmer, University of Pennsylvania

The tenth annual International Solid-State Circuits Conference was held at the University of Pennsylvania and the Sheraton Hotel in Philadelphia. In addition to a Friday afternoon session on optoelectronics there was also an informal discussion session on Thursday evening—primarily a panel discussion—which included questions and comments from the audience. The moderator of this session was G. Wade *Raytheon*, and the topic was coherent optical techniques and applications. The panel

continued on page 823

Application of the Sénarmont Polariscope to Analysis of Optical Maser Light

David Hellerstein

A Sénarmont polariscope suitable for optical maser work has been constructed. It employs an optically active wedge and an analyzing polarizer to map the azimuthal angle onto a linear field, indicating this angle by null positions on a photographic plate. It measures the azimuth of linearly polarized light over a range of 180° with an accuracy at present of ±1.5° and distinguishes between right and left circularly polarized light. This device is compact and relatively inexpensive; it requires no auxiliary electronic apparatus.

Introduction

The pulse duration of optical masers is normally tenths of milliseconds. Most optical polarization analyzers, such as polarizers, biquartz, and various compensators,[1] are not useful for pulses; in general, they have moving parts which must be oriented while the beam is passing through them. Electro-optical systems, which scan the polarization field electronically[2] or electromechanically,[3,4] are more useful; scanning frequencies of 10 or 20 kc/sec are easily attained. However, we were interested in measurements on a maser employing *Q*-spoiling, i.e., one in which maser action is prevented until population inversion is maximized. Pulses from such a maser approach nanoseconds in length, requiring scanning frequencies outside the range of present systems. We wished to measure the azimuth of linearly polarized light (LPL) over the entire range of 180° and to identify left and right circularly polarized light (CPL). The Sénarmont polariscope,[5] although designed for a system with moving parts, is readily adapted to these requirements by means of photographic techniques. The heart of this system is two wedges of optically active material, specifically quartz, across whose exit face is placed an analyzing polarizer. The wedges, one of *l*-rotatory quartz, the other of *d*-rotatory quartz, are geometrically identical cut with the optic axis normal to one face of the prism. They are placed together with optical axes colinear, to form a rectangular parallelopiped (Fig. 1). Light passes through the quartz wedges parallel to the optic axes.

The active element actually used in this study consisted of a single quartz wedge immersed in a mineral oil of approximately the same refractive index as quartz (see Fig. 2). The face of the wedge had an average diameter of 4 cm, and the wedge angle was 32°. HN-22 polarizers were used.

A collimated beam of linearly polarized, monochromatic light, with a diameter at least as great as that of the active element, passes through this element and the analyzing polarizer to fall on a photographic plate. At some distance y along the exit face of the device a null in transmitted intensity is observed. This is the locus of light paths along which the azimuthal angle of polarization of the incident beam is rotated through the angle necessary to cross it with the analyzer. Azimuthal rotation is a function of position along the face of the active element, specifically:

$$\zeta(y) = dL - \frac{L}{W}(d - l)y \tag{1}$$

$$= A + by, \tag{2}$$

where $\zeta(y)$ is the total rotation in degrees of any ray parallel to the z axis; d is the rotatory power of the d-rotatory quartz in + degrees/mm; l is the rotatory power of the l-rotatory quartz in + degrees/mm (note $l < 0$); L and W are the length and width, respectively, of the active element, and A and b are constants defined by the equation.

We measure y from the edge of the active element to the null position on the photographic plate; the other parameters are known or measurable. ζ can thus be found. ζ and the orientation of the analyzer determine the unknown polarization.

The author is with Baird-Atomic, Inc., Cambridge 38, Massachusetts.

Received 13 December 1962.

This work was supported in part by U. S. Air Force Office of Scientific Research.

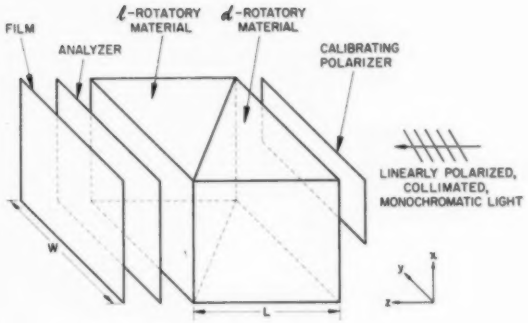

Fig. 1. Diagram of polarization analyzer.

More direct measurements are made by calibrating the photographic image with LPL of known azimuth and of the same wavelength as the light to be analyzed. A polarizer or in practice several polarizers of known orientation are placed across part of the entrance face of the apparatus. The active element is designed to provide at least one 180° difference in rotation between $y = 0$ and $y = W$. If the analyzer is properly oriented, the polarizer will cause at least two nulls to appear on the film. Since $\zeta(y)$ is a *linear* function of y [Eq. (2)], the azimuthal angle varies linearly from 0 to 180° over the distance between the two calibrating nulls. LPL of arbitrary azimuth passing through the unshielded section of the equipment will cause a null to appear at some y position between the calibrating nulls. The distance of this null from the calibrating null nearer $y = 0$ is directly proportional to the azimuthal angle of the incident light, and b, the constant of proportionality, is determined by the 180° distance between the calibrating nulls. By this technique we find the azimuthal angle of polarization by measuring the azimuth of the calibrating polarizer and distances on the photographic plate, thereby eliminating measurements on the active element.

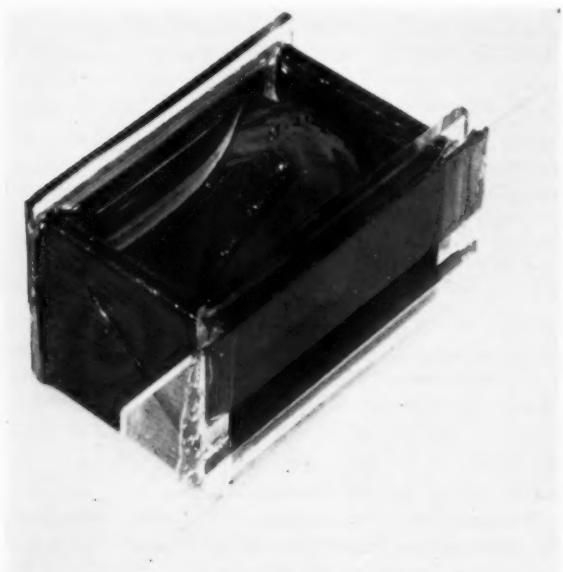

Fig. 2. Polarization analyzer used for photographs in Fig. 5 and for measurements described in this paper.

Mathematical Analysis

In this section we investigate by means of the Mueller calculus[6,7] the passage of LPL, CPL, and elliptically polarized light (EPL) through the polarization analyzer. Let us consider a plane wave of EPL moving in the positive Z direction of a right-handed coordinate system. Following the notation of Shurcliff,[6] α is the azimuthal angle (all azimuthal angles are in the XY plane and are measured counterclockwise from the X axis), and ω is defined as $\tan^{-1} b/a$, where b/a is the ratio of the semi-minor to semi-major axis of the ellipse. The normalized Stokes vector representation of the light is:

$$L_{ep} = \begin{bmatrix} 1 \\ \cos 2\omega \quad \cos 2\alpha \\ \cos 2\omega \quad \sin 2\alpha \\ \sin 2\omega \end{bmatrix}. \tag{3}$$

For LPL this becomes,

$$L_{lp} = \begin{bmatrix} 1 \\ \cos 2\alpha \\ \sin 2\alpha \\ 0 \end{bmatrix}, \tag{4}$$

and for CPL we have

$$L_{cp} = \begin{bmatrix} 1 \\ 0 \\ 0 \\ \pm 1 \end{bmatrix}, \tag{5}$$

where the plus and minus signs refer to right and left CPL, respectively. If the intensity of the light is different from unity, the entire normalized Stokes vector is multiplied by a scalar equal to this intensity.

Each optical component that the light passes through on its way to the film is represented by a square matrix; the effect of each component on the light is determined by multiplying the incident light vector by the component matrix.

Specifically:

(a) Counterclockwise rotation of the azimuth α by an angle ζ is represented:

$$R(\zeta) = \begin{bmatrix} 1 & 0 & 0 & 0 \\ 0 & \cos 2\zeta & -\sin 2\zeta & 0 \\ 0 & \sin 2\zeta & \cos 2\zeta & 0 \\ 0 & 0 & 0 & 1 \end{bmatrix}. \tag{6}$$

(b) A linear polarizer transmitting only LPL of azimuth θ is represented:

$$P(\theta) = \tfrac{1}{2}\begin{bmatrix} 1 & \cos 2\theta & \sin 2\theta & 0 \\ \cos 2\theta & \cos^2 2\theta & \sin 2\theta \cos 2\theta & 0 \\ \sin 2\theta & \sin 2\theta \cos 2\theta & \sin^2 2\theta & 0 \\ 0 & 0 & 0 & 0 \end{bmatrix}. \quad (7)$$

(c) A $\lambda/4$ plate, whose fast axis is at $+\pi/4$ from the X axis, is represented:

$$\frac{\lambda}{4} = \begin{bmatrix} 1 & 0 & 0 & 0 \\ 0 & 0 & 0 & -1 \\ 0 & 0 & 1 & 0 \\ 0 & 1 & 0 & 0 \end{bmatrix}. \quad (8)$$

Let LPL of azimuth α fall on the front surface of the polarization analyzer. Through the unshielded face

$$L_T \equiv L_{\substack{\text{transmitted} \\ \text{to film}}} = P(0)R[\zeta(y)]L_{lp} = \cos^2[\alpha + \zeta(y)]\begin{bmatrix} 1 \\ 1 \\ 0 \\ 0 \end{bmatrix}. \quad (9)$$

This is LPL, of azimuth 0, and of amplitude $\cos[\alpha + \zeta(y)]$. A null occurs on the film at y_α where

$$\alpha + \zeta(y_\alpha) = \frac{\pi}{2} + n\pi, \qquad n = 0, \pm 1, \ldots \quad (10)$$

A calibrating polarizer of azimuth β is placed partially across the entrance face of the device, as in Fig. 2. Light passing through this section of the device may be represented:

$$L_T = P(0)R[\zeta(y)]\ P(\beta)L_{lp} \quad (11)$$

$$= \cos^2[\zeta(y) + \beta]\cos^2(\alpha - \beta)\begin{bmatrix} 1 \\ 1 \\ 0 \\ 0 \end{bmatrix}, \quad (12)$$

where β is determined by direct measurements on the polarizer. L_T is LPL of amplitude $\cos[\zeta(y) + \beta]\cos(\alpha - \beta)$. Nulls occur if

$$\zeta(y_m) + \beta = \frac{\pi}{2} + m\pi, \qquad m = 0, \pm 1, \ldots, \quad (13)$$

or

$$\alpha - \beta = \frac{\pi}{2} + k\pi, \qquad k = 0, \pm 1, \ldots, \quad (14)$$

If condition (14) exists then the entire calibrating field is dark. This difficulty may be eliminated by use of several calibrating polarizers at different β (see Appendix). If the entire field is not dark, nulls must occur at y_m. The constant of proportionality b in Eq. (2) is determined by combining (13) and (2) with the distance between consecutive nulls:

$$\zeta(y_{m+1}) - \zeta(y_m) = [(m+1) - m]\pi = b(y_{m+1} - y_m), \quad (15)$$

$$b = \frac{\pi}{y_{m+1} - y_m}. \quad (16)$$

By subtracting Eq. (13) from Eq. (10) and combining the results with Eq. (2) α may be found [up to a trivial term $(n - m)\pi$]:

$$\alpha = \beta + \pi\frac{(y_m - y)_\alpha}{y_{m+1} - y_m}. \quad (17)$$

So the azimuth of polarization is calculated from measurements on the film (y_m, y_{m+1}, y_α) and on the calibrating polarizer (β).

To analyze CPL a $\lambda/4$ plate with the azimuth of its fast axis at $\pi/4$ is placed in front of the polarizer. Light through the system is represented:

$$L_T = P(0)\,R[\zeta(y)]\,\Lambda/4\,L_{cp} \quad (18)$$

$$= \sin^2(\zeta)\begin{bmatrix} 1 \\ 1 \\ 0 \\ 0 \end{bmatrix} \text{ for right CPL} \quad (19)$$

$$= \cos^2(\zeta)\begin{bmatrix} 1 \\ 1 \\ 0 \\ 0 \end{bmatrix} \text{ for left CPL.} \quad (20)$$

Nulls appear at $\zeta = 0, \pi$ or at $\zeta = \pi/2$ for right CPL and left CPL, respectively. The calibrating section is used with CPL as with LPL since the calibrating polarizer converts all light incident on it into LPL at azimuthal angle β. If the calibrating polarizer is oriented so that $\beta = \pi/2$ its nulls will appear at $\zeta = 0, \pi$. Right CPL may then be distinguished from left CPL by whether the nulls of the $\lambda/4$ section appear respectively alongside or halfway between the nulls of the calibrating section.

We are currently considering adaptation of this device for analysis of EPL. Our approach will be to place a variable retardation plate, in particular a Babinet compensator, between the optically active element and the analyzing polarizer, so that retardation δ varies linearly with x. If $\delta(x)$ and $\zeta(y)$ are known, theory indicates that both the azimuth and the ellipticity of the EPL may be determined from the location of null points on the photograph.

Operating Notes

Several methods of varying degrees of accuracy were used to determine the relative positions of nulls on the photographic plate. Ideally, the intensity of light falling on the film will vary as $\sin^2\pi y/\Delta y$, where Δy = distance between calibrating nulls. The response of the film to this light varies with exposure. Visually locating the center of a photographed null is most accurately accomplished when this image is a narrow line with well-defined edges. Narrowing the line-width is accomplished by moderate overexposure and overdevelopment. Negatives are enlarged onto very high contrast paper (No. 5). Line-width is thus reduced to 4% of the field width, and line edge uncertainty to about 0.5%. For negatives examined directly, line-

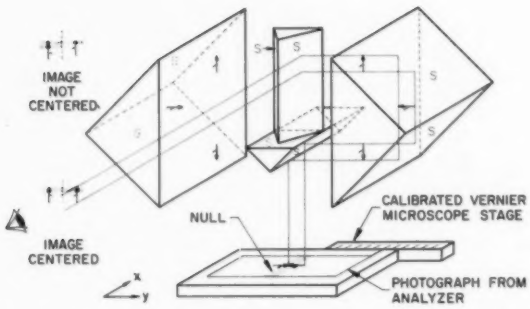

Fig. 3. S: silvered. An optical comparator for determining the relative positions of null lines on analyzer photographs. When the null image appears as a single line, the null is centered under the comparator, and its position may be read from the vernier.

width varies with intensity of the transmitted light.*

Our measurements were made on both pulsed maser light and on continuous light. Measurements from any one picture when the center of the null was located visually were repeatable to ±2°, or about 1%, regardless of the size of the picture. The inaccuracy was due in part to the inability of the eye to locate the darkest part of a dark field. We have constructed an optical comparator which splits the null into two parts and recombines them in such a way that when the two sections of the null appear aligned, the position of the null may be measured (Fig. 3). This is more accurate (±1/2 deg for any one picture) because (a) the eye observes intensity differences at a discontinuity more accurately than over a continuum, and (b) the rate of change of the emulsion density is greater at the edges of the null, where comparison may now take place, than at the nadir. The comparator is a simple and inexpensive device. Electronic measurement systems are equally accurate, but more expensive. Measurements were made with a Baird-Atomic densitometer-comparator and a Bristol recorder. Examples of densitometer traces are shown in Fig. 4. Measurements made on different photographs taken under apparently identical conditions varied by ±1.5°, whether maser light or an appropriate continuous source was used.

We used a C-cut cylindrical ruby maser with plane parallel end plates. The interference pattern over the maser face varies with the energy of the pumping light, and the geometry of the pumping system.[8] These patterns caused difficulty in locating nulls. In Fig. 5, three pictures taken through the analyzer are shown, two of maser light [Figs. 5(a) and (b)] and one

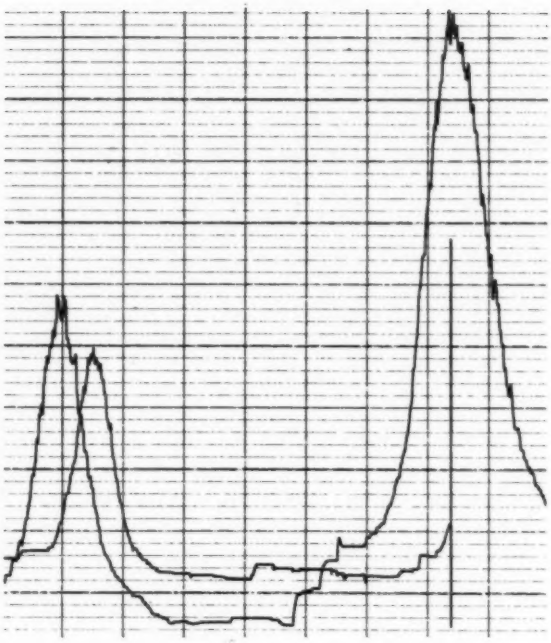

(a)

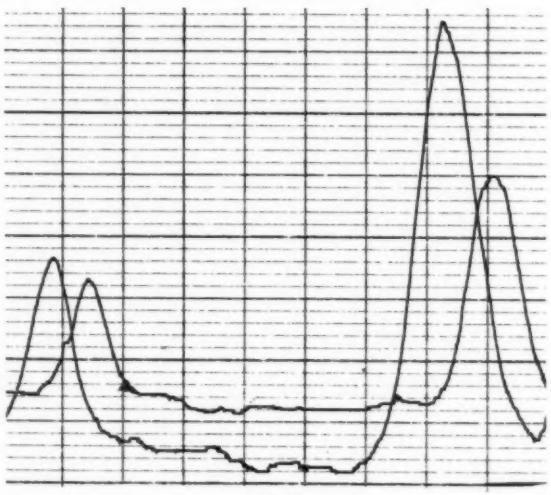

(b)

Fig. 4. Emulsion density vs distance across analyzer face. Densitometer trace of analyzer photograph made with maser light. Trace of calibrating nulls (first and third peaks) superimposed on trace of incident nulls (second peak). (a) Focused; (b) defocused.

of linearly polarized continuous light [Fig. 5(c)] The maser photographs are characterized by rough null edges, especially apparent when the maser is operated near threshold pump light energy [Fig. 5(b)]. This produced a ragged densitometer trace, pictured in Fig. 4(a). To facilitate measuring, we

* Film sensitivity at ruby maser wavelength (6943 Å) is generally down. The pictures shown were taken with Ansco Hypopan, developed in straight Dektol at 24°C for 6 minutes. Polaroid speed 3000 film was also used successfully.

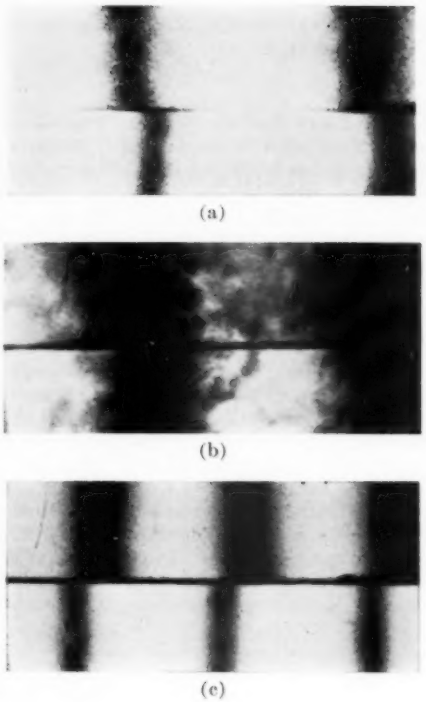

(a)

(b)

(c)

Fig. 5. Photographs taken through polarization analyzer. Upper nulls from calibrated light; lower nulls from incident light. (a) Maser light—normal pump light energy; (b) maser light—pump light energy near threshold of maser action; (c) collimated, linearly polarized, continuous, monochromatic, green light.

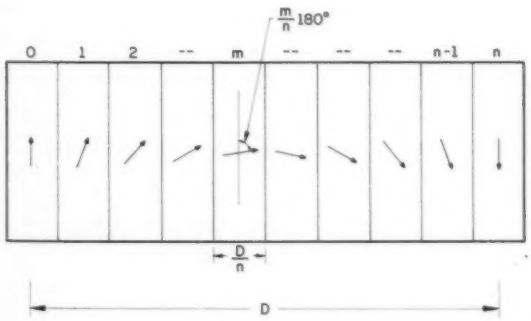

Fig. 6. A calibrating polarizer providing n-calibrating nulls per 180° of azimuthal angle.

averaged over the ragged curve by defocusing the densitometer. The result was a smooth trace, as shown in Fig. 4(b).

We had some difficulty with the optically active element. Rotation was not a linear function of y. This was due (a) to twinning in the quartz, which caused the optic axis to change direction part way through the quartz, and (b) to the optic axis being off normal to the entrance face of the active element.

Monochromatic light must be used, since optical activity is in general dispersive. The light beam under analysis must be well collimated and parallel to the optic axis, or rotation will become nonlinear, and a function of x as well as of y.

Appendix

A Calibrating Polarizer Providing n-Calibrating Nulls per 180° of Azimuthal Angle

Let 180° correspond to a distance D across the exit face of the analyzer at some given wavelength. The calibrating polarizer is constructed of $n + 1$ vertical elements, each of width D/n, as in Fig. 6. The strips are cut and oriented so that the strip with its center at $(m/n)D$, $0 \leq m \leq n$, has its orientation at an angle (m/n) 180°. Unpolarized light of the proper wavelength is passed through the system, and the analyzer oriented until nulls appear across the exit face. There will be nulls every $180/n$ degrees. Errors due to nonlinearity of the $\zeta(y)$ function will be reduced.

We wish to express our deepest thanks to Jack T. Smith for his ideas, assistance, and encouragement throughout the work described. In particular, we gratefully acknowledge his suggesting an optical comparator for null position measurements, and use of calibrating polarizers on the front face of the active element. We wish also to thank Antonio F. Quesada for helpful discussions.

References

1. H. G. Jerrard, J. Opt. Soc. Am. **38**, 35 (1948).
2. H. Takasaki, J. Opt. Soc. Am. **51**, 462 (1961).
3. T. Lentz and J. Miyata, J. Opt. Soc. Am. **51**, 890 (1961).
4. W. Budde, Appl. Opt. **1**, 201 (1962).
5. M. H. de Sénarmont, Ann. Chim. Phys. Troisième Série **28**, 279 (1850).
6. W. A. Shurcliff, *Polarized Light* (Harvard University Press, Cambridge, Mass., 1962).
7. A. F. Quesada, "General considerations regarding polarization of plane harmonic waves," unpublished.
8. V. Evtuhov and J. K. Neeland, Appl. Opt. **1**, 517 (1962).

September Feature

Spectroscopic Instrumentation

Books for review should be submitted to the Managing Editor, APPLIED OPTICS, 1155 16th St., N.W., Washington 6, D.C.

Lasers, Generation of Light by Stimulated Emission. By B. A. LENGYEL. Wiley, New York, 1962. $6.95. 125 pp.

Dr. Lengyel belongs to that fortunate generation of physicists whose research careers encompassed the development of microwave radar in World War II, the postwar developments in ferrites and semiconductors, masers, and finally lasers. The applications of the physics of the period 1900–1940 have dominated this exciting era in electrical engineering.

The preface tells us that "in the confusion of newspaper publicity and the scrambling for contracts, scientific fact, engineering achievement, and promotional optimism merged in such chaos that even the workers in the field became uncertain about what had already been accomplished, what was earnestly and logically hoped for, and what was brightly predicted or lightly promised." The newspaper publicity given lasers and masers has indeed far exceeded that which might have been reasonably regarded as necessary to inform the public about these developments. Science reporters have made a sincere effort to be accurate and objective. They have not succeeded too well because a number of physicists have not given the news media accurate impressions of the importance of their work and its relation to that of others. What is even worse is that inaccurate and incomplete accounts have often been accepted by much of the scientific community. One of the motivations for Dr. Lengyel's book is this problem, which was created by some of our best-known physicists, a few universities, and our largest research laboratories. Perhaps an equally talented effort can be made to improve matters.

This book then proceeds to the task of leading the reader through the laser field. This is done in a manner which is absorbing, objective, and clear. First we have a short discussion of the laws of radiation, coherence, and stimulated emission. This is followed by a description of ruby lasers. The motivation for the development of four-level rare earth lasers is explained nicely. The improved understanding of the modes in a Fabry-Perot interferometer, due to Fox and Li, is summarized in a useful way. A detailed discussion of the ruby laser is then given. This includes: the causes and cure of the relaxation oscillations, the sapphire coated cylinder, and the continuous-operating ruby laser. This is followed by description of the rare earth lasers. Chapter 14 discusses the possibility of liquid lasers employing chelates. The clear and concise descriptions are continued, taking us through the electrical discharge method of creating inverted populations in a gas, and the helium-neon laser. A realistic discussion of the current outlook and current problems terminates the book.

A thin volume (125 pp.) could hardly be expected to be complete. There are no rigorous discussions of photon correlations, nonlinear phenomena, relaxation phenomena, or certain features of the quantum theory which had to be thoroughly understood by the research workers who developed the first devices. It was inevitable that the early publication would result in omission of some important later developments such as: the semiconductor laser, the europium benzoylacetonate laser, and the negative result in the attempt of Sanders to confirm the coherent amplification of light which Butayeva and Fabrikant claimed to have observed in 1957.

The specialist in this field will find here some hours of enjoyable reading. The nonspecialist who reads this book carefully will be rewarded by an interesting, often exciting introduction to this new field of technology.

J. WEBER

Advances in X-Ray Analysis. Vol. 5. Proceedings of the Tenth Annual Conference on Application of X-Ray Analysis, August, 1961, Sponsored by the University of Denver and Denver Research Institute. Edited by WILLIAM M. MUELLER. Plenum Press, New York, 1962. 564 pp. $17.50.

In the eleven years (through 1962) of its existence the Denver X-Ray Conference has firmly established itself as a model kind of symposium for reporting progress and exchanging ideas within one area of science, albeit one growing in size and complexity. As James P. Blackledge says in his foreword to this published collection of contributions at the Tenth Annual Conference in 1961: "Knowledge, unlike money, cannot be given away; when shared, it remains more than ever the possession of the giver while at the same time cherished by the receiver." The present volume is the fifth of the published proceedings, since unfortunately the first five Conferences representing the tentative growing stages were not put into permanent recorded form.

Of greatest interest is to follow the real advances in x-ray analysis through the five volumes; to find clearly the evidences of contagious enthusiasm in sharing new ideas and approaching mutual problems, successfully materializing in a succeeding volume; to feel even from the printed page the fraternal spirit drawing devotees of x-ray science more closely together. It is safe to say that the Denver Conference has done more than meetings of any kind to generate the progress which is so highly characteristic of x-ray analysis today. Part of this is due to the elimination of extraneous activities of the large national society meetings; part is due to the expert management of Professor Mueller and his associates of the University of Denver and the Denver Research Institute; another part is due to the complete willingness to consider practical applications of x-ray techniques to modern industry, without apology, but at the same time to face without fear the mathematical complexities of single-crystal analyses if need be; and a large part to the fact that the carefully written and edited presentations are easily within reach of those who keep their libraries as well as ideas up to date.

The 10th Conference recorded in Volume 5 was surely one of the very best in diversity of topics, in clear evidence of the lines of advance since the 9th Conference and Volume 4, and in the participation of a distinguished group of foreign x-ray experts whose names and work are known even to the novice—Guinier of Paris with the first article on the evaluation of 20 years of progress in x-ray diffraction techniques, appropriately anticipating the 50th anniversary of the Laue discovery of crystal diffraction; Nowotny of Vienna, great expert in crystal chemistry, as is Goldschmidt of Birmingham, England; Leroux, Claisse, and Samson of Canada. And then a group of Americans who make one swell up with pride—representatives of universities, institutes, government agencies, industries including a remarkable number from those concerned with aircraft, space research, and electronics. The remarkable contributions on very soft x rays by Henke and associates whose pioneer achievements come from a comparatively small college, Pomona, are a real impetus to creative research everywhere. This volume comprises 49 articles, together with the record of pertinent discussion which followed the presentation of each paper. For several years there has been an interesting competition in the growth, improvement, usefulness of x-ray fluoresence spectrometry for elemental analysis, and x-ray diffraction analysis of crystalline materials. Here the score turns out to be 26 for diffractometry and 22 for spectrometry. Among the former are 10 articles on high-temperature

continued on page 832

Hole-Burning Model of Oscillation of Ruby Laser

A. J. DeMaria and R. Gagosz

A STL high-speed image converter camera has been used to study the time variation of the output radiation from a 15-cm long ruby laser, the latter being operated with detached external reflectors separated by 61 cm. These data offer additional support for the "hole-burning" model type of oscillation for ruby lasers. The simultaneous oscillation during one pulse of a ruby laser at two optical frequencies corresponding to the eigenwavelength of the Fabry–Perot cavity has been photographed.

Introduction

The fact that the output radiation from ruby optical masers (lasers) consists of pulses which vary randomly with time and position across the crystal face was recognized early in the development of these quantum devices.[1,2] The position and time variation of these pulses of coherent radiation have been studied using a variety of experimental techniques,[3–12] but, in general, the investigations have been limited to studying the emitted radiations from a ruby laser utilizing a relatively short separation between the Fabry–Perot reflectors. This paper reports the results of a study of the emitted radiation from a ruby laser utilizing a relatively long separation between the Fabry–Perot reflectors.

Of particular interest is: (1) the presentation of additional data supporting the "hole-burning" effect on the R_1 line profile as suggested by Hughes[5]; (2) evidence that two portions of the ruby rod may simultaneously undergo oscillation at two different optical frequencies thereby yielding beats where the two areas intermix; and (3) the simultaneous oscillation at two optical frequencies corresponding to the eigenwavelengths of the Fabry–Perot cavity has been photographed.

Experimental Apparatus

The experimental apparatus is schematically illustrated in Fig. 1. A 15-cm long, 0.6-cm diam, 90-deg oriented ruby crystal having two detached 13-layer dielectric reflectors of reflectivity 98 to 99% was energized by two EGG FX-45 flash lamps. The reflector separation was 61 cm. The ruby rod and the flash lamps were housed in a circular aluminum cavity with the inside surfaces polished. A small portion of the laser beam was coupled into the camera by the angular positioning of a fused quartz optical flat. The image of the external reflector was centered on a horizontal slit having a width of approximately 250 μ. The slit was then imaged on the photocathode of a Space Technology Laboratories, Inc., image converter camera.[6] In this manner the slit image can be streaked across the photographic film at various velocities and time durations. The emitted light from the other Fabry–Perot reflector was used to trigger the camera and an oscilloscope on the first pulse by using a fiber-optic, phototube, and trigger amplifier arrangement having a delay of approximately 30 nsec.

Experimental Results and Discussion

A typical streak photograph of the radiation emitted from the 250-μ slit of the center portion of the end of the ruby rod when operated approximately 100% above threshold is illustrated in Fig. 2(a). The time duration between the individual micropulses was calculated from a knowledge of the streak velocity and optical image magnification of the camera, and this also is shown in Fig. 2(a). The number of pulses per unit time and the time relationship between the camera shutter opening and the laser pulses as recorded by a dual beam oscilloscope is illustrated in Fig. 2(b). The streak velocity and shutter opening time were 3.3 mm/μsec and 10 μsec, respectively; the oscilloscope sweep was 5 μsec/div. The decay time constant of the photodetector was made purposely long in order to permit easy observation of the laser pulses at the 5 μsec sweep speed. Figures 3 and 4 illustrate typically the radiation emitted from the slit when the quantum device was operated between 30–50% and 10–20% above threshold, respectively. The streak velocity

The authors are with the United Aircraft Corporation Research Laboratories, East Hartford 8, Connecticut.

Received 7 January 1963.

Note in proof: A Letter referring to the work of Tang *et al.* will appear in a later issue.

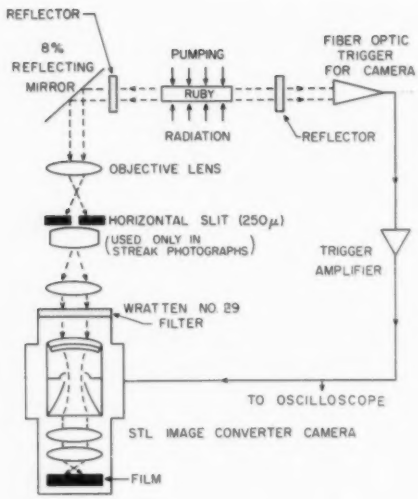

Fig. 1. Experimental apparatus.

and the shutter opening durations were identical to those used to obtain the results shown in Fig. 2.

In general, the data reveal that for the ruby rod under investigation under the stated pumping intensities, and reflector separation, the pulsed nature of the radiation emitted from this ruby may be categorized as

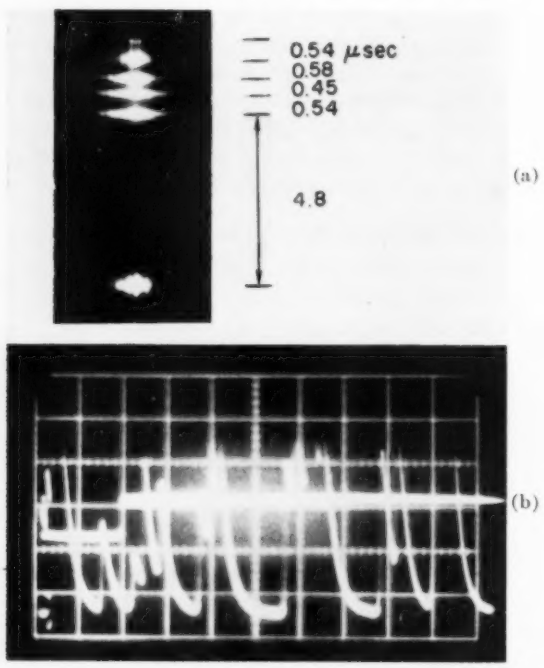

Fig. 2. (a) Streak photograph of the radiation emitted from the ruby laser when operated approximately 100% above threshold. (b) Dual-beam oscilloscope trace of time relationship between camera shutter opening and laser pulses. Streak velocity: 3.3 mm/μsec; open shutter duration: 10 μsec; oscilloscope sweep: 5 μsec/div. Time is increasing from top to bottom of Fig. 2(a).

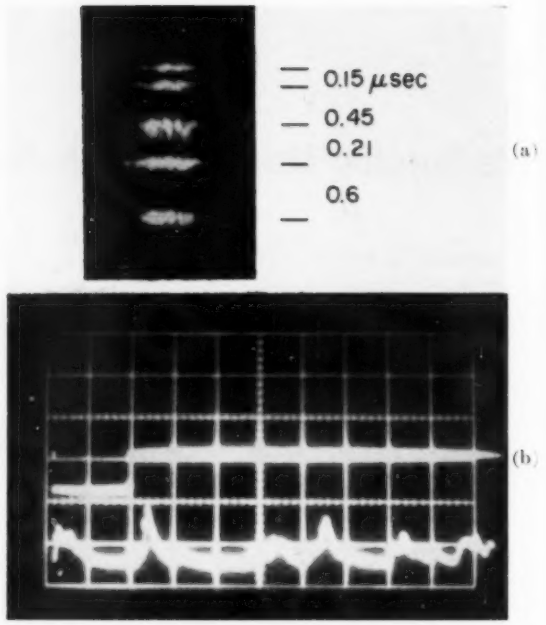

Fig. 3. Streak photograph of the radiation emitted from the ruby laser when operated between 30–50% above threshold. All other parameters were identical to those used to obtain the results of Fig. 2.

follows: (1) a burst of radiation approximately 1 μsec in duration with a time interval between bursts (which is dependent on the pumping intensity) of between 3 to 10 μsec, (2) a micropulse of radiation whose time duration and time interval between micropulses are measurable in tenths of microseconds and a number of which make up the aforementioned bursts. It was also noted that the number of bursts and the number of micropulses contained within the bursts increased with increasing power excess above threshold.

The occurrence of the ensemble of micropulses is believed to be due to the small frequency separation between the eigenwavelengths of the Fabry–Perot cavity resulting from the relatively large separation of the reflectors. The micropulses ensemble can be explained as due to a rapid depletion of the excited Cr^{3+} ions in the portion of the ruby E-energy level that is superimposed by the eigenwavelengths of the Fabry–Perot cavity as suggested by Hughes.[5] As the population of the E-energy level increases with respect to the ground state, the eigenwavelength of the Fabry–Perot cavity lying nearest the peak of the R_1 line profile will be the first to achieve population inversion sufficient to sustain maser action, and an output micropulse will result. If during this process, the rate of stimulated emission, which is greatly intensified by the positive feedback effect of the Fabry–Perot cavity, is larger than the rate of input of excited Cr^{3+} ions into the E-energy level, the excited ions lying in and around this

eigenwavelength will be depleted to a point where maser action will cease. A short while later, the next eigenwavelength further down on the R_1 line profile will repeat the process, etc. For a given pumping intensity, maser action will be possible only for a given wavelength range due to the increasing slope of the line profile as one moves further from the peak and the tendency of the competing relaxation processes to fill in the "burned holes" in the line. In agreement with this model, the data show an increase in the number of micropulses making up a burst ensemble with increasing pumping power. The frequency separation of the eigenwavelength for the 15-cm long ruby laser with detached reflectors separated by 61 cm is approximately 200 Mc/sec. One would then expect from the model (and it is verified by the data) that for the stated pumping intensities, the time interval between the micropulses is much shorter than the time interval between the micropulse ensembles. The fact that past investigations have been limited to studying the emitted radiation from a ruby laser utilizing a relatively short separation between the Fabry–Perot reflectors is believed to be the reason why the ensemble of micropulses were not previously reported.

The fact that radiation is emitted simultaneously from separate points on the crystal face as illustrated by Fig. 4 is evidence of a strong cross-coupling within the crystals.[6] Patterns of this type are believed to be caused by high-order modes as photographed by Hughes and Young[9] for ruby lasers.

In order to observe more closely the time and position variation of the micropulses of radiation emitted by the laser, the camera streak velocity was increased to 16 mm/μsec and the shutter speed was reduced to 2 μsec. All other conditions were identical to those employed in Fig. 3. The resulting streak photograph (Fig. 5) shows that two portions of the ruby rod were simultaneously undergoing oscillation at two optical

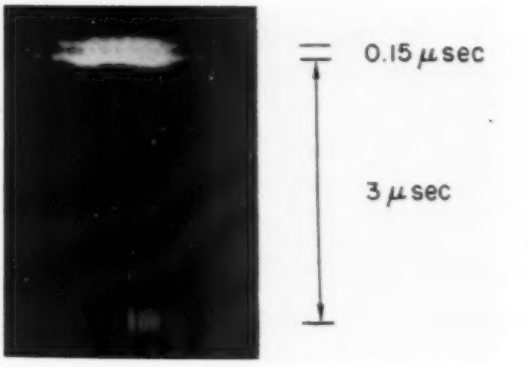

Fig. 4. Streak photograph of the radiation emitted from the ruby laser operated between 10–20% above threshold. All other parameters were identical to those used to obtain the results of Fig. 2.

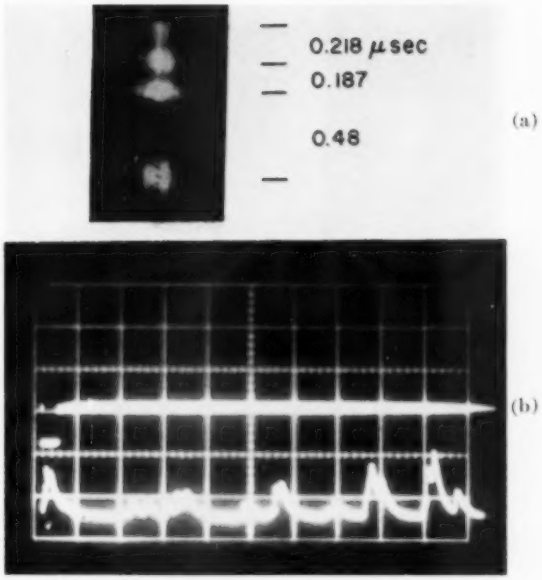

Fig. 5(a). Streak photograph illustrating 11.5 Mc/sec beats in radiation emitted from the ruby laser when operated between 30–50% above threshold. Streak velocity: 16 mm/μsec; open shutter duration: 2 μsec; oscilloscope sweep: 5 μsec/div. Time is increasing from top to bottom of Fig. 5(a).

frequencies, differing in frequency by approximately 11.5 Mc/sec, thereby yielding 11.5 Mc/sec rf beats where the two areas intermixed. Periodic emission with a frequency of 16 Mc/sec have also been observed from this ruby rod. Present theory does not account for this type of behavior but Clark *et al.*[6] have suggested that it may be related to the resonant cavity properties.

At a streak velocity of 66 mm/μsec, the separation between the light bands corresponding to a 200 Mc/sec intensity modulation of the radiation emitted from the slit would equal 0.17 mm. Since this separation can be resolved from a photograph, an attempt was made to photograph the 200 Mc/sec beats resulting from the simultaneous oscillation of the ruby laser at two adjacent eigenwavelengths as previously detected by McMurtry and Siegman[12] by means of a microwave phototube. As nearly as can be determined by a visual measurement with a graduated mm scale on a magnifying glass, the first micropulse of the ensemble illustrated in Fig. 6(a) shows light bands whose separation corresponds to a 200 Mc/sec light modulation. Figure 6(b) shows the light beats in more detail. Figure 6 offers additional support for the "hole-burning" model type of oscillation for ruby lasers. The fact that light beats were not always obtained on repetitive firing of the laser under seemingly identical conditions, appears to rule out the possibility of faulty focusing being the cause of the observed light beats.

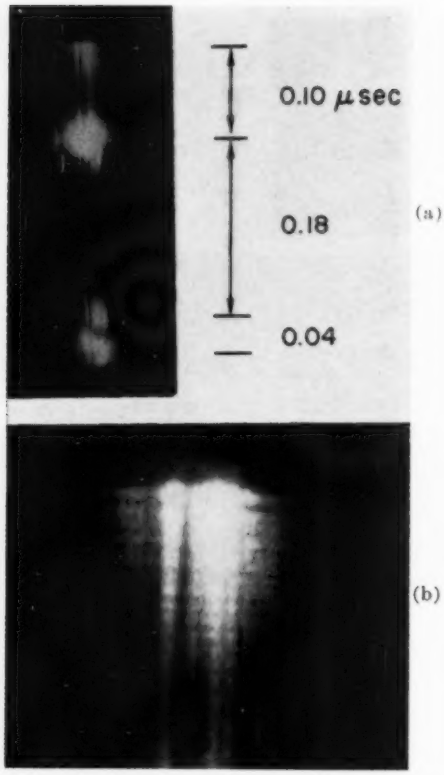

Fig. 6. Streak photograph illustrating the simultaneous oscillation of the ruby laser at two adjacent eigenwavelengths of the Fabry–Perot cavity. Streak velocity: 66 mm/μsec; open shutter duration: 0.5 μsec. Time is increasing from top to bottom. (a) Complete ensemble of micropulses; (b) enlarged photograph of the first micropulse showing 200 Mc/sec beats.

Conclusions

For the ruby rod employed in this investigation and for a relatively large separation between the Fabry–Perot reflectors, the data reveal that at the beginning of laser action, the laser oscillated in bursts made up of an ensemble of individual micropulses of radiation. The occurrence of these ensembles of micropulses of radiation have been explained as due to a rapid depletion of the excited Cr^{3+} ions in the ruby E-energy level by a so-called "hole-burning effect" superimposed on the eigenwavelengths of the Fabry–Perot cavity. It has also been found that present theory does not account for the periodic emission of optical radiation by a ruby laser at various rf frequencies. The photographing of the 200 Mc/sec beats corresponding to the simultaneous oscillation of the ruby laser at two adjacent eigenwavelengths offers additional support for the "hole-burning" model type of oscillation.

It is a pleasure to acknowledge the assistance of T. J. Healey of Space Technology Laboratories, Inc., in the operation of the image converter camera. In addition, thanks are due to V. A. Suprynowicz for reading and making comments on the manuscript and to G. Barnard for assistance in the taking of the data.

References

1. R. J. Collins, D. F. Nelson, A. L. Schawlow, W. Bond, C. G. B. Garrett, and W. Kaiser, Phys. Rev. Letters **5,** 303 (1960).
2. T. H. Maiman, R. H. Hoskins, I. J. D'Haenens, C. K. Asawa, and V. Evtuhov, Phys. Rev. **123,** 1151 (1961).
3. M. Hercher, Appl. Opt. **1,** 665 (1962).
4. G. R. Hanes and B. P. Stoicheff, Nature **195,** 587 (1962).
5. T. P. Hughes, Nature **195,** 325 (1962).
6. G. L. Clark, R. F. Wuerker, and C. M. York, J. Opt. Soc. Am. **52,** 878 (1962).
7. M. S. Lipsett and M. W. P. Strandberg, Appl. Opt. **1,** 343 (1962).
8. E. S. Dayhoff and B. Kessler, Appl. Opt. **1,** 339 (1962).
9. T. P. Hughes and K. M. Young, Nature **196,** 332 (1962).
10. I. D. Abella and C. H. Townes, Nature **192,** 957 (1962).
11. M. Ciftan, A. Krutchkoff, and S. Koozekanani, Proc. Inst. Radio Engrs. **50,** 84 (1962).
12. B. J. McMurtry and A. E. Siegman, Appl. Opt. **1,** 51 (1962).

ERRATA

O. H. Olson, "Selected Ordinates for Solar Absorptivity Calculations," Appl. Opt. **2,** 109 (Jan. 1963).

On p. 110, Table III under the first and second columns:

No.	λ(μ)
4	0.511

On p. 110, Table III under the third and fourth columns:

No.	λ(μ)
7	0.852

W. T. Powers and R. S. Aikens, "Image Orthicon Astronomy at the Dearborn Observatory," Appl. Opt. **2,** 157 (Feb. 1963). *On p. 157,* the equation in the footnote referring to Arcese results should read: $[e/(e+1)]^{1/2}$. That is, the exponent applies to the entire expression—not just the denominator.

On p. 159, Eq. (5) should read:

$$m_s = 2.5\left(5.2 - \log\left\{\frac{d}{7600}\,\frac{[1-(1+4QN_{pb})^{1/2}]}{2Qt}\right\}\right),$$

where

$Q = ekp/2S^2 \ldots$

Interference Rings in Ruby Maser Beams

B. P. Stoicheff and A. Szabo

Interference rings are observed when a ruby maser beam falls on a photographic plate placed normal to the beam, without the use of any lenses. The rings produced by several different ruby rods at distances of 40–700 cm from the ruby rods have been studied. Measurements of the ring radii along with other observations are in good agreement with a simple theory which predicts such ring fringes. The interpretation given here is that these fringes arise from the interference of "off-axis" rays produced by scattering of light in the axial modes at the surfaces or within the ruby rod.

I. Introduction

Several studies[1–3] of the light emitted by a ruby optical maser have demonstrated the occurrence of interference rings concentric with the main beam in the focal plane of a lens (far-field pattern). Abella and Townes[1] have carried out a detailed study of these ring structures. They have shown that the series of rings corresponds to the well-known pattern of a Fabry-Perot interferometer and moreover, that the emission in these rings is of precisely the same frequency and coherent in phase. Their interpretation of the ring structure is that it arises from oscillating angular modes which are coupled to the axial Fabry-Perot resonances as a result of transfer of light between them by a scattering mechanism.

A somewhat similar ring structure has been reported in the direct maser beam, *without the use of any lens.*[1,4,5] A photograph of a typical ring structure obtained in this way is shown in Fig. 1. Maiman *et al.*[4] have stated that the ring radii vary as $(n + a)^{1/2}$, where n is 1,2,3 ... and a is a constant. However, no other experimental results have yet been reported which might help in understanding the origin of these ring structures. The occurrence of such ring structures in the *near field* is implied in the above interpretation of Abella and Townes.[1] On the other hand, Wagner and Birnbaum[6] suggest that they may arise from "off-axis" oscillating modes in the ruby cavity when the cavity length is such that no axial mode is in resonance with the emission line.

In the present paper are reported the results of observations of the near-field ring patterns obtained with several different rubies at various distances from the rubies. Other experiments bearing on the origin of these ring patterns are also described. In addition, an interpretation of the ring pattern based on a simple optical model is given which appears to be in agreement with our experimental observations.

The authors are with the Division of Pure Physics and the Radio and Electrical Engineering Division of the National Research Council, Ottawa, Canada, respectively.

Received 13 September 1962.

II. Experiments and Observations

A. Ruby Patterns

The experimental arrangement for photographing the ring structures is straightforward. The direct maser beam was allowed to strike a photographic plate (Kodak IF and IIIF) at various distances from the ruby, the beam being suitably attenuated by neutral density filters. Five different rubies were used but only four of them produced fringes. Photographs were taken at various distances from the rubies in the range 40–700 cm.

The general appearance of the patterns was similar to the example given in Fig. 1, (except for the angular variations in intensity which differed for the various rubies). Most of the patterns were circular or very slightly elliptical (the latter being due to the lack of exact parallel alignment of the ruby end faces). With one ruby, a part of the pattern (on opposite sides of the central spot) was linear but joined continuously to the ring structure. With another ruby, a part of the ring pattern was double but the spacing was too large to be due to the adjacent longitudinal mode separation.

Although the fractional intensity in the rings was not measured, rather wide variations were observed ranging from barely observable rings to estimated intensities of a few percent of the main beam. The rings were observed at threshold for maser emission and at input

power about 100% above threshold and were unchanged in appearance although of higher intensity. Identical patterns were observed with one ruby at temperatures of 20°, −10°, −70° and −100°C. Ring structures were observed with 0° and 90° ruby rods and with square as well as circular cross sections. For 90° rods the light in the rings had the same polarization as that in the main beam. The occurrence of the ring structures seemed to be unaffected by the conditions of the side wall surfaces or by the silvering of the ends (from a few percent transmission to no silver on one end or none on both ends). In one case, however, rings were observed only after recoating the ends; in another case, improvement of the end polish resulted in much weaker rings.

B. Ring Radii

The ring radii of several photographs were measured with a photoelectric comparator, and the results are given in Table I. Graphs of the ring radii (maxima and minima of intensity) were plotted against the ring number $n^{1/2}$. A typical graph is given in Fig. 2. It is seen that all the experimental points lie on a straight line. Moreover, the line extrapolates to zero at $n = 0$ within experimental error. Similar results were obtained for all of the measurements. These combined results imply that the wavelength of the light in all of the rings is identical and moreover is the same as the axial Fabry-Perot resonances in the main beam. The measured slopes of the resulting straight lines are given in the third column of Table I.

Fig. 1. A typical ring pattern observed when the ruby maser beam falls on a photographic plate placed normal to the beam some distance away from the ruby. This pattern was produced with a ruby rod 4.1 cm long and with a plate to ruby separation of 81.5 cm.

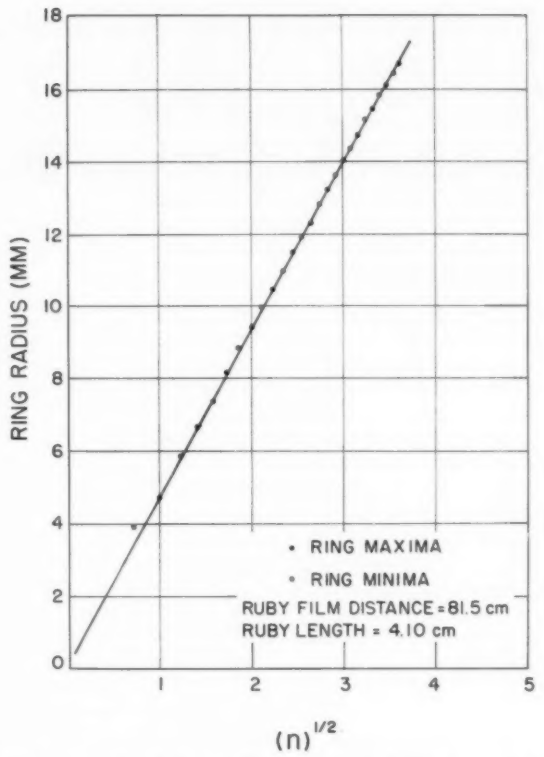

Fig. 2. Graph of ring radii (maxima and minima of light intensity) plotted against $(n)^{1/2}$, where $n = 1,2,3 \ldots$ for the maxima and $n = 1/2, 3/2, 5/2 \ldots$ for the minima.

C. Source of Light in Rings

In an attempt to localize the source of the light producing the rings, the ring pattern of Fig. 1 was allowed to fall on a screen with a 1-mm aperture (small enough to sample one ring at a time), and the ruby face was photographed by placing a lens immediately behind this aperture. Photographs of the ruby face with

Table I. Experimental and Calculated Values of $L(\mu\lambda/t)^{1/2}$ From Ring Radii

Ruby dimensions	Plate distance (cm)	Experimental value (mm)	Calculated value (mm)
4.1 cm (5 mm diam)	40.6	2.45 ± 0.10	2.25
	81.5	4.55 ± 0.10	4.45
	100.0	5.65 ± 0.10	5.46
6.0 cm (4 × 4 mm)	81.5	3.83 ± 0.20	3.68
4.05 cm (8 mm diam)	75.5	4.17 ± 0.10	4.15
5.78 cm (4 × 4 mm)	176.0	8.17 ± 0.10	8.10
	700.0	31.5 ± 1.0	32.2

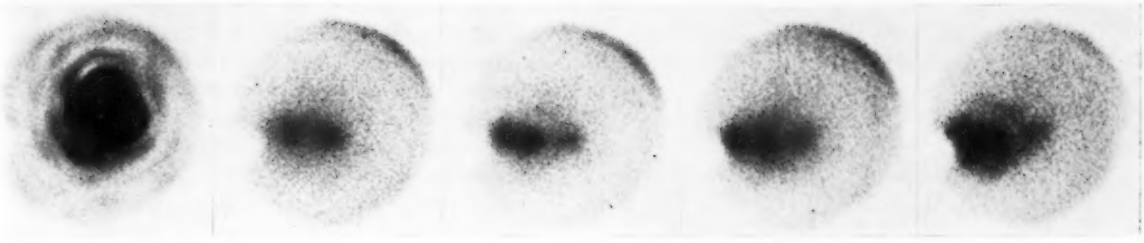

(a) (b) (c) (d) (e)

Fig. 3. Photographs of the ruby emitting face (5 mm diam) taken through a 1-mm diam aperture. (a) Aperture in center of maser beam; (b) aperture 1 cm left of center; (c) 1.1 cm left; (d) 1.2 cm left; (e) 1.3 cm left of center. The photographs are oriented as the ruby face would appear to the eye looking through the apertures. A marker was painted on the left side of the ruby face.

the aperture (together with lens) in various positions in the ring region are shown in Fig. 3.

With the aperture in the main beam, a large emitting area on the ruby face is observed, [Fig. 3(a)]. As the aperture is moved into the ring region, the size of the emitting area on the ruby face becomes smaller. The emitting area consists of two or three small regions which lie approximately in line with the direction of movement of the aperture. Furthermore, the emitting area changes in position on the ruby face as the aperture is moved. While the exact position of the aperture in the ring system was not known in Fig. 3, later experiments in which the aperture was precisely moved through the ring maxima and minima showed corresponding maxima and minima of intensity on the ruby face. In Fig. 4 are shown similar photographs with a 1-cm diam aperture. Here the spot pattern is not observed since the large aperture is sampling several rings at a time (see Sec. III). However, the shift in the emitting area with changing position of the aperture is clearly shown.

D. Inducing the Rings

Since off-axis rays in the ruby are involved in the ring formation, attempts were made to induce the rings by depositing scattering centers such as fine powder on the output end of the ruby. This procedure was unsuccessful; however, partial ring structures were induced by reflecting a portion of the output beam at an angle back into the ruby. This was done using a glass plate a few cm in front of a ruby whose output end was unsilvered. By adjustment of the plate angle near the parallel condition, the original maser beam was seen to be accompanied by a second beam. The variation of the distance between the two beams with plate angle, as well as the intensity of the second beam (more intense than the main beam) indicated clearly that the second beam originated from partial reflection of the main beam at the glass surface and subsequent amplification within the ruby.

When the second beam was made to fall on the ring structure of the main beam, enhancement of the structure was observed in the region of overlap (Fig. 5). As the second beam was brought closer to the center, its interference pattern became linear and tangent to the rings. Also the widths of the fringes were essentially the same as the widths of the rings. These experiments demonstrated conclusively that off-axis rays of the same wavelength as the main beam can lead to the observed ring structures.

III. Theory and Discussion

A. Ring Formation

In the initial attempts to account for the Fabry-Perot-like rings seen in the near field, the question arose as to why rings were observed without a lens following the etalon. That this is possible has been shown by

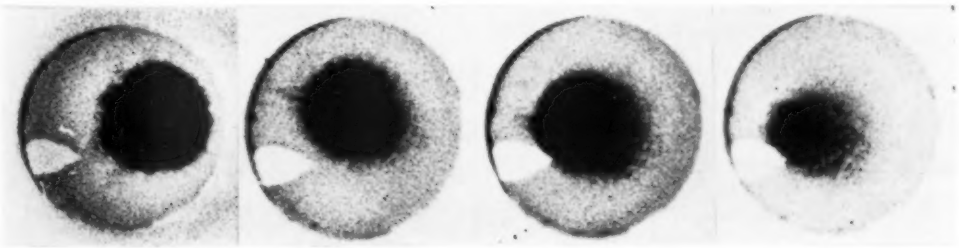

(a) (b) (c) (d)

Fig. 4. Photographs of the ruby emitting face through a 1-cm diam aperture. Aperture to ruby distance = 70 cm. (a) Aperture in center of maser beam; (b) aperture 1 cm left; (c) 1.25 cm left; (d) 1.5 cm left of center.

Fig. 5. Enhancement of the ring pattern when part of the maser beam is reflected at an angle back into a ruby whose output end is unsilvered. A second beam is observed which enhances the ring structure of the main beam on the left.

Tolansky[7] who studied the case of a monochromatic point source of light outside an etalon and the resulting light pattern observed on a distant screen. He showed that the rings were nonlocalized, they diverge in cones from the source and extend outwards from the interferometer into space.

The model which will be analyzed here is that of a point source of monochromatic light between Fabry-Perot plates. In a practical solid-state maser, such a point source (for small angles) may arise by scattering[8] of the light in the oscillating axial resonance modes from inhomogeneities in the crystal or from surface defects in the Fabry-Perot plates. With the aid of Fig. 6, consider first the interference condition for the two lowest-order beams which start from a point source S and arrive at the point P on the observation plane. The optical path length for the first beam (solid line) is

$$S_1 = \frac{\mu a}{\cos\theta_1'} + \frac{L}{\cos\theta_1} \cong \mu a + L + \frac{\theta_1^2}{2\mu}(a + \mu L), \qquad (1)$$

where μ is the index of refraction of the medium in the etalon, and for small angles $\theta_1 = \mu\theta_1'$ and $\cos\theta = 1 - \theta^2/2$. Similarly, the optical path length for the second beam (broken line) is

$$S_2 \cong a(a + 2t) + L + \frac{\theta_2^2}{2\mu}(a + \mu L + 2t). \qquad (2)$$

The small angles θ_1 and θ_2 are related by the equation

$$\theta_2 = \frac{(a + L)\ \mu}{(a + \mu L + 2t)}\theta_1. \qquad (3)$$

The optical path difference is

$$S_2 - {}_1S = 2\mu t - \frac{\theta_1^2(a + \mu L)t}{\mu(a + \mu L + 2t)}. \qquad (4)$$

For constructive interference in the nth ring

$$\theta_1 = \left[\frac{|n \pm \gamma|\,\lambda\mu(a + \mu L + 2t)}{(a + \mu L)t}\right]^{1/2}. \qquad (5)$$

In deriving this result from Eq. (4), we have considered the general condition $2\mu t = (m + \gamma)\lambda$, where m is an integer and $0 < \gamma < 1$. However, if λ is assumed to be the same as in the axial modes, then $\gamma = 0$ because of the cavity resonance condition $2\mu t = m\lambda$. In this case, the radius r_n of the nth bright ring is $L\theta_1 + (a\theta_1/\mu)$, that is,

$$r_n = L\left[\frac{n\lambda\mu}{t}\left(1 + \frac{2(a + t)}{\mu L}\right)\right]^{1/2}. \qquad (6)$$

This reduces to

$$r_n = L\,(n\lambda\mu/t)^{1/2}, \qquad (7)$$

$n = 0, 1, 2 \ldots$ when second and higher order terms are neglected. The radii at which destructive interference occurs are given by Eq. (7) when n has half integral values. To first order, the same results are obtained for beams which start out in the backward direction. When interference between the first and higher order beams is considered, it is found that the various contributions to the total intensity occur at slightly different radii than those given by Eq. (6) and therefore contribute to the widths of these rings. For a line of point sources, the second-order dependence on a also affects the ring widths. An analytic solution to the problem of the radiation pattern produced by scattering centers distributed over a finite volume inside the etalon has not been obtained. It might be noted, however, that the problem is similar (except for the coherence and amplification aspects) to that analyzed by Kastler,[9] namely, the investigation of the interference pattern from a medium between Fabry-Perot plates emitting incoherently.

Table I gives a comparison of the theoretical slope [Eq. (7)] of plots of r_n vs $(n)^{1/2}$ with experiment. For the calculation, $\mu = 1.76$ and $\lambda = 6940$ Å were assumed. The calculated and observed constants in Table I show a tendency for the theoretical values to be smaller than the experimental values by about 5 %. This is of the correct sign and magnitude which the second-order terms in the theory contribute, depending, however, on an arbitrary choice of a in Eq. (6).

An explanation of the spot pattern on the ruby face

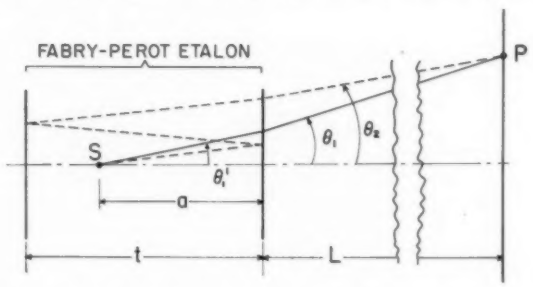

Fig. 6. Two light beams from a monochromatic point source S within a Fabry-Perot etalon arrive at point P on the observation plane and produce interference effects.

observed by photographing the face through a small aperture in the ring region can be given in terms of the model. The spots can be interpreted as the multiple beams which leave the ruby face and interfere to produce each ring. Referring to Fig. 6, the multiple beams (only two shown here) are seen to leave the face in different regions, each of which is displaced from the region producing the main beam. The observed spot spacings were in approximate (±30%) agreement with the theory. For an aperture which samples several rings as in Fig. 4, the spot pattern is no longer observed presumably because the multiple beams for the various rings overlap to form a continuum. An over-all shift of the pattern, however, would still be expected.

B. Ring Widths

One of the most puzzling aspects of the ring structure, which at first glance is not readily explained by the preceding model, is that ring widths are observed which are much smaller than the oscillating cross section in the ruby. For a source of finite dimensions which is spatially incoherent, the ring widths would be strongly affected by the source size[10] since each small emitting volume produces a ring pattern which adds to patterns produced by other volumes. Thus an incoherent source which is large compared to the ring spacings would not exhibit ring structure because of overlap. When the source is spatially coherent, these simple considerations are no longer valid and an analysis must consider both the phase and amplitude from each source point in the oscillating volume. Coherence over the entire oscillating volume of ruby maser is, in fact, strongly implied from recent measurements on maser beams which indicate coherence over the entire wavefront[2,11] and a coherence length of ~3000 cm.[12]

C. Diffraction

Diffraction of the beam inside the ruby etalon will contribute off-axis rays which may then interfere to produce rings. However, this source of off-axis radiation is present in *all* optical maser cavities while experimental observations show a wide variation in ring intensity for different rubies having similar size oscillating regions and hence presumably similar diffraction losses.[13] This observation, it would appear, favors the idea that surface or volume inhomogeneities[8] are the main source of the nonaxial light.

D. Off-Axis Oscillation

Theories[6,14] of oscillation modes in Fabry-Perot cavities have been advanced which predict off-axis oscillation, and the question naturally arises whether the rings are caused by such oscillation. The experimental results do not favor this interpretation for the following reasons. According to theory, off-axis oscillation occurs at a higher threshold than axial oscillation. Experimentally, however, the rings appear as soon as threshold is reached for the axial modes. Also, the theories predict that the propagation angles (and hence the ring radii) are dependent on the position of the axial cavity resonances relative to the center of the emission line. This position would certainly strongly depend on the ruby temperature, however the rings are observed, at the same radii over a wide range of temperatures.

Conclusions

It has been shown that nonlocalized interference rings are obtained with ruby maser beams under a variety of experimental conditions. The ring radii are found to vary with the order number as $(n)^{1/2}$ and not as $(n + \gamma)^{1/2}$, where $0 < \gamma < 1$. This result implies that the light in the rings has the same wavelength as the light in the axial modes of the ruby cavity. These observations are in agreement with a simple optical model proposed here to explain the origin of the rings, namely, that light from the axial modes is scattered within or on the end faces of the ruby in all directions and that interference takes place at certain angles which are almost the same as for the usual Fabry-Perot fringes (using a lens). In this optical model it is not necessary to invoke oscillating "off-axis" cavity modes.

We wish to acknowledge the skillful fabrication of the ruby rods by J. N. Cairns, the technical assistance given by E. L. Dimock and E. Pfitzer, and interesting correspondence with J. I. Masters.

References

1. I. D. Abella and C. H. Townes, Nature **192,** 957 (1961).
2. J. I. Masters and G. B. Parrent, Jr., Proc. Inst. Radio Engrs. **50,** 230 (1962).
3. M. S. Lipsett and M. W. P. Strandberg, Appl. Opt. **1,** 343 (1962).
4. T. H. Maiman, R. H. Hoskins, I. J. D'Haenens, C. K. Asawa, and V. Evtuhov, Phys. Rev. **123,** 1151 (1961).
5. R. J. Collins (private communication).
6. W. G. Wagner and G. Birnbaum, J. Appl. Phys. **32,** 1185 (1961).
7. S. Tolansky, *An Introduction to Interferometry* (Longmans, Green and Co., London, 1955), p. 191.
8. W. Kaiser and M. J. Keck, J. Appl. Phys. **33,** 762 (1962).
9. A. Kastler, Appl. Opt. **1,** 17 (1962).
10. S. Tolansky, ref. 7, p. 195.
11. D. F. Nelson and R. J. Collins, J. Appl. Phys. **32,** 739 (1961).
12. D. A. Berkley and G. J. Wolga, Phys. Rev. Letters **9,** 479 (1962).
13. A. G. Fox and T. Li, Bell System Tech. J. **40,** 453 (1962).
14. J. Kotik and M. C. Newstein, J. Appl. Phys. **32,** 178 (1961).

Papers to appear in subsequent issues

Interferometric Measurement of Vibration Amplitudes—*Bowie*
Infrared Transmission through Fogged Salt Windows—*Morrow and Turk*
A Simple Grating Calibrator for the Visible and Vacuum Ultraviolet—*Hammer, Arakawa, and Birkhoff*
Photorefractometer II Measurement of N and K—*Kapany and Pontarelli*
The Use of Polarized Infrared Radiation in Magneto-optical Studies of Semiconductors—*Palik*
An Optical Null Double-Beam Double-Pass IR Spectrophotometer—*Minami*
A Photomultiplier Circuit for Precision Spectrophotometry—*Budde*
Large-Scale Photoelectric Planimeter for Leaves—*Carman*
A New Method for High-Speed Motion Picture Photography of Transparent Drops—*Pfeiffer*
Photometric Accuracy of Infrared Spectrophotometers—*Stewart*
Study of the Fabrication of Aspherical Surfaces—*Sakurai and Shishido*
Transmission of Isotropic Radiation Across an Interface Between Two Dielectrics—*Stern*
Isosceles Total Internal Reflectors as Optical Elements—*Rothstein*
Test of Theoretical Absorption Band Model Approximations—*Burch and Williams*
Performance of Curved Crystals in the Range 3 to 12 Å—*Jones, Paschen, and Nicholson*
Optics in Norway—*Hisdal and Omholt*
Use of an Analog Computer in Side-on Arc Spectroscopy—*Shumaker and Yokley*
The Evaporation Rate of Filament Material from Alternating Current Heated Filaments—*Wilson*
Attenuation by Ozone and the Earth's Albedo in the Middle Ultraviolet—*Green*
Double Monochromator Systems—*Christensen and Potter*
Experiments with the Optical Excitation of Mercury Vapor for the Production of Isolated Fluorescence—*Zito and Schraeder*
Observations of Near Infrared Radiation from the Solar Atmosphere—*Taylor and MacQueen*
Irradiance on a Flat Object Underwater—*Tyler and Shaules*
Kirchhoff Diffraction Pattern Calculations—*Moore*
Electronic Flash Illumination of a Large Wilson Cloud Chamber—*Edgerton*
Interference Filter Spectrometer for Low Intensity Extended Sources—*Carter, MacRae, Nelson, Birkhoff, and Arakawa*
A Universal Spectrophotometer—*Kaye*
The Stressed-Plate Shutter: A New Moderate-Speed Electro-Optical Light Modulator—*Hauser, Smith, and Marlowe*
Infrared Transmission of the Atmosphere to Solar Radiation—*Gates and Harrop*
Measurement of Energy Flux Density Distribution in the Focus of an Arc Image Furnace—*Beyer, McCulley, and Evans*
Irradiance Linearity Corrections for Multiplier Phototubes—*Baker and Wyatt*
Optics in Australia—*Steel*
A New Family of Flat-Field Cameras—*Gelles*
Dispersion in the Vicinity of an Optical Resonance—*Fork and Bradley*
Design for a Wide-Angle, Linear-Output, Horizon-Sensor Optical System—*Palser*
Spectroscopy of Shock-Excited Powdered Solids—*Nicholls, Parkinson, and Reeves*
An Atomic Absorption Spectrophotometer—*Kahn and Slavin*
The PEPSIOS Purely Interferometric High-Resolution Scanning Spectrometer. I—The Pilot Model—*Mack, McNutt, Roesler and Chabbal*
A Two-Wavelength Two-Frequency Ratio Recording Infrared Spectrometer Analyzer—*Bartz and Ruhl*
Predisperser for High-Resolution Grating Spectrographs—*Reader, Marquet, and Davis*
A Redetermination of Some Optical Properties of Calcium Fluoride—*Malitson*
Test Methods in Spectrophotometry: Stray Light Determination—*Poulson*
The Scattering of Infrared Radiation from Clouds—*Bauer*
Beer's Law and the Optimum Transmittance in Absorption Measurements—*Hughes*
Temperature Measurements with an Optical Pyrometer under Adverse Conditions—*Paul*
An Absolute Reflectometer for Use at Low Temperatures—*Hartman and Logothetic*
Field Photometer with Nine-Element Filter Wheel—*Frentress, Young, and Edwards*
On the Astrophysical Work of W. W. Coblentz—*Strong*
Jet-Controlled Arc II: Excitation of Third Spectra—*Moore, Thygesen, Derwin, and Eward*
Illumination of the Slit Source of the Hough-Powell Digitizer—*Rosin*
Bubble Chamber Optics—*Welford*
Illumination of the 60-in. (203-cm) Bubble Chamber—*Rosin*
A Flying Spot Measuring Machine Employing Crossed Glass Fibers—*Palmer*
Absorption Coefficients of Krypton in the 600–996 Å Wavelength Region—*Huffman, Tanaka, and Larabee*
Optical Properties of "Liumogen": A Phosphor for Wavelength Conversion—*Kristianpoller and Dutton*
Optical and Mechanical Properties of Bubble-Chamber Windows—*Reitmayer and Deeg*
Exfocal Pumping of Optical Masers in Elliptical Mirrors—*Roess*
Power Dip of Line Center of Gaseous Lasers—*S. Winsberg*
Optical Harmonic Generation in Two Ferroelectric Crystals—*Smith*
Spectroscopy Applied to Hypersonic Atmospheric Penetration—*Planet*
A New Grazing Incidence Spectrometric Mounting—*Landon*
Coblentz's Contribution to Infrared Spectroscopy—*Jones*
A Technique for Evaluating Half-Wave and Quarter-Wave Plates—*Hall*
Spherical Mirror Oscillating Interferometer—*Herriott*
Spectral Emittance of Refractory Materials—*Blau and Jaspers*
The Influence of W. W. Coblentz on Radiometry—*J. A. Sanderson*
The Trigger Circuit for the 60″ (203-cm) Bubble Chamber Light Source—*Yamamoto and Sims*
Feasibility of a Reflecting Coronagraph—*Zirin and Newkirk*
The Infrared Transmittance of Carbon Dioxide—*Stull, Wyatt, and Plass*
An Automatic Calibrating Apparatus for Standard Scales by Counting Interference Fringes—*Doi, Shimizu, Tsuboi, and Kouno*
Data Processing System for the Automatic Transformation of Observed Plasma Intensities into Their Radial Distribution—*Paquette and Wiese*

Tilted-Plate Interferometry with Large Plate Separations

H. W. Moos, G. F. Imbusch, L. F. Mollenauer, and A. L. Schawlow

With very highly collimated monochromatic light sources, such as optical masers, multiple-beam interference fringes between nearly parallel surfaces are obtained at large separations. Sharp fringes displaying the surface contours have been observed with separations as large as 20 cm. The requirements and limitations of the device are described, as well as some possible applications.

I. Introduction

If a well-collimated beam of monochromatic light passes through a Fabry–Perot etalon, the usual circular fringes are not observed. As there is only a single wavelength and a single angle of incidence, the light is either transmitted or not, depending on how close it comes to satisfying the usual interferometer condition $n\lambda = 2d\cos\theta$ where θ is the angle of incidence, d is the spacing, λ is the wavelength, and n is an integer. With a camera lens focused for infinity, only the central spot of the usual ring pattern is obtained. If the lens is not used, the entire aperture of the interferometer is equally light or dark.

If one of the interferometer plates is tilted slightly, the spacing varies across the plates. Then transmission takes place at those places where the distance between the plates satisfies the above condition. Thus, the pattern of transmission, observed on a screen or photographic plate just behind the interferometer plates, is a map of contours of the interferometer spacing. If the plates are flat, the contours are straight lines.

This arrangement of a Fabry-Perot interferometer with tilted plates is quite similar to the usual Fizeau–Tolansky method for studying surfaces.[1] Its use has been limited to small plate spacings[2] because of the spread in angle and wavelength from most light sources. The spread in angle can be overcome by using a collimator.[3] The extension of the method to large separations requires light sources which are monochromatic as well as collimated. These requirements are just those which can now be readily satisfied with optical masers. The resulting instrument can be used to study surface contours at large separations. Moreover, as the fringe position is very sensitive to the wavelength, the tilted-plate interferometer can also be used for high resolution spectroscopy. For this application, it has some unusual properties which will be described.

II. Theory

The basic difference between the work done previously[1,2] and that described here is the large distance between plates permitted by the extreme parallelism and monochromaticity of the beam. Much of the theory[4] which has been worked out for two very close tilted plates is applicable here. We will review some of these results here, emphasizing certain aspects related to using the interferometer in spectroscopy and at large separations.

The spacing between the plates of the tilted plate interferometer is given by

$$d = d_0 + \alpha x, \tag{1}$$

where x is the distance along the plate and α is the tilt of the plate. For normal incidence, the bright fringes correspond to positions along the plate where

$$n\lambda = 2d. \tag{2}$$

Light entering the instrument is initially perpendicular to one plate and strikes the other at an angle of incidence α. After each successive pair of reflections, the angle of incidence increases by 2α. Thus, rays which have been reflected more times diverge more from the axis, but they also become weaker. If α is small (a typical value would be less than 10^{-4} radians), all beams of appreciable intensity are within a small angle near the axis. Thus, the pattern is sharply defined near the plates and remains so for a considerable distance. In other words, the fringes are localized

The authors are at the Department of Physics and W. W. Hansen Laboratories of Physics, Stanford University, Stanford, California.

This work was jointly supported by the U. S. Army Signal Corps, U.S. Air Force, and U.S. Army.

Received 16 January 1963.

near the interferometer plates, but the divergence of the reflected rays is so small that the plane of observation is not at all critical. In fact, the divergence is so small, that they can be photographed with a camera having a lens, as long as that lens is not actually focused for infinity. By this means a smaller or larger replica of the pattern can be obtained with good sharpness.

For such small values of α, one may as a first approximation neglect the changes in path direction due to the reflection from the tilted plate. The fringe intensity distribution is the same as that of a Fabry–Perot interferometer, except that here the relative phase between beams is a function of position along the plate whereas usually it is a function of the angle of the beam.

The resolving limit may be found by asking how small the distance between two fringes, Δx, may be and the Rayleigh criterion obeyed. From Eq. (2) the resolution in wave numbers is then found. This is similar to the analysis of the Fabry–Perot.[5] One finds then that

$$\Delta\bar{\nu} = \frac{1}{2dN}, \tag{3}$$

where the equivalent number of beams

$$N = \frac{\pi\sqrt{R}}{1-R}. \tag{4}$$

The resolving power of the tilted-plate interferometer is as great as that of the Fabry–Perot interferometer if the effect of the tilt of the plates may be neglected. Moreover, the finesse of the Fabry–Perot interferometer is determined at high reflectivities by the flatness of the plate over the aperture. In the tilted-plate interferometer, since a given fringe uses only a small part of the aperture, the finesse is not critically dependent on flatness of the plates. Inexpensive mirrors used this way can provide very high resolution. However, if one wishes to measure accurately distances from fringe to fringe, a topographical mapping of the contours[3] on the plates may be useful to correct for shifts of the fringes. Finally, it should be pointed out that, since the fringes are localized in the vicinity of the plate, at large plate separations a long focal length lens system is not needed.

One must now consider the effects of the tilt of the plates and the requirements as to how normal the beam should be. Consider a plane wave incident on a tilted-plate interferometer. The angular tilt of the plate is α and the angle of the wavefront to the normal axis is θ. Keeping only the largest terms, the phase difference due to different path lengths between the 0th and nth beams at a point of plate separation d is[6]

$$\beta_n = \frac{2\pi}{\lambda}\left\{2dn\left(1-\frac{\theta^2}{2}\right) - \frac{4}{3}\,d\alpha^2n^3\right\}. \tag{5}$$

The angle θ of the incoming beam leads in second order to a shift in the position of the fringes. Thus the degree to which the incoming beam must be kept normal is not especially stringent. The incoming beam will not be perfectly collimated, however, and there will be a divergence θ_0 in the incoming rays giving a fringe width Δx_{θ_0}. The ratio of this width to the interorder distance Δx is

$$\frac{\Delta x_{\theta_0}}{\Delta x} = \frac{2\theta_0^2 d_0}{\lambda}. \tag{6}$$

For $\theta_0 = 10^{-4}$ rad, $\lambda = 6 \times 10^{-5}$ cm, $\Delta x_{\theta_0}/\Delta x \sim 1$ at about $d_0 = 3 \times 10^3$ cm.

In the case when θ is so small that it may be neglected, Eq. (5) becomes

$$\beta_n = n\beta_0 - \delta n^3, \tag{7}$$

where

$$\beta_0 = \frac{2\pi}{\lambda}\,2d, \tag{8a}$$

and

$$\delta = \frac{8\pi}{3\lambda}\,d\alpha^2. \tag{8b}$$

The intensity is then a modified Airy distribution,

$$I = I_0T^2\left|\sum_{n=0}^{\infty} \mathrm{Re}^{in\beta_0}e^{-i\delta n^3}\right|^2. \tag{9}$$

The effect of the component,

$$e^{-i\delta n^3} \cong 1 - i\delta n^3 - \frac{\delta^2 n^6}{2}, \tag{10}$$

for δn^3 sufficiently small, is to mix components 90° and 180° out-of-phase into the waves which are adding at the point of interest. Thus, the fringe will be slightly less intense at the center and not go to as low an intensity in the dark regions. δ is small, however, and if δn^3 becomes appreciable only at a point where R^n is so small that the succeeding terms do not contribute to the series, there will be no effect on the fringes. Not-

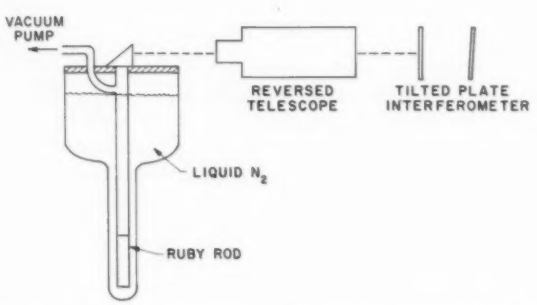

Fig. 1. Optical maser source. The rod was pumped by being placed at the focus of an elliptic cylinder with a linear lamp at the other. Threshold was about 50 J.

Fig. 2. Two fringes from He–Ne optical maser with output at 6328 Å appear vertically. The interferometer separation was 20 cm. The horizontal cross-hatching is due to reflections from air–glass interfaces.

ing the expansion of Eq. (10), a sufficient criterion will be that

$$\frac{8\pi}{3\lambda}\, d\alpha^2 R^n n^3 \ll 1, \tag{11}$$

for all n. This quantity has its maximum value at

$$n = \frac{3}{1-R}\ . \tag{12}$$

For the values of R generally used, this value of n is almost the same as the equivalent number of beams given by Eq. (4).

For a spacing of 10 cm, a tilt, α corresponding to a distance between fringes of 2 cm at 6900 Å, and a high reflectivity giving $n = 50$, Eq. (11) has a maximum value of 0.31. For very high reflectivities and very large distances, larger diameter plates must be used in order to decrease α (at least 2 bright fringes are usually desired on the plate). However, these plates do not need to be extremely flat. Because of the strong dependence on n and hence R, extremely high reflectivities may sometimes be a disadvantage.

III. Sources

Several types of sources were used in our study. The one almost always used was an optical maser, whose output was passed backward through a telescope further to improve collimation (see Fig. 1). The composite ruby rods[7] of about 0.05% concentration were immersed in liquid N_2 and operated very near threshold. The rods are not silvered on the output end, giving an optical cavity of relatively low Q. These rods do not spike at liquid N_2 temperatures. Near threshold the output of this source is highly parallel and monochromatic[8] (as against the usual polychromatic output of an optical maser), the frequency being primarily determined by the maximum of the fluorescence line.

One of the problems with the present source is that it is difficult to distinguish changes in angle from changes in frequency, since both lead to fringe broadening. This problem could be removed by using two lenses and a pin hole collimator between the optical maser and the reversed telescope. The degree of collimation would then be chosen so that the width due to angular divergence [see the discussion with Eq. (6)] is small.

We have also used an He–Ne gas maser with an output in the visible[9] at 6328 Å. Because it is a continuous wave device, we have found it to be very useful for aligning the interferometer and studying materials. Figure 2 shows fringes obtained at 20 cm. At these plate separations, if the reflectivity is very high, one may obtain spurious effects such as ghost fringes. [See the discussion with Eq. (11) and ref. 6.]

Light sources other than masers can be used and studied with this interferometer, but useable plate spacings are limited[2] for even the best of them. For example, the green line from a water-cooled Hg^{198} lamp has a width of 0.018 $cm.^{-1}$ Thus, if we wish to have fringes of width less than a tenth of the inter-order spacing, we are restricted to plate separations less than 3 cm. However, visible fringes can be obtained at larger spacings. For example, Fig. 3 shows that 4358 Å line of mercury from an air-cooled Hg^{198} lamp with an interferometer spacing of 6.1 cm. The light from the lamp was collimated by the usual pin hole and lens combination. Pictures were taken with no lens, and the film about 10 cm from the plates. Exposure time was about 5 sec on Polaroid type 47 film. From the width of the fringes (about 0.6 of the inter-order spacing), the line-width of the lamp is seen to be about 0.05 cm^{-1} under these conditions.

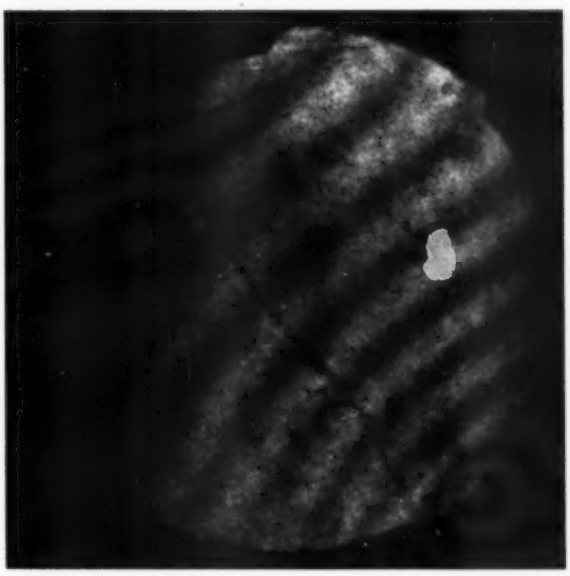

Fig. 3. Hg^{198} 4358 Å line at a separation of 6.1 cm. The exposure time was roughly 5 sec on Polaroid type 47 film.

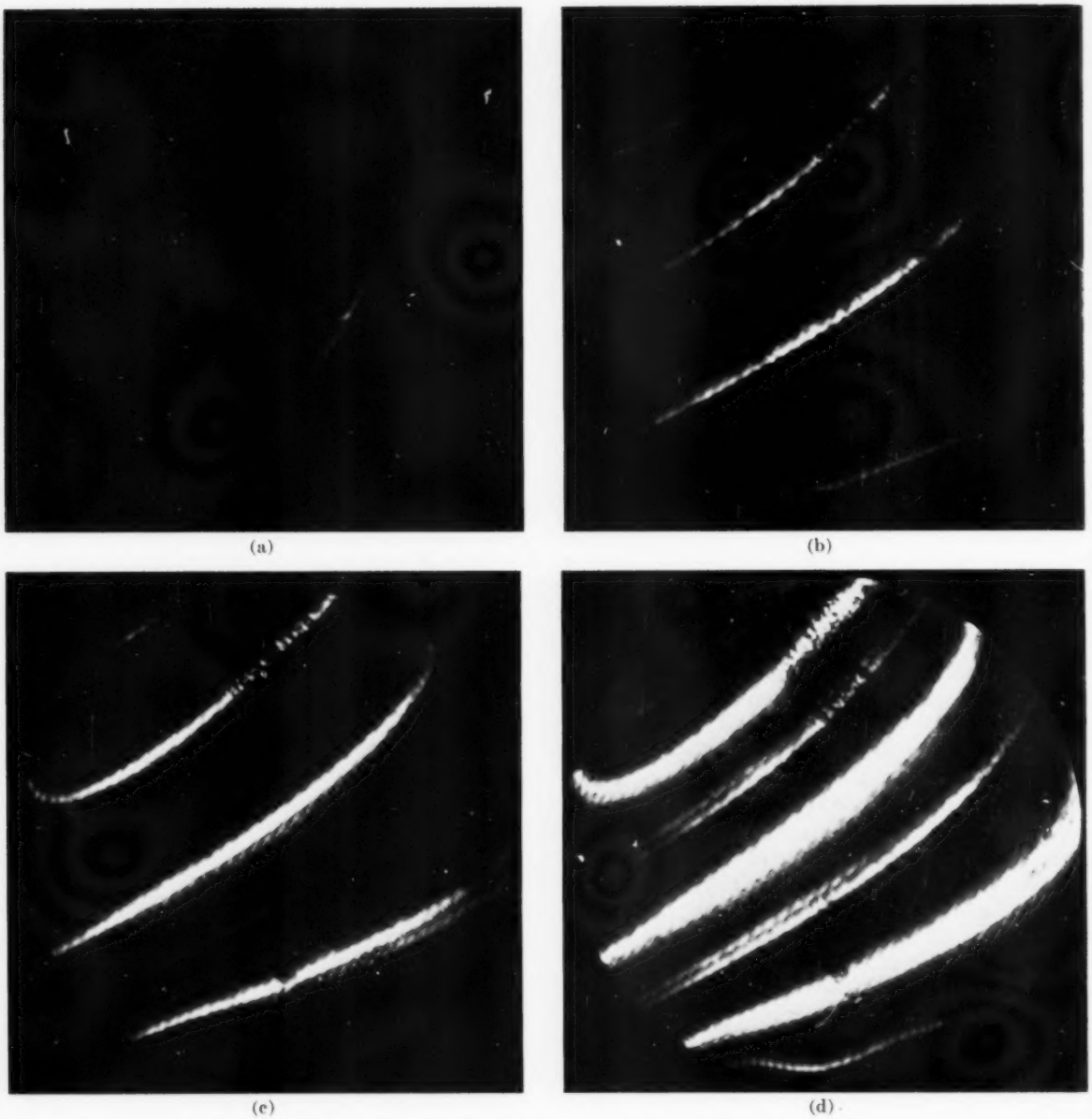

Fig. 4. Output of optical maser source at (a) 0%, (b) 2%, (c) 8%, and (d) 16% above threshold input power. The composite rod was 3 cm long and silvered on one end. The plate separation was 0.6 cm.

An interference filter was used to separate the various spectral lines. If a wedge filter were placed with its apex at 90° with respect to that of the tilted-plate etalon, the various spectral lines would appear at different vertical positions on the plate. Thus, one would have two tilted-plate interferometers in tandem. It should be noted that the aperture of a Fabry–Perot interferometer is generally higher[10] than that of a spectrograph.

IV. Applications

The primary application which we have made of tilted-plate interferometry is as a tool for studying the output of an optical maser. In Figs. 4(a)–(d) are shown a series of single-flash photographs taken with increasing power at a spacing of 0.6 cm. As the power increases, the lines broaden. At these spacings, this is due to changes in frequency rather than beam di-

vergence [see Eq. (6)]. In Figs. 4(c), 4(d), and 7 there is a second fainter fringe whose separation from the bright fringe corresponds to the ground-state splitting. The satellite splitting of the fringes appearing in Fig. 4(d) are probably real. It might be noted that, although the quartz plates used were not flat, as indicated by the curvature of the fringes, the narrow fringes in Fig. 4(a) indicate a high coefficient of finesse. The reflectivity of the silver film was estimated to be between 80 and 90%.

In Fig. 5 is shown the fringes from the optical maser source near threshold at a spacing of 10.5 cm. The width of these fringes is no more than $^1/_{20}$ order, which indicates a total width in the output of less than 2.5×10^{-3} cm^{-1}, or 75 Mc/sec.

Several other applications to the study of the optical maser might be noted. Since the angle may be made very small, the transverse motion of the fringes with frequency variations may be made very large. This high dispersion may be useful in detecting frequency modulated light. If the plates are made completely parallel, the device becomes a discriminator changing frequency variations to amplitude variations. For this application it has the unusual property that the dispersion and resolution can be separately controlled without limit.

One may use the optical maser fringes to align a Fabry–Perot etalon at large separations, by adjusting the plates until the fringes disappear. We have used these fringes with 10- and 20-cm etalons.

Since these fringes may be used to align flats with considerable separations, this can serve as a very accurate method of aiming masers or telescopes. For example, if a flat of diameter a is positioned to within an error of one wavelength from side to side, its angular position is determined within λ/a, which is the diffraction limit for an aperture of that size. With the tilted-plate multiple beam interferometer, considerably greater accuracies are readily obtainable.

When the method is used to study surface contours, with large spacings it is limited by the requirement that the angles between the surfaces be fairly small at all points. This means that only a few fringes can be observed at any one setting, and there is little information about contours at other points on the plates. However, the plate separation may be changed by small fractions of wavelength yielding new contours lying between those previously observed. For this purpose, a mounting,

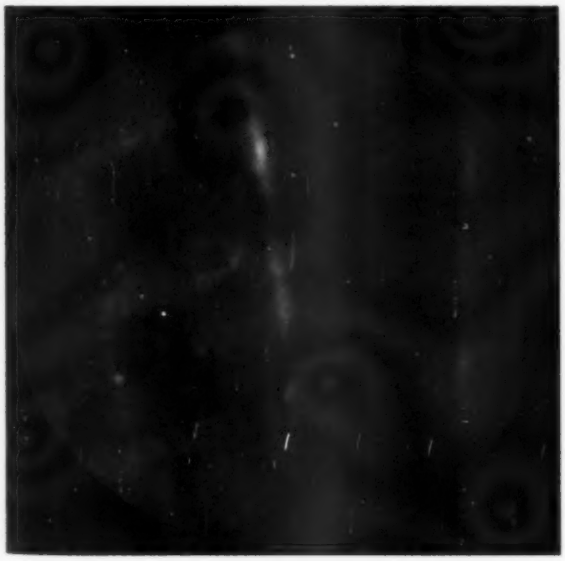

Fig. 5. Optical maser source fringes near threshold. The etalon spacing was 10.5 cm.

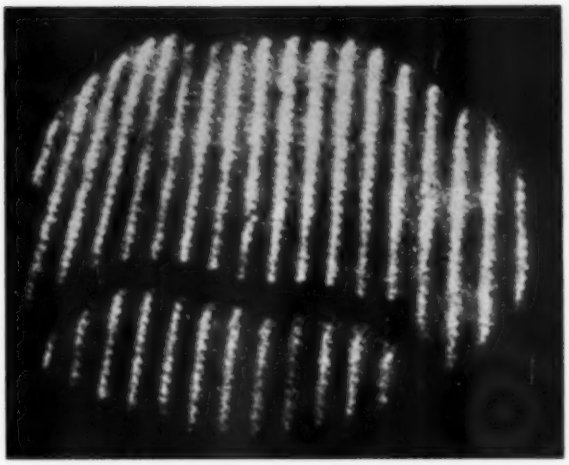

Fig. 6. Tilted-plate fringes showing the shadow of a wire in a plane parallel to the two plates.

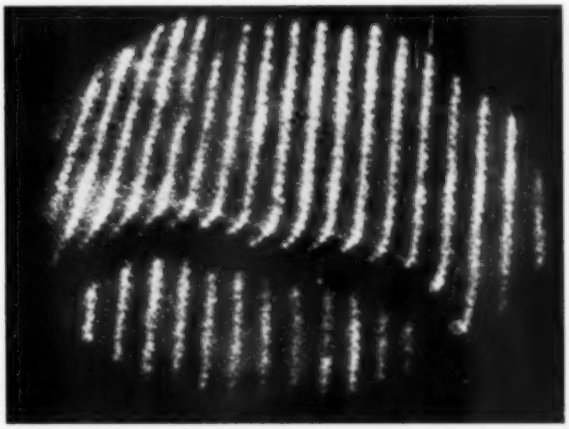

Fig. 7. The distortion of the fringes by the warming of the wire.

similar to that described by Bradley[11] provides a means of moving the plates apart without changing the tilt.

One obvious application is to study the variation of the index of refraction in a material. Since the multiple beam fringes can be made quite sharp, much smaller shifts in fringe position can be seen than with the usual two beam methods. As a demonstration of the sensitivity of the method, the distortion of the fringes by a warm wire was recorded. In Figs. 6 and 7 the wire is in a plane between and parallel to the plates, which are separated by several cm. In Fig. 6 the wire is at room temperature, while in Fig. 7 it has been warmed by passing a current through it. Because of the sharpness of the fringes, very small displacements may be detected. The temperature of the wire was not measured. However, the wire felt scarcely warm when touched by the hand. These pictures were taken with the ruby optical maser source. With a 20-cm etalon, it is estimated that a fractional change in refractive index of one part in 10^7 would be readily observable.

V. Conclusion

With highly collimated monochromatic light sources, such as optical masers, multiple-beam Fizeau fringes are obtained with nearly parallel surfaces at large separations. These fringes have been observed with separations as large as 20 cm. Because of the very small tilt of the plates, the interferometer has the same resolution as that of a Fabry–Perot except at very large separations and very high reflectivities. We have used the instrument primarily to study optical masers. However, because the fringes are localized and also very sharp it should prove to be an excellent tool for studying variations of the index of refraction in materials such as transparent solids, gases, and plasmas.

We wish to thank C. F. Quate for allowing us to use his visible helium–neon optical maser. W. Scott, S. Sears, and G. West provided valuable assistance in the experiments. One of us (A. L. S.) acknowledges a stimulating discussion with N. I. Adams, which helped to suggest this investigation.

References

1. S. Tolansky, *Surface Microtopography* (Interscience, New York, 1960).
2. S. Tolansky, *High Resolution Spectroscopy* (Pitman, New York, 1947) p. 141 *ff*.
3. J. B. Saunders, J. Res. Nat. Bur. Std. **47,** 148 (1951).
4. S. Tolansky, *Multiple Beam Interferometry* (Oxford University Press, London, 1948), Chap. II; J. Brossel, Proc. Phys. Soc. (London) **59,** 224 (1947); M. Born and E. Wolf, *Principles of Optics* (Pergamon, New York, 1959), p. 350 *ff*.
5. F. Jenkins and H. White, *Fundamentals of Optics* (McGraw-Hill, New York, 1957), 3rd ed., pp. 276–278
6. M. Born and E. Wolf, *Principles of Optics* (Pergamon, New York, 1959), p. 352.
7. G. Devlin, J. McKenna, A. May, and A. L. Schawlow, Appl. Opt. **1,** 11 (1962).
8. L. F. Mollenauer, G. F. Imbusch, H. W. Moos, and A. L. Schawlow, Bull. Am. Phys. Soc. **7,** 445 (1962).
9. A. D. White and J. D. Rigden, Proc. Inst. Radio Engrs. **50,** 1697 (1962).
10. P. Jacquinot, J. Opt. Soc. Am. **44,** 761 (1954).
11. J. Bradley, Proc. Roy. Soc. (London) **A262,** 529 (1961).

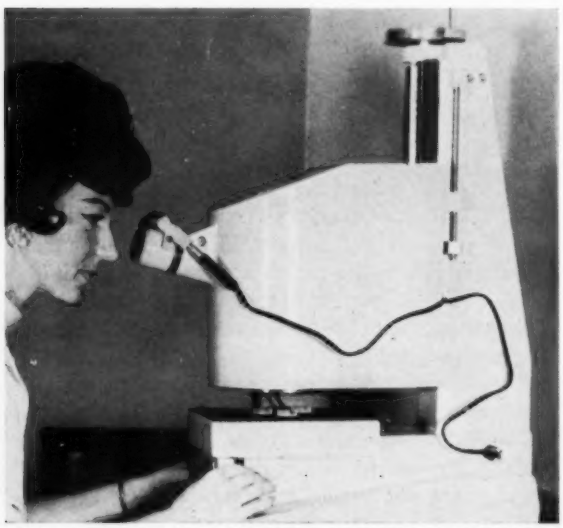

Vivian Santee *Davidson Optronics* uses Davidson D-309 Plano-Interferometer applying the phenomena of mutual interference of light waves to inspect optical windows and flat mirrors for lasers development.

Frederick Brech (left) and John Schuch, co-inventors of the Jarrell-Ash Laser Microprobe, an instrument for bridging the gap between conventional analysis and x-ray micropobe analysis. It should now be possible to make analyses regardless of the electrical conductivity of the sample, the size of the sample, or the position of an element in the periodic table. We hope to have a paper from Mr. Brech on this in the March '64 issue.

Spurious Harmonic Generation in Optical Heterodyning

H. Z. Cummins, N. Knable, and Y. Yeh

An experiment is described in which the simultaneous photodetection of two incoherent light beams chopped at different frequencies yields a direct measurement of the cross-modulation coefficient of a photocathode. This is a technique generally applicable to the measurement of small nonlinearities in photodetectors.

Optical heterodyning or photomixing was first observed by Forrester, *et al.*, in 1955,[1] and has subsequently been employed by several authors in the investigation of optical masers.[2,3] Townes[4] has proposed the application of optical maser heterodyning to Raman spectroscopy and to the measurement of Brillouin doublets. A detailed analysis of the theory of photomixing with both coherent and incoherent light sources has been given by Forrester.[5]

Photomixing occurs at the photocathode of a photoelectric device (usually a photomultiplier), and the current produced is assumed to be proportional to the square of the total electric field strength. The assumption of perfect square-law response is based both on the theoretical E^2 dependence of the photoelectric effect and on the observed linear relationship between light intensity and photoelectric current over a wide range of intensities for real photoelectric devices.

Suppose two plane light waves, $E_1 \sin\omega_1 t$ and $E_2 \sin\omega_2 t$ [where $(\omega_1 - \omega_2) \ll \omega_1$ or ω_2], are allowed to fall with coplanar wavefronts on a photocathode whose response $i(E)$ is given by:

$$i = \alpha_0 + \alpha_1 E + \alpha_2 E^2 + \ldots + \alpha_n E^n + \ldots, \qquad (1)$$

where $E = E_1 \sin\omega_1 t + E_2 \sin\omega_2 t$. If all the α_n except α_0 and α_2 were, in fact, zero (as is usually assumed), the resultant current would contain only one low-frequency component; the difference frequency signal $\alpha_2 E_1 E_2 \sin(\omega_1 - \omega_2)t$. If higher order α's are not strictly zero, they would give rise to signals at harmonics of the difference frequency. Specifically, a term $\alpha_{2n} E^{2n}$ would generate a component at $n(\omega_1 - \omega_2)$.

This process will evidently be very large when the light intensity is great enough to saturate the photocathode, since the departure from linearity of the current vs. light intensity characteristic is then extreme. Even in the supposedly linear region, however, small departures from linearity are of importance since the spurious harmonics generated may be confused with normal beat signals resulting from the presence of other frequency components in the incident light. Such effects would be particularly undesirable in optical maser spectroscopy of the type considered by Townes, since there is particular interest in measurement of harmonics of the fundamental Brillouin shift whose existence has previously been reported by Gross.[6] The harmonics are probably quite small compared to the fundamental and may therefore be masked by spurious harmonics generated in the mixing of the fundamental components with the optical local oscillator.

One could, in principle, measure the α coefficients directly with two single-mode optical masers. Interpretation of optical difference frequency measurements is complicated, however, by the imperfect coherence of real sources which leads to a heterodyning efficiency which may be considerably less than one. We have, therefore, employed another technique which is a simple extension of a method used to measure intermodulation effects in electronic devices.

The detector receives simultaneously the signals from two incoherent sources which are chopped at different frequencies. Since the sources are incoherent, the heterodyning efficiency is negligibly small, and the signals produced at optical difference frequencies are not detected. However, the $\alpha_{4n} E^{4n}$ terms also produce dc signals, and these are modulated at harmonics of the difference between the two chopping frequencies.

The authors are at Columbia University, New York, New York.

Received 28 December 1962.

Work supported by the National Science Foundation, the Army Research Office (Durham), and the Joint Services (U. S. Army, the Office of Naval Research, and the Air Force Office of Scientific Research).

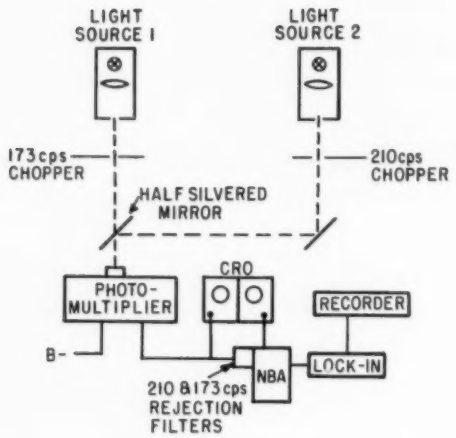

Fig. 1. Schematic diagram of apparatus.

The amplitudes of these modulated signals do not depend on the specific spectral character of the two sources, and may be related simply to the coefficients of Eq. (1).

The apparatus is illustrated schematically in Fig. 1. Two incoherent light sources L_1 and L_2 are arranged to illuminate the photomultiplier PM. (The photomultiplier used was an E.M.I. 9558B with S-20 photocathode which has a quantum efficiency of about 7 % at 6328 Å, the wavelength of the output of a visible helium-neon maser.) The two light beams were chopped mechanically at frequencies ν_1^M and ν_2^M, where $(\nu_1^M - \nu_2^M) \ll \nu_1^M$ or ν_2^M. The two light signals may be represented by $A_1(t)E_1 \sin(\omega_1 t + \psi_1)$ and $A_2(t)E_2 \sin(\omega_2 t + \psi_2)$, respectively, where the phase factors ψ_1 and ψ_2 are randomly varying in time, and the amplitude modulation $A(t)$ is determined by the appropriate mechanical chopper. For a perfectly sinusoidal chopper, the intensity modulation would be given by $(1/2)(1 - \cos\omega^M t)$, where ω^M is the angular frequency of the chopper, and the amplitude modulation would therefore be $A(t) = (1/\sqrt{2})(1 - \cos\omega^M t)^{1/2}$. The total electric field E is thus:

$$E = (1/\sqrt{2})(1 - \cos\omega_1{}^M t)^{1/2}E_1 \sin(\omega_1 t + \psi_1) + (1/\sqrt{2})(1 - \cos\omega_2{}^M t)^{1/2}E_2 \sin(\omega_2 t + \psi_2). \quad (2)$$

If the photomultiplier were a perfect square-law device, we would expect no heterodyning since $E_1E_2 \sin(\omega_1 t + \psi_1) \sin(\omega_2 t + \psi_2)$, the cross term in E^2, has a time average of zero. Only the individual squared terms would contribute, giving rise to signals at ν_1^M and ν_2^M. Spurious heterodyning or intermodulation will occur, however, through the terms α_4E^4, α_8E^8, $\alpha_{12}E^{12}$, etc., since the time average of terms $\sin^{2n}(\omega_1 t + \psi_1) \sin^{2n}(\omega_2 t + \psi_2)$ is not zero. Thus, the group of terms $\alpha_{4n}E^{4n}$ will generate signals at harmonics of the difference chopping frequency $(\nu_1^M - \nu_2^M)$. Unfortunately, deviations from perfectly sinusoidal modulation will tend to confuse the harmonics of the modulation difference frequency generated by the various E^{4n} terms. For example, the α_4E^4 term contains $A_1^2(t)A_2^2(t)$ which contributes a component at $(\nu_1^M - \nu_2^M)$ due to the fundamental terms in the chopping waveforms, but which will also give rise to components at multiples of $(\nu_1^M - \nu_2^M)$ proportional to the products of the appropriate Fourier components in imperfectly sinusoidal chopping waveforms. These components at $n(\nu_1^M - \nu_2^M)$ are indistinguishable from the components generated by the fundamental chopping frequencies through the $\alpha_{4n}E^{4n}$ terms. One could only separate the terms if the Fourier components of the chopping waveforms were accurately determined beforehand by examining the photocurrents produced by each chopped light beam individually. We have, however, limited ourselves in this experiment to a measurement of the fundamental difference frequency $(\nu_1^M - \nu_2^M)$, which can arise only from the α_4E^4 term through the product of the fundamental chopping frequencies.

In this experiment, the two choppers C_1 and C_2 were run at 210 and 173 cps respectively, and the photomultiplier signal was processed with a narrow-band amplifier and lock-in detector tuned to 37 cps. Rejection filters at 210 and 173 cps were included to avoid mixing in the N.B.A., and the last few dynodes of the photomultiplier were biased from a low impedance source to avoid modulation of the dynode voltages. Initially, the photocathode was strongly overdriven in order to produce a large beat signal for tuning the N.B.A. and lock-in. The light intensity was then reduced to bring the photomultiplier well within its nominally linear range. With each light source adjusted to produce a photomultiplier anode peak current of 0.2 mA, the beat signal was measured for total anode to cathode voltages between 700 and 1500 V. At 1100 V (photomultiplier gain = 1.5×10^5) the beat signal was 0.005 mA, or approximately 1% of the peak photomultiplier current. At higher gains, with less incident light required to produce the 0.2 mA anode current, the beat signal was smaller, while for lower gains,

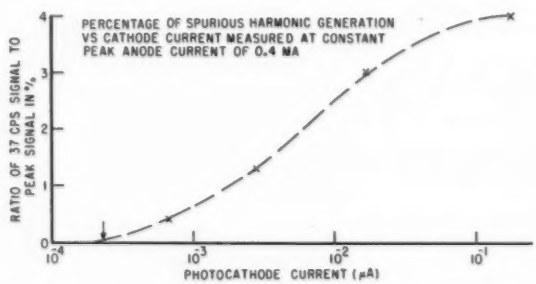

Fig. 2. Experimentally determined spurious harmonic content

the beat power was larger. A plot of the ratio of beat signal to peak photomultiplier current vs. cathode current is shown in Fig. 2. The smallest ratio measured was 5×10^{-4} at a current of 2.3×10^{-4} μA. Measurements at lower currents were precluded by instrumental limitations. For total light inputs of 0.01 μW/cm² to the photocathode, the ratio α_4/α_2 is approximately 10^{-3}.

Conclusions

The technique described above is generally applicable to the measurement of small nonlinearities in photodetectors. The use of incoherent light sources permits the α coefficients of the response function [Eq. (1)] to be measured directly. Once these coefficients have been determined for a particular detector, they may be used to compute the spurious harmonic content which should be anticipated in optical beating experiments with coherent light sources.

For the particular case of a photomultiplier, the measured nonlinearities should be considered as a property of the entire device (photocathode plus dynode chain) rather than of the cathode alone, since spurious harmonics may be generated either through departures from square-law response of the photocathode, or through nonlinear amplification of the fundamental heterodyne signal at the dynodes.

References

1. A. T. Forrester, R. A. Gudmundsen, and P. O. Johnson, Phys. Rev. **99,** 1691 (1955).
2. A. Javan, W. R. Bennett, Jr., and D. R. Herriott, Phys. Rev. Letters **6,** 106 (1961).
3. H. Kogelnik and C. K. N. Patel, Proc. Inst. Radio Engrs. **50,** 2365 (1962).
4. C. H. Townes, *Advances in Quantum Electronics,* ed. by J. R. Singer (Columbia University Press, N. Y., 1961), p. 3.
5. A. T. Forrester, J. Opt. Soc. Am. **51,** 253 (1961).
6. E. Gross, Nature **126,** 201, 400 (1930).

Meeting Reports *continued from page 800*

consisted of C. J. Peters, who spoke on traveling wave phase modulation, E. I. Gordon, who discussed resonant modulation, R. H. Rediker, whose topic was modulation of injector lasers, and J. A. Armstrong, who discussed modulation by propagation in nonlinear media.

Traveling-wave phase modulation of masers and lasers makes use of the linear electro-optic effect, that is, the change in the index of refraction with electric field strength that occurs in certain substances, among which are potassium diphosphate (KDP) and cuprous chloride (CuCl). Dr. Peters described a device in which a crystal of KDP is placed between two parallel metallic bars that constitute a waveguide. As an electromagnetic wave travels from one end of the waveguide to the other, the changing electric field in the KDP changes the index of refraction for the light beam traveling in the KDP and thus changes the velocity of propagation of the light. The velocity of the microwave radiation in the waveguide must be adjusted to be equal to the phase velocity of the light in the crystal by a proper choice of the thickness of the crystal. Composite crystals up to 1 m in length have been employed successfully. This method of modulation appears to be quite satisfactory. In resonance modulation of a light beam, one also makes use of the electro-optic effect. Gordon combined a Fabry-Perot interferometer made from a KDP crystal for the light with a resonant microwave cavity for the modulation at microwave frequencies. This has the disadvantage that the unit heats up while it is being used, with the consequence that it will not stay in tune. Rediker discussed the use of GaAs *p-n* junction-injection lasers. On applying a forward voltage bias electrons are injected from the *n* into the *p* region where they recombine radiatively with holes. At an appropriate bias voltage, there is a population inversion of the energy bands leading to stimulated emission. The rate of recombination of holes and electrons, which determines the rate of light emission, is determined by the rate at which electrons are supplied to the *n* material. Thus, the rate of emission of light depends on the current. The coherent light produced by recombination of the injected carriers can be modulated simply by varying the input current. This is a major advance over optical or electrical discharge pumping for modulating the laser beam. One of the important advantages of GaAs is that the recombination time is very short—just how short is not yet known. But modulating frequencies of well over 1 Gc/sec are possible. Some people think the modulating frequency can be as high as 100 Gc/sec. Armstrong discussed harmonic generations and sum and difference frequency formation by propagation in nonlinear media. For harmonic generation, he makes use of a long birefringent crystal which is cut in such a way that for the direction of propagation chosen the phase velocity of the extraordinary ray of *twice the frequency of the incident light* is the same as the phase velocity of the ordinary ray. This results in energy being transferred from the original frequency to twice that frequency. The nonlinear optical properties in an electro-optic crystal lacking a center of symmetry are determined by a 3×9 tensor of the third rank similar to the piezoelectric tensor. In forming the combination frequencies, the relations $\omega_1 + \omega_2 = \omega_3$, and $k_1 + k_2 = k_3$ apply.

On Friday afternoon, two papers were presented on GaAs in optoelectronic devices. The first of these described a junction diode made of GaAs, which is a high-efficiency, high-speed incoherent source with durable qualities. The second one described a GaAs coherent source of radiation, i.e., a laser. We have already pointed out the advantages of such a laser. A third paper described the CuCl light modulators, for which many advantages were claimed. A fourth paper described a PIN junction diode as a detector of light modulated at microwave frequencies. This diode was made of germanium. The discussion included a consideration of the dependence of noise on frequency. The last paper of the afternoon by R. V. Bez considered switching light with light, absorption edge modulation. Bez claims that, as the speed of operation of electronic digital computers increases, new problems arise of such a nature that it will be advantageous to proceed to a new type of machine designed to operate with light rather than wires and electrons. In such a machine, there is need for an element that will have its transmittance of one optical signal depend on a second optical signal. Semiconductors offer selective optical absorption by any one of four processes for such purposes.

29th Annual Meeting of the American Society of Photogrammetry, Washington, D.C., 24–29 March 1963

Reported by J. V. Sharp, IBM

The papers presented at this conference were primarily in the application, areas of photographic interpretation, mapping and charting projects, instrumental improvements and usage, and mapping and charting subsystems.

In the photographic interpretation area, the papers included applications to counter-guerilla warfare, geographic research, geophysical research, highway design, forestry, satellite photography, and surveys of scientific and military uses. In this P.I. area also, improved techniques were reported in P.I. key usage, measurements of small lake depths, inventory measurements, information extraction, human factors, techniques in the Soviet Union, and progress in automated techniques of photo interpretation. Photo interpretation equipment developments were reported in photo viewing equipment and automated photo interpretation.

Papers on mapping and charting projects included mapping glaciers in Canada, resources in Chile, lunar charts, topographic maps, tidal current charting, highway design, dam site design, and Peace Corps projects. Others covered mapping and charting equipment, usage and improvements were Kelsh plotters, underwater cameras, automatic plotters, ballistic cameras, electronic printers, C-4 stereoplotters, analytical stereoplotters, electro-tapes, Tellurometers, and Geodimeters.

Papers on mapping and charting subsystems reported optimizing stereoplotting, aero-triangulation, airborne electronic surveying, automatic map compilation, radar network adjustment, and satellite systems—geodetic and meteorological. Additional papers of wide interest were presented on matter and energy in photographic systems, equipment calibration techniques, education and training status and proposals, and stability and dodging of photographic film and plates.

The exhibits were for the most part directly related to the projects and equipment discussed in the papers above. Two outstanding new equipment exhibits were the operational prototype exhibits of the super wide angle (120°) Kelsh plotter and the T. R. W. automatic stereoplotter.

PIB Symposium on Optical Masers, New York, 16–18 April 1963

Reported by Donald R. Herriott, Bell Telephone Laboratories

The attendance at the Polytechnic Institute of Brooklyn Symposium on Optical Masers showed that the interest in optical masers is still growing rapidly. The symposium, which was sponsored jointly by the Optical Society of America, the Institute of Electrical and Electronic Engineers, the Air Force Office of Scientific Research, the Office of Naval Research, and the U.S. Army Research Office, along with the Polytechnic Institute of Brooklyn, was attended by over 1200 conferees. The program consisted of a balance between papers reviewing the theoretical considerations of masers, materials and optics, discussions of broad fields of experimental investigation, and specific papers on new devices and techniques. A few of the papers that were of particular interest to the reviewer are mentioned here.

Professors Kallmann, Bloembergen, and Wolf opened the meeting with papers about the electromagnetic theory of maser action, nonlinear theory of optical materials, and the coherence of light including the statistical characteristics of the source and detector. Professor Kallmann entered a special plea for stronger financing of basic research in these as well as in other areas, without as much restriction as is usual.

There were a number of talks describing experimental investigations into general areas. A. L. Schawlow described experiments aimed at removing the cavity from frequency control of solid-state masers. G. H. Dieke described his work in the spectroscopy of rare earths. D. S. McClure and Z. Kiss described work on divalent rare earth ions in crystals. C. G. B. Garrett presented a survey of the results obtained in expanding the wavelengths of gaseous maser operation. W. P. Dumke, A. E. Michel, and E. J. Walker described in two papers the GaAs laser diode and the distribution of light from it. In the area of materials, K. Nassau discussed the growth of $CaWO_4$ crystals, R. D. Maurer described fluorescence and stimulated emission in oxide glasses, and E. I. Gordon, A. D. White, and J. D. Rigden considered the interaction of maser levels in HeNe. In the area of systems and devices, one of the outstanding new ideas was a modulation method presented by K. Gurs and R. Muller from Germany. By varying the coupling out of a maser cavity, they can obtain the low power requirements usually associated with modulation in the cavity without the frequency limitations usually inherent in cavity modulation. W. M. Macek *et al.* described the characteristics of a gas laser rotational rate sensor. A. J. DeMaria, R. Gagosz, and G. Barnard described the control of maser spiking with ultrasonic waves in the material. The distribution of energy in optical cavities using the Fresnel Integral was considered, in papers by L. Bergstein and H. Schacter, and using aberrations in spherical mirror cavities by G. Toraldo di Francia. L. K. Anderson discussed the operation of photodiodes as maser detectors. The meeting was rounded out by a large number of other papers, covering almost every facet of the optical maser gem.

THE SCIENCE OF COLOR

is being reprinted

Applied Optics Reporters

These reporters submit information from which are compiled in part the news columns of *APPLIED OPTICS*. They have a rather thankless and seldom properly recognized task, and the *APPLIED OPTICS* editors are very grateful to them.

L. H. Chasson, *San Francisco*
T. K. McCubbin, *Pennsylvania*
Stanley S. Ballard, *Florida*
E. Scott Barr, *Southeast*
J. L. Rood, *Rochester*
E. M. Wormser, *Connecticut*
R. A. Oetjen, *Japan*
R. H. Tourin, *New York City*
D. J. Lovell, *Michigan*
R. Kraushaar, *New Jersey*
Mary E. Warga, *Greater D.C. and Baltimore*
R. K. McDonald, *Northwest*
M. Kent Wilson, *Boston*
David M. Gates, *Denver*
K. M. Baird, *Canada*
C. S. Williams, *Texas*
A. J. Cussen, *Los Angeles*
J. R. Holmes, *Hawaii*
G. L. Clark, *Illinois*
A. Walsh, *Australia*

A New Condenser for a Sun-Powered Continuous Laser

P. H. Keck, J. J. Redmann, C. E. White, and R. E. DeKinder, Jr.

A new optical condenser to concentrate sunlight effectively from a parabolic collector into a laser rod is described. The condenser has a conical part made of material of high refractive index with a field lens on the wider end of the cone, which faces the parabolic collector. Radiant flux concentrated into the narrow end of the cone is transferred into a small solid integrating sphere with highly reflecting walls. The laser rod is embedded in the sphere and is pumped from all sides by radiation reflected from the walls. Photometric data and performance characteristics of this condenser used with an arc-lamp source are presented. A sun-powered system is proposed and compared to the arc-lamp system.

Several designs for condensers to concentrate sunlight from a parabolic collector into a laser rod have been suggested,[1,2] but these do not yield uniform pumping. This paper describes a new condenser, which achieves effective pumping from all sides of the laser rod and discusses results of tests in which an arc-lamp source was used.

Radiant Flux from the Sun

The radiant-flux density of sunlight on earth in the 560–600 mμ band, in which a considerable part of the total pumping for neodymium-doped laser crystals takes place, is about 5.85 mW/cm² for an air mass of unity.[3] Additional pumping energy in the bands centered at 530, 740, 810, and 880 mμ is neglected in the present analysis.

Figure 1 shows a proposed sun-laser system and gives data on available pumping power. Two flat mirrors are used to relay a beam of sunlight into an $f/1$ parabolic mirror of 100-cm focal length. If we assume losses of 10% at the surface of each flat mirror and of the parabolic mirror, a loss of 5% for shadowing of the parabola by the laser head and support, and a loss of 15% for reflection and light absorption in filters, we have an optical efficiency of 50%. The total pump power collected is:

$$(0.5)\cdot\frac{\pi}{4}\cdot(100)^2\cdot(5.85\times10^{-3}) = 23.2\ \text{W}.$$

The sun image formed by the mirror is 0.935 cm in diameter.

The authors are with Texas Instruments Incorporated, Dallas, Texas.

Received 17 December 1962.

Presented by J. J. Redmann at the Fall Meeting of the Optical Society of America, Rochester, New York, 3–5 October 1962.

Cone-Sphere Condenser

The radiant power concentrated in the sun image is fed into the laser rod by means of a cone-integrating-sphere condenser, which is described below.

The condenser (Fig. 2) consists of a solid conical light funnel with a field lens on the large end and an integrating sphere on the small end. A laser rod is embedded in the sphere.

The field lens is placed at the focus of the parabolic sun mirror and is designed to image this mirror within the integrating sphere near the apex of the cone. The solid conical light funnel allows radiant energy incident on the field lens within an angle α of the axis to be propagated by multiple reflections at the cone walls into the sphere. The cone walls may have a high reflectance coating if any of the rays reflected from them are incident at less than the critical angle.

The relationship between the size of the entrance and exit apertures of a conical condenser to the angle of acceptance has been treated by Williamson.[4] He showed that a meridional ray (i.e., a ray in an axial plane) that enters the entrance aperture of the cone is able to reach the exit aperture only if the extension of the ray intercepts or is tangent to the circle in the meridional plane with center at the vertex of the cone and with the line of intersection of the exit aperture and the meridional plane as a chord of this circle. Figure 3 shows a meridional plane of a solid cone with a field lens on the entrance surface. The ray incident on the center of the field lens at angle α is refracted and, before subsequent reflections from the cone wall, forms angle β with the axis. The dashed straight line is an extension of this ray. The dashed circle is constructed with center at the vertex of the cone and tangent to the dashed straight line. The intersection of the circle with

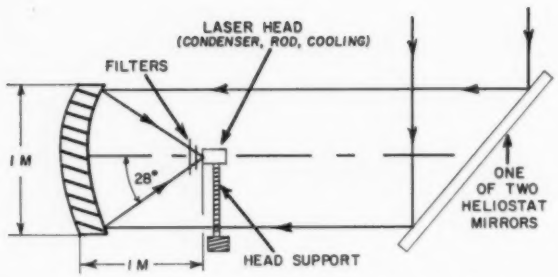

Fig. 1. Proposed sun–laser system. Flux density (0.56–0.60 μ): 5.85×10^{-3} W/cm^2. Mirror area: 7854 cm^2. Optical efficiency: 0.50. Sun-image size: 0.935-cm diam, 0.685-cm^2 area. Flux (0.56–0.60 μ) at image: 23.2 W.

the cone determines the chord d_L, which is the diameter of the smallest exit aperture that the ray in question will reach. The dashed circle in Fig. 3 is not to be confused with the integrating sphere. The diameter and center location of the integrating sphere are not subject to the restrictions placed on this dashed circle. If the exit aperture is reduced, the ray in question will be reflected from the wall in such a manner that it never reaches the exit aperture, but instead propagates back toward the entrance aperture.

The field lens is designed to image the mirror at the plane shown, which causes the extension of all meridional rays incident on the entrance aperture at an angle equal to α or less to be tangent to or to cut into the dotted circle. This implies that all such rays will reach the exit aperture.

The relationship between the cone entrance-aperture diameter d_I, the acceptance angle α, and the minimum diameter d_L of the exit aperture which can be reached by all rays incident at angles less than or equal to α is:

$$d_L/d_I = r/L = \sin\beta = \sin\alpha/n.$$

The first equality follows from properties of similar triangles, the second from the fact that $r = L\sin\beta$, and the third from Snell's law. The equation also shows that the length of the cone does not affect the minimum exit diameter. However, if the cone is made too short, the radius of the field lens becomes so steep that Fresnel reflection losses are high, or the radius of curvature becomes less than $d_I/2$, reducing the entrance face, so that for practical reasons the minimum length of the cone is somewhat restricted.

The minimum exit diameter of the cone for use with the 1-m $f/1$ parabolic sun mirror is tabulated for several materials in Table I. We had decided to make the cone-sphere condenser of strontium titanate. For this material, as seen from Table I, the minimum allowed cone exit aperture is 1.8 mm. In order to gain mechanical strength, we designed the sphere so that it intercepts the cone at a 3.5-mm diameter. This means that we

Table I. Minimum Cone Exit Diameter for an $f/1$, $f = 100$-cm Sun Parabolic-Mirror Image: 0.935 cm $= d_I$. $\alpha = 28°$

Material	Index	Minimum exit diameter (cm)
Air	1.0	0.438
Glass	1.54	0.285
Sapphire	1.76	0.249
$SrTiO_3$	2.41	0.182

are well above the minimum diameter, and all the pumping flux will be funneled into the sphere without exceeding the range of total reflection on the cone wall. The slightly larger entrance aperture of 3.5 compared to 1.8-mm diam for the integrating sphere is less than 1% of the sphere surface and therefore its influence on the efficiency of the integrating sphere will be small.

The high-refractive index material is beneficial for concentrating the light into the integrating sphere, but we have to pay for this advantage by a poor match of the refractive index at the interface between sphere and laser rod. In the actual experiments, we used Canada balsam of index 1.53 between the laser rod of index 1.9 and the strontium titanate of index 2.41. As a consequence, light incident on the rod at an angle higher than the critical angle is totally reflected and will contribute to pumping only after being repeatedly reflected back from the sphere wall and arriving at the rod at an angle smaller than the critical.

The sphere surface is coated with a film having a high reflectivity, at least in the main pumping bands. Experimental evidence indicates that the performance of an integrating sphere is not seriously degraded if the walls deviate slightly from ideally diffuse reflection.[5] Therefore, the walls may have a finely ground or lightly polished finish before the application of the reflecting coating.

The flux density at the walls of an integrating sphere is[6]

$$\phi/4\pi r_s^2 \times R/(1 - R). \qquad (1)$$

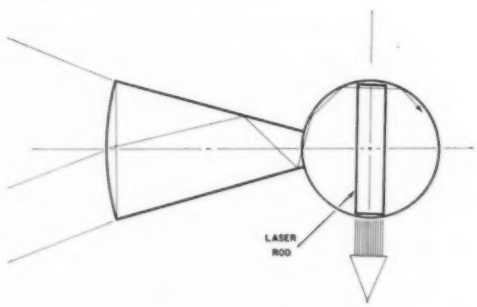

Fig. 2. A cone-sphere condenser.

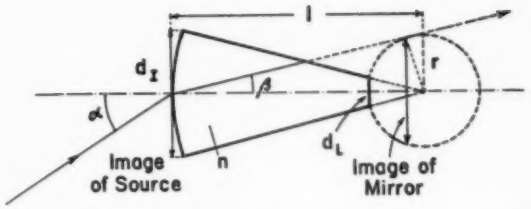

Fig. 3. Relationship between the acceptance angle, entrance-face diameter, and minimum-exit diameter of a cone condenser.

$$\frac{d_L}{d_I\, l} = r = \sin\beta = \frac{\sin\alpha}{n}, \text{ since } r = l\sin\beta.$$

Here, ϕ is the flux from the source entering the sphere, r_s is the radius of the sphere, and R is the reflectance of the sphere wall. The flux ϕ which in our case enters the sphere from the cone condenser is equal to the product of the flux ϕ_i, incident on the cone-entrance face and the transmittance T of the cone condenser. The flux density at the entrance aperture of the cone condenser with the radius r_c is

$$\phi_i/\pi r_c^2. \tag{2}$$

Substituting $\phi_i T$ for ϕ in Eq. (1) and considering Eq. (2), we obtain the ratio of the flux density in the sphere to that at the cone entrance.

$$Tr_c^2/4r_s^2 \times R/(1-R). \tag{3}$$

It is obvious that the larger this ratio is, the more effectively can pumping be achieved. T will be close to 1, if an antireflecting coating is applied at the front surface of the cone and if all internal reflections occur at angles larger than the critical angle for total reflection, which is the case for the strontium titanate cone. Next, the sphere r_s should be made as small as is compatible with the size of the laser rod. Furthermore, R should be as large as possible. The average effective reflectance will be somewhat lower than the actual reflectance of the sphere wall, due to the relatively small area where the cone enters the sphere, the joints, and laser-rod surface through which the laser beam exits, since these areas have a low reflectance. The effective reflectance R in our experiments was estimated to be between 0.90 and 0.93.

This relationship, Eq. (1), holds for an integrating sphere without absorbing material within the sphere. In our case, the laser rod acts as an absorbing body; and it would seem that the level of absorption, and therefore the neodymium concentration in the laser rod, influences the pumping efficiency of the cone-sphere condenser, through both the factor $R/(1-R)$ and the uniformity of excitation throughout the rod volume.

Since we wanted to use rods of various sizes (in particular, 1 mm and 2 mm thick by 12 mm long), we made spacer plates to fit between the cone-hemisphere part

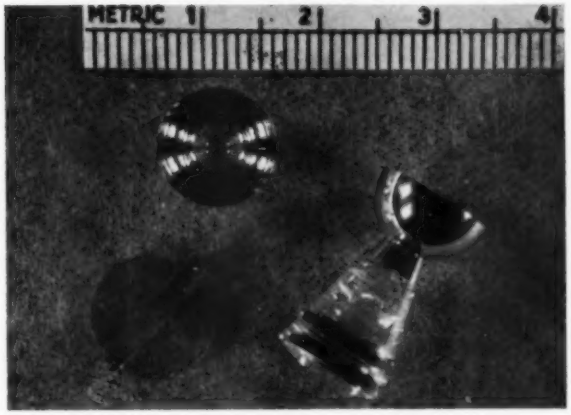

Fig. 4. Components of cone-sphere condenser. Cone-hemisphere, hemisphere, and laser rod with spacer plates. (in mm)

and the other hemisphere, which left a groove for the laser rod to lay in. Figure 4 shows a 2×2×12-mm laser rod cemented between the flat spacer plates on the lower left, the cone-hemisphere on the right, and the hemisphere in the center.

The outer surfaces of the hemispheres, the surface of the cone near the sphere, and the outer edges of the spacers are aluminized.

Figure 5 shows a fixture for supporting and cooling the condenser. Water is circulated around the condenser. A protective coating of aluminum and silicon monoxide was applied over the dielectric multilayer at one end of the rod. The other end of the rod extended out through the sphere a short distance and was covered by an aluminum cap having a Vycor window.

Experimental Results

At this point, we would like to describe briefly the results of tests in which the strontium titanate cone-

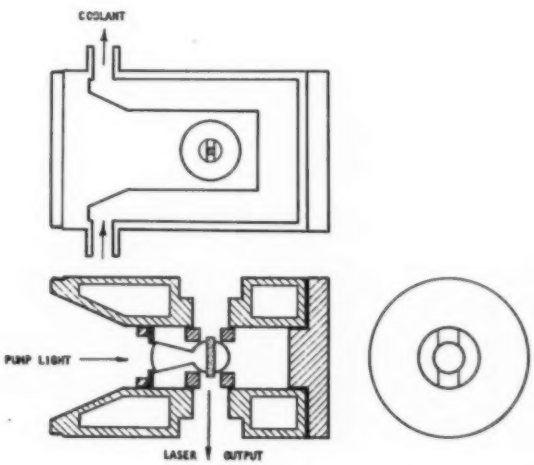

Fig. 5. Fixture for supporting and cooling cone-sphere condenser.

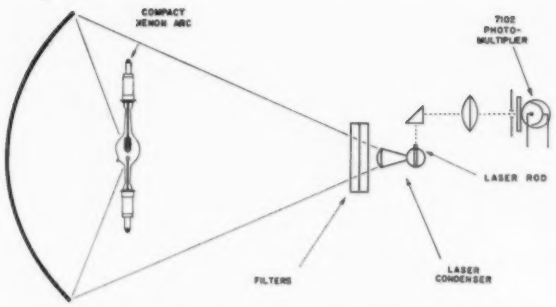

Fig. 6. Experimental optical setup for pumping laser rod and detecting laser output.

sphere condenser was used in pumping a neodymium-doped calcium tungstate laser rod.

Since a sun mirror suitable for the pumping experiment was not available, we decided to test the cone-sphere condenser with the Texas Instruments cw laser pump, which uses an $f/0.4$ ellipsoidal mirror with a xenon compact arc lamp at the near focus.

With this pump, the cone-sphere condenser can be used, since its acceptance angle is larger than the required 23° for the arc lamp. On the other hand, its 10-mm entrance aperture intercepts only 77% of the energy in the arc image. The field lens of the cone is equally suitable for both the sun mirror and the ellipsoidal mirror because the distance between the image planes in the two cases is only a fraction of a millimeter.

The optical setup with the arc lamp is shown schematically in Fig. 6. The 61-cm diam ellipsoidal mirror focuses the arc of the Osram XB0-1600 W compact xenon lamp, which is located at the near focal point, onto the entrance face of the cone-sphere condenser, placed at the far focal point.

For filters we use a water tank with quartz windows placed near the condenser face, containing a Corning 3-69 yellow glass filter. Flowing water cools the glass filter and provides infrared absorption. The arc lamp is operated continuously from a dc power supply. A shutter, not shown in Fig. 6, is located between the filters and the condenser and may be opened and closed by an electromagnet. The output from the laser rod is directed by a reflecting prism to a lens through filters and onto a 7102 photomultiplier.

Figure 7 shows an oscilloscope trace of the photomultiplier output with continuous pumping. The upper trace shows the output below threshold, and the lower trace shows laser action evidenced by the spiking pattern. The time scale is 10 msec per division. The 360-cps ripple on the lamp arises from rectification of three-phase ac by the dc power supply.

The term "pump input power" refers to the electrical power supplied to the arc lamp.

Table II compares the flux in the 560–600 mμ band incident on the cone-sphere condenser from the sun to that from the arc lamp at the 14-kW and 16.95-kW levels, corresponding to the oscilloscope traces of Fig. 7. The sun image is entirely intercepted by the condenser. The arc-lamp image is larger, and only 77% of the energy in this image is intercepted. The radiant flux in the arc image, measured calorimetrically with no filters, is 820 W and 975 W at the two power levels shown. The fraction of the arc-lamp power in the spectral region in question is 3.02%. The transmission of the filters is 85% in this band. The resulting radiant flux is 16.1-W pump power in the band in question for 14-kW input to the lamp, and 19.2-W for 16.95-kW, at which level laser action commenced. More recent experiments, using the same experimental setup as shown previously in Fig. 7, but operating the arc lamp as a flash lamp, show that the use of a Schott GG-14 filter in place of the Corning 3-69 decreases the threshold by a factor of 1.22. This improvement is attributable to more efficient transmission of the 530-mμ pumping band. Moreover, laser rods fabricated recently from calcium tungstate having a neodymium concentration of 2-mole % have exhibited a threshold only one-half as great as the rods used in the experiment described here. Use of the newer rods and the Schott filter will reduce the lamp input power to about 7 kW, which gives a flux intercepted by the cone-sphere condenser of about 7.8 W in the 560–600 mμ range. Other condensers of conical and chisel shape, described by the authors,[7] have permitted continuous-wave laser action at a flux of 3.5 W in this spectral band. The 7.8 W for the cone-sphere condenser and the 3.5 W for the conical and chisel condensers compare with 23.2 W from a 1-m $f/1$ sun mirror. This comparison does not take into account the fact that the xenon arc spectrum contains a somewhat higher percentage of energy in the longer wavelength pumping regions than the sun spectrum, which means that the xenon arc lamp is somewhat more efficient than it seems to be in this comparison with the sun.

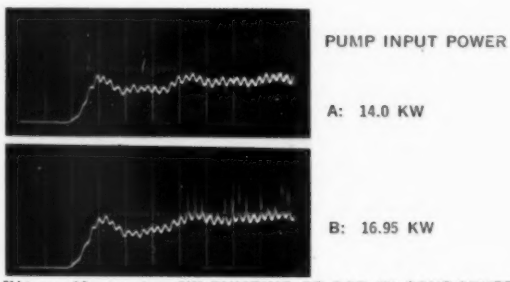

Fig. 7. Oscilloscope traces of the photomultiplier output with continuous pumping.

Table II. Comparison of Fluxes Incident on Condenser from the Continuous Pump to That from the Sun

	cw pump		Sun
Electrical input	14 kW	16.95 kW	—
Radiant flux in arc image (without filters)	820 W	975 W	—
Fraction intercepted by condenser	0.77	0.77	1.00
Fraction in 560–600 mμ band	0.0302	0.0302	—
Reduced by 15% loss in filters	0.85	0.85	0.85
Flux incident on condenser in 560–600 mμ band	16.1 W	19.2 W	23.2 W

It should be mentioned that the laser rod used in the earlier experiment was cut from a crystal supplied by the Linde Company and had approximately 0.3-mole % neodymium concentration. Its threshold was approximately 50 J when measured with an FT-524 helical flash lamp. The material for the later laser rods had a 2-mole % neodymium concentration and was supplied by the Solid State Materials Corporation. The threshold was approximately 25 J as determined with the FT-524 flash lamp.

In conclusion, we state that a cone-sphere condenser has been built that achieves continuous pumping of a 2×2×12 mm neodymium-doped $CaWO_4$ laser rod above threshold using a compact xenon arc lamp. The required spectral flux in the main pumping region of 560–600 mμ was found to be 19.2 W, and improved filters and rods should reduce this to 7.8 W. This compares to an available spectral flux of 23 W, if a sun mirror of 1 m focal length and an opening of $f/1$ were to be used.

It is a pleasure to acknowledge the support and interest of Howard E. Sorrows as well as many useful discussions with him.

References

1. P. H. Keck, Bull. Am. Phys. Soc. **7,** 15 (1962).
2. G. R. Simpson, J. Opt. Soc. Am. **52,** 595 (1962).
3. Based on data reported by Parry Moon in "Proposed Standard Solar Radiation Curves for Engineering Use," J. Franklin Inst. (November 1940), as quoted in Illuminating Engineering Society, *IES Lightning Handbook*, (IES, New York, 1962), 3rd ed., pp. 7–11.
4. D. E. Williamson, J. Opt. Soc. Am. **42,** 712 (1952).
5. R. Ulbricht, *Das Kugelphotometer* (Oldenbourg, Munich, 1920), pp. 58–59.
6. R. S. Longhurst, *Geometrical and Physical Optics* (Longmans, Green and Co., New York, 1957), pp. 388–390.
7. P. H. Keck, J. J. Redmann, C. E. White, and D. E. Bowen, Jr., Appl. Opt. **2,** 801 (1963).

William E. Bell (left) and Arnold L. Bloom measuring wavelength and intensity with a Perkin-Elmer 98-G monochromator with a 1-m gas laser used for research purposes at Spectra-Physics. This laser is permanently connected to a vacuum system and has interchangeable ends—Brewster windows and mirrors—so that a large variety of experiments can be done on it.

Books *continued from page 806*

diffraction studies and several on very high precision, thus illustrating that instrumental developments and measurement techniques have met the challenge, probably originally issued at these Conferences. All the articles are extremely well written because of the dedication of the authors, and because each could revise and perfect the text following the oral presentations. The book itself is well printed by an offset process, and thanks to the care of the authors and of the editor and his staff there are singularly few errors. The reviewer after 40 years in the x-ray field has been able to live through the unbelievable progress, beginning only 10 years after the Laue discovery. It is deeply satisfying to say "Well done" to the eleven Denver Conferences and the five published volumes to be joined by the sixth for the 1962 session. The shadow of the stature of this annual refresher and inspirer of x-ray research and control scientists will long remain undimmed. It is unthinkable that it should ever be discontinued.

GEORGE L. CLARK

Fifty Years of X-Ray Diffraction. P. P. EWALD and numerous crystallographers. A. Oosthoek, Utrecht, The Netherlands, 1962. 720 pp. $11.25.

The crystallographers of all nations met in Munich, 25 July to 1 August 1962 to commemorate the fiftieth anniversary of the discovery of x-ray diffraction. As the reader may recall, x-rays were discovered by Roentgen in 1896 and were immediately applied to all radiographic problems, but the realization that they could be diffracted from crystals did not occur until 1912 when Professor Von Laue with the help of his students Friedrich and Knipping discovered it. In Munich during these early experiments was Paul Ewald, then a student of Summerfeld and now president of the International Union of Crystallography. Professor Ewald, in preparation for the commemoration meeting in Munich, corresponded with those crystallographers whom he considered most intimately acquainted with the intricate steps in the scientific progress by which x-ray diffraction became useful for atomic location in the simplest salts and metals to the determination of structures of giant molecules in medicine and biology. Through this correspondence, Professor Ewald obtained the cooperation of a host of authors to write the unusual book *Fifty Years of X-Ray Diffraction*.

The first half of this book is intended as a scientific history, but it is really an informative discussion of crystal structure analysis, x-ray spectroscopy, and crystal optics in the widest sense, by such authors as W. L. Bragg, Linus Pauling, J. Monteath Robertson, Fritz Laves, Hume-Rothery, Ralph Wyckoff, Kathleen Lonsdale, and Manne Siegbahn. In one of the sections, "Dynamical X-Ray Optics", Professor Ewald himself wrote 17 concentrated and interesting pages (not to mention about 170 other pages and dozens of pages of translations).

Approximately in the center of this 700-page book there are 90 pages devoted to the memory of the twenty or so famous crystallographers who are no longer with us. These pages bring the early days of x-ray diffraction very near and remind us how young the field really is, with so many pioneers still living. About 100 pages are used to discuss the activities of some of the great schools and laboratories of the various nations.

The last large section gives the personal reminiscences of thirty-four noted scientists in x-ray crystallography. Among these is R. W. James who wrote *The Optical Principles of the Diffraction of X-Rays*, a book which is hailed by crystallographers and physicists alike as an authoritative treatise on the most fundamental aspects of diffraction of x rays. All thirty-four of these authors weave the story of their scientific lives into a close coordination with the lives of other scientists over the past fifty or more years in Europe and the United States. This part of the book is of great importance in the history of science and almost sure to be a source of entertainment and inspiration to all young people who read it.

The present reviewer would highly recommend *Fifty Years of X-Ray Diffraction* to all crystallographers and physicists for reading and personal ownership. I would like to warn each student in crystallography, however, not to feel disappointed with his professor if the professor's name is not the chief adornment of the book, because, although this book does attempt to give some credit to all the pioneers in the field, complete coverage is naturally impossible. Just remember that the late A. H. Compton, senior author of the great book *X-Rays in Theory and Experiment*, does not make a very big splash in this memorial volume either.

DAN MCLACHLAN, JR.

Photographic Instrumentation. BY KENNETH SHAFTAN AND DEAN HAWLEY. Society of Photographic Instrumentation Engineers, Redondo Beach, California, 1962. xlviii + 336 pp. $20.00.

The greatly increased research activity brought into being by the requirements of national defense and by space exploration has created a new demand for the creation and use of elaborate specialized photographic equipment for making and recording observations which, otherwise, would be quite impossible. As in so many other branches of engineering, the possibilities and capabilities of such equipment has been greatly extended by the utilization of the many developments associated with electronics. The result is the accumulation of a mass of engineering accomplishments, skills, and data sufficiently homogeneous to be considered a new field of engineering—photographic instrumentation. As a consequence we have the Society of Photographic Instrumentation (SPIE). The first issue of its new journal, *Society of Photographic Instrumentation Engineers Journal*, has just appeared. Kenneth Shaftan was one of the pioneers who greatly stimulated the idea that photographic instrumentation was of sufficient importance to justify special study as a separate branch of engineering. During World War II he was a commander in the USNR. He was Officer in Charge of the Photographic Branch, Bureau of Ships, where he supervised extensive work in technical photography applied to scientific research, and later, as a member of Joint Task Force One, he designed instrumentation for the Bikini target ship, for airborne high-speed recording, and for the data interpretation of its results. After the war he became director of photoinstrumentation with J. A. Maurer, Inc. Shaftan and his colleague, Dean Hawley of Origins, Inc., were killed in the crash of a private plane in the spring of 1953. Had Shaftan lived he would undoubtedly have played a leading role in the organization and policy direction of SPIE.

The text of the book under review, *Photographic Instrumentation*, is a portion of the report resulting from the United States Navy, Office of Naval Research Contract N80NR-65301. The purpose of this contract was to finance "A survey of the Navy scientific and engineering projects to determine, in the field of photographic instrumentation, the techniques available, their application, and the problems in this field deserving attention." This presented a problem of fascinating interest to Shaftan into which he entered wholeheartedly. "Visits were made to 67 research and development activities engaged in military or related projects . . . . 128 research projects were discussed, approximately 1250 reports were assembled and reviewed, including articles in the scientific literature, manufacturers' literature, and texts." The results of this work appear as 232 pages (not counting the bibliography and appendices) written in brief notebook

continued on page 839

Performance of a Continuous-Wave Neodymium Laser

P. H. Keck, J. J. Redmann, C. E. White, and D. E. Bowen

A high-pressure compact xenon arc lamp with an ellipsoidal collector of 61-cm diameter and an opening of $f/0.4$ served as pumping source. The flux available from this source is concentrated into the $2 \times 2 \times 12$ mm laser rods of neodymium-doped calcium tungstate by either a straight cone condenser or by a chisel-shaped condenser. Both condenser designs are discussed. Continuous laser action has been achieved for periods up to more than one hour, using water cooling at room temperature.

This paper describes experiments with a continuous neodymium-doped calcium tungstate laser,[1] operated at room temperature, using water cooling.

The Pump Source

The Texas Instruments' laser pump, which has been described recently,[2] served as a source (see Fig. 1). It contains an Osram XBO-1600 W compact xenon arc lamp which has an electrode distance of approximately 4 mm. An ellipsoidal front surface pyrex mirror of 61-cm diam with an opening of about $f/0.4$ collects a substantial percentage of the radiation and produces a three times magnified arc image. The total radiant flux through a 12×12 mm aperture in this image plane is approximately 6% of the electric input power of the lamp. This holds with good approximation for an input between 1 and 10 kW. For a 10-kW lamp input, for instance, we obtain through the image plane a total radiant flux of 600 W. The energy distribution of the xenon source for various spectral bands is indicated in Table I. The spectral flux in the major pumping region for neodymium between 560 and 600 mμ is, in this case, $600 \times 3.02\% = 18.12$ W. In addition, we have in the region between 740 and 880 mμ three neodymium absorption bands which contribute to pumping. In this range, the spectral flux through the 12×12 mm aperture is $600 \times 11.96\% = 71.8$ W.

Design of the Laser Condenser

There have been described in the past a number of optical systems which concentrate the radiant flux into a laser rod of relatively small size. For practical reasons we have standardized on rods of $2 \times 2 \times 12$ mm. In the following we would like to concentrate on two condenser designs: (a) The straight cone which has the laser rod in the cone axis, as described at a previous meeting[3] and (b) a chisel-shaped condenser which provides a high pumping flux through one of the side faces of the laser rod. In contrast to the straight cone, the rod axis is in this case perpendicular to the pumping direction. The condenser is sketched in Fig. 2. The cross section in one plane is of wedge shape whereas in a perpendicular plane we have a rectangular shape. The arc source is imaged on the condenser front face which has a square opening of 12×12 mm. The rectangular shape of the condenser on the other end matches the side faces of the $2 \times 2 \times 12$ mm rods.

Let us now consider the effect of light concentration by a cone or wedge-shaped condenser. A ray entering in the center of the front surface, as seen in Fig. 3, and forming an angle β with the axis, will be reflected forward and can exit through the nose only, as Williamson[4] has shown for a cone condenser, if β is equal or smaller than the tangent to the circle with radius r determined by the nose. As seen from Fig. 3, the ratio of the nose to the front opening d_L/d_I of the wedge is determined by the maximum angle α of the incident rays and by the refractive index n of the wedge. Note that this ratio

Table I. Spectral Energy Distribution of the Xenon Arc Lamp

Wavelength range (mμ)	Percentage of total radiation Xe lamp
200– 400	5
400– 700	23.6
700–1400	71
500– 600	7.28
560– 600	3.02
740– 880	11.96

The authors are at Texas Instruments Incorporated, Dallas, Texas.

Received 17 December 1962.

Presented in part at the Fall Meeting of The Optical Society of America, Rochester, New York, 3–5 October 1962.

This work was partly supported by a contract with the Air Force Cambridge Research Laboratories.

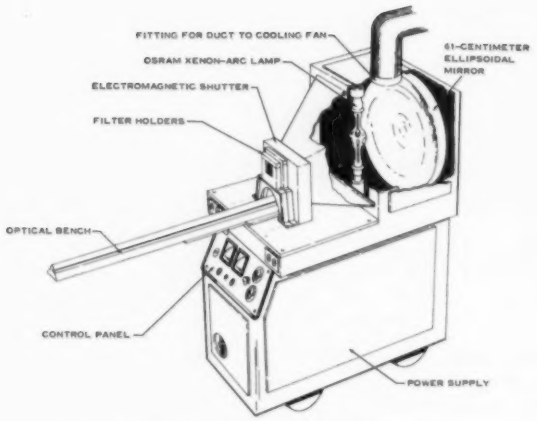

Fig. 1. The Texas Instruments laser pump.

is independent of the length l of the cone. The arc image, which is focused on the front surface, is in our case d_I = 12-mm diam. It should be noted that the front face of the condenser is shaped into a field lens which images the collector mirror into the plane defined by the tangents to the nose circle. This field lens is spherical in the case of the straight cone and, of course, is cylindrical for the chisel condenser.

For a front opening of 12 mm and a maximum angle $\alpha = 23°$, we have listed in Table II the minimum nose opening d_L for condensers made out of materials of various refractive indexes. It is quite obvious that with higher refractive index materials a stronger concentration of the radiant flux into the laser crystal can be achieved. We have fabricated straight-cone condensers out of fused quartz and sapphire and chisel condensers out of sapphire and strontium titanate. The strontium titanate, as can be seen from Table II, is best fitted to match a 2 mm wide laser rod.

Over most of its length total reflection occurs on the cone or wedge surface except for a narrow range near the nose end where the angle of total reflection is exceeded. This range, which is in our case small, depends on the cone angle and the refractive index of the cone and its ambient. It was calculated for the various combinations, and reflecting aluminum coatings were evaporated over this range.

Table II. Concentration Power of Condenser Depending on Refractive Index. Wedge-Type Condenser for 12-mm Front Opening and $\alpha = 23°$

Nose end (mm)	Material	Refractive index
4.67	Air	1
3.03	Glass	1.54
2.65	Sapphire	1.76
1.95	Strontium titanate	2.41

Mounting of the Laser Rod

To avoid large reflection losses it is important to have a good optical contact between the condenser proper and the laser rod. We have in progress various approaches to make the joints. However, since the results are not yet conclusive we will report here on the use of Canada balsam only. Canada balsam was found to withstand the high pumping intensity for a considerable period, provided that an ultraviolet and infrared absorption filter was inserted in the pump beam and that the condenser was cooled with water. Figure 4 shows a straight sapphire cone condenser with a $CaWO_4$ laser rod cemented in the tip area. The cone is made of two halves with V grooves to accommodate the square rod. The pumping radiation is entering the laser rod through the four cemented side faces. Figure 5 shows a laser rod cemented onto a strontium titanate chisel condenser. The small flat end surfaces of the laser rods have multilayer dielectric coatings with 98 to 99% reflection at 1.06 μ. One of these end faces was usually aluminized on top of the multilayer coating while the other end was used to observe the laser beam. The losses due to reflection at the interfaces strontium titanate–Canada balsam–calcium tungstate have been estimated to be approximately 25%. Part of these

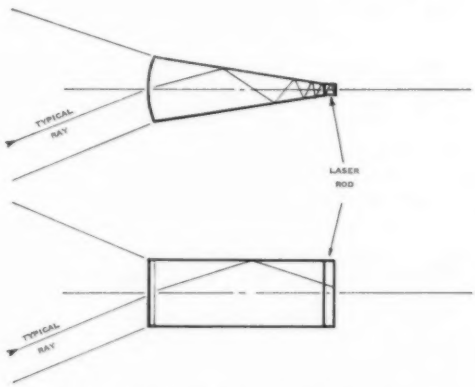

Fig. 2. Design of chisel-type condenser.

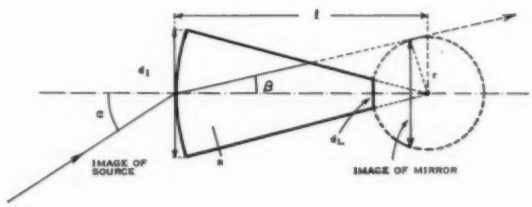

$$\frac{d_L}{d_1} = \frac{r}{f} \sin \beta = \frac{\sin \alpha}{n},$$

SINCE $r = f \sin \beta$

Fig. 3. Ray concentration by a cone or wedge-shaped condenser.

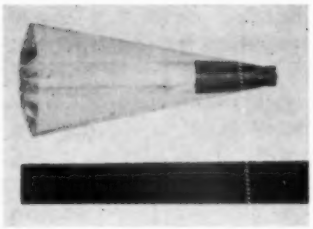

Fig. 4. The straight-cone condenser with laser rod.

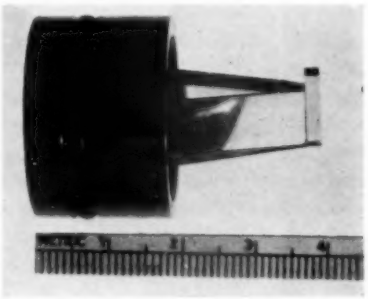

Fig. 5. The chisel-type condenser with laser rod in holder.

losses can be avoided by a better matching of the refractive index of the intermediate layer and by proper coatings on both the chisel edge and the joining face of the laser rod.

As indicated in Fig. 6, the condenser with the mounted laser rod was placed in a water-cooled holder in front of the laser pump so that the arc image was focused in the front aperture of the condenser. With the chisel-type condenser the laser beam emerges perpendicular to the pumping direction and was reflected into the 7102 type photomultiplier by a 90° prism. In the case of the cone condenser, the laser beam was axially directed into the photomultiplier.

In most experiments we used as a filter in front of the condenser a water tank with fused quartz windows and a Corning yellow filter 3-69, 3 mm thick, immersed in the water. The yellow filter has approximately 50 % transmission at 530 mμ. Other yellow filters used in place of 3-69 included the Schott filters GG14 and GG15.

Experimental Results

Let us now discuss characteristic results obtained with 2 × 2 × 12 mm laser rods of neodymium-doped calcium tungstate, cemented to the condenser with Canada balsam.

Figure 7 shows, as an example, the laser action for a chisel-type condenser at room temperature. This condenser was made of sapphire and its side faces were aluminized. The laser rod had a neodymium concentration of approximately 0.3 mole % and was cut from a single crystal obtained from the Linde Company. The flash threshold measured with a General Electric spiral lamp was approximately 50 J. The top frame (a) of Fig. 7 indicates the fluorescence and pump radiation below threshold. The visible ripples correspond to 360 cps due to the 3-phase input power. For these experiments we have intentionally left out a ripple suppressor which we have actually built, because these ripples serve as a convenient indication for laser action. In the middle and lower frame the threshold has been exceeded, and it will be noticed that some spiking occurs in the bottom picture besides a general amplification of the power supply ripples. Figure 8 shows the same system with a five times increased sweep rate. The bottom frame contains considerable detail of the laser action.

The laser threshold with this condenser occurs at a total input into the arc lamp of 11.4 kW, which of course is a considerable overload. This was measured with the water tank and the yellow filter 3-69 in front of the laser condenser. The total radiant flux into the condenser amounts in this case to: 42 % × 6 % × 11.4 kW = 288 W, since the filter combination transmits 42 %, as measured calorimetrically. This corresponds

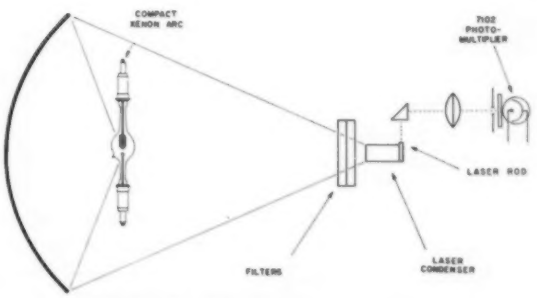

Fig. 6. Continuous-wave laser arrangement.

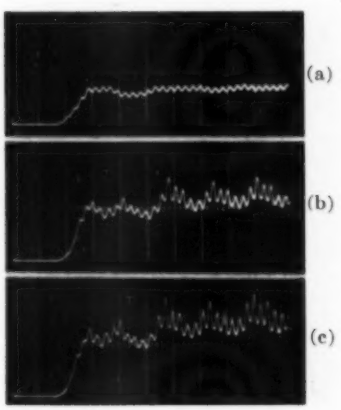

Fig. 7. Laser output with chisel-type condenser. Pump input power: (a) = 5.5 kW; (b) = 11.4 kW; (c) = 13.4 kW. Vertical scale: 0.5 V/cm. Horizontal scale: 10 msec/cm.

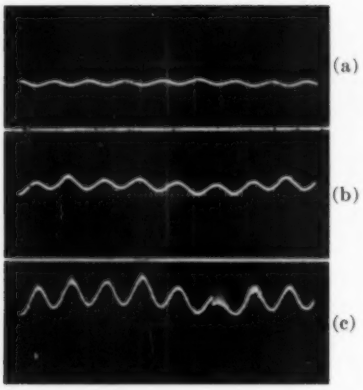

Fig. 8. Laser output with chisel-type condenser. Pump input power: (a) = 5.5 kW; (b) = 11.4 kW; (c) = 13.4 kW. Vertical scale: 0.5 V/cm. Horizontal scale: 2 msec/cm.

to an estimated spectral flux of 15.5 W in the main pumping range between 560 and 600 mμ.

Figure 9 shows the oscillogram for a laser rod cemented in a straight sapphire cone condenser. The rod was also cut from the Linde crystal and had the same flash threshold of approximately 50 J (as measured with a General Electric spiral tube type FT 524). As seen from the middle frame (b) the laser threshold was reached in this case at an input power of 5.5 kW using also the water tank and yellow filter 3-69 in front of the laser condenser. The radiant flux into the condenser for laser threshold is in this case 140 W corresponding to a spectral flux of 7.5 W in the range between 560 and 600 mμ.

Experiments with a series of calcium tungstate crystals, supplied by the Solid State Materials Corporation, having neodymium concentrations between 0.5 and 2 mole % showed that the threshold for lasing decreased approximately linear with increasing concentration. For laser rods with 2 mole % neodymium we obtained continuous lasing with a pump input power between 2.5 and 4 kW. This reduces the total radiant flux into the laser condenser to values between 65 and 100 W, corresponding to a spectral flux between 3.5 and 5.4 W in the 560 and 600 mμ range. We usually carried out the cw experiments for short intervals; however, several rods have been operated continuously up to more than one hour. The cw output power was estimated to be in the milliwatt range.

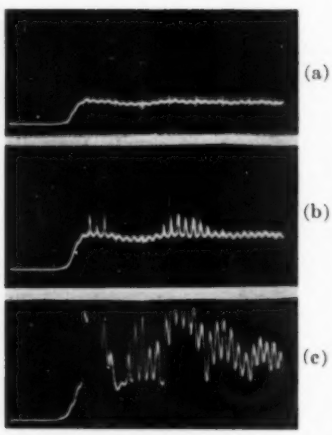

Fig. 9. Laser output with straight-cone condenser. Pump input power: (a) = 3.36 kW; (b) = 5.5 kW; (c) = 8.8 kW. Vertical scale: 0.5 V/cm. Horizontal scale: 10 msec/cm.

It was thought that excitation in both flash and continuous modes under identical optical conditions would provide valuable comparative data on spiking and steady state lasing. Therefore, we modified the pump source so that we could run the xenon compact arc lamp in either continuous or flash operation. Figure 10 is a flash excitation of the same rod and condenser which has been used in Figs. 7 and 8. The threshold to occur at the 1-volt level of the photomultiplier output where we observed the beginning of laser action in Figs. 7 and 8 will be seen. Note that the sweep in Fig. 10 is ten times faster than in Fig. 8. It is quite striking that we observe in the oscillograph trace of Fig. 10 both a strong spiking as well as a sizable increase of the amplitude. Another advantage of the addition of the flash operation is to provide a means to compare accurately the efficiency of different optical arrangements and to study the influence of various parameters of the laser system.

Fig. 10. Flash laser with chisel-type condenser: 400 μF, 1800 V Vertical scale: 0.5 V/cm. Horizontal scale: 0.2 msec/cm.

Conclusions

Continuous laser operation of neodymium-doped laser rods of 2 × 2 × 12 mm size has been demonstrated at room temperature, using as the light source a xenon compact arc lamp with a 610 mm diam $f/0.4$ ellipsoidal mirror as a collector. Two types of laser condensers were investigated: (a) A straight cone with the laser rod axially cemented in the cone tip section with Canada balsam; (b) A chisel-shaped condenser with the laser rod axis perpendicular to the pumping direction. It was found that the total radiant flux into the laser condenser aperture necessary to produce laser action was between 65 and 288 W depending on the threshold of the laser rods and on the design of the condenser. This corresponds to a spectral flux in the main pumping

range between 560 and 600 mμ, of 3.5 and 15.5 W, respectively. The lowest value was obtained with the sapphire straight-cone condenser. This is an indication that this type is optically somewhat more efficient than the chisel condenser. However, the chisel design provides the advantage of better cooling since a larger surface area of the laser rod is directly exposed to the cooling water. A somewhat higher efficiency of the straight cone condenser can be qualitatively understood because the cone concentrates the pump light in all directions perpendicular to the axis, while the chisel condenser concentrates essentially only in one direction. A more accurate comparison of the condenser is more involved and has to take into account the effective path of the pump radiation in the laser rods together with their absorption characteristic.

Continuous laser operation for periods up to one hour using the best rods and condensers required an input to the arc lamp of about 2.5 kW. Under these conditions the arc lamps were found to have a lifetime better than several hundred hours.

It is a pleasure to acknowledge the support and interest of this work by Howard E. Sorrows as well as many useful discussions with him.

References

1. The first continuous laser operation on neodymium-doped calcium tungstate has been shown by L. F. Johnson, G. D. Boyd, K. Nassau, and R. R. Soden, Phys. Rev. **126**, 1406 (1962).
2. H. J. Auvermann, P. H. Keck, and C. E. White, Bull. Am. Phys. Soc. **7**, 330 (1962).
3. P. H. Keck, Bull. Am. Phys. Soc. **7**, 15 (1962).
4. D. E. Williamson, J. Opt. Soc. Am. **42**, 712 (1952). See also J. H. McLead, J. Opt. Soc. Am. **44**, 592 (1954).

Applied Optics January 1962

featuring **OPTICAL PUMPING AND MASERS**
editor B. H. Billings

Magnetic Resonance in Radiating or Absorbing Atoms—Francis Bitter

Composite Rod Optical Masers—G. E. Devlin, J. McKenna, A. D. May, and A. L. Schawlow

Atomes à l'Intérieur d'un Interféromètre Perot-Fabry—A. Kastler

Synthetic Maser Ruby—Robert D. Olt

Proposal for an Electron Accelerator Using an Optical Maser—Koichi Shimoda

Recent Developments in Maser Devices and Materials—Hendrik J. Gerritsen

The Interference between Beams from the Opposite Ends of a Ruby Optical Maser—P. Kisliuk and D. J. Walsh

Photomixing Experiments with a Ruby Optical Maser and a Traveling-Wave Microwave Phototube—B. J. McMurtry and A. E. Siegman

Properties of the Hydrogen Maser—Daniel Kleppner, H. Mark Goldenberg, and Norman F. Ramsey

Principles of Operation of the Rubidium Vapor Magnetometer—Arnold L. Bloom

$2.00 a copy
cash with
order preferred

See order card facing page 852
Order from APPLIED OPTICS Back Numbers
AIP Attn. Mr. Uszak, 335 E. 45th St., New York, 17, N.Y.

Books *continued from page 832*

style but with an abundance of illustrations. The methods considered are largely those concerned with transient phenomena and with rapidly moving objects which require the different types of high-speed cameras. Topographic photogrammetry which, economically, is probably the most important field of photographic instrumentation is not considered, perhaps because of its routine character resulting from its long period of development and present established position. However, there are elaborate installations of photographic instrumentation for the precise determination of the positions of projectiles and bombs in flight which could well be included in a complete treatment of photographic instrumentation. No developments that have arisen since 1953 are included, such as the elaborate photographic instruments that have been developed for tracking artificial satellites.

The first three chapters discuss, in a general way, the different types of equipment and the different techniques such as still, motion picture, streak, shadowgraph, schlieren, interferometric photography, and many others. The capabilities and limitations of the different procedures are well presented. Chapter 4, which is much the longest chapter, describes the types of equipment that are required for the different techniques that have been referred to in the earlier chapters. Considerable attention is given to the different illuminants that must be employed for special purposes, and some to the different types of photographic emulsions that are available. Very little space is devoted to the chemistry of the photographic processes because this is considered to not fall within the scope of this book. Chapter 5 presents the results of the visits to the "67 research and development activities engaged in military or related projects." The field of interest of the military in the field of photographic instrumentation is so all pervasive that this chapter contains brief sketches of nearly all types of applications of photography to research work and in most instances a government or university laboratory is indicated where each particular application is being effectively used. This chapter, therefore, tells not only what is being done with admirable conciseness but also where one can go for first-hand additional information from people who are actively experienced in the respective application.

The main text of the book is followed by a bibliography containing 440 references and by appendices giving engineering specifications and data relating to illuminants classified as continuous source—gaseous discharge, mercury vapor; continuous source—incandescent; transient source—single flash; and transient source—repetitive flash. Another appendix gives very complete data concerning "high-speed, very high-speed, and ultra high-speed motion picture cameras", and finally, a table of specifications of hydrogen thyratons.

This work will prove to be a valuable reference work of an engineers' handbook type for use by anyone concerned with the methods and applications of photographic instrumentation. Also, it may be considered to be the framework about which one could write a most excellent encyclopedia presenting the methods, the possibilities, and the instrumentation for the extremely interesting and varied applications of photography as an aid to scientific research and development.

IRVINE C. GARDNER

Tables of Einstein Functions: Vibrational Contributions to the Thermodynamic Functions. By JOSEPH HILSENRATH AND GUY G. ZIEGLER. National Bureau of Standards Monograph 49. U.S. Government Printing Office, Washington, D.C., 1962. 258 pp. $2.75.

This book tabulates the contributions of a quantum-mechanical harmonic oscillator to the thermodynamic functions. It includes two tables and a short introduction. In Table 1 the thermodynamic functions are tabulated in dimensionless units as a function of the dimensionless ratio of the vibrational frequency to the temperature. The functions tabulated are Gibbs free energy, enthalpy, entropy, and heat capacity. Also tabulated are first differences between successive entries for each function. The tables extend from values of the argument at the lower end of 0.0010 to 16.0 at the upper end. The close spacing of the entries facilitates linear interpolation between the entries, which are tabulated to five figures to the right of the decimal. Table 2 differs from Table 1 only in that the enthalpy function is omitted, and the entries are tabulated in units of calories per mole per degree K. Also, the format of Table 2 is somewhat different from Table 1: the argument explicitly includes both the frequency (in wave-number units) and the temperature (in °K). For each temperature, the entries are tabulated as a function of the wave number from 100 cm^{-1} to 4000 cm^{-1}, at intervals of 10 cm^{-1}. The temperature range extends to 5000°K in 100°K intervals, except for the first two arguments, which are 273.15°K and 298.15°K, respectively.

These tables should be useful to the thermodynamicist who frequently must make rapid estimates of the thermodynamic properties of materials, such as molecular gases from elementary vibrational (and other) motions of their constituent atomic and molecular particles, and for whom a high speed computer either is not available or would be unprofitable to use. Though, strictly speaking, the atomic and molecular vibrators are anharmonic, the amount of anharmonicity is usually quite small when the vibrators are close to their lowest quantum states, and this is usually the case when the dimensionless ratio of the frequency to the temperature is somewhat less than unity. Even at somewhat more elevated temperatures, the harmonic-oscillator approximation is often a useful result about which to perform an expansion to obtain the contributions for the anharmonic vibrations that actually occur. Finally, this writer frequently has had occasion to use a similar set of tables that is now out of print [N. L. Johnston, L. Savedoff, and J. Belzer, *Contributions to the Thermodynamic Properties by a Planck-Einstein Oscillator in One Degree of Freedom* (U.S. Government Printing Office, Washington, D.C., 1949)]. For purposes of comparison, it should be noted that the present tables have considerably more entries and should prove more convenient to use.

L. HAAR

From the Department of Incidental Information*

WEBSTER (2nd ed.)

laser, *n.* [L.] *Pharm.* **a.** A drastic purgative gum resin obtained from laserwort. **b** = ASAFETIDA.
laserwort, Any plant of the genus *Laserpitium*, esp. the herb frankincense.

OXFORD

Laser. [a. L. *läser.*] A gum-resin mentioned by Roman writers obtained from an umbelliferous plant called *laserpicium* or *silphium.*

* via J. A. Sanderson

M. P. Thekaekara *Georgetown University* (left), H. K. Hammond, III *National Bureau of Standards*, and A. I. Mahan *Applied Physics Laboratory* during a meeting of the Local Sections.

Electro-Optic Light Modulation with Cubic Crystals

C. F. Buhrer, L. R. Bloom, and D. H. Baird

Analysis of the linear electro-optic effect in crystals of classes containing a threefold rotation axis is carried out. It is shown that such crystals display a dual transverse electro-optic effect in which the magnitude of an electric field transverse to the light direction controls the electro-optic retardation and the direction of the field controls the orientation of the fast and slow polarization axes. The most desirable crystals for utilization of this effect are those of cubic class $\bar{4}3m$ since they are optically isotropic in zero field and are not optically active. Using a crystal of this type, for example, zinc sulfide, analysis shows it is possible to modulate a light beam simultaneously with two independent signals in the form of mutually perpendicular fields both transverse to the light beam. The signals are recoverable at the receiver by photodetectors responding to appropriate polarization components of the beam. If the fields applied to the crystal consist of appropriate combinations of the modulating signals, the latter appear as upper or lower sidebands of the optical carrier. Differences of the polarization states of sidebands and carrier make it easily possible to achieve single-sideband suppressed-carrier transmission. Receiver design for superheterodyne detection of such signals is described. Results of experiments are given demonstrating the modulation and reception techniques described.

I. Introduction

The production of coherent light by optical masers has stimulated interest in light communications systems and therefore in optical modulation techniques. The most generally useful of these employs the linear electro-optic (Pockels) effect in crystals. It is the purpose of this paper to discuss the electro-optic properties of certain classes of crystals which are found to be particularly useful for optical modulation, to describe the principles of several types of optical modulator which have been realized with such crystals, and to give the experimental results obtained with these modulators.

In an anisotropic medium, such as a crystal, the dielectric constant is a tensor with six independent components. This has the consequence that for light propagating in any given direction in the medium two different plane polarizations at right angles to each other (and to the direction of propagation, of course), are permitted. Waves of the two polarizations travel with different velocity v, or have different refractive indices c/v. The refractive indices of the two waves are conveniently obtained with the use of an ellipsoidal surface, known as the indicatrix, that one may draw in the crystal. The most general form of the equation of the indicatrix is

$$\frac{1}{n_1^2}x^2 + \frac{1}{n_2^2}y^2 + \frac{1}{n_3^2}z^2 + \frac{2}{n_4^2}yz + \frac{2}{n_5^2}zx + \frac{2}{n_6^2}xy = 1. \quad (1)$$

The refractive indices for light traveling in a given direction may be obtained from the central section of this ellipsoid perpendicular to the light direction. This central section is an ellipse. Its major and minor axes are the allowed polarization directions for light traveling perpendicular to its plane. The refractive index for either of the allowed polarization directions is equal to half the length of the ellipse axis in that direction. If beams of the two polarizations, to be denoted by the subscripts α and β, start together through the crystal the retardation Γ in radians of one relative to the other after they have traversed a thickness d of crystal is

$$\Gamma = \frac{2\pi}{T}\left(\frac{d}{c/n_\alpha} - \frac{d}{c/n_\beta}\right) = \frac{2\pi d}{\lambda}\Delta n, \quad (2)$$

where T is the period of the vibration, Δn is the difference in the refractive indices, and λ the free space wavelength.

The Pockels effect consists of a linear variation in refractive index due to electric field that is described in terms of the coefficients in (1) by

$$\frac{1}{n_i^2} = \left(\frac{1}{n_i^2}\right)_{E=0} + \sum_{j=1}^{3} r_{ij}E_j, \quad (3)$$

where E_j is one of the components of the electric field. Since i may take on six values, corresponding to the six independent components of the dielectric constant tensor, and j three values, there may be eighteen inde-

The authors are with the General Telephone and Electronics Laboratories, Inc., Bayside, New York.

Received 1 January 1963.

pendent electro-optic coefficients r_{ij}. The symmetry of the crystal introduces relations among these that reduce this number.

The linear variation of refractive index with field implicit in (3) when the sum on the right is much smaller than one (as is the case for attainable field strengths in virtually all known electro-optic crystals) means that Δn and, therefore, Γ in (2) also depend linearly on field strength. It is this dependence of the retardation on field which is useful for the modulation of light. It is a great simplification in this application for the retardation in the absence of the field to be zero, i.e., for the crystal to be cubic and, therefore, optically isotropic or for the light path to be along the optic axis of an anisotropic crystal. Cubic crystals are much to be preferred since very stringent requirements on the parallelism of the light beam itself and of the light beam with the optic axis must be imposed if the natural birefringence of an anisotropic crystal is not to decrease the efficiency of the modulation process.

The crystals most commonly used in electro-optic modulators are KH_2PO_4 (KDP) and its isomorphs which are of tetragonal structure and therefore optically uniaxial. Their use has been dictated by their high electro-optic sensitivity and their ready preparation as large single crystals. Their behavior in an electric field has been described by Billings.[1] Using such crystals it is possible to produce amplitude, phase, double sideband or single sideband[2] modulation of light at frequencies as high as 10 Gc./sec.[3] However, these crystals have a fundamental limitation in that their point group symmetry ($\bar{4}2m$) requires that the modulating field be along the light path. This arrangement necessitates the use of large voltages to produce useful values of retardation and also makes for more difficulty in the problem of optical modulator design, particularly at the higher frequencies, than would be the case for transverse modulating fields.

The present discussion is concerned with the modulation techniques made possible by available types of crystal which overcome these disadvantages of the KDP type of material. The properties of these crystals of particular importance are the following:

(1) They respond to fields transverse to the light path, simplifying problems of modulator design and permitting reduction in the voltage by the use of a light path large compared with the distance over which the field is impressed.

(2) They possess what may be termed a "dual transverse" Pockels effect which permits simultaneous modulation of the light with two independent signals by the use of two mutually perpendicular transverse fields.

(3) They are cubic and hence possess no natural birefringence. The problems of alignment and beam parallelism are, therefore, minimized as compared with those found in the use of naturally birefringent crystals such as KDP.

In the following section discussion is given of the requirements on crystal symmetry which must be fulfilled to yield these properties. It may be noted that earlier data[4,5] show at least two crystals satisfying these requirements, cubic zinc sulfide and cuprous chloride, to have electro-optic sensitivities comparable to that of KDP.

II. Dual Transverse Pockels Effect

The dual transverse Pockels effect will be shown to exist in any crystal with a threefold rotation axis in its point group so long as the over-all symmetry is not so high as to prohibit any linear electro-optic effect. To do so we calculate the effect of an electric field of arbitrary direction in the plane normal to such a threefold axis and show the dependence of the optical properties of the crystal on the magnitude and on the direction of this field.

Consider that we have light propagating along such a threefold axis. To determine the refractive indices we need the cross section of the indicatrix normal to the axis. In the absence of an electric field, this cross section is circular and there is no birefringence. Stated differently, in noncubic crystals a threefold axis is always the optic axis. On application of a field transverse to this axis, the cross section becomes elliptical. If the threefold direction is taken as the z direction, the electric field may be specified by

$$\begin{aligned} E_x &= E_m \cos\alpha, \\ E_y &= E_m \sin\alpha. \end{aligned} \tag{4}$$

To write the equation for the indicatrix cross section in the $z = 0$ plane we need only the coefficients n_1, n_2, and n_6 of Eq. (1). According to (3) these are

$$\begin{aligned} \frac{1}{n_1^2} &= \frac{1}{n_0^2} + r_{11}E_x + r_{12}E_y, \\ \frac{1}{n_2^2} &= \frac{1}{n_0^2} + r_{21}E_x + r_{22}E_y, \\ \frac{1}{n_6^2} &= r_{61}E_x + r_{62}E_y, \end{aligned} \tag{5}$$

where n_0 is the refractive index in the absence of electric field. As deduced from symmetry considerations, the most general form of the r_{ij} matrix for this orientation, with the three or z axis parallel to the threefold axis, is

$$\begin{pmatrix} r_{11} & -r_{22} & r_{13} \\ -r_{11} & r_{22} & r_{13} \\ 0 & 0 & r_{33} \\ r_{41} & r_{42} & 0 \\ r_{42} & -r_{41} & 0 \\ -r_{22} & -r_{11} & 0 \end{pmatrix}. \tag{6}$$

With the use of (5), (6), and (1) we obtain for the desired equation of the indicatrix cross section

$$\left[\frac{1}{n_0^2} + (r_{11}E_x - r_{22}E_y)\right]x^2 + \left[\frac{1}{n_0^2} - (r_{11}E_x - r_{22}E_y)\right]y^2 + 2[-r_{22}E_x - r_{11}E_y]xy = 1. \quad (7)$$

To obtain the indices of refraction in the allowed polarization directions we must rotate the x and y axes to coincide with the principal axes of the ellipse, x' and y'. In the usual way it is found that the angle of rotation θ required to do this is given by

$$\sin 2\theta = -\frac{r_{22}E_x + r_{11}E_y}{\sqrt{r_{11}^2 + r_{22}^2}\,E_m}, \quad (8)$$

while the equation of the ellipse referred to its principal axes is

$$\left(\frac{1}{n_0^2} + \bar{r}E_m\right)x'^2 + \left(\frac{1}{n_0^2} - \bar{r}E_m\right)y'^2 = 1, \quad (9)$$

where

$$\bar{r} = \sqrt{r_{11}^2 + r_{22}^2}. \quad (10)$$

By expanding in powers of $\bar{r}E_m$, which is very small, and keeping only terms linear in E_m, we obtain for the index of refraction $n_{x'}$ of the ray polarized in the x' direction

$$n_{x'} = n_0 - \frac{1}{2}\,n_0^3\bar{r}E_m, \quad (11a)$$

and for the ray polarized in the y' direction

$$n_{y'} = n_0 + \frac{1}{2}\,n_0^3\bar{r}E_m. \quad (11b)$$

Thus the indices of refraction are dependent only on the magnitude of the field and not on its direction. As a consequence the retardation Γ, given by (2), will also depend only on the magnitude of the field. The orientation of the ellipse, however, does depend on the field direction. From (8) and (4) the angle between the x' and x axes is given by

$$\sin 2\theta = -\frac{r_{22}}{\bar{r}}\cos\alpha - \frac{r_{11}}{\bar{r}}\sin\alpha$$

$$= -\sin(\alpha + \Phi),$$

where

$$\Phi = \arcsin r_{22}/\bar{r}. \quad (12)$$

Thus

$$-2\theta = \alpha + \Phi. \quad (13)$$

The fixed angle Φ, independent of the field direction, occurs because of the choice of the coordinate system for which the matrix r_{ij} was written. This system is such that if the field is in the x direction (i.e., if $\alpha = 0$) the principal axis x' is $-\Phi/2$ from that direction. It is easily seen that choice of the coordinate system can always be made such that the x and x' directions coincide when $\alpha = 0$, i.e., such that $\Phi = 0$.

The discussion above shows that electro-optic crystals of the symmetry described are unique in that their optical properties are subject to control by two variables: the magnitude of the applied electric field and its direction. This is in contrast with such materials as KDP where only the magnitude of the field is a useful control variable. The application of crystals showing this dual transverse Pockels effect to the problem of light modulation is discussed in succeeding sections.

Crystal classes whose symmetry elements include one or more threefold axes, and which therefore show the dual transverse effect, occur in the trigonal, hexagonal, and cubic systems. In cubic crystals, the [111] directions are threefold rotation axes. The dual transverse effect is therefore obtainable from cubic crystals of those classes in which additional symmetry elements do not eliminate a linear electro-optic effect, namely 23 and $\bar{4}3m$. Of these, crystals of class $\bar{4}3m$ are more desirable in that they can possess no complicating optical activity. In the cube axis system ordinarily used for describing cubic crystals, the electro-optic tensor has only 3 nonzero components which are all equal, $r_{63} = r_{52} = r_{41}$. In terms of this parameter, the value of $\bar{r}$ in (11) is found to be $^2/_3 r_{41}$. In cubic crystals, an induced polarization direction coincides with the field when the latter is along a [112] direction. Additional crystal classes compatible with the dual transverse effect are 3, 32, and $3m$ of the trigonal system and $\bar{6}$ and $\bar{6}m2$ of the hexagonal. Crystals of these classes are less desirable than cubic crystals because of the restricted light apertures due to their natural birefringence.

III. Duplex Polarization Modulation

Passage of polarized light through an electro-optic crystal does not alter its total intensity but produces a modulation of its polarization state. With a crystal exhibiting the dual transverse effect described in the preceding section, it is possible simultaneously to apply two modulating signals to one beam and subsequently to separate them at a receiver. The effects of such duplex modulation on the polarization state of the beam are shown in this section.

A left circularly polarized beam of light traveling in the $+z$ direction in a right-hand coordinate system enters the electro-optic crystal as shown in Fig. 1. Let the incident light have

$$E_x = E_l\cos\omega_l t,$$

$$E_y = E_l\sin\omega_l t, \quad (14)$$

and let the fast polarization direction be along x' when the electric field, E_m, is at an angle α from x. As discussed earlier, we may choose the x, y directions such that x' coincides with x for $\alpha = 0$. Then the angle θ between x and x' is $-\alpha/2$ as shown in Fig. 1. The field in the crystal is the resultant of two independently

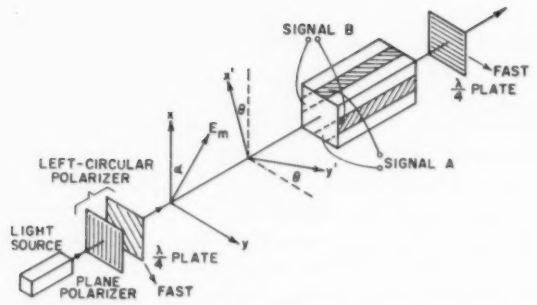

Fig. 1. Schematic representation of the optical arrangement for duplex polarization modulation. Light propagates along the threefold axis of the electro-optic crystal to which the signals A and B are applied.

varying component fields A(t) and B(t) applied along the x and y directions. Thus we have

$$E_m = (A^2 + B^2)^{1/2},$$
$$\tan\alpha = B/A. \tag{15}$$

This field produces a relative phase shift between rays polarized along x' and y' given by (2) and (11) as

$$\Gamma = \frac{2\pi d}{\lambda} n_0^3 \bar{r} E_m \equiv 2kE_m. \tag{16}$$

After traversing the crystal, the electric vector of the light in the x', y' system is

$$E_{x'} = E_l[\cos\theta \cos(\omega_l t + \Gamma/2) + \sin\theta \sin(\omega_l t + \Gamma/2)],$$
$$E_{y'} = E_l[\cos\theta \sin(\omega_l t - \Gamma/2) - \sin\theta \cos(\omega_l t - \Gamma/2)]. \tag{17}$$

After conversion to the x, y system and elimination of θ using (13) and (15)

$$E_x = E_l\left[\cos(\Gamma/2)\cos\omega_l t - \frac{A}{E_m}\sin(\Gamma/2)\sin\omega_l t - \frac{B}{E_m}\sin(\Gamma/2)\cos\omega_l t\right],$$
$$E_y = E_l\left[\cos(\Gamma/2)\sin\omega_l t - \frac{A}{E_m}\sin(\Gamma/2)\cos\omega_l t + \frac{B}{E_m}\sin(\Gamma/2)\sin\omega_l t\right]. \tag{18}$$

The first terms in E_x and E_y correspond to the left circularly polarized carrier reduced in amplitude by $\cos(\Gamma/2)$ indicating that sideband energy appears at the expense of the carrier in the modulation process. The second terms and the third terms in E_x and E_y correspond to two right circularly polarized vibrations differing in phase by 90°. In the small signal approximation [$\sin(\Gamma/2) = (\Gamma/2)$], the amplitudes of these vibrations are seen to be proportional to modulating signals A and B, respectively. As is shown in the next section, A and B are separately recoverable under these circumstances. We call the modulation process described above "duplex polarization" modulation.

Duplex polarization modulation having a linearly polarized carrier can be obtained by the addition of a quarter-wave birefringent plate at the output of the electro-optic crystal. If this is oriented with its slow polarization direction along x, its output is

$$E_x = E_l\left[\cos(\Gamma/2)\cos\omega_l t - \frac{A}{E_m}\sin(\Gamma/2)\sin\omega_l t - \frac{B}{E_m}\sin(\Gamma/2)\cos\omega_l t\right],$$
$$E_y = E_l\left[\cos(\Gamma/2)\cos\omega_l t + \frac{A}{E_m}\sin(\Gamma/2)\sin\omega_l t + \frac{B}{E_m}\sin(\Gamma/2)\cos\omega_l t\right]. \tag{19}$$

The first terms now represent the carrier linearly polarized at 45° to the x direction; the second and third terms represent the modulated components linearly polarized at −45° to the x direction and differing by 90° in phase.

The polarization states resulting from sinusoidal modulation applied as field A or B are shown in Fig. 2 for the cases of both circularly and linearly polarized carriers. The ellipses represent the loci of points taken by the positive end of the electric vector of the light wave during one optical cycle as the oncoming beam is viewed. The circularly polarized carrier becomes elliptically polarized during modulation, its axes depending upon whether the signal is applied as field A or B as shown in the first two rows. The light output with linearly polarized carrier has polarizations dependent upon fields A or B as shown in the last two rows. With both fields A and B the output light varies both in ellipticity and orientation.

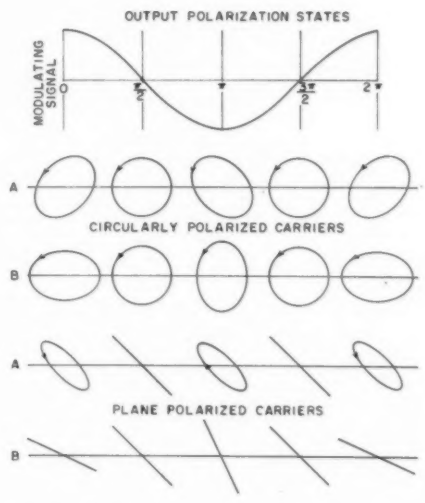

Fig. 2. Polarization states of modulated light beam for sinusoidal modulation applied as signal A or B. These states are shown both for circularly polarized and plane polarized carriers.

IV. Detection of Polarization Modulated Light

In the process of polarization modulation, no light absorbing elements are involved and, therefore, the beam intensity is constant. Detection by a photocell insensitive to the polarization state would give no information recovery, and so polarization filters are needed at the receiver. If two modulating signals are present as in the preceding examples, the particular polarization component transmitted to the detector determines which signal is recovered.

Examination of the circularly polarized output (18) shows the intensities of the components linearly polarized along x and y to be

$$I_x = |E_x|^2 = E_l^2\left(1 - \frac{B}{E_m}\sin\Gamma\right) \cong E_l^2(1 - 2kB),$$
$$I_y = |E_y|^2 = E_l^2\left(1 + \frac{B}{E_m}\sin\Gamma\right) \cong E_l^2(1 + 2kB), \tag{20}$$

where the final expression corresponds to the small signal approximation $\sin\Gamma = \Gamma$. The intensities of the linearly polarized components at $\pm 45°$ with respect to x are

$$I_{x,y} = |E_{x,y}|^2 = E_l^2\left(1 - \frac{A}{E_m}\sin\Gamma\right) \cong E_l^2(1 - 2kA),$$
$$I_{x,-y} = |E_{x,-y}|^2 = E_l^2\left(1 + \frac{A}{E_m}\sin\Gamma\right) \cong E_l^2(1 + 2kA). \tag{21}$$

Therefore, use of a photocell preceded by a plane polarizer oriented along either x or y results in detection of signal B; use of a photocell preceded by a plane polarizer oriented at 45° to x results in detection of signal A. Conversion of the receiver from one channel to the other is achieved by a 45° rotation of the polarizer.

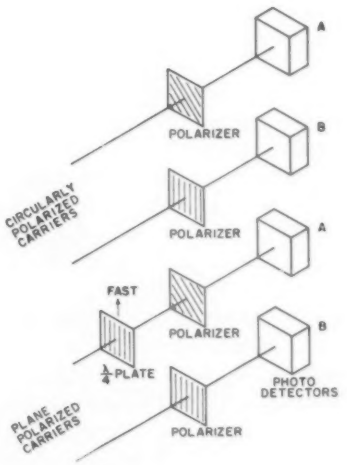

Fig. 3. Receivers for detection of each modulating signal of duplex polarization modulated light for cases of circularly polarized and plane polarized carriers.

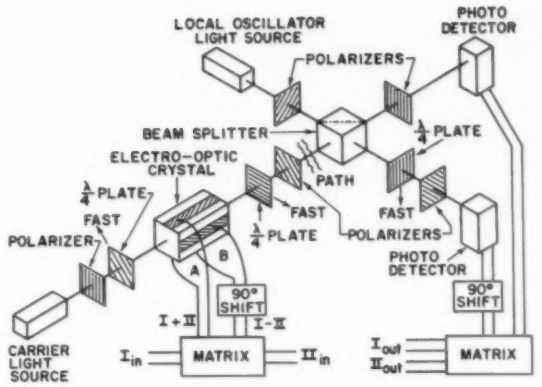

Fig. 4. Schematic diagram of the electrical and optical arrangements for duplex optical transmission and reception with suppressed carrier.

The quarter-wave birefringent plate which converts the circularly polarized output (18) to the linearly polarized output (19) affects the relative phases, but not the amplitudes, of the x and y components. These are, therefore, given again by (20). This plate, however, converts the components linearly polarized at $\pm 45°$ to x into circularly polarized components whose amplitudes are therefore given by (21). In the case of a linearly polarized carrier, therefore, a photocell with a linear polarizer along x or y detects signal B, while a photocell with a circular polarizer of either sense detects signal A. In applications where the receiver may rotate slightly about the beam axis, this type of operation affords more certain separation of the two signals than does operation with a circularly polarized carrier. This is because the operation of the circular polarizer required for detection of signal A is independent of rotation about the axis. Rotation of the plane polarizer required for detection of B from the optimum orientation reduces the intensity of B at the photocell but does not produce mixing of A with B. Receivers of both types are shown in Fig. 3, the circular polarizer consisting as is shown of a plane polarizer at 45° to the axes of a preceding quarter-wave plate.

The minimum crosstalk between signals A and B is that due to the nonlinearities of (20) and (21). Thus the output of a photocell responding to the x component of the incident beam will be proportional to the intensity of this component, which may be written

$$|E_x|^2 = E_l^2\left(1 - 2kB\frac{\sin\Gamma}{\Gamma}\right). \tag{22}$$

Powers of Γ in the expansion of (22) represent spurious products in this output.

V. Single-Sideband Modulation and Reception

The dual transverse linear electro-optic effect described above is also most useful in generating single-

sideband modulation. Consider two independent signals

$$\begin{aligned} \mathrm{I} &= V_1 \sin\omega_1 t, \\ \mathrm{II} &= V_2 \sin\omega_2 t, \end{aligned} \tag{23}$$

from which, using a sum and difference matrix and phase shifter, are derived

$$\begin{aligned} w\mathrm{A} &= V_1 \sin\omega_1 t + V_2 \sin\omega_2 t, \\ w\mathrm{B} &= V_1 \cos\omega_1 t - V_2 \cos\omega_2 t, \end{aligned} \tag{24}$$

in which w is the effective distance across which fields A and B exist. Substituting (24) into (18) and using (16) one obtains for the light amplitude

$$\begin{aligned} E_x &= E_l \left[\cos(\Gamma/2) \cos\omega_l t \right. \\ &\quad \left. - \frac{k \sin(\Gamma/2)}{w(\Gamma/2)} \left\{ V_1 \cos(\omega_l - \omega_1)t - V_2 \cos(\omega_l + \omega_2)t \right\} \right], \\ E_y &= E_l \left[\cos(\Gamma/2) \sin\omega_l t \right. \\ &\quad \left. + \frac{k \sin(\Gamma/2)}{w(\Gamma/2)} \left\{ V_1 \sin(\omega_l - \omega_1)t - V_2 \sin(\omega_l + \omega_2)t \right\} \right], \end{aligned} \tag{25}$$

in which the first terms represent a left circularly polarized carrier, and the following terms represent right circularly polarized lower and upper sidebands respectively. Thus it is seen that, if two independent signals (23) are first converted into the form (24) and then applied to the polarization modulator of Fig. 1, each appears on a different optical sideband. Addition of a quarter-wave plate to the modulator as before, (19) converts the carrier frequency components to plane-polarized light and the sidebands to light plane polarized 90° from the carrier.

Recovery of signals I and II can be achieved using photodetectors preceded by polarizing filters oriented as in Fig. 3 to obtain voltages proportional to A and B. These are given a 90° relative phase shift and added or subtracted to isolate I or II, an operation which is the inverse of (24).

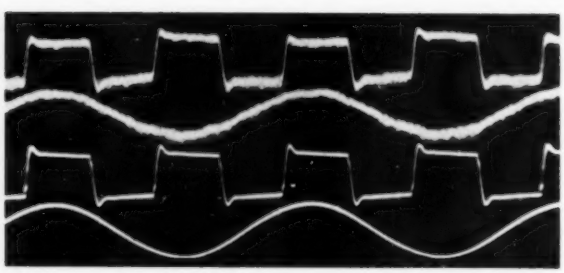

Fig. 5. Oscillogram showing the modulating signals and the received signals in a duplex polarization modulation experiment. The lower traces are the signals A and B applied as shown in Fig. 1 and consisting respectively of a 1000-cps square wave and a 500-cps sine wave. The upper traces are the corresponding output signals from the appropriate receivers of Fig. 2.

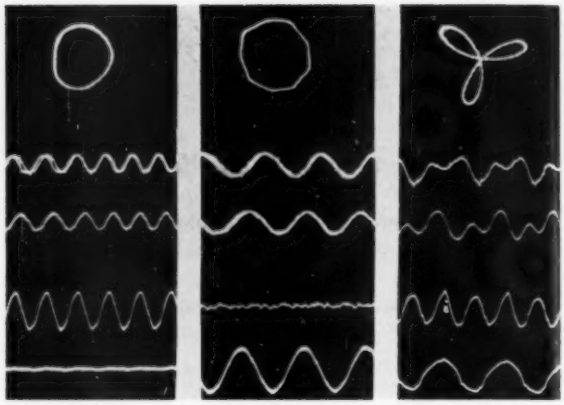

(a) (b) (c)

Fig. 6. Oscillograms showing, from top to bottom, a plot of field A vs field B, the output of the two photodetectors and the recovered signals in duplex single-sideband generation and reception. Fields A and B were derived from the input signals I_1 and II_2 according to Eq. (24). In (a) I_1 is a 1000-cps sine wave and $\mathrm{II}_2 = 0$; in (b) $\mathrm{I}_1 = 0$ and II_2 is a 500-cps sine wave; in (c) I_1 is a 1000-cps sine wave and II_2 is a 500-cps sine wave.

VI. Suppressed-Carrier Transmission and Reception

Optical sidebands must be demodulated by mixing them with their carrier frequency in a square law detector such as a photocell. The carrier can either be transmitted to the receiver with the sidebands as described above, or generated locally at the receiver.[6] In the latter case both the suppressed carrier and the carrier reinserted at the receiver must be coherent and have nearly the same frequency, since any error will appear as a frequency shift in the recovered signal.

For modulating signals in the microwave range, such shifts due to the frequency instability of optical masers should be tolerable. A much more severe requirement is that of phase synchronism between the suppressed and reinserted carriers, but this is removed if one sideband is suppressed in either the transmitter or the receiver. Using the phasing technique described above, single-sideband operation of both transmitter and receiver is possible permitting simultaneous use of both sidebands by two independent signals without the requirement of phase synchronism of the reinserted carrier. A similar system at radio frequencies has been described by Norgaard.[7,8]

One possible configuration of a suppressed-carrier optical transmitter and receiver is shown in Fig. 4. The transmitter is similar to that in Fig. 1, but includes a polarization filter before the transmission path to absorb the carrier. The quarter-wave plate and polarizer comprising this filter convert the beam given by (25) to the form

$$E_x = -E_y = -E_l \frac{k \sin(\Gamma/2)}{w(\Gamma/2)} \{V_1 \cos(\omega_l - \omega_1)t - V_2 \cos(\omega_l + \omega_2)t\}. \quad (26)$$

After traversing the transmission path this duplex signal is combined with a synthetic carrier from a local oscillator source having

$$E_x = E_y = E_c \cos(\omega_l t + \delta), \quad (27)$$

in which δ is an arbitrary phase angle. (In this equation, and in others to follow that describe beams traveling in the same direction, the x and y refer to a coordinate system related to the coordinate system of the modulator by a reflection in a plane containing the beam-splitter reflecting surface.) Each component entering the beam splitter is halved in intensity when it emerges so that each of the resulting composite beams has

$$E_x = \frac{\sqrt{2}}{2}\left[E_c \cos(\omega_l t + \delta) - E_l \frac{k \sin(\Gamma/2)}{w(\Gamma/2)} \{V_1 \cos(\omega_l - \omega_1)t - V_2 \cos(\omega_l + \omega_2)t\}\right], \quad (28)$$

$$E_y = \frac{\sqrt{2}}{2}\left[E_c \cos(\omega_l t + \delta) + E_l \frac{k \sin(\Gamma/2)}{w(\Gamma/2)} \{V_1 \cos(\omega_l - \omega_1)t - V_2 \cos(\omega_l + \omega_2)t\}\right].$$

Selected polarization components of these beams are demodulated by the photodetectors. If $E_c \gg E_l$, terms in E_l^2 comprising the photocurrents can be neglected, and under such linear operating conditions the output can be shown to be proportional to

$$I_{\text{linear}} = \frac{E_c^2}{4} - \frac{E_c E_l}{2} \frac{k \sin(\Gamma/2)}{w(\Gamma/2)} \{V_1 \cos(\omega_l t + \delta) - V_2 \cos(\omega_2 t - \delta)\} \quad (29)$$

from the detector with the linear polarization filter and

$$I_{\text{circ}} = \frac{E_c^2}{4} + \frac{E_c E_l}{2} \frac{k \sin(\Gamma/2)}{w(\Gamma/2)} \{V_1 \sin(\omega_l t + \delta) + V_2 \sin(\omega_2 t - \delta)\} \quad (30)$$

from the detector with the circular polarization filter. If the latter is phase shifted by 90° and combined with the former the sum and difference each contain only one sideband.

Thus, it can be seen that the phasing method of single-sideband reception[8] is applicable to optical superheterodyne reception. For two signals transmitted as opposite sidebands on a suppressed-carrier, signal separation is independent of the reinserted carrier phase δ.

VII. Experimental

A natural sphalerite crystal (ZnS) was cut and polished with two parallel (111) faces 6 mm square and 10 mm apart. Metal electrode strips, 2 × 10 mm, were evaporated onto the center of each rectangular face and connected so that field A was along $[11\bar{2}]$ and field B was along $[\bar{1}10]$. This crystal was incorporated into the polarization modulator shown in Fig. 1. The light source was a dc operated sodium vapor lamp with a Corning CS 3-66 yellow filter. A plane polarizer and quarter-wave plate circularly polarized the beam which was focused on the center of the ZnS crystal. The light traveled along the [111] direction in the crystal and then was passed through a quarter-wave plate as shown. Two test signals, a 1000-cps square wave and 500-cps sine wave, were amplified separately and applied to the electrodes on the crystal to produce fields A and B, respectively. These signals appeared as sidebands on the emerging plane-polarized carrier.

The two signals were simultaneously received by splitting the beam and bringing each half into one of the two receivers shown in the lower half of Fig. 3. Multiplier phototubes (1P21) served as detectors. An oscillogram showing, from top to bottom, the two output signals and two input signals is shown in Fig. 5. A similar experiment in which the carrier was circularly polarized by leaving out the second quarter-wave plate of Fig. 1, and which used the first two receiver configurations of Fig. 3, gave identical results.

Single-sideband generation and reception was then demonstrated using the same equipment as above except for the signal sources. Fields A and B were derived from two input signals I_1 and II_2 according to Eq. (24). This operation involved the use of a phase inverter, a resistive matrix and an audio frequency phase shift network which produced a phase difference of 90° between voltage wA and wB for frequency components between 300 and 3000 cps. The two detector outputs, after a correction for a difference in the detector sensitivities, were given a 90° relative phase shift, then combined in a resistive matrix to recover signals I and II separately as described above. Oscillograms obtained during these tests are shown in Figs. 6(a)–6(c). These show, from top to bottom, respectively, a plot of field A against field B which represents the motion of the electric field in the (111) plane of the crystal; the voltages appearing at each of the two photodetectors; and the output signals I and II. Figure 6(a) was obtained with a 1000-cps sine wave as I_1 and with $II_2 = 0$. As shown by Eq. (25), only a lower sideband was present and output II is seen to be zero. Figure 6(b) is similar but with $I_1 = 0$ and a 500-cps sine wave as II_2. Here no lower sideband was generated, output I is zero, and output II is the demodulated upper sideband. With both frequencies applied as opposite sidebands, as in Fig. 6(c), the photodetectors contain both signals, but the outputs I and II each contain the appropriate single-frequency signal.

Experimental verification of the system shown in Fig. 4 has not been achieved because of the poor optical quality of the ZnS crystals available. A similar ex-

periment in which two KDP crystals were used to produce single-sideband suppressed-carrier light as previously described[2] was carried out instead. Two optical maser beams at 6328 Å served as the transmitter carrier source and receiver local oscillator source. The necessary relative frequency stability was obtained by taking the beams from opposite ends of one gas laser. This experiment and its results have been described elsewhere.[9]

VIII. Conclusion

The symmetry properties of the Pockels effect in crystals having a threefold rotation axis in their point group have been analyzed and shown to lead to a dual transverse linear electro-optic effect. Using this effect, light modulators having two signal inputs can be constructed to produce various types of duplex modulation. Crystals in class $\bar{4}3m$ should be most useful, since their symmetry forbids both natural birefringence and optical activity, thus permitting long optical paths in modulators.

References

1. B. H. Billings, J. Opt. Soc. Am. **39,** 797 (1949).
2. C. F. Buhrer, V. J. Fowler, and L. R. Bloom, Proc. Inst. Radio Engrs. **50,** 1827 (1962).
3. I. P. Kaminow, Phys. Rev. Letters **6,** 528 (1961).
4. Susumu Namba, J. Opt. Soc. Am. **51,** 76 (1961).
5. C. D. West, J. Opt. Soc. Am. **43,** 335 (1953).
6. A. T. Forrester, J. Opt. Soc. Am. **51,** 253 (1961).
7. D. E. Norgaard, Proc. Inst. Radio Engrs. **44,** 1718 (1956).
8. D. E. Norgaard, Proc. Inst. Radio Engrs. **44,** 1735 (1956).
9. L. R. Bloom and C. F. Buhrer, Proc. Inst. Elect. and Elect. Engrs. **51,** 610 (1963).

Archie Mahan *APL* (left), Rudolph Kingslake *Eastman Kodak*, David Richardson *Bausch & Lomb*, John Howard *AFCRL*, Joanne Conlon and Mary Warga *OSA*, and E. D. McAlister *UCSD*.

photo D. L. MacAdam

Information for Contributors

Scope: Papers are welcomed in the broad areas of applied optics, in disciplines related to optics and employing optical techniques. Papers should be sent to *The Editor, APPLIED OPTICS, 1155 Sixteenth St. N.W., Washington 6, D.C.* Manuscripts may be submitted in English, French, German, or Russian, and the presentation should be as succinct as comprehension will permit. In general, the metric system of units is preferred. One original and one carbon copy of the manuscript, with two sets of all illustrations, must be sent in. Manuscripts should be typed double or triple spaced on one side of 22 × 28 cm (8½ × 11 in.) paper, leaving a 3.8 cm (1½ in.) margin all around. Equations must be typed not hand written wherever possible. Papers on the more fundamental aspects of experimental and theoretical optics should be sent to *The Editor, JOURNAL OF THE OPTICAL SOCIETY OF AMERICA, National Bureau of Standards, Washington 25, D.C.*

An **abstract,** adequate as an index and a summary, of not more than 100 words should appear at the beginning of the paper after the *title, author's name, affiliation, and address.* In the case of papers in a non-English language, they must be accompanied by an abstract in English as well as an abstract in the language of the paper. It should be borne in mind that this abstract may be used in toto by the abstracting journals, therefore it should be self-contained.

Figures suitable for printer's use should be sent. Bear in mind that illustrations will normally be reduced to column width (8.4 cm—3⅜ in.—20 picas). *Halftones:* two sets of glossy prints are needed, which should be mailed flat, with any proportion or framing indicated on a working copy. *Line drawings* should be suitable for reproduction and be not larger than 22 × 28 cm (8½ × 11 in.). *Captions* should be listed on a separate sheet in addition to each caption appearing on each illustration.

Tables should be typed on separate sheets and the data therein be intelligible, by title, without reference to the text. Tables should include a minimum of vertical ruling.

References must be typed on a separate sheet, be numbered consecutively in the order of their appearance in the text, and follow this form:

1. F. C. Brown, Phys. Rev. **12,** 345 (1821).
2. J. Culpeper, *Space Optics* (Georgetown Institute of Technology Press, Washington, D.C., 1861), pp. 12, 345.

A list of abbreviations for the names of journals is published in *Chem. Abstr. List of Periodicals 1961.* To make for uniformity of presentation generally, the American Institute of Physics *Style Manual,* second edition, should be used. In general, *APPLIED OPTICS* differs from the *Style Manual* only inasmuch as footnotes appear at the bottom of the page of text, while references are listed numerically at the end of the paper.

There will be no **page charge** for publishing in *APPLIED OPTICS* for the time being.

Letters to the Editor should follow the above suggestions, but no abstract is required.

Analysis of Stimulated Raman Scattering of a Giant Laser Pulse

R. W. Hellwarth

When a Raman active material is placed inside the optical Fabry-Perot cavity resonator of a giant pulse ("Q-switched") laser, the high-power laser light pulse induces gain in the Raman material at frequencies shifted from the giant pulse frequency by well-known Raman frequencies. If this gain is large enough to overcome cavity losses, a strong buildup of coherent light at the shifted frequency(s) may ensue; the process is analogous to stimulated fluorescence and is an example of stimulated Raman scattering. We calculate here the Raman output power as a function of time and its spectral content when the Raman material is in the laser cavity. From the resulting expressions (which contain no undetermined parameters) we calculate the properties of the light generated by nitrobenzene inside a giant pulse ruby laser and find that the results agree with (as yet incomplete) observations that have been made on that system.

I. Introduction and Formulation

When a Raman active material is in an optical cavity which is sufficiently excited around one frequency, then light will build up strongly in the cavity at one or more other frequencies differing by Raman shift(s).[1] This is a simple form of stimulated Raman scattering which has been observed from a number of organic liquids which were placed in a Fabry-Perot optical cavity excited by a giant optical laser pulse from ruby. We will analyze the results of these and related experiments here, calculating the scattered intensity as a function of time, giant pulse characteristics, the reflectivities of the end plates at the ruby and scattered frequencies, the pertinent Raman scattering cross sections, and other known parameters.

We need not review the mechanism for the production of a giant optical pulse in the optical cavity, but only review its pertinent properties.[2,3] Strong pulses are the result of suddenly reducing cavity losses several times below the level of gain that has been prepared in the laser material. Hence the ensuing buildup of laser light has a rise time constant several times shorter than the normal cavity decay time. This means that the energy stored in the initially prepared (ruby) population excess is converted to photons inside the cavity in a time short compared with the cavity response time. We will find that under any reasonable conditions the level of Raman scattered light does not become appreciable until several time constants have elapsed. Hence it is quite accurate to approximate the initial phase of the process of interest here as a cavity in which there are: (a) a high number of n_α of photons in each of several cavity modes around the laser frequency ω_a; (b) a laser material in which the population excess has been driven to almost exactly zero (by the formation of the giant pulse) and, by virtue of the relatively slow pumping and relaxation rates, remains zero throughout the subsequent Raman scattering of the photons which have been emitted into the cavity; and (c) a Raman active material which is in thermal equilibrium (at room temperature in experiments to date). The laser material (ruby), therefore, takes no further part in the process other than normal scattering and possibly small absorption of light in the cavity, the effects of which can be lumped into over-all cavity losses. We will picture the optical cavity modes as essentially consisting of waves of equal magnitude running in opposite directions, and assume that these waves are essentially plane waves in character over some cross-sectional area a, and zero outside this region. (The ruby excites only one polarization.) These rays pass through the Raman active material in traversing the cavity and create gain g_β per cm at various Raman shifted frequencies ω_β (and wave vectors $\mathbf{k}_\beta$, polarizations $\mathbf{e}_\beta$) in the illuminated parts of this material which causes light waves of frequency(s) ω_β to become growing waves. Although in general gain exists for wave vectors $\mathbf{k}_\beta$ in all directions, we will be interested only in those directed along the axis between the Fabry-Perot end plates of the cavity where growing waves will be regeneratively fed back and forth through the Raman material many times thus causing a large buildup of light at ω_β when

$$g_\beta l > \gamma_\beta. \tag{1}$$

The author is with Hughes Research Laboratories, Malibu, California.

Received 10 February 1963.

Here l is the length of Raman active material measured along the cavity axis and γ_β is the average loss in nepers suffered by the light in traversing the cavity once. (The natural decay time of the nearly longitudinal cavity modes in which we will be interested, therefore, is τ/γ_β, where τ is the time it takes light to traverse the cavity once.)

According to the theory of stimulated Raman scattering, the gain in a Raman active material at a temperature T which is subjected to plane waves (of wave vector and polarization symbolized by α) of intensity I_α photons per cm^2/sec is[4]

$$g_\beta = \Sigma_\alpha I_\alpha \sigma_{\alpha\beta} \lambda_\beta^4 [1 - \exp(-\hbar\Delta_{\alpha\beta}/kT)]/c_\beta \text{ cm}^{-1}. \quad (2)$$

Here λ_β is the wavelength of the scattered wave β and c_β its velocity as measured in the material. $\Delta_{\alpha\beta} \equiv \omega_\alpha - \omega_\beta \cdot \sigma_{\alpha\beta}$ is the Raman scattering cross section from wave α to wave β per unit wavelength (in the material) per steradian per unit volume of the material. If the recoil of the Raman scatterers can be neglected, then, for the scattering of linearly polarized light, $\sigma_{\alpha\beta} = A \cos^2\theta + B$, where θ is the angle between $\mathbf{e}_\alpha$ the polarization of the incident wave α and $\mathbf{e}_\beta$ the polarization of the scattered wave. A and B are positive functions of ω_α and $\Delta_{\alpha\beta}$ which vary smoothly with ω_α but exhibit peaks as a function of $\Delta_{\alpha\beta}$. These peaks are called Raman lines. If a Raman line has $B = 0$ it is said to be "polarized"; if $B = 3A$ the line is cal'ed depolarized; if $0 < B < 3A$ the line is called partially polarized.[5] No other values of B are possible. The values of A and B have been measured by McClung and Weiner around some of the lines in several of the liquids in which stimulated Raman scattering has been observed[6]; we will use their results later for numerical calculations of stimulated Raman scattering from nitrobenzene which has been the material most studied to date.

The question next arises as to whether the Raman material stays nearly in thermal equilibrium throughout the stimulated scattering process so that (2) remains valid with T constant. The answer is "yes" in any experiments resembling those to date. In a ruby giant pulse the number of photons emitted cannot exceed half the total number of Cr ions, which number would result from 100% inversion. In practice there are many fewer; the most intense pulses used to date have produced total fluxes of around 3×10^{18} photons per cm^2 at $\omega_\alpha \approx 2.7 \times 10^{15}$ rad per sec. Therefore, there can be no more than this number of Raman transitions. We may think of the Raman material as approximately made up of a number of independent scattering molecules all, or a sizable fraction, of which are in their ground vibrational and electronic state. At least several centimeters length of liquid is typically required for sufficient gain, so that roughly one Raman active molecule in 10^4 makes a transition from the ground state even if every incident photon is scattered. The factor $\exp -\hbar\Delta_{\alpha\beta}/kT$ in (2) represents the ratio of the number of molecules in the final Raman level to that in the ground state; it is small initially and is negligibly altered by such a fractionally small number of Raman transitions. Even if the number of photons scattered were larger, relaxation processes which cause excited molecules to return to the ground state might still maintain thermal equilibrium and hence the validity of (2); we need not examine this point further here. Note that (2) is valid (for thermal equilibrium) even if the scattering molecules interact (or are even bound as in a solid) and cannot be considered to be independent or recoiless.[4]

Having established the nature of the experimental process and the applicability of Eq. (2), it is a straightforward matter to compute in what manner photons are scattered from the "incident" cavity modes (α) to the scattered (β) modes. The number of photons n_β in each scattered cavity mode must obey

$$dn_\beta/dt = n_\beta(g_\beta l - \gamma_\beta)/\tau. \quad (3)$$

We neglect here effects of the reflections at dielectric interfaces existing between the cavity end plates; these can be made small by careful anti-reflection coating of the ruby and other elements in the beam. Note that in (3) we have included ordinary cavity loss mechanisms and stimulated Raman scattering, but have not included the contribution of ordinary Raman scattering. This omission can be rectified by putting $1 + n_\beta$ for n_β according to the quantum rules for writing the matrix elements for photon creation. This would be a needless complication because we will be interested in the classical limit where $n_\beta \gg 1$. However, this point will affect our choice of the initial condition of n_β, for rather than take n_β ($t = 0$) to be the thermal average $\langle n_\beta \rangle$, we see it is much more accurate to use instead $\langle 1 + n_\beta \rangle$, especially (as is most often the case) when $\langle n_\beta \rangle$, which equals $[\exp(-\hbar\omega_\beta/kT) - 1]^{-1}$, is less than unity.

It remains to construct the equation governing the time behavior of g_β. To do this it is most convenient to re-express g_β in terms of the numbers n_α of photons in each of the incident cavity modes, for n_α equals $I_\alpha' \tau a$ (a = cross-sectional area of the mode). Here I_α' is the sum of the intensities of both left and right traveling waves in the mode, each of which contributes equally to g_β because of the properties of $\sigma_{\alpha\beta}$ discussed above. Therefore, from (2)

$$g_\beta = \Sigma_\alpha \sigma_{\alpha\beta} n_\alpha \lambda_\beta^4 (1 - \exp - \hbar\Delta_{\alpha\beta}/kT)/(c_\beta \tau a) \quad (4)$$

and

$$dn_\beta/dt = n_\beta(\Sigma_\alpha n_\alpha \Gamma_{\alpha\beta} - w_\beta), \quad (5)$$

where

$$\Gamma_{\alpha\beta} = \sigma_{\alpha\beta}\lambda_\beta^4(1 - \exp - \hbar\Delta_{\alpha\beta}/kT)l/(c_\beta \tau^2 a), \quad (6)$$

and the w_β ($\equiv \gamma_\beta/\tau$) are the natural mode decay rates of the cavity. The sum over incident modes α in (5) signifies scattering from each α mode; one photon is subtracted from an α mode for each added to a β mode, from which it follows that

$$dn_\alpha/dt = -n_\alpha(\Sigma_\beta n_\beta \Gamma_{\alpha\beta} + w_\alpha). \quad (7)$$

Perhaps the most difficult part of the analysis of the problem is determining just how many modes we should include in the mode sums over α and β. Because the incident light is very monochromatic compared with the width of the peaks in $\Gamma_{\alpha\beta}$, the Raman material cannot distinguish the effect of the light in the various α modes. Furthermore, since the α modes which are excited by the ruby all have about the same loss w_α, it is quite accurate to assume that the total of incident photons $x(t) = \Sigma_\alpha n_\alpha$ behave as if they were in a single mode with damping rate w, and therefore to remove the sum on α in (5). The sum over β modes in (7) cannot be eliminated. We know it must include longitudinal modes separated in angular frequency by π/τ; there are generally hundreds of these modes within one resonance of $\Gamma_{\alpha\beta}$. However, we do not know exactly how many transverse modes of a given longitudinal wavenumber to include in the sum on β in (7). The number probably depends on accidental irregularities in the end faces and the materials in the cavity. In mode studies of a strongly pumped ruby laser one sees typically 10–100 different transverse mode patterns.[7] For numerical computation we will assume that 10^2 transverse modes (which have high enough Q's to participate) exist for each longitudinal index, but keep in mind that this is only a guess and deserves further study. Fortunately such results as the threshold giant pulse intensity will depend very little on this number of modes. Now, barring complications which we mention later, Eqs. (5) and (7), along with the boundary conditions discussed above, should completely describe stimulated Raman scattering of a giant pulse by material in a Fabry-Perot optical cavity. These equations consist of a large number of coupled nonlinear differential equations and, in general, cannot be solved in a closed form. However, we will be able to obtain enough quantitative information from them by looking at various limiting cases to learn a good deal about the behavior of stimulated Raman scattering. For example, even before attempting to solve (5) and (7) one can see that the total number of photons scattered from the α to the β modes increases monotonically as w_α and w_β decrease; that is, the effect is always enhanced by raising the Q's of any of the cavity modes participating. Since in practice about the same Q is obtainable at ω_α as at ω_β the most interesting case will be $w_\alpha = w_\beta$. However we will continue to study the more general case of different Q's.

II. Case of a Small Fraction of Incident Photons Scattered

In most of the experiments to date in which stimulated Raman scattering of a giant pulse has been observed, only a small fraction (10^{-3} to 10^{-1}) of the incident photons is scattered. (This is, of course, a very much larger fraction than would be observed for ordinary Raman scattering.) Fortunately, this low-efficiency limit is easy to analyze because the incident number of photons $x(t)$ is negligibly disturbed from its normal decay $x_0 \exp - wt$ and each of the Eqs. (5) can be integrated to give

$$n_\beta = \eta \exp [\Gamma_\beta x_0(1 - e^{-wt})/w - w_\beta t]. \quad (8)$$

Here x_0 is the total number of photons produced initially by the giant pulse; $\eta = [1 - \exp - \hbar\omega_\beta/kT]^{-1}$ is the number initially present in each β mode and for molecular vibrational Raman transitions is nearly unity; $\Gamma_\beta = \Gamma_{\alpha\beta}$ but the subscript α has been dropped as each α mode is assumed to have the same effect. We expect the number of modes participating to be of the order 10^4 and the output (at ω_β) is not a significant fraction of the incident photon number until around 10^{15} photons have been scattered, or an average of $\sim 10^{11}$ photons into each mode. Therefore, we see from (8) that the dimensionless ratio r_β of the initial gain in a β mode to the loss in the α mode satisfies

$$r_\beta = \Gamma_\beta x_0/w >> w_\beta/w, \quad (9)$$

in order to accomplish such a large growth before the incident photon number has decayed to where the gain vanishes.

With the above observations in mind we first calculate the total instantaneous scattered power $\phi(t) \equiv \Sigma_\beta w_\beta (n_\beta - \eta)$ (in photons per sec) delivered by the β modes, all or a portion of which are typically monitored by a photon detector and fast scope. By the time that ϕ has grown large enough to give a discernible signal, $r_\beta(1 - e^{-wt})$ is so large that a central limit approximation of the sum on β is very accurate. That is, take $r_\beta \approx r(1 - f^2)$ where, for a Lorentzian line, f is the frequency displacement of the mode β from the line center in units of the half-intensity displacement. The modes may be considered to be continuously distributed with number density ρ per half-width of the line at half-intensity. Therefore, from (8) (assume w_β is a constant W)

$$\phi(t) \to W\rho\eta\pi^{1/2}[r(1 - e^{-wt})]^{-1/2} \exp [r(1 - e^{-wt}) - Wt], \quad (10)$$

soon after the scattering begins (i.e., for $wt > r^{-1}$). This output has its peak at a time t_m nearly given by

$$wt_m = \ln(rw/W), \quad (11)$$

which may be several time constants w^{-1} because $r \gg W/w$ for significant laser action. This means that the

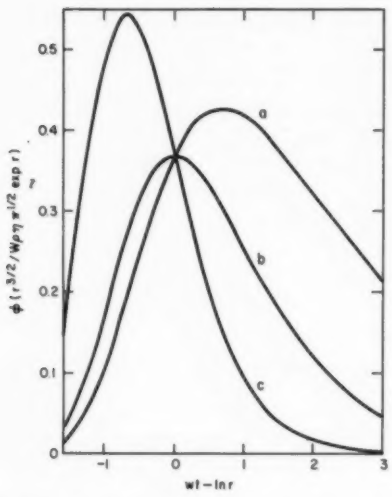

Fig. 1. A plot of Eq. (10) for the scattered power ϕ (normalized by factors defined in the text), as a function of time t (times w the natural decay rate of the incident light modes) minus ln r (where r is the ratio of the peak initial Raman gain $x_0\Gamma$ to incident mode losses w) and valid for weak scattering. The curves (a), (b), and (c) are for $W/w = 1/2$, 1, and 2, where W is the natural decay rate of the scattered modes.

peak output power ϕ_m is nearly

$$\phi_m \backsimeq W\rho\eta(W/wr)^{W/w}e^{r-W/w}(\pi/r)^{1/2}. \tag{12}$$

We have approximated the factor $(1 - \exp - wt)^{-1/2}$ in (11) by unity (the factor is very near unity during the body of the pulse; also according to more detailed estimates its deviation from unity is of doubtful significance anyway). With this approximation we can draw universal curves (one for each value of W/w) for ϕ as a function of $wt - \ln r$, as are shown in Fig. 1.

It is also of experimental interest to know the total fraction ξ_β of initial photons available x_0 which are scattered into β modes at different deviations f from line center (this is what would be recorded photographically by a calibrated spectrograph), and also to know the total fraction $\Sigma_\beta\xi_\beta$ that is scattered (this would be proportional to the integrated output of a photodetector sensitive near ω_β). According to (5)

$$\xi_\beta = \Gamma_\beta\int_0^\infty ds\; n_\beta(s)x(s)/x_0, \tag{13}$$

which from (8) is ($v \equiv re^{-wt}$)

$$\xi_\beta = \eta r_\beta{}^{-W/w}(\exp r_\beta)\int_0^r dv\; e^{-v}v^{W/w}/x_0. \tag{14}$$

We know that $W/w \ll r$ for significant scattering. Therefore, for the important β modes near the center of the output, the integrand in (14) is so small at $v = r$ that the upper limit r may be replaced by ∞ with no significant error; whence we have [$\Gamma(x)$ is the gamma function]

$$\xi_\beta \approx r_\beta{}^{-W/w}x_0{}^{-1}\Gamma(1 + W/w)\exp - r_\beta. \tag{15}$$

From this we see that the half-width at half-intensity of the total scattered output is narrowed over the normal Raman line by a factor $f_{1/2}$ given by

$$f_{1/2} \approx [(\ln 2)/r]^{1/2}. \tag{16}$$

Because we are studying the "weak" scattering case, this spectral narrowing is not spectacular. We will find that for large scattering (i.e., $\xi \to 1$) the narrowing is greater and still approximately given by (16). Of course, (16) gives the over-all spread of radiating modes, each of which emits a very narrow spectrum.

To find the total fraction ξ scattered we may sum (15) over β by using the central limit approximation used to obtain (10), whence ($x_0{}^{-1} < \xi \ll 1$)

$$\xi \to \rho\eta r^{-1/2-W/w}\Gamma(1 + W/w)\pi^{1/2}e^r/x_0. \tag{17}$$

This is essentially the same result that would have been obtained by integrating (10) for the photon flux ϕ over all time or by calculating $\int_0^\infty \Sigma_\beta w_\beta n_\beta dt$ which is the total of scattered photons plus $\Sigma_\beta\eta$.

From (17) one can calculate the size x_0 of a giant pulse required to obtain a given fraction ξ of the photons converted by stimulated Raman scattering to a different frequency. To aid this we have plotted $\xi x_0/[(\pi^{1/2}\rho\eta\Gamma(1 + W/w)]$ versus r for $W/w = 1/2$, 1, and 2 in Fig. 2.

III. Case of High-Fractional Scattering

It has been reported that stimulated Raman scattering from nitrobenzene has produced as much as 30% of the giant pulse photons (from ruby) scattered into

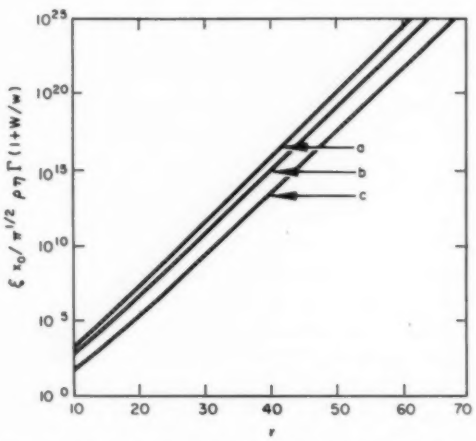

Fig. 2. A plot of Eq. (17) for the total fraction ξ of photons, available initially from the giant pulse, which are scattered as a function of the giant plus intensity x_0 photons (expressed in the dimensionless ratio r of the peak initial gain $x_0\Gamma$ in the scattered modes to the incident mode loss rate w) and valid for weak scattering. The curves (a), (b), and (c) are for $W/w = 1/2$, 1, and 2 where W is the loss rate of the scattered modes.

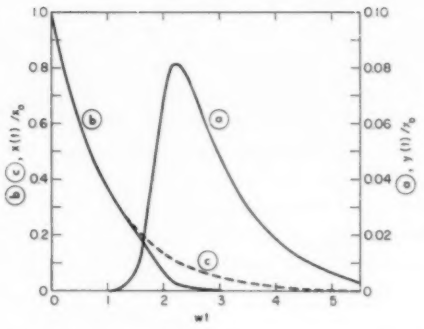

Fig. 3. Curve (a), using right side ordinate, gives a plot of Eq. (21) for the number of photons y in the scattered modes (in units of the number of photons x_0 produced by the giant pulse) as a function of time t (times the cavity loss rate w) for the parameter values indicated by the circle in Fig. 4. Curve (b), using the left-side ordinate, gives the number of photons x (in units of x_0) in the incident cavity modes as a function of wt during the output pulse of curve (a). Curve (c) gives x as it would evolve with time wt without stimulated Raman scattering.

the 1430 cm^{-1} line at 7650 Å[1]; no doubt further experimenting will increase this fraction. [We will find that Eq. (5)–(7) show that in principle any arbitrarily large fraction, approaching unity, of incident photons will be scattered if the number of photons incident initially is made large enough.] An accurate solution of (5) and (7) for large coupling becomes extremely sensitive to very small variations in w_β and Γ_β with β, and these variations are not easy to predict. However, other physical considerations suggest that the accuracy of the equations themselves, for any given Raman material, may be poor at high conversion, and it would not be worthwhile to undertake to solve them very accurately anyway. For example, the inhomogeneous character of the broadening of Raman lines in gases, liquids, and, quite possibly, solids will affect the output more and more for faster and more intense pulses (just as inhomogeneous broadening commonly affects operation in ordinary lasers.) Also the fractional rise of radiation in a mode becomes significant during the time for a single pass of scattered light. Because the modes are separated by less than π/τ, this causes the modes to broaden into each other; in fact, the whole idea of modes seems to lose its meaning in this case. We built up our equations (5)–(7) using the ideas of oppositely traveling growing waves and formulated the mode properties so that qualitatively they would still be sensible even under these indistinct conditions. To proceed, we will ignore inhomogeneous line broadening, and modify (5)–(7) by supposing that all the important scattered photons see essentially the same loss $w_\beta = W$ and same gain $\Gamma_\beta = \Gamma$ and hence behave the same in time. Call the sum of these photons $y(t)$, then (5) and (7) become

$$dy/dt = y(x\Gamma - W) \tag{18a}$$

$$dx/dt = -x(y\Gamma + w), \tag{18b}$$

where Γ is now the peak value that is derived from (6). The initial value y_0 of y is even harder to assess than for the weak scattering case. Presumably, y_0 is the number of thermal (plus zero point) photons available in modes which are encompassed by the final narrow pulse spectrum. From (18) we will be able to estimate the width of the output spectrum and make a guess for y_0; fortunately, the value of x_0 required for a given strength of operation will not be sensitive to the choice of y_0. The first step in solving (18) is to divide each side of (18a) by the corresponding side of (18b) whence dt cancels and the remaining equation is separable in x and y. Integrating gives

$$(x - x_0 + y - y_0)\Gamma w/W = \ln(xy_0/yx_0). \tag{19}$$

This, in principle, gives $x(y)$ which may be substituted in (18) and integrated to give $x(t)$. Because the mathematics is cumbersome for the general case we will solve only the optimum and most interesting case where $w = W$. In this case adding (18a) to (18b) gives

$$x + y = (x_0 + y_0)e^{-wt}, \tag{20}$$

which with (19) gives

$$y = be^{-wt}\{1 + d\exp[\Gamma b(e^{-wt} - 1)/w]\}^{-1}, \tag{21}$$

where $b \equiv x_0 + y_0$ and $d \equiv x_0/y_0$. Equation (21) is plotted for $x_0\Gamma/w = 40$, $d = 10^{15}$ in Fig. 3.

Figure 3 also shows $x(t)$. One can see that what happens in the strong conversion limit is that $x(t)$ decays normally like $x_0 \exp -wt$ until $y(t)$ has had time to grow from its relatively small initial value to near maximum. During the last rise time constant, which is of order $(rw)^{-1}$ and quite short, $x(t)$ suddenly drops to nearly nothing, giving essentially all the photons that were left in the incident modes to the scattered light. The scattered light then decays in a normal exponential fashion; x is so small that stimulated scattering is no longer important. One can see from (21) that the time t_m to reach maximum in the scattered pulse obeys the same relation (11) as in the weak scattering case.

With these observations we can estimate the spectral width of the output by assuming a uniform density of modes ρ per line-width. In each mode radiation builds up according to (8) until the time t_m after which all decay at the normal rate (without scattering). For those modes near line center, nearly all the photons which are emitted during the entire pulse are present at t_m, therefore, the total number scattered into each mode is approximately given by putting $t = t_m$ in (8). Near line center we take $r_\beta = x_0\Gamma_\beta/w \approx r(1 - f^2)$, which, substituted in (8), gives the fraction of the natural line-width $f_{1/2}$ at which the mode intensities are down by one-half from peak value. The result is identical with that given in (16) for the weak scattering

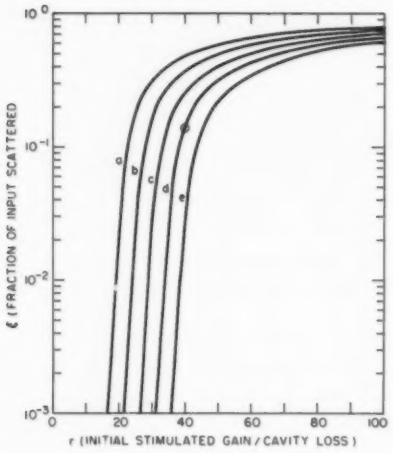

Fig. 4. A plot of Eq. (23) for the total fraction ξ of giant pulse photons scattered to output cavity modes as function of giant pulse intensity x_0 (expressed in dimensionless units $r = x_0\Gamma/w$) and valid for strong scattering. Curves (a)–(e) correspond to $d(= x_0/y_0) = 10^9$, 10^{11}, 10^{13}, 10^{15}, and 10^{17}, respectively, where y_0 is the number of (thermal plus zero point) photons present initially in those modes in which most of the scattered output is concentrated.

case. Assuming that only modes inside the half-width are important we estimate that the initial condition for y is approximately

$$y_0 \approx \rho\eta[(\ln 2)/r]^{1/2}, \tag{22}$$

when we treat strong scattering with Eqs. (18).

We may use (18) to estimate the total fraction scattered by integrating Wy/x_0 over all time:

$$\xi = r^{-1}\ln[(d + e^{r(1+1/d)})/(d + 1)], \tag{23}$$

where $r \equiv \Gamma x_0/w$ as before. A plot of ξ vs r is shown in Fig. 4 where one sees graphically how little the scattering differs for initial values of (y_0/x_0) eight orders of magnitude apart, once r becomes high.

IV. Application to Nitrobenzene

In this section we will use our analysis to calculate the number of giant pulse photons x_0 which are required in order to scatter the fraction ξ that was observed in the Raman emission in ref. 1 under the conditions stated there for nitrobenzene (NB). We will show that this number agrees with the actual giant pulse size that was used and also calculate how much might be converted if the apparatus were optimized for stimulated Raman scattering. We will also calculate line narrowing consistent with that observed.

The peak cross section per unit volume of NB per unit wavelength per steradian $\sigma_{\alpha\beta}$ for the 1345 cm^{-1} Raman line of interest has been measured (by scattering from an ordinary ruby laser) to be 2.3 cm^{-2} with input and scattered polarizations parallel (the line is almost purely polarized).[6] The error in this figure is now set at $\pm$ 50% but will be improved.[6] The full width at half-intensity of this line is 8 cm^{-1} or 24 $\times$ 10^{10} cps. (This means that the total scattering cross section per NB molecule for this line is 6 $\times$ 10^{-30} cm^2.) The area of the laser beam was observed to be 0.12 cm^2. The time τ for light to pass once between the end plates was 1.6 nsec. The scattered wavelength (in air) is 7660 Å and the index of refraction is 1.55. The length along the beam l of the NB liquid was 5 cm. These numbers used in (6) give for the peak value Γ of Γ_β

$$\Gamma \approx 1.15 \times 10^{-3}\ \text{sec}^{-1}. \tag{24}$$

The natural cavity decay rate w at the driving frequency (calculated from the stated end plate losses of 0.17 Np per pass) was 10^8 sec^{-1}, and the decay rate W at the scattered frequency was about 3 times this. The number of longitudinal cavity modes within the line-width is 24 $\times$ 10^{10} $\tau/\pi \cong 120$ or the total number of modes ρ within a line-width is $\sim 10^4$. The initial number of photons η in each mode is ~ 1.

First we ask for the x_0 required for $\xi = 10^{-2}$ which was the lower fractional scattering that was reported.[1] The weak scattering formula (17) should be appropriate and, with the above values of parameters, gives $r = 38$. Therefore, the giant pulse intensity required is nearly

$$x_0 \backsimeq 3.3 \times 10^{17}\ \text{photons}, \tag{25}$$

which is 0.1 J and agrees well within the experimental errors with the giant pulse power used. It is instructive to use the strong scattering formulas (22) and (23) to compute the same thing (for which we must assume $W = w = 10^8$ as we did not calculate the more general case). This gives $r = 33$, or $x_0 = 2.9 \times 10^{17}$ photons, and, if we had properly treated the fact that $W < w$, then this result for r would have been higher. The two limiting theories, therefore, are seen to dovetail quite well.

Let us use (22) and (23) to calculate what giant pulse energy $x_0\hbar w_\alpha$ would be required to achieve $\xi = {}^1/_2$ in the same apparatus except with losses lowered so that $w = W = 0.3 \times 10^8$ sec^{-1} which corresponds to about as low a loss (0.05 Np per pass) as might be realized in practice. Doing this gives $r = 63$ or $x_0 \approx 1.6 \times 10^{17}$ photons (0.05 J). Therefore, very large Raman conversion ($\sim$ unity) can be expected with existing techniques, as had indeed already been indicated in ref. 1.

According to (16) the spectrum of the integrated Raman scattered output in the first case ($\xi = 10^{-2}$) should be 0.14 times the normal width of 4 Å or about 0.6 Å in agreement with spectrographic data. It should also be possible to check the predictions for the pulse power behavior in time by new high-speed photometric techniques. Measurements of Raman

NEW SUBSCRIPTION ORDER

APPLIED OPTICS

Please enter my/our subscription* and continue until countermanded:

- ☐ OSA member rate $6.00 per year
- ☐ Other AIP Societies' rate $8.00 per year
- ☐ Regular rate $10.00 per year
- ☐ Please send OSA membership information
- ☐ check enclosed ☐ bill me
- ☐ Single copy of issue $2.00

Name ..... Membership No. .....

Address .....

.....

*Subscriptions entered for calendar year only.

Please allow eight weeks for order processing.

NEW SUBSCRIPTION ORDER

APPLIED OPTICS

Please enter my/our subscription* and continue until countermanded:

- ☐ OSA member rate $6.00 per year
- ☐ Other AIP Societies' rate $8.00 per year
- ☐ Regular rate $10.00 per year
- ☐ Please send OSA membership information
- ☐ check enclosed ☐ bill me
- ☐ Single copy of issue $2.00

Name ..... Membership No. .....

Address .....

.....

*Subscriptions entered for calendar year only.

Please allow eight weeks for order processing.

FIRST CLASS
Permit No. 18297
New York, N. Y.

BUSINESS REPLY MAIL
No postage stamp necessary if mailed in the U. S. A.

POSTAGE WILL BE PAID BY

APPLIED OPTICS
American Institute of Physics
335 E. 45th Street
New York 17, N. Y.

FIRST CLASS
Permit No. 18297
New York, N. Y.

BUSINESS REPLY MAIL
No postage stamp necessary if mailed in the U. S. A.

POSTAGE WILL BE PAID BY

APPLIED OPTICS
American Institute of Physics
335 E. 45th Street
New York 17, N. Y.

scattering cross sections for other lines in NB and in other materials will be available soon,[6] and the calculations here may be easily repeated for these other cases.

In ref. 1 it was observed that the scattered light is often strong enough to produce further stimulated scattering to multiple Raman shifts. When the stimulated scattering is strong, Eq. (21) shows that the scattered light suddenly exists almost by itself in the cavity and therefore scatters essentially according to the same relations we have developed here for the scattering of the giant laser pulse.

References

1. G. Eckhardt, R. W. Hellwarth, F. J. McClung, S. E. Schwarz, D. Weiner, and E. J. Woodbury, Phys. Rev. Letters **9**, 455 (1962).
2. R. W. Hellwarth, in *Advances in Quantum Electronics* (Columbia University Press, New York, 1961), p. 334.
3. F. J. McClung and R. W. Hellwarth, Proc. IEEE **51**, 46 (1963).
4. R. W. Hellwarth, Phys. Rev. **130**, 1850 (1963).
5. G. Herzberg, *Infrared and Raman Spectra* (Van Nostrand, Princeton, N.J., 1959).
6. F. J. McClung and D. Weiner (private communication).
7. T. P. Hughes and K. M. Young, "Mode Sequences in Ruby Laser Emission" (to be published).

From the Editor

One of our chief trepidations, when first we began to function as an editor, was how to face up to writing editorials. An editorial is rather like a sermon: it is supposed to be both wise and pious. Inasmuch as your editor has a wide circle of associates who suspect that he is neither pious nor wise, this poses certain risks of reproach. Then, as every young cleric must remember, one must be firmly against sin and waywardness without specifically offending those sinners in the congregation who are wealthy or influential. This does not leave much to write about except the weather and the bright and glorious future of optics. As we write this, it is a pleasant spring day in New England.

If we write that we need to produce more or better-trained optics personnel we receive indignant communications that we have distorted the capabilities or capacities of the existing academic facilities. If our own background in physics causes us mentally to consider optics as a subdivision of physics, we are accused by the engineers, chemists, astronomers, and others of neglecting their very important contributions. This is why we stick to discussions of units and terminology and similar noncontroversial matters, such as the use of the metric system.

There is however one other source of material for this column which appears to be substantial and which will doubtless help fill many future paragraphs. This consists of the clarifications and explanations which we must make concerning mistakes, errors, and misunderstandings we manage to perpetrate in prior editorials. For example, some of you have pointed out that our listing of former Russian units in the March editorial is not spelled according to the latest Webster, which has *versta* instead of *wersta*. Our own home encyclopedia happens to be a Brockhaus, rather than a Brittanica, and transliterations differ. Remember that the editorial is usually written under the duress of barely meeting the deadline, and there is no opportunity ordinarily to check out our recollections in the references of the local library.

Another reader felt that we were being very unfair to the ancient Romans to ask how many times does XIV go into MCMLX. These letters, he said, represented cardinal numbers, such as are carved on the cornerstones of PVBLIC LIBRARIES, and were not used in day-to-day calculations. This is at least partly true, and we apologize to any other Romans, Rhodes Scholars, or Harvard graduates who noted this. (*Excusat abjecto, editor illitteratus.*)

The Greeks had words for their numbers, but in writing them used Greek letters α = one, β = two, etc. (Plus special symbols vau for 6, koppa for 90, and sampi for 900.) Apart from these special symbols, sets of numbers looked just like words (with a line over them or an accent at the end to indicate that they were numbers). Mathematical manipulations, however, were performed on an abacus. Similarly, the average Roman, if he could count at all, counted on an abacus, or lacking that, on his fingers and toes, and then wrote down the answer in Roman numerals. On the abacus there were rows of nine beads, and they slid on wires representing I, X, C, $\bar{\text{I}}$, $\bar{\text{X}}$, $\bar{\text{C}}$, etc. It seems to be universally accepted that the decimal system derives from the fact that we have ten fingers and ten toes. After *decem* the Romans counted *undecim*, *duodecim*, and then went to *decem et tres*, etc. The Greeks had a similar system. It is interesting to note that the early Germanish (from whose speech evolved German, Anglo-Saxon, and Scandinavian) found the climate too cold to remove their shoes for eleven and twelve; they simply said *an-laf* and *twa-laf* (one left over and two left over).

We found a fascinating book about early mathematics: *Science Awakening* by B. L. van der Waerden [Oxford University Press, New York (1961)]. This book explains in detail the mathematical manipulations of Egyptians, Sumerians, Babylonians, and up to the Greeks. With this book one can solve the problems of pyramid building and such problems (from the Rhind papyrus) as how to divide 6 loaves among ten men (answer, $\bar{2} + \bar{10}$ or one half plus one tenth each), and how to do it in hieroglyphics, if one wishes to be authentic.

This book tells how the Hindu-Arabic numerals reached northern Europe from Moorish Spain. The bishop and mathematician Gerbert (b. 940) who later became Pope Sylvester II, traveled widely in Spain, and in his book of mathematics introduced Arabic numerals. People did not like these numbers at first, especially the little circle (*cifra*, or zero, which derived from the Arabic *alsifr*, meaning empty). There was no zero on an abacus. As late as 1299 the city of Florence prohibited the use of Hindu numerals, because it was too easy to falsify a 0 to a 6 or a 9. In 1494 the mayor of Frankfurt cautioned clerks to use these numerals sparingly. In 1594 an Antwerp canon warned merchants not to use numerals in contracts or drafts. Five hundred years ago practically everybody north of the Alps still calculated with the abacus and used Roman numerals. To return to today's message, the theme of the editorial, it is simply that awkward, clumsy systems die hard.

We would also like to confess here, just privately between us, that when we asked how many times does XIV go into MCMLX (Ans. CXL), we did not really work it out in cardinal numbers, nor even on an abacus. We cheated and translated from Arabic.

JOHN N. HOWARD

The Optical Society of America

Officers of the Society

President	STANLEY S. BALLARD, Department of Physics, University of Florida, Gainesville, Fla.
President-Elect	RICHARD C. LORD, Spectroscopy Laboratory, MIT, Cambridge 39, Mass.
Past President	DAVID L. MACADAM, Research Laboratories, Eastman Kodak Company, Rochester 4, N.Y.
Executive Secretary	MARY E. WARGA, OSA, 1155 16th Street N.W., Washington 6, D.C.
Treasurer	ARCHIE I. MAHAN, Applied Physics Laboratory, 8621 Georgia Avenue, Silver Spring, Md.
Editor of the Journal of the Optical Society of America	DEANE B. JUDD, National Bureau of Standards, Washington 25, D.C.
Editor of Applied Optics	JOHN N. HOWARD, AFCRL, Bedford, Mass.

Directors-at-Large

* *Term expires December 31 of the indicated year.*

RUDOLF KINGSLAKE (63)* Eastman Kodak Company, Rochester 4, N.Y.
EARLE K. PLYLER (63)* Department of Chemistry, Florida State University, Tallahassee, Fla.
DAVID RICHARDSON (63)* Bausch & Lomb, Inc., Rochester 2, N.Y.
GEORG H. HASS (64)* ERDL, Fort Belvoir, Va.
R. CLARK JONES (64)* Polaroid Corp., Cambridge, Mass.
E. D. MCALISTER (64)* Scripps Institution of Oceanography, La Jolla, Calif.
W. LEWIS HYDE (65)* University of Rochester, Rochester 20, N.Y.
JOHN A. SANDERSON (65)* Naval Research Laboratory, Washington 25, D.C.
GEORGE WALD (65)* Biological Laboratories, Harvard University, Cambridge 38, Mass.

Local Sections

Rochester
JOSEPH L. ROOD *President*
ROBERT M. BLAKNEY *President-Elect*
JOSEPH H. ALTMAN *Secretary*
Research Laboratories
Eastman Kodak Co.
Rochester 4, N.Y.
VERNON L. PARKS *Treasurer*

Detroit
RICHARD MAJKOWSKI *President*
CARL LEISTNER *President-Elect*
DANIEL L. HARMON *Secretary*
16152 Parkside, Detroit 21, Mich.
SAMUEL COHEN *Treasurer*

Niagara Frontier
E. SCHUSTIK *President*
THOMAS FROST *President-Elect*
CALVIN W. YOUNG *Secretary*
Carborundum Metals Co.
Box 32, Akron, N.Y.
RAY ANNINO *Treasurer*

New England
DAVID S. GRAY *President*
CHARLES KOESTER *Vice-President*
GEOFFREY HARVEY *Secretary*
Itek Corporation
10 Maguire Rd.
Lexington, Mass.
WILLIAM J. DAVIS *Treasurer*

Texas
CHARLES S. WILLIAMS *President*
P. O'B. MONTGOMERY *Vice-President*
HARRY J. AUVERMANN *Secretary-Treasurer*
LTV Research Center
P.O. Box 5003
Dallas 22, Tex.

Delaware Valley
F. J. WARZAK *President*
J. E. TUDOR *Secretary*
General Electric Company MSVD
3316 Spring Garden Street
Philadelphia, Pa.
M. CONSHERRY *Treasurer*

Pittsburgh
THOMAS P. VOGL *President*
JEROME J. WOLKEN *President-Elect*
GEORGE L. BUC *Secretary*
Fisher Scientific Company
717 Forbes Street
Pittsburgh 19, Pennsylvania
IRVING S. STAPSY *Treasurer*

Chicago
FRED CLARKE *President*
DONALD PONTARELLI *Vice-President*
RICHARD STECK *Secretary*
4556 North Oakview
Chicago 31, Ill.
HOWARD PADGITT *Treasurer*

Southwestern Connecticut
LEONARD EISNER *President*
ROBERT C. GORE *Vice-President*
MARTIN ROME *Secretary*
Machlett Laboratories, Inc.
1063 Hope Street
Springdale, Connecticut
EDWARD SPEYER *Treasurer*

Southern California
ERNEST DAVIDSON *President*
WM. S. GALLAWAY *Vice-President*
MILTON LAIKIN *Secretary*
Korad Corp.
2520 Colorado Blvd.
Santa Monica, Calif.
JEROME J. ROSENBLATT *Treasurer*

Northern California
ANDREW L. JORGENSEN *President*
CLYDE C. SHAW *Vice-President*
HARVEY MORTON *Secretary-Treasurer*
Tinsley Laboratories
2448 Sixth Street
Berkeley, Calif.

National Capital
MATTHEW P. THEKAEKARA *President*
FREDERICK W. PAUL *First Vice-President*
HARRY K. HAMMOND, III, *Secretary*
National Bureau of Standards
Washington 25, D.C.
RICHARD S. HUNTER *Treasurer*

San Diego
JOHN E. TYLER *President*
JOHN H. TAYLOR *Vice-President*
JOHN M. HOOD *Secretary-Treasurer*
Bldg. 4, U.S. Navy Electronics Laboratory
San Diego 52, Calif.

Detroit
CARL J. LEISTNER *Chairman*
W. K. LESNICK *Chairman-Elect*
D. L. HARMON *Secretary*
University of Detroit
Detroit, Mich.
SAMUEL COHEN *Treasurer*

The Optical Society of America was organized in 1916 **"to increase and diffuse the knowledge of optics in all its branches, pure and applied, to promote the mutual interests of investigators of optical problems, of designers, manufacturers and users of optical instruments and apparatus of all kinds and to encourage cooperation among them."** The Society invites to membership all who are interested in any branch of optics, either in research, in instruction, in optical or illuminating engineering, in the manufacture and distribution of optical goods of all kinds, or in physiological and medical optics. Further information may be obtained from the Executive Secretary of the Society. **Annual Dues:** Regular members and Fellows, $17.00; Associate members, $13.00; Corporate members, $125.00. These dues include subscription to the Society's official journal, the **Journal of the Optical Society of America**, but not to its other publications.

Optical Quality and Radiation Patterns of Ruby Lasers

C. Martin Stickley

A comparison is made of near- and far-field radiation patterns for two different ruby laser crystals of known and differing optical quality. It is shown that ring-width in far-field patterns is directly related to optical quality as measured using a Twyman-Green interferometer. Near-field patterns of the higher quality crystal ($\lambda/10$) that were observed using high-speed photographic equipment always appeared to be transverse modes of a cylindrical resonator whereas this was not true for the poorer quality crystal ($\lambda/4$). An approximate mode sequence during firing of the $\lambda/10$ laser rod shows a reproducible mode development (in time). A sudden switching to higher-order modes was observed and several factors are suggested which could explain this.

Introduction

Extensive measurements have been made on a number of ruby laser crystals of varying degrees of optical quality. These measurements include strain patterns, variation in optical path length, image distortion through the crystal, time-integrated far-field radiation patterns, and short duration exposures of the end of the laser rod when it is oscillating. Data on the best two of these crystals are given. Correlation can be shown between the average optical quality (determined by using a Twyman-Green interferometer[1]) and the width of the rings in the far-field radiation pattern when the laser is pumped near threshold. On the basis of short duration photographs (0.1 μsec) of the end of the laser crystal (near-field radiation pattern) one can see a much more orderly behavior for the higher quality crystal (one-tenth wavelength path variation or less) than for the crystal of lesser quality[2] (one-quarter wavelength or longer). The patterns from the high quality crystal are interpreted as higher-order transverse modes of an open cylindrical resonator of the type described by Fox and Li[3] and Barone.[4] The time sequence of these modes of the $\lambda/10$ crystal show that they change from spike-to-spike and develop in complexity in a reproducible manner. Some reasons for the switching from the lowest order to higher-order transverse modes are suggested below.

Optical Quality

Several means of assessing the optical quality of ruby laser crystals were used in this work. The simplest of these is by examination through crossed polaroids with the polarizer adjusted so that the electric vector is normal to the plane of the crystal axis. If a region of the crystal is strained, it will rotate the plane of polarization of the light and will therefore be passed by the crossed analyzer. Variations from cases of extreme strain to essentially no strain have been observed in ruby laser crystals.*

A second method is the one developed by Hercher,[1] which allows a direct measurement to be made of the variations in optical path length in the crystal. When the laser rod (without reflecting coatings) is placed in one arm of the Twyman-Green interferometer,[5] the interference pattern that is observed approximates a contour map of the optical thickness of the rod.

The third method that has been used[6] employs a collimator to examine and compare the quality and position of a cross hair image that has passed through the rod twice with the image that has reflected from the front, uncoated end of the rod. The rear flat end of the rod is usually left coated to ensure maximum brightness of the return image. If the return image is very fuzzy compared to the image from the front face of the crystal, then discrete optical path variations, strain, and scattering exist in the crystal. If it is displaced from the primary image, then either the ends are not mechanically parallel or a smooth variation in optical path length exists in the crystal. Combinations of these two cases can, of course, occur.

Thirty crystals have been examined by the first and

The author is with the Air Force Cambridge Research Laboratories, L. G. Hanscom Field, Bedford, Massachusetts.

Received 1 April 1963.

* We are indebted to a referee for pointing out that the rotation need not be caused by strain in the usual sense, but rather by local deviations of the crystal's optic axis which are not eliminated by annealing. He suggests the word "lineage". Its effects are not thoroughly understood.

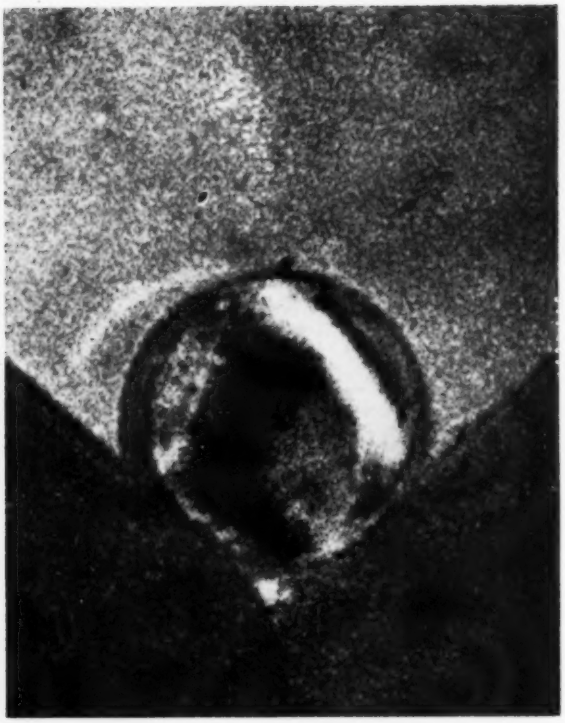

Fig. 1. Interferogram of crystal 32.

third methods and four by the second. Table I is a tabulation of data on two crystals: 32, because it is the best ruby rod we have studied, and 19, because it is of fair optical quality (compared to others we have seen) and because we have a large amount of data on it. Figure 1 is the interferogram for 32 which illustrates the path-length variations for parallel rays normal to the end of the laser rod. The light was polarized with the **E** vector perpendicular to the *c* axis. The path-length variations for 32 are approximately $\lambda/10$ in the center half of the crystal where the laser action develops. A crystal of this quality is by no means common and it represents the best ruby rod that we (and Hercher) have seen when examined using this method. Figure 2 is a similar photograph for 19. Its average path variations are approximately $\lambda/4$ to $\lambda/10$ but they are not smooth (the change in path length between a dark and a bright fringe is $\lambda/4$ for both 32 and 19 since their change in physical length ΔL is zero[1]). It is felt that this is in qualitative agreement with the severe strain that is seen using method 1 and the fuzzy image using method 3.

Table I. Properties of Crystals 32 and 19

Crystal No.	32	19
Length	3.81 cm	3.17 cm
Diameter	4.72 mm	5.00 mm
Lateral surface	Polished	Rough ground
c-axis orientation	57°	$1^1/_2$°
Strain	None	Severe
Path-length variations	$\lambda/10$ (smooth)	$\lambda/4$ (sharp)
Return image	20 sec of arc wide	2 min of arc wide

Far-Field Radiation Patterns

Theory

It is well known in the field of optics that the response of an infinite aperture Fabry-Perot interferometer which is illuminated at all angles with monochromatic light is[7]

$$\theta_p = \sqrt{\frac{n\lambda}{L}(p - 1 + e)}, \tag{1}$$

where θ_p = the angle of the pth ring measured with respect to the normal of the Fabry-Perot; n = refractive index, λ = wavelength of the light, L = separation of the plates, p = ring number counting from the center, and e = fractional excess, $0 \leq e \leq 1$.

The lasers that are discussed in this article have flat, parallel, and mirrored ends. The wavelengths that are emitted correspond (approximately) to longitudinal resonances, $e = 1$, and the separation $\Delta\lambda$ between the emitted wavelengths is $\lambda^2/2nL$. For the case of a ruby laser, $\lambda = 6943$ Å.

[It may be helpful to digress by presenting another viewpoint toward the same phenomenon. The theory of interference between parallel reflecting surfaces is also used in x-ray analysis of crystals[8] and propagation in a waveguide.[9] For the waveguide case one is interested in propagation of power between two parallel metal walls and in the direction of the waveguide.

Fig. 2. Interferogram of crystal 19.

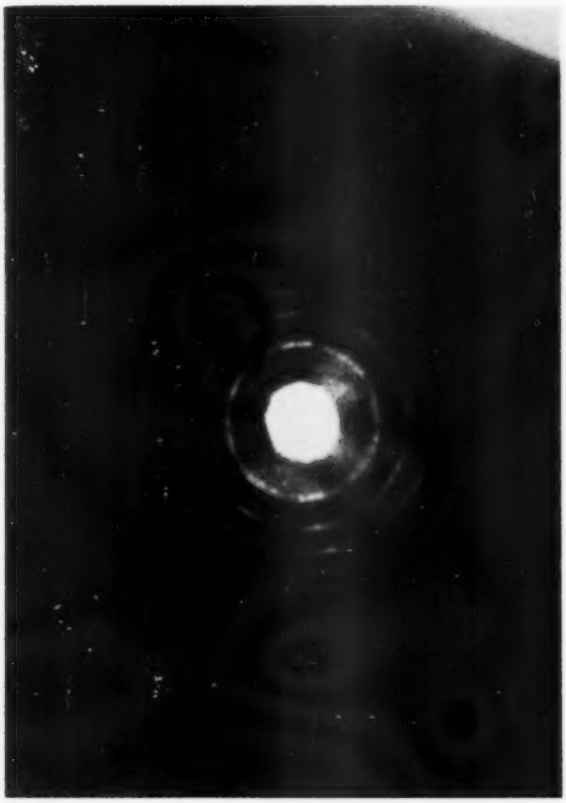

Fig. 3. Far-field radiation pattern of 32 fired 3% over threshold.

Kraus[9] shows that the condition for which this occurs is

$$2L \sin\theta = k\lambda, \tag{2}$$

where L is the separation between the walls of the waveguide, θ = the angle of the Poynting vector measured with respect to the walls, and k is the mode number (an integer). Cutoff for mode number k in the waveguide occurs where $\theta = 90°$ or

$$\lambda_{co}(k) = 2L/k. \tag{3}$$

The term "cutoff wavelength" for a waveguide implies that $k = 1$ and λ_{co} is equal to $2L$. By virtue of Eq. (1), if the waveguide were to be fed from a source that emitted *plane* waves with wavelength λ, power could propagate only at discrete angles, $\theta(k)$. The laser is very much analogous to the waveguide if one lets L equal the length of the laser rod. Since it is self-powered (compared to a waveguide) it oscillates at $\lambda = 2L/k$ (where k is now of the order of 100,000 rather than an integer close to unity) and power can propagate with a component parallel to the plates at the angles given by Eq. (2). These angles are exactly the angles of the rings seen in the far-field radiation pattern of a laser.]

Consider the case where there are optical path-length variations in the laser such that one region has a length of nL and the other, a length $(nL + \lambda/q)$ where q is an integer. Assume that the wavelength λ_0 of oscillation is determined by the region of length nL and that there is some mechanism (the detailed nature of which is not agreed upon at the time of this writing) which maintains energy at wavelength λ_0 in the longer region. The expression that determines the angles θ_p' at which maxima occur in the far-field radiation pattern is (from standard Fabry-Perot theory)

$$2(nL + \lambda_0/q)\cos(\theta_p'/n) = (k_0 - p)\lambda_0, \tag{4}$$

where $k_0 = 2nL/\lambda_0$. Using the approximation $\cos x = 1 - x^2/2$ for small x, one gets

$$\theta_p' = \sqrt{\left(p + \frac{2}{q}\right)\frac{\lambda_0 n}{L}}. \tag{5}$$

The ring width Δr_p would be given by $r_p' - r_p$ where $r_p' = f\theta_p'$ and $r_p = f\theta_p = f\sqrt{p\lambda_0 n/L}$. f is the focal length of the lens used to observe the far-field radiation pattern. This gives

$$\Delta r_p = f\sqrt{\frac{n\lambda_0 p}{L}}\left[\sqrt{1 + \frac{2}{qp}} - 1\right]. \tag{6}$$

Experimental Verification

Figure 3 is the far-field pattern of 32 when it was pumped 3% over threshold; Fig. 4 is the pattern for 19 when it was pumped about 10% over threshold.

Fig. 4. Far-field pattern of 19 fired 10% over threshold.

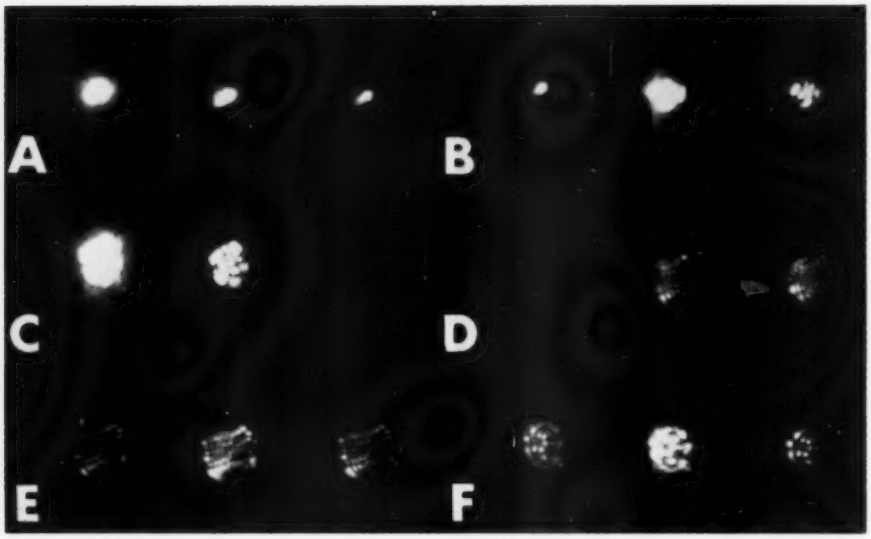

Fig. 5. Approximate mode sequence for 32 fired 15% over threshold. (A) 0.1-μsec exposure and taken at 0, 10, and 20 μsec with reference to the start of oscillation. Each exposure is of a different spike. (B) 0.05-μsec exposure occurring at 12, 22, and 32 μsec with reference to the start of oscillation. Each photograph is of a different spike. (C) 0.2-μsec exposure with 0.5-μsec separation; delay after start of oscillation was 200 μsec. (D) and (E) 0.05-μsec exposure with 0.5-μsec separation and 200-μsec delay; (F) 0.05-μsec exposure with 0.5-μsec separation; 500-μsec delay (near end of oscillation)

It should be mentioned at this point that the star-like feature of the far-field radiation pattern for 32 is not understood (it was present in the radiation patterns for all of the rods that were cut from the same boule as 32). Both laser rods were silver-coated with one end opaque and the other end transmitting about $^1/_2$% so that the ring widths will be limited by optical imperfections rather than by low reflectivity. The pump lamp was a FT 524; the same pumping system was used when the near-field photographs were made which will be discussed in the next section.

Ring-widths were measured from these photographs and are compared with the calculated value [using Eq. (6)] in Table II.

The excellence of the agreement for 32 between calculated and measured values for the less intense portion of the ring is probably fortuitous, considering the approximations that have been made to optical quality, the difficulty in determining 3 dB points on film, the neglect of possible effects of gain mechanisms on ring width, and the fact that Eq. (6) gives the separation between two infinitely sharp components which will, using a more complete theory, have finite width. The ring width in the star pattern is broader than theory would predict but the rings are considerably overexposed in this region. The agreement for 19 is good when compared to the measured value in the bright region. The film is not overexposed in this region but it appears to be underexposed in the dark regions since the rings are barely observable. A third crystal that was examined using the Twyman-Green interferometer was found to have path-length variations of three wavelengths, and its far-field radiation pattern showed no ring pattern at all. Further confirmation of this theory is described in a Letter to the Editor in this issue of *Applied Optics* entitled "Far Field Fabry-Perot Diffraction Patterns of a Neodymium in Glass Laser" by C. Martin Stickley and Rudolph A. Bradbury (see page 873).

Table II. Measured and Calculated Ring-Widths for Ring Number 3

Crystal No.	Δr_3 calc. (mm)	Δr_3 meas. (mm)	Portion of ring
32	0.36	0.38	Dark
		0.5 –0.64	Bright (in star pattern)
19	0.86	0.38–0.5	Dark
		0.76–1.0	Bright

The general agreement between theory and experimental results shows that the ring-widths are good indicators of the optical quality of the laser rod when the reflectivity $R \cong 1$. The model also can explain often seen fine structure in the far-field radiation patterns of some crystals as well as the smooth structure for the cases of 32 and 19.

Ring broadening due to generation of multiple axial frequencies with different refractive indices is entirely negligible; even if the laser rod were good to $\lambda/100$, this contribution would be only about 1% of the ring width. The observed ring-width compared to the ring separation in the far-field pattern is directly related to resolving power of the laser rod if it could be used as

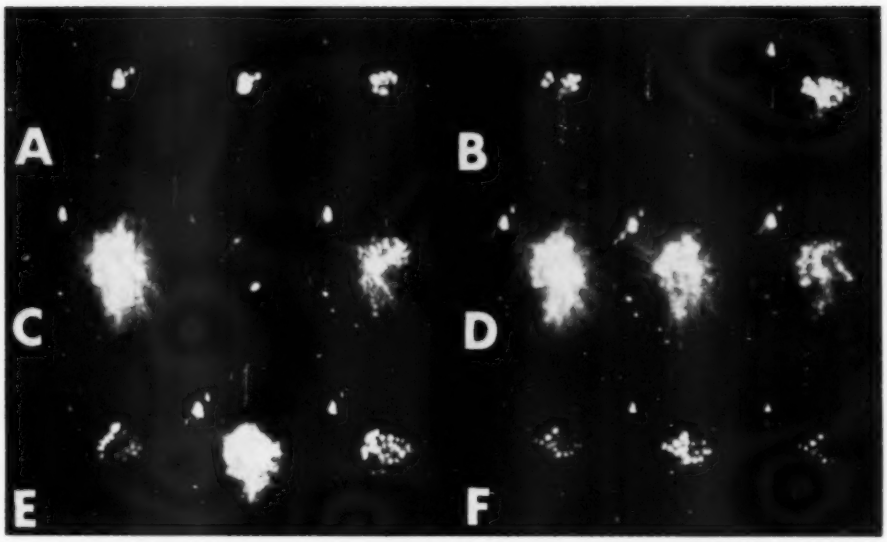

Fig. 6. Approximate mode sequence for 19 fired 15% over threshold. Frame exposure times were all 0.2 μsec; each exposure is of a different spike except for groups E and F. (A) 5-μsec separation at 0, 5, and 10 μsec after start of oscillation; (B) and (C) 5-μsec separation at 200 μsec after start of oscillation; (D) 10-μsec separation at 200 μsec after start of oscillation; (E) and (F) 0.5-μsec separation at 200 μsec after start of oscillation.

a Fabry-Perot interferometer (i.e., if the absorption in the laser material did not exist).

Near-Field Radiation Patterns

Several investigators[2,10,11] have reported their observations of near-field radiation patterns but no attempt was made to correlate these with their optical quality. We have made detailed studies of the near-field patterns of crystals 32 and 19 using an STL image converter camera operating in the framing mode.

Figures 5 and 6 are each complications of six groups of photographs; each group contains three exposures of duration and separation as indicated in the figure captions. These figures are attempts to construct the transverse mode sequences during a firing of the laser even though each group of three was taken during a different firing. For each figure the group photographs were all taken with identical pumping energies and crystal temperatures but with different time delays from the first spike that was emitted.

Figure 5 is the approximate mode sequence for 32 and Fig. 6 is a similar sequence for 19. Before general conclusions are drawn from these photographs, some specific comparisons should be made: (a) For the first 20 to 30 μsec, 32 always oscillates in the lowest order mode (a smooth continuous distribution in intensity) independent of pumping energy, whereas 19 does not do this. Instead, the pattern of the first spike always consists of four dots as shown in the first group of Fig. 6. Note that 32 (Fig. 5, group B) switched to a higher order mode at $t = 22$ μsec. (b) Crystal 32 has no regions that oscillate preferentially over others whereas several of these can be seen for 19. The preferential spots in the patterns for 19 could be locations of relative extrema in optical path as suggested by Hercher.[1] This would be in agreement with the contours seen in its interferogram. The interferogram for 32 does not show any relative extrema, and it has no preferential spots where oscillation occurs. (c) The emitting area for 32 is always confined to a region in the center of the crystal and has a diameter which is equal to about one-third of the rod diameter. This is in qualitative agreement with the analysis of Devlin *et al.*,[12] which showed that the exterior portion of the rod diameter acts as a lens and focuses the radiation into the center of the rod. Crystal 19 starts oscillating in the center but, for very intensive spikes, does spread out toward the edge of the rod in some directions. This is in general agreement with the observations of Aagard *et al.*[13] They mentioned that a ruby sample with rough sides emitted over the whole end of the rod. This is due, presumably, to the lateral surface acting as a scattering device for the pump radiation rather than as a lens. (d) Crystal 32 always exhibits a near-field pattern which is interpreted to be a transverse mode or combination of transverse modes of a cylindrical resonator,[3,4] whereas the patterns for 19 cannot always be construed to be this. They do not have circular symmetry but do appear to be curved in a manner similar to those photographed by Dayhoff.[2] In general, the near-field patterns of 19 do not have the degree of order and symmetry exhibited by those of

32. Further evidence that these are mode patterns is that beat frequencies have been detected between simultaneously occurring modes,[14] and the range of these beat frequencies is in agreement with the predicted range using the mode theory for a cylindrical resonator. Photographic evidence that simultaneous modes can occur and can change within a spike is shown in Fig. 5D. In this group the first two exposures are similar but the third is more complex and yet it retains the features of the first two. Beat frequencies[15] have also been observed to be of shorter duration than the spike width.

There are many effects in a ruby laser that might have bearing on the mode switching observed in 32. We should like to mention three. First, heating of the ruby may cause distortion of the cavity. Second, as the active volume of the laser initially increases, it encompasses a greater number of defects so that oscillation is taking place in a less perfect cylindrical resonator. Fox and Li's theory[16] for a resonator with tilted or distorted plates indicates extreme sensitivity of relative losses in different modes to perturbations of the resonator. Finally, we believe that saturation would lead to that transverse mode being most stable whose average intensity distribution most closely approximated the pump intensity distribution.* Calculations[13,16] have shown that the pump intensity (and consequently the degree of population inversion) is constant for the case of zero absorption within a central region of radius R/n of a laser rod with radius R. If this calculation is assumed to be valid for 32 (light doping and small diameter), then the lowest order mode would not be the most stable since its average intensity is lower near the edge of the highly pumped region than the intensity of a higher order mode. Therefore, one might expect this effect to cause it to switch from the lowest to a higher order mode.

Conclusions

We have presented evidence that there is an intimate relationship between the optical quality of a ruby laser and the radiation patterns that it generates. The narrowness of the rings in the far-field patterns can be directly related to the average path-length variations that exist in the rod. Correlation has been established between the optical quality of two laser rods and their performance as cylindrical resonators in that the near-field patterns of a high quality ruby rod are characteristic of the mode patterns of this type of resonator while the patterns of another, lower quality rod were not clearly recognizable as such. Mode switching is seen which is consistent with a number of prevailing beliefs concerning laser oscillation in ruby.

The writer is deeply indebted to R. A. Bradbury and P. Schweitzer for their help through many stimulating discussions. Other contributors to this work and to whom we express many thanks are D. W. Lipke (now at NASA), who took many of the photographs in Figs. 5 and 6, M. Hercher of the Institute of Optics, who took the interferograms, and J. Mason, for his critical review of the manuscript.

References

1. M. Hercher, Appl. Opt. **1,** 665 (1962).
2. E. S. Dayhoff, Proc. Inst. Radio Engrs. **50,** 1684 (1962).
3. A. G. Fox and T. Li, Bell System Tech. J. **40,** 453 (1961).
4. S. R. Barone, J. Appl. Phys. **34,** (1963).
5. S. Tolansky, *An Introduction to Interferometry* (Wiley, New York, 1955), p. 109.
6. R. A. Bradbury (to be published).
7. M. Born and E. Wolf, *Principles of Optics* (Pergamon Press, New York, 1959), p. 329.
8. C. S. Barrett, *Structure of Metals* (McGraw-Hill, New York 1952), p. 70.
9. J. D. Kraus, *Electromagnetics* (McGraw-Hill, New York 1953), p. 445.
10. T. P. Hughes and K. M. Young, Nature **196,** 332 (1962).
11. V. Evtuhov and J. K. Neeland, Appl. Opt. **1,** 517 (1962).
12. G. E. Devlin, J. McKenna, A. D. May, and A. L. Schawlow, Appl. Opt. **1,** 11 (1962).
13. R. L. Aagard, D. L. Hardwick, and J. F. Ready, Appl. Opt. **1,** 537 (1962).
14. C. M. Stickley, Proc. IEEE **51,** 1848 (1963).
15. O. Svelto, Appl. Opt. **1,** 745 (1962).
16. A. G. Fox and T. Li, Proc. IEEE **51,** 80 (1963).

* We are grateful to a referee whose remarks have led to clarification that this must be a saturation effect.

V. Z. Williams *Perkin-Elmer* and Elmer Hutchisson *AIP*.

Applied Optics

Letters to the Editor

Letters to the Editor should be addressed to the Editor, APPLIED OPTICS, 1155 16th St., N.W., Washington 36, D.C.

Influence of Magnetic Fields upon Gas Discharge Lasers

Rudolf G. Buser, J. Kainz, and J. Sullivan

U.S. Army Electronics Research and Development Laboratory, Fort Monmouth, New Jersey.
Received 25 January 1963.

The recent development of continuous-wave gaseous lasers[1-3] opens up a number of interesting applications for laboratory experiments in the field of plasma physics. Here, as well as in the communications aspect, the problems of modulation, intensity adjustment, intensity control, and mode selection are important. In the following we present some experiments in which we studied the influence of a magnetic field upon the light output of a gas laser. In all measurements we used a Perkin-Elmer Spectra-Physics gas phase laser which provides a linearly polarized light beam at 6328 Å, 11,523 Å, and 33,912 Å. A more complete description of this work is given by Buser *et al.*[4]

For excitation we used an rf oscillator (Mc/sec range) capacitively or inductively coupled. No effort has been made to measure the high-frequency coupling and to correct for the change in coupling produced by the changing impedance in the presence of a magnetic field. In general the latter effect was small.

For detection we used either an RCA 6914 image converter, 1P21 photomultiplier recorder system, or a RCA 7102 photomultiplier together with an oscilloscope with the proper filters (at 11,523 Å) or a monochromator (at 6328 Å).

In Fig. 1 we show the relative laser intensity as a function of a longitudinal magnetic field. Parameters: λ = 11,523 Å; capacitive coupling; homogeneous field. With weak excitation the emission drops to zero at $\approx$ 200 Oe (the remaining intensity is fluorescent light passing through the imperfect filter). At moderate to normal excitation a larger magnetic field is necessary to reduce the light intensity towards zero. Changing from capacitive to inductive coupling produces no essential change.

In Fig. 2 we study the dependence of this effect on the polarity of the magnetic field. Here we use two magnetic coils, placed 17 cm apart, and measure the light emission in a parallel and antiparallel field. Parameters: λ = 11,523 Å, capacitive coupling; inhomogeneous field. No essential change, compared to Fig. 1, can be found. Measurements made on different lasers and at different frequencies (λ = 6328 Å) show essentially the same behavior.

Obviously, after an initial rise the intensity of the laser emission soon reaches a maximum and then decreases continuously as the magnetic field is increased. The effect depends on electron concentration n_- (which is a function of power input): At low electron concentration the entire laser action is easily suppressed, at higher concentration the influence of the magnetic field is reduced. The general behavior is independent of the direction of the magnetic field and the type of high-frequency excitation (TE mode or TM mode). If the magnetic field changes with time, we find, at low frequencies, a behavior exactly corresponding to the dc case. At higher frequencies a more complex behavior is found.

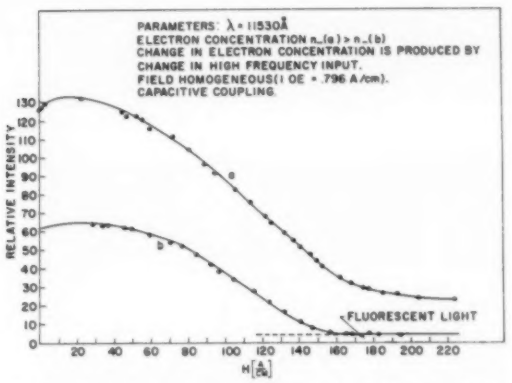

Fig. 1. Laser intensity versus magnetic field strength H. Parameters: λ = 11,523 Å; $n_-(a) > n_-(b)$; field homogeneous capacitive coupling.

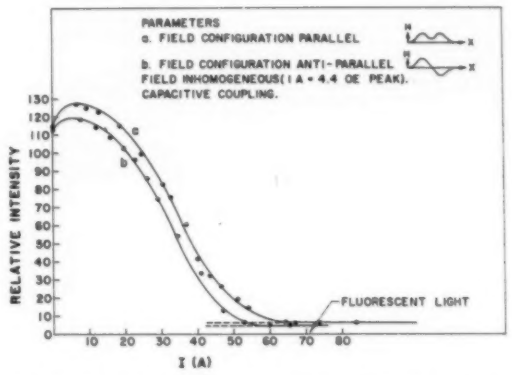

Fig. 2. Laser intensity versus magnetic field strength H. Parameters: λ = 11,523 Å; inhomogeneous field; (a) field configuration parallel; (b) field configuration antiparallel; capacitive coupling.

From a magnetic field we expect the following effects on the emission of a gas discharge laser: influence upon the line emission (Zeeman splitting),[5,6] upon the light propagation (Faraday rotation), and upon the discharge mechanism (energy and particle balance). The conditions of the experiments reported above exclude a marked influence of Faraday rotation and favor an explanation of the effect in terms of diffusion of electrons to the wall and the electron temperature as a function of the magnetic field, and by Zeeman splitting. There is little known about light emission of a high-frequency discharge in the presence of a magnetic field. We can only compare the results of measurements on a dc discharge, and indeed those show a very similar behavior[7] as compared with our observations. On the other hand, Zeeman effect will at higher fields broaden the linewidth of the particular transition involved, reduce the gain, and

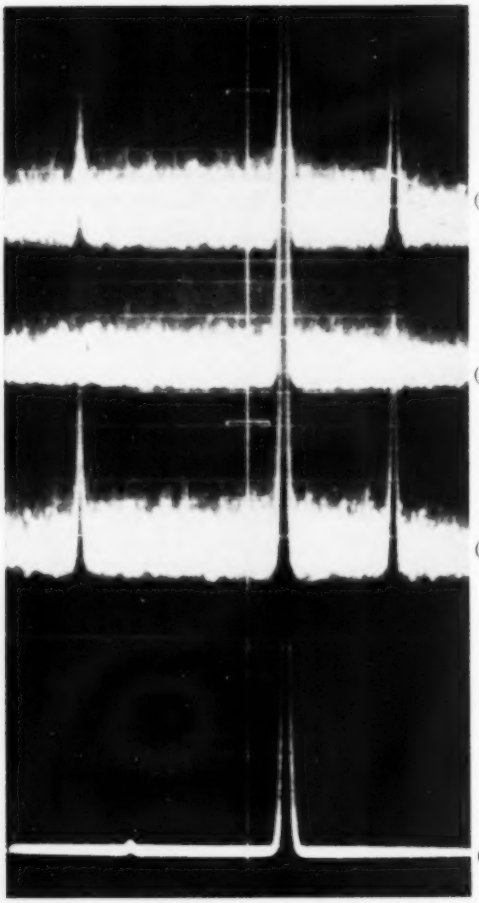

Fig. 3. Influence of the magnetic field upon the beating frequencies; (a) signal with $H = 0$; (b) signal with $H \approx 200$ A/cm; (c) signal with $H = 0$; (d) signal with laser light blocked off (center peak is a reference peak of the instrument at 125 Mc/sec, distance between signals is approximately 1 Mc/sec).

therefore reduce the observed intensity. The reduced influence of the magnetic field at higher excitation could be explained by the increased gain and the increased number of longitudinal modes present. Further work will be needed to study both effects independently.

It is interesting to observe the influence of the magnetic field upon the beating of the optical frequencies as found with a conventional rf spectrum analyzer.[8] Preliminary measurements indicate that, at high magnetic fields, indeed all peaks of the output signal disappear as shown in Fig 3. By turning on and off magnetic fields of different intensities the measurements indicate several possible reactions of mode switching.[9]

We are indebted to the Perkin-Elmer Corporation for supplying the lasers.

References

1. A. Javan, W. R. Bennett, Jr., and D. R. Herriott, Phys. Rev. Letters **6,** 106 (1961).
2. W. R. Bennett, Jr., W. L. Faust, R. A. McFarlane, and C. K. N. Patel, Phys. Rev. Letters **8,** 470 (1962).
3. C. E. N. Patel, W. R. Bennett, Jr., W. L. Faust, and R. A. McFarlane, Phys. Rev. Letters **9,** 102 (1962).
4. R. G. Buser, J. Kainz, and J. Sullivan, "Influence of a dc and ac Magnetic Field upon a Gas Discharge Laser," USAELRDL TR 2322 (Jan. 1963) and TR 2322A (to be published).
5. H. Statz and R. Pannanen, J. Appl. Phys. **33,** 2319 (1962).
6. R. Pannanen, C. L. Tang, and H. Statz, Proc. IEEE, **51,** 63 (1963).
7. G. W. Rokhlin, J. Phys. (U.S.S.R.) **1,** 347 (1939).
8. D. R. Herriott, J. Opt. Soc. Am. **52,** 31 (1962).
9. A. L. Schawlow and C. H. Townes, Phys. Rev. **112,** 1940 (1958).

Analysis of Transients and Stability in an Idealized Two-Level Laser System

J. E. Ludman

Air Force Cambridge Research Laboratories, Bedford, Massachusetts.

Received 1 March 1963.

There have been some recent discussions of the stability and transient behavior (spiking, etc.) in various lasers. The analysis of three-or four-level laser systems involves several coupled differential equations which do not yield analytical solutions.

It is the purpose of this note to point out a relatively simple analytical solution to an idealized two-level laser system. Such a two-level system bears a resemblance to the diode laser system.

The equations describing the idealized two-level system shown in Fig. 1 may be written as follows

$$dn_2/dt = -An_2 - B\rho n + R + B\rho n_1, \tag{1}$$

$$d\rho/dt = -B\rho n_1 + B\rho n_2 - \alpha\rho + An_2, \tag{2}$$

where n_1 and n_2 are the populations of the lower and upper states (electrons per unit volume).

$\rho(t)$ is the radiation field intensity (photons per unit volume). [Since there is only one frequency, the frequency dependence has been neglected. Also the energy density would be $h\nu\rho(t)$.]

R is the rate at which electrons are pumped from state 1 to state 2 (electron per unit volume per sec). The pump rate R is constant.

α is the attenuation constant and $\alpha\rho$ is the energy loss rate of the system (photons per unit volume per sec). [For a unit volume laser with the radiation in one plane, $\alpha = 3 \times 10^{10}/\text{sec}^{-1}(1 - r)$, where r is the reflectance of the walls.]

$n_1 + n_2 = c$ (constant).

A is the coefficient of spontaneous emission.

B is the coefficient of stimulated emission. [The frequency dependence of B, like $\rho(t)$, is neglected.]

The addition of (1) to (2) leads to

$$\frac{d\rho}{dt} + \frac{dn_2}{dt} = R - \alpha\rho. \tag{3}$$

If a steady-state condition of the laser system does exist, then both dn_2/dt and $d\rho/dt$ must be zero leading to

$$R = \alpha\rho. \tag{4}$$

This indicates that if a steady state exists (to be shown), then the pump rate (R) must equal the loss rate ($\alpha\rho$).

Use Eq. (1) and $n_1 = c - n_2$ and rearrange

$$dn_2/dt = R + B\rho c - An_2 - 2B\rho n_2. \tag{5}$$

Use Eq. (2) and $n_1 = c - n_2$ and rearrange

$$d\rho/dt = -\alpha\rho - B\rho c + An_2 + 2B\rho n_2. \tag{6}$$

(n_2 shall be simply n from here on.)

The last term in Eqs. (5) and (6) being a cross term prevents a general solution in closed form, so as a subterfuge is in order.

Define ρ_0 and n_0 as follows:

$$\rho_0 = R/\alpha, \tag{7}$$

$$n_0 = \frac{\alpha R + BRc}{A\alpha + 2BR}. \tag{8}$$

These values are chosen so that in a steady-state condition $n = n_0$ and $\rho = \rho_0$.

Now

$$\rho = \rho_0 + (\rho - \rho_0)$$

and

$$n = n_0 + (n - n_0),$$

$$\rho n = -\rho_0 n_0 + n_0\rho + \rho_0 n + (\rho - \rho_0)(n - n_0). \tag{9}$$

When $\rho \sim \rho_0$ and $n \sim n_0$ (i.e., near the steady-state position), the last term in (9) is small and may be neglected. This approximation will not hold at points far from the steady state but will permit the determination of the stability of the system near the point of steady-state operation. If the laser is stable about this point, the subsequent solutions will describe its behavior.

Inserting the approximation in Eqs. (5) and (6), we obtain:

$$dn/dt = R + 2B\rho_0 n_0 + (Bc - 2Bn_0)\rho - (A + 2B\rho_0)n, \tag{10}$$

$$d\rho/dt = -2B\rho_0 - (\alpha + Bc - 2Bn_0)\rho + (A + 2B\rho_0)n. \tag{11}$$

Rewrite Eq. (10) and differentiate

$$\rho = \frac{1}{(Bc - 2Bn_0)}\left(\frac{dn}{dt} + (A + 2B\rho_0)\,n - (R + 2B\rho_0 n_0)\right), \tag{10a}$$

$$\frac{d\rho}{dt} = \frac{1}{(Bc - 2Bn_0)}\left(\frac{d^2n}{dt^2} + (A + 2B\rho_0)\frac{dn}{dt}\right). \tag{10b}$$

Use (10a) and (10b) to remove ρ dependence in (11),

$$\frac{d^2n}{dt^2} + (A + 2B\rho_0 + \alpha + Bc - 2Bn_0)\frac{dn}{dt} + \alpha(A + 2B\rho_0 n) - [(\alpha + Bc - 2Bn_0)R + 2\alpha B\rho_0 n_0] = 0 \tag{12}$$

$$\frac{d^2n}{dt^2} + D\frac{dn}{dt} + En + F = 0. \tag{12a}$$

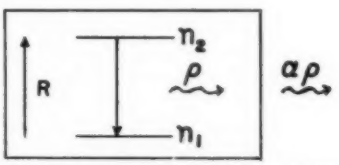

Fig. 1. Idealized two-level laser with populations n_1 and n_2, radiation density ρ, loss rate $\alpha\rho$, and pump rate R.

Solving this in the usual manner:

$$\left(\frac{d}{dt} + \frac{D + \sqrt{D^2 - 4E}}{2}\right)\left(\frac{d}{dt} + \frac{D - \sqrt{D^2 - 4E}}{2}\right)n + F = 0. \tag{13}$$

The general solution is then given by

$$n = c_1 \exp\frac{-D + \sqrt{D^2 - 4E}}{2}t + c_2 \exp\frac{-D - \sqrt{D^2 - 4E}}{2}t + \frac{F}{E}, \tag{14}$$

where

$$D = A + 2B\rho_0 + \alpha + Bc - 2Bn_0,$$

$$E = \alpha(A + 2B\rho_0),$$

$$F = (\alpha + Bc - 2Bn_0)R + 2\alpha B\rho_0 n_0,$$

and c_1 and c_2 are integration constants to be determined by the boundary conditions.

The expression $\alpha + Bc - 2Bn_0$ appears in both D and F. Insertion of the value for n_0 [Eq. (8)] leads to

$$\alpha + Bc - 2Bn_0 = \frac{A\alpha^2 + AB\alpha c}{A\alpha + 2BR} \tag{15}$$

Equation (15) may be used to remove the only negative term in D and F; therefore D, E, and F are all positive constants.

Equation (14) may now be inspected to determine the nature of the solution in the vicinity of the steady-state position. The steady-state position for (14) is just $n = F/E$ and the rate at which any deviations from the steady state will be damped out is just $\exp(-Dt/2)$. If $4E > D^2$, then the second part of the exponential $[\sqrt{(D^2 - 4E)}/2t]$ is of the form $\exp(i\omega t)$ and the approach to steady-state operation will be a damped oscillation with the frequency given by $\omega = \sqrt{(4E - D^2)}/2$. If $D^2 > 4E$, then (14) is critically damped and shows no oscillation whatsoever. Since D and E are both positive constants, the exponentials in (14) cannot become positive, therefore the laser cannot become unstable.

It may be concluded, then, that this two-level laser would achieve a steady-state operation with constant pump rate. After a momentary disturbance of the steady state by some means, such as injection of a light pulse or addition of a pulse to the pump, the laser would return to its steady-state operation with a damped oscillation transient. The same transient is expected when the laser pump is first turned on.

Letters *continued overleaf*

J. W. Kupperian *NASA* (left) and R. H. Tourin *Warner and Swasey*, reporter for New York City.

Improved Cathode for Extreme Ultraviolet Schueler Lamp

R. G. Newburgh

Air Force Cambridge Research Laboratories, Bedford, Massachusetts.

Received 10 April 1963.

A Schueler lamp (hollow cathode) for use as a light source in the extreme ultraviolet (xuv) has been described recently by Newburgh *et al.*[1] Stability was a problem in the original design, especially when helium was used as the discharge gas. The original cathode used was short, open at both ends, and separated from the gas inlet by about 16 cm. Because of the high ionization potential of helium, 24.46 eV, the discharge had a tendency to strike in the region between the cathode and the gas inlet. When this occurred, the discharge was not within the hollow cathode and gave very weak spark spectra. For gases of lower ionization potential, such as hydrogen, argon, and neon, the tendency to strike outside the cathode was much less.

To confine the discharge the structure shown in Fig. 1 was built. The cathode is connected directly to the gas inlet. The cathode (1) is seamless drawn tantalum tubing, approximately 200 mm long, 12.7 mm o.d., and 11.7 mm i.d. It is inserted in an aluminum support (2), and surrounded by a Vycor tube (3) of 17 mm o.d. and 14.5 mm i.d., held in place by three set screws. The Vycor tube protects the cathode from positive ion bombardment.

With this structure the operation is more stable, even with helium, and the discharge easier to strike. By containing the discharge there appears to be less loss of energy to the space outside the cathode, since the observed source intensity for comparable power input is higher by a factor of 2.

The source is convenient for several applications in the xuv region. There is no problem of sorting orders from a continuum, since the lamp is a line source. It is quiet electrically and therefore can be used with counting techniques. It is useful in the same spectral region as a Penning discharge source (PIG) described by Deslattes *et al.*[2] However, the two sources differ in some experimentally important properties. Whereas the PIG suffers from considerable cathode sputtering (for heavier materials the rate of matter removal is 1 mm/hr), this is not a problem with the Schueler lamp. With the improved cathode described in this note, the Schueler discharge can be operated continuously for at least 10 hours. The cathodes themselves can be used apparently indefinitely. One has been operated for several hundred hours and is still completely serviceable.

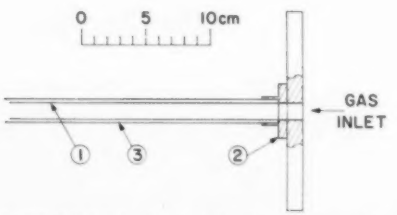

Fig. 1. Modified Schueler lamp cathode. (1) Tantalum cathode. (2) Aluminum cathode support. (3) Vycor tube.

References

1. R. G. Newburgh, L. Heroux, and H. E. Hinteregger, Appl. Opt. **1,** 733 (1962).
2. R. D. Deslattes, T. J. Peterson, Jr., and D. H. Tomboulian, J. Opt. Soc. Am. **53,** 302 (1963).

A Technique for Evaluating Half-Wave and Quarter-Wave Plates

A. C. Hall

Socony Mobil Oil Company, Inc., Field Research Laboratory, Dallas, Texas.

Received 16 April 1963.

Both quarter-wave and half-wave plates are of considerable importance for the analysis of polarized light. The former are used to convert elliptically polarized light to linearly polarized light, and the latter to locate precisely the azimuth of a linearly polarized beam. Since mica has the requisite optical properties and can, in addition, be cleaved relatively easily,[1] it is commonly used to fabricate both quarter-wave and half-wave plates. However, it is difficult to split mica with sufficient precision to obtain plates of the correct thickness (±0.005 mm) and it is necessary to test each specimen.

A micrometer may be used to check thickness,[2] but an optical method is preferable because, among other reasons, the plate may contain inhomogeneities not detectable by a micrometer. If a given plate, illuminated normally by a beam whose plane of vibration includes an angle of 45° with the axes of the plate, transmits circularly polarized light, then it is indeed a quarter-wave plate. Similarly, a putative half-wave plate may be examined to determine whether it rotates the plane of vibration of an incident linearly polarized beam through an angle of 2θ, where θ is the angle contained by the plane of vibration of the incident beam and an axis of the plate.

Although plates which are not exactly quarter-wave may be used for the analysis of elliptically polarized light, exact plates are more convenient. Inexact half-wave plates cannot be used in polarimetry. Thus it is of interest to provide a method which distinguishes quickly and clearly between exactness and inexactness.

The device shown in Fig. 1 uses a single large (50 × 50 × 25 mm) rhombohedron of calcite, P, as polarizer and analyzer. Calcite has, of course, greater transparency than Polaroid, and besides being readily available,[3] is much less expensive than any polarizing prism. M is a partially reflecting mirror and M_1 a front-silvered mirror. The light source is a mercury arc, A, with a filter, F, corresponding to the wavelength for which half-wave and quarter-wave plates are desired (5461 A in this instance). The beam is collimated as shown using a 2-mm aperture at the focus of a 23-mm objective. A second aperture, S, of 2 mm is used to produce a beam of conveniently small cross section.

Without a mica specimen in place, an image of the aperture is seen by an observer behind M. If a mica plate, c, is inserted, three images of the aperture appear along a principal section of

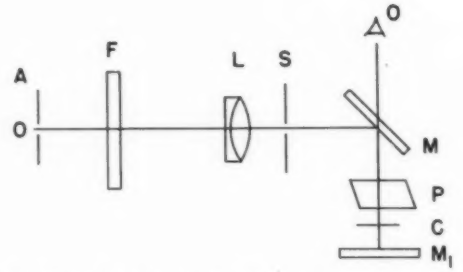

Fig. 1. System for inspecting half-wave and quarter-wave plates. A—mercury arc; F—5461 Å filter; L—collimating lens; S—stop; M—partially silvered mirror; P—calcite rhomb; C—wave plate; M_1—front surface mirror; O—observer.

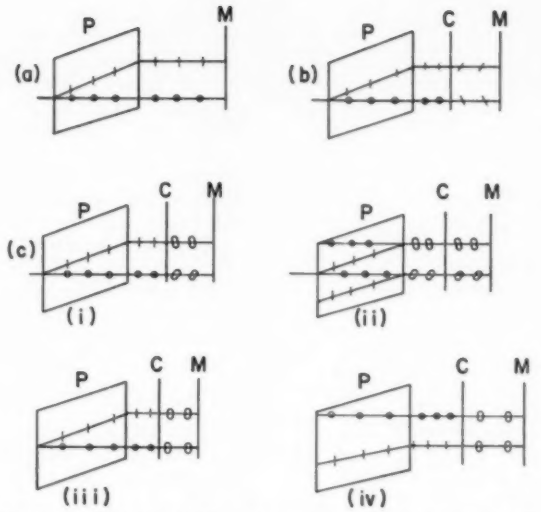

Fig. 2. (a) Calcite rhomb and mirror; one image. (b) Calcite rhomb, half-wave plate and mirror; one image. (c) Calcite rhomb, inexact quarter-wave plate and mirror; incident rays (i). Same case, reflected rays; three images (ii). Calcite rhomb, quarter-wave plate and mirror; incident rays (iii). Same case, reflected rays; two images (iv).

the calcite rhomb, except in certain cases. As the specimen is rotated in the plane perpendicular to the beam, the central image passes through successive minima of brightness, while the outer pair are at maximum illumination. Again, the outer pair are extinguished simultaneously as the central image passes through maximum brightness. If the specimen chances to be an exact half-wave plate then only the central image is seen, and its brightness does not vary with rotation. If the specimen is a quarter-wave plate, the central image is extinguished in certain orientations. The explanation of these observations is made clear by Fig. 2.

In Fig. 2(a), with no plate between P and M, the ordinary and extraordinary rays are reflected unchanged back through P and converge to form a single image. This will also be the case whenever the planes of vibration of the E and O rays coincide with the fast and slow axes of C. Figure 2(b) shows C as an exact half-wave plate. Whatever the angle between the axes of C and the principal section of P, the E and O rays are each resolved into components along the axes of C and recombine upon emerging from C with a phase difference of π. These plane polarized beams are reflected at M and upon passing through C again their components acquire a further phase difference of π. The total change of 2π obviously gives a result identical with that of 2(a).

Figure 2(c) shows the case for a plate of arbitrary retardation (i, ii), and also that of an exact quarter-wave plate (iii, iv). The incident and reflected rays are shown separately in both cases for the sake of clarity. In general it is seen that three images are formed. After traversing C the E and O rays have become elliptically polarized and each resultant beam has E and O components. For an exact quarter-wave plate the O ray and E ray will be resolved into components having phase difference of $\pi/2$. If the components are equal, that is, if the planes of vibration of the E and O rays form angles of 45° with the axes of C, circularly polarized light is produced and reflected from the mirror. In passing the quarter-wave plate again a further difference of $\pi/2$ is introduced, resulting in a total difference of π. Thus the E ray becomes purely an O ray and vice versa. There is then no central image. If the plate is not exactly quarter-wave then the central image will still be at minimum brightness at these 45° positions.

Evaluation of quarter-wave and half-wave plates depends upon extinction of an image in the first instance, and upon invariance of image brightness (and the disappearance of E and O rays) in the second. Extinctions can, of course, be detected with good accuracy. Variation of image brightness is also a sensitive test provided the brightness is not too great. It is advisable to reduce the light intensity by use of a neutral filter, or by substituting an ordinary light bulb for the mercury arc. Since the quarter-wave and half-wave plates are, in effect, evaluated as half-wave and full-wave plates, respectively, deviations from exactness produce twice the effect that they have in actual use. In a sense, therefore, these tests are more exacting than the usual techniques. It will be seen, also, that the use of a single calcite crystal in this way leads to somewhat simpler results than would the use of two calcite crystals in, say, an ordinary polarimeter.

The author wishes to acknowledge permission of the Socony Mobil Oil Company, Inc., to publish this paper.

References

1. C. Benedicks, Phys. Z. **32**, 561 (1931).
2. F. A. Jenkins and H. E. White, *Fundamentals of Optics* (McGraw-Hill, New York, 1957), 3rd ed., p. 557.
3. Ward's Natural Science Establishment, Inc., Rochester 3, New York. Opposite faces of the crystal were polished after the procedure given in J. Strong, *Procedures in Experimental Physics* (Prentice-Hall, New York, 1943).

Spherical-Mirror Oscillating Interferometer

Donald R. Herriott

Bell Telephone Laboratories, Inc., Murray Hill, New Jersey.
Received 17 April 1963.

A high-Q, multiple-pass, spherical-mirror interferometer with one mirror oscillating in axial position to scan wavelength has been constructed for the measurement of spectral characteristics of continuous optical masers. This instrument has been used to obtain direct scans of the distribution of energy in the separate modes of oscillation of a gaseous He–Ne maser as shown in Fig. 1. Reflectors of radius in the range from the plano mirrors of a multiple-beam Fizeau interferometer to the special case of confocal geometry have been used. Spacings of between 10 and 50 cm, with films of 99% reflectance, give resolutions at 1-μ wavelength of between 60 and 300 million with free spectral range of 1500 to 300 Mc/sec.

Conventional instrumentation is not generally suitable for this type of measurement. Spectrographs do not have adequate

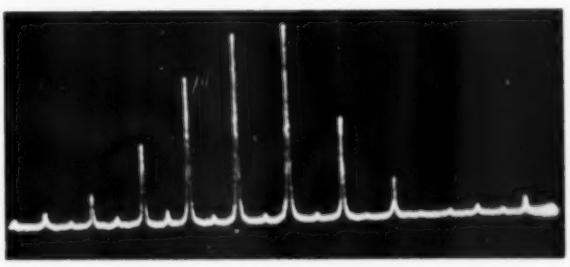

Fig. 1. Spectrum of output of He–Ne maser showing simultaneous axial modes at 112 Mc/sec spacing.

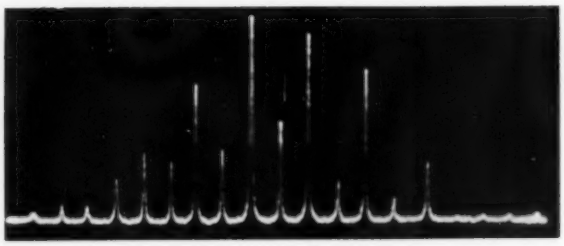

Fig. 2. Increase in energy in the off-axis modes of measuring cavity causes spurious peaks.

resolution to separate modes which are spaced at 100 Mc/sec or 0.0033 Å. Fourier analysis spectroscopy, as originally used to observe these modes,[1,2] has since been extended by the author to 20-m path differences but, in addition to requiring very long path differences for high resolution, this method gives an ambiguous result unless phase measurements are also made. Mixing of modes and observing beats at radio frequency[2,3] gives indirect information and requires a broad-band optical detector such as a photomultiplier tube which is sensitive only to visible and near infrared wavelengths.

Spherical-Mirror Interferometer. The spherical-mirror, multiple-pass interferometer[4,5] has advantages over the plane surface Fabry-Perot or Fizeau interferometers. The maximum resolution of an interferometer with 99% reflecting mirrors is determined very strongly by the surface flatness of the reflectors. The diameter of the axial mode in a spherical mirror interferometer is smaller than that in the plano case and therefore the surface quality of the reflector is critical over a smaller diameter, in the order of 2 mm. It is much easier to obtain the high surface quality over a 2-mm diam than over a 25-mm diam which would be suitable in the plano case. The smaller diameter of the distribution of energy also reduces the diffraction loss.

Illuminating the Spherical Interferometers. The resonances of a spherical interferometer when illuminated off-axis are very different from those when illuminated on-axis.[6] It is therefore necessary to illuminate only the axial mode. To do this, the diameter of the illuminating beam must be adjusted to match the distribution of the energy in the interferometer and the shape of the wavefront should be curved to match the radius of the mirror surface.

The off-axis resonances of the cavity can be seen in Fig. 1 as the small peaks between the primary maser modes. If the conditions of illumination are not proper, the energy in these modes is increased as shown in Fig. 2.

A second condition that is important in using this type of interferometer is the feedback effect of the measuring interferometer on the maser resonator. Maser output is reflected back into the maser cavity by the measuring interferometer and modifies the characteristics of the output beam. This can be eliminated in two ways. A circular polarizer consisting of a plane polarizer followed by a quarter-wave plate oriented at 45° can be inserted between the cavities. This isolator will absorb any of the light reflected from the measuring cavity as the sense of rotation of the circular polarized light is inverted when it is reflected so that it will not be transmitted back through the circular polarizer. An absorption filter can also be placed between the two cavities to attenuate their interaction if adequate energy is available.

Oscillating Cavity. The energy as a function of wavelength can be obtained by varying the separation of the mirrors of the cavity, thereby scanning in wavelength as has been done by Tolansky and Bradley.[7]

The instrument that was constructed (Fig. 3), scans in wavelength by an axial periodic oscillation of the position of one mirror. The mirror is mounted so that it is free to move only in the axial direction. A coil wound on one end of the mirror structure is positioned in the annular gap of a permanent magnet so that a current in the coil results in an axial force. A sinusoidal current applied to the coil causes an axial oscillation of the mirror over the range of about one wavelength of light. The same driving signal is used to drive the horizontal position of the beam of an oscilloscope displaying the signal from the optical detector of the output of the interferometer. The oscilloscope thus displays a linear plot of signal vs spacing of the mirrors.

The system can be used with a narrow-band detector such as the photoconductive types available throughout the infrared because the bandwidth required is only that needed to plot the curve on the oscilloscope. The frequency of oscillation can be reduced from the 60 cps that was used if required for use with narrow-band detectors.

The spherical-mirror, oscillating interferometer provides a means of obtaining very high optical resolution in measuring the direct spectral output of the new high-energy narrow-band sources. This method obviates the necessity of broad-band detectors which are required in mixing and beating techniques.

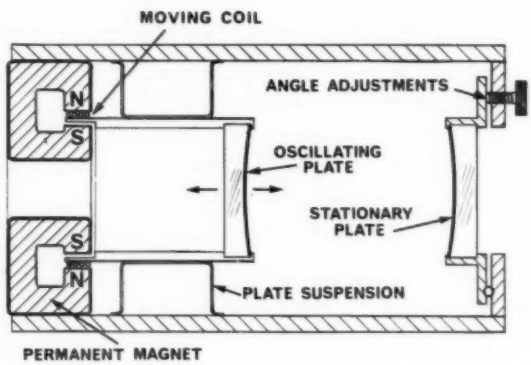

Fig. 3. Diagram of resonant interferometer construction.

References

1. A. Javan, W. R. Bennett, Jr., and D. R. Herriott, Phys. Rev. Letters **6,** 106 (1961).
2. D. R. Herriott, J. Opt. Soc. Am. **52,** 31 (1962).
3. A. T. Forrester, R. A. Gudmundsen, and P. O. Johnson, Phys. Rev. **99,** 1691 (1955).
4. P. Connes, Rev. Optique **35,** 37 (1956).
5. G. D. Boyd and H. Kogelnik, Bell System Tech. J. **41,** 1347 (1962).
6. D. R. Herriott, H. Kogelnik, and R. Kompfner, to be published.
7. S. Tolansky and D. J. Bradley, *Interferometry*, Natl. Phys. Lab. Symposium #11 (Her Majesty's Stationery Office, London, 1960), p. 375.

Letters *continued on facing page*

ERRATUM

B. Schurin, D. E. Williamson, and S. A. Clough, "Direct Recording of Integrated Band Intensities from a Linear Wavelength Spectrometer", Appl. Opt. **2,** 611 (June 1963).

At the time of the writing of this article D. E. Williamson was with the Williamson Development Company, West Concord, Mass. He is now with Cordis Corporation, Miami 37, Fla.

Far-Field Fabry-Perot Diffraction Patterns of a Neodymium in Glass Laser

C. Martin Stickley and Rudolph A. Bradbury

AFCRL, Optical Physics Laboratory, Bedford, Massachusetts.
Received 1 April 1963.

Many investigators have observed the ring-type radiation patterns that are generated by ruby lasers since they are easily seen if the beam is directed onto a scattering surface. The angles at which the rings are produced agree completely with the angles that would be predicted using passive Fabry–Perot interferometer theory,[1] and the widths of the rings are well correlated[2] with the optical quality of the ruby rod.

We report here the observation of a similar ring structure emitted by a Nd in glass laser rod made by Eastman Kodak. According to the manufacturer, it contains from 3% Nd. The rod is 2.54 cm long and 6.2 mm in diameter, and is roughly ground on the cylindrical surface. The mirrors were multilayer dielectrics with a geometric mean reflectivity of 98%. It was tested in an interferometer by Kodak and met their minimum specification of having less than one-tenth wavelength path-length variation. Figure 1 is the far-field pattern taken ½% over threshold (all photographs were made using a sensitized Type Z emulsion). This pattern is not at all like the far-field photographs of high-optical quality ruby rods in which a well-defined circular spot can be seen. Instead, Fig. 1 appears to consist of a large number of interfering crossed hyperbolas. As the pumping energy is increased (Fig. 2, 10% over threshold), strong radiation is observed in seven radial directions. This general feature of the far-field radiation pattern has been observed from other glass rods of this type.[3] Where the beam is highly attenuated, seven small dots having an angular span of 5 mrad can be seen. There is a strong suggestion that there is a relation between these dots and the seven radial rays since similar correlation has been seen in a high quality ruby rod.

A time-integrated photograph of the end of the laser rod shows that the strongest emission is occurring from the central one-third of the rod. Less intense emission occurs throughout the remainder of the rod which is modulated with a poorly defined radial structure. The only optical imperfection that can be seen is a bubble 0.1 mm in diameter that is near the center of the rod and very close to the mirror surface. This is visible as a shadow in the near-field photograph.

The diameter of the rings seen in Fig. 2 agree, within the limits of measurement errors, with the values given by the expression

$$D_p = 2f\sqrt{p\,\lambda n/L}, \qquad (1)$$

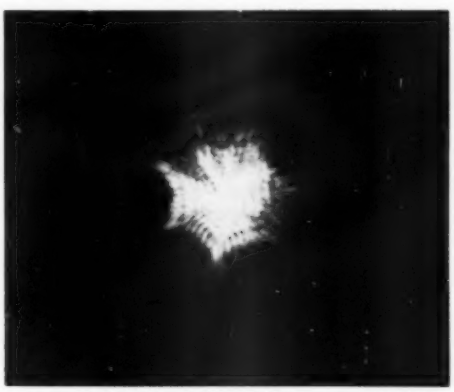

Fig. 1. Far-field pattern ½% over threshold.

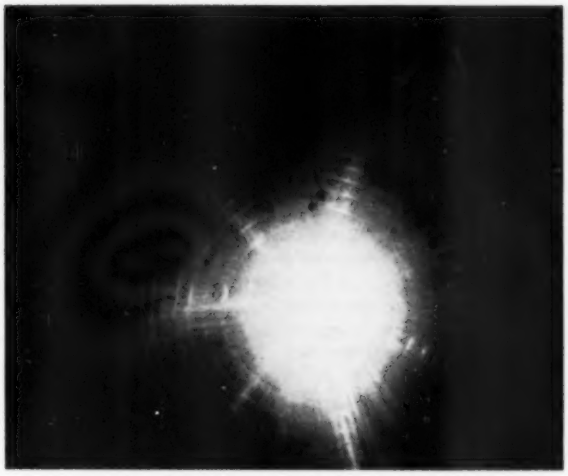

Fig. 2. Far-field pattern 10% over threshold.

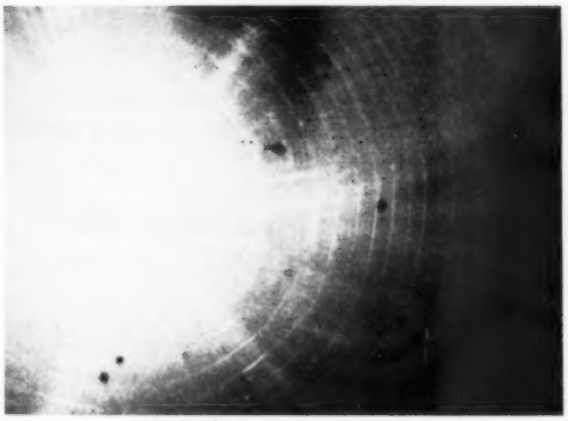

Fig. 3. Magnification of a portion of Fig. 2 showing the diffraction structure between the rings (see also cover of this August issue).

where D_p is the diameter of the pth ring, f is the focal length of the lens, λ is the wavelength of oscillation (1.06 μ), n is the refraction index of the glass (1.70), and L is the length of the laser rod. A striking feature of the rings is their extreme narrowness. Upon close examination (see Fig. 3) it can be seen that the "background" exposure between the rings consists in turn of a number of fine, closely spaced lines. In a portion of the pattern between the eighth and ninth Fabry-Perot rings where the fine structure was quite distinct, seven maxima could be counted. Using Eq. (1), the angular difference between the eighth and ninth rings was computed and was then divided by eight to get the angular separation between the fine structure. This was found to be 1.8×10^{-4} rad. Similar measurements made from other portions of the pattern gave angular separations ranging from 1.8 to 2×10^{-4} rad. Assuming that the full diameter of the laser rod is illuminated by plane waves, one can calculate (using $\theta = 1.22\,\lambda/d$, where d is the diameter of the rod) that the angular difference between successive maxima in the Fraunhofer diffraction pattern of the circular aperture should also be 2.0×10^{-4} rad.

It is tempting to conclude that the fine structure is due to Fraunhofer diffraction for which the total diameter of the laser rod is the aperture since it is impossible for two adjacent maxima to be more closely spaced than this.

The angular width of the eighth ring was measured to be 4.0 $\times 10^{-4}$ rad. It would be of interest to know what the optical quality of the laser rod must be if this ring width is limited by diffraction. It has been shown that the separation between two components of the same Fabry–Perot ring due to a step discontinuity in optical length of λ/q is

$$\Delta\vartheta_p = \theta_p\left[\sqrt{1+\frac{2}{pq}}-1\right]. \qquad (2)$$

Setting $\Delta\theta_p$ equal to 1.22 λ/d (the Rayleigh criterion for resolution) and $p = 8$, one can calculate that $q \geq 14$. That is, if the optical quality of the glass rod is better than $\lambda/14$ the two components of the Fabry–Perot ring due to this difference in optical length will not be resolvable, and the ring width will be governed by diffraction. The expression $q = 14$ is in good agreement with the specification ($q \geq 10$) on optical quality for this type laser rod.

The writers are indebted to E. Hoell and H. Miller for their assistance in the experimental work.

References

1. M. Born and E. Wolf, *Principles of Optics* (Pergamon Press, New York, 1959), p. 329.
2. C. M. Stickley, Appl. Opt. **2**, 861 (1963).
3. P. Mauer, Eastman Kodak Co., private communication.

Measurement of the Direct Electro-Optic Effect in Quartz at UHF

D. D. Eden and G. H. Thiess

Apparatus Division, Texas Istruments, Inc., Dallas, Texas.
Received 22 May 1963.
This work was supported by a U.S. Army ERDL contract.

The existence of the "direct" electro-optic effect[1] in quartz has been experimentally verified at this laboratory at a frequency of 830 Mc/sec.

A linearly polarized, nearly monochromatic, light beam was passed through a sample of crystalline quartz, subjected to a modulating electric field of approximately 1000 V/cm. The light beam, upon emerging from the crystal, was then directed through a linear analyzer, oriented as closely as possible for extinction, and finally to a light detector. The experimental layout is shown in Fig. 1.

The light source was a helium–neon gas phase optical maser (6328 Å) operating in the hemispherical condition with several of its axial modes excited. The frequency separation between the axial modes was approximately 125 Mc/sec. The quartz sample was oriented so that the light traveled along the crystallographic y axis with its plane of polarization inclined 45° with respect to the crystallographic x and z axes. The modulating electric field was applied along the crystallographic x axis. The optical detector consisted of a 7102 photomultiplier and a spectrum analyzer. Due to the presence of the laser modes, "optical mixing" took place at the detector[2] with the result that the modulating signal was found at various frequencies integrally related to the sums and differences of the 830 Mc/sec signal, and multiples of the mode separation. Of the many signals we observed, the strongest occurred at 80, at 205, and at 330 Mc/sec.

The quartz sample was in the form of a rectangular bar whose dimensions coincided with the crystallographic axes. Here y = 50 mm, X = 1 mm, Z = 3 mm. The induced difference in

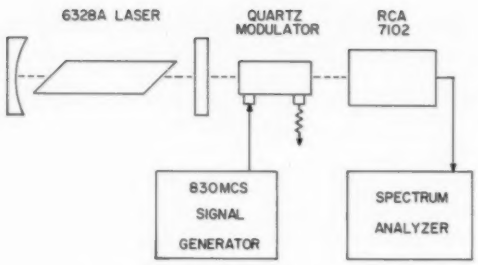

Fig. 1. Experimental arrangement.

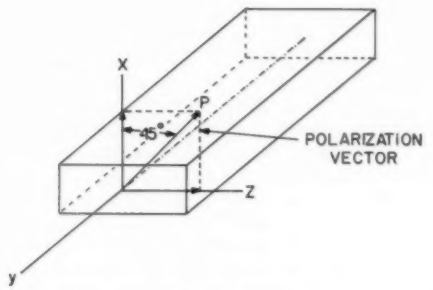

Fig. 2. Relative orientation of polarization vector and crystallographic axes.

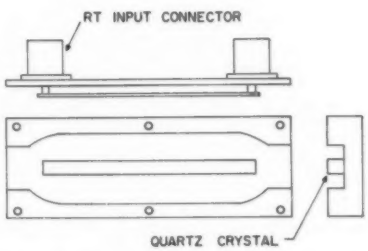

Fig. 3. TEM traveling wave modulator.

phase ($\Delta\phi$, in radians) generated between the two orthogonally polarized light components (into which the incident light is decomposed—see Fig. 2) is given by the equation which follows:

$$\Delta\phi = \frac{\pi y N_0^3 r_{11} E_m}{\lambda_0},$$

where λ_0 = free-space light wavelength, N_0 = ordinary index of refraction, r_{11} = electro-optic coefficient, and E_m = modulating electric field.

The formula above for $\Delta\phi$ is valid provided either one of two possible conditions holds: i.e., (a) the travel time for the light beam in the sample is much less than the period of the applied modulation (low-frequency case), or (b) though the light beam travel time may be equal or greater than the period of the applied modulation, the phase velocities of the light and the traveling microwave modulation in the crystal must be matched, and the induced *change* in the travel time of the light beam through the sample must be much less than the period of the modulation.

For maximum modulation, the crystal was placed in a traveling wave TEM structure where, in the quartz, the uhf phase velocity and the optical phase velocity were matched through the

use of an inhomogeneous dielectric loading.[3] Details of the modulator are illustrated in Fig. 3.

The effect we observed depends upon the electro-optic or "Pockels" coefficient r_{11}. Cady[4] has calculated the direct contribution to r_{11} as 0.23×10^{-10} cm V^{-1} based on the "dc" measurement of Pockels[5] and Gunther,[6] and the known piezoelectric and piezo-optic constants. At present we are able to conclude from our measurements that r_{11} is of the order of 10^{-11} cm V^{-1} at uhf.

Our results seem to indicate that the relaxation of this "direct" electro-optic effect in quartz occurs at frequencies higher than uhf.

By orienting the polarization of the incident light to be along the crystallographic x axis, phase modulation can also be obtained without the aid of the analyzer. If the phase modulation is rapid (i.e., the modulation frequency is high), significant frequency modulation is effected. A frequency modulation-to-amplitude modulation conversion scheme recently reported on[7] uses a suitably oriented doubly refracting crystal of appropriate length. The basic idea is that the difference in phase retardation between the ordinary and extraordinary rays, when passing through the material, is wavelength-dependent. Rutile has been used successfully in such a converter at this laboratory at uhf modulation frequencies.

The use of quartz as a microwave light modulator shows great promise for realizing extremely wide modulation bandwidths and high optical and microwave efficiencies.

Traveling-wave TEM structures seem to be quite suited to this material. The advantage here is that the over-all effect is no longer directly proportional to the applied voltage only, but depends upon the optical path length as well. This means that applying large voltages to the material is no longer of prime importance since a smaller peak voltage may be made up for by an increased optical path length. It is, therefore, not necessary to be too greatly concerned with high electro-optic activity. Of equal and perhaps greater concern are the optical and dielectric properties of the material. In this regard, quartz is at least an order of magnitude better than any other electro-optic material.

References

1. W. G. Cady, *Piezoelectricity* (McGraw-Hill, New York, 1946), p. 721.
2. A. T. Forrester, R. A. Gudmundsen, and P. O. Johnson, Phys. Rev. **99,** 1691 (1955).
3. R. E. Collin, *Field Theory of Guided Waves* (McGraw-Hill, New York, 1960), p. 242.
4. Ref. 1, p. 723.
5. F. Pockels, Abhandl. Gött. **39,** 1–204 (1894).
6. N. Gunther, Ann. Physik **13,** 783 (1932).
7. S. E. Harris, Record of Northeast Electronics Research and Engineering Meeting, 1962.

Jameson Dane Rigden, codeveloper of the visible helium-neon laser, has joined the Perkin-Elmer Corporation, Norwalk, Conn., as group leader in gas laser research and development in the Optical Maser Department.

Power Dip at Line Center of Gaseous Lasers

S. Winsberg

The author was at TRG, Inc., Syosset, New York. Present address: Kollsman Instrument Corp., Elmhurst, New York.

Received 30 April 1963.

This research is a part of Project DEFENDER, sponsored by Advanced Research Projects Agency, Department of Defense, and technically monitored by the Air Force Office of Scientific Research, under an Air Force contract.

A dip may occur in the power output from gaseous lasers as the oscillating frequency is scanned over the Doppler line. This effect has been observed by McFarlane *et al.*[1] and Javan[2] in the He–Ne system. Experiments to measure this effect in optically pumped Cs vapor have been described by Rabinowitz and Jacobs.[3] The theory of this effect has been discussed by Lamb[4] and Bennett[5,6] from different points of view. Bennett's discussion[6] is restricted to conditions of low fields and the case that $\Delta\nu_{\text{Doppler}} \gg \Delta\nu_{\text{natural}}$. Our treatment has the first restriction but not the second. Both methods agree for conditions under which the second restriction is satisfied.

continued overleaf

The Publications of W. W. Coblentz on Infrared Spectroscopy

The principal work of the late W. W. Coblentz on infrared spectroscopy originally appeared in three Publications of the Carnegie Institution of Washington. Publication No. 35, issued in 1905, dealt with his investigations at Cornell University of the infrared absorption spectra of some 135 organic compounds, with shorter supplementary sections on transmission and reflection spectra. Publication No. 65 (1906) and Publication No. 97 (1908) are concerned with later work on the transmission and reflection spectra of minerals and other inorganic compounds carried out at the U.S. Bureau of Standards.

These classical investigations form the basis of most modern work on analytical infrared spectroscopy. The journals have long been out of print, but, with the kind permission of the Carnegie Institution, they have recently been reprinted in a single volume under the joint sponsorship of the Coblentz Society and the Perkin-Elmer Corporation.

All concerned with modern applications of infrared spectroscopy to problems of chemical structure and analysis should be conversant with this early work, which provides the basis for much of the modern technique. To maintain a properly balanced outlook on the subject, this volume should accompany the standard modern texts on the library shelf of the spectroscopy laboratory.

A limited number of copies of the first reprinting are still available at $3.50 per copy on application to Dr. H. B. Kessler, The Secretary, c/o The Perkin-Elmer Corporation, Norwalk, Connecticut.

We present results of an analysis based on the rate equations for the populations and fields. When the field is oscillating at a specific frequency, two groups of atoms will respond, each possessing a Doppler-shifted central frequency equal to the applied frequency. When the applied frequency equals the central frequency of a stationary atom, the two groups coalesce, and, depending on the ratio of the natural width to the Doppler width, the power output decreases. The ratio of the power output at the oscillating frequency, ω, to that at the central frequency, ω_0, is given by:

$$\frac{\rho(Q)}{\rho(0)} = \frac{\left\{\int d\mathrm{Re}^{-R^2}\left[\frac{1}{W_1}+\frac{1}{W_2}-\left(\frac{1}{W_{1TH}}+\frac{1}{W_{2TH}}\right)\right]\right\}}{\left\{\int d\mathrm{Re}^{-R^2}\left[\frac{2}{W_0}-\left(\frac{1}{W_{1TH}}+\frac{1}{W_{2TH}}\right)\right]\right\}} \frac{\left\{\int d\mathrm{Re}^{-R^2}\left[\frac{4}{W_0^2}\right]\right\}}{\left\{\int d\mathrm{Re}^{-R^2}\left(\frac{W_1+W_2}{W_1W_2}\right)^2\right\}},$$

where

$R = v/c_1$,

v = velocity of the atom,

$c_1 = 2\sqrt{\ln 2}$ Doppler velocity width,

$(c_1\omega_0)/c = 2\sqrt{\ln 2}$ Doppler width (frequency units),

$W_1 = (Q+R)^2 + U^2$,

$W_2 = (Q-R)^2 + U^2$,

$W_{1TH} = (Q_{TH}+R)^2 + U^2$,

$W_{2TH} = (Q_{TH}-R)^2 + U^2$,

$W_0 = R^2 + U^2$,

$$U = \frac{\text{natural width}}{2\sqrt{\ln 2}\ \text{Doppler width}},$$

$$Q = \frac{(\omega-\omega_0)c}{c_1\omega_0} = \frac{\text{oscillating frequency} - \text{central frequency}}{2\sqrt{\ln 2}\ \text{Doppler width}},$$

$$Q_{TH} = \frac{(\omega_{TH}-\omega_0)c}{c_1\omega_0} = \frac{\text{threshold frequency} - \text{central frequency}}{2\sqrt{\ln 2}\ \text{Doppler width}},$$

ω_{TH} = the frequency at which threshold occurs.

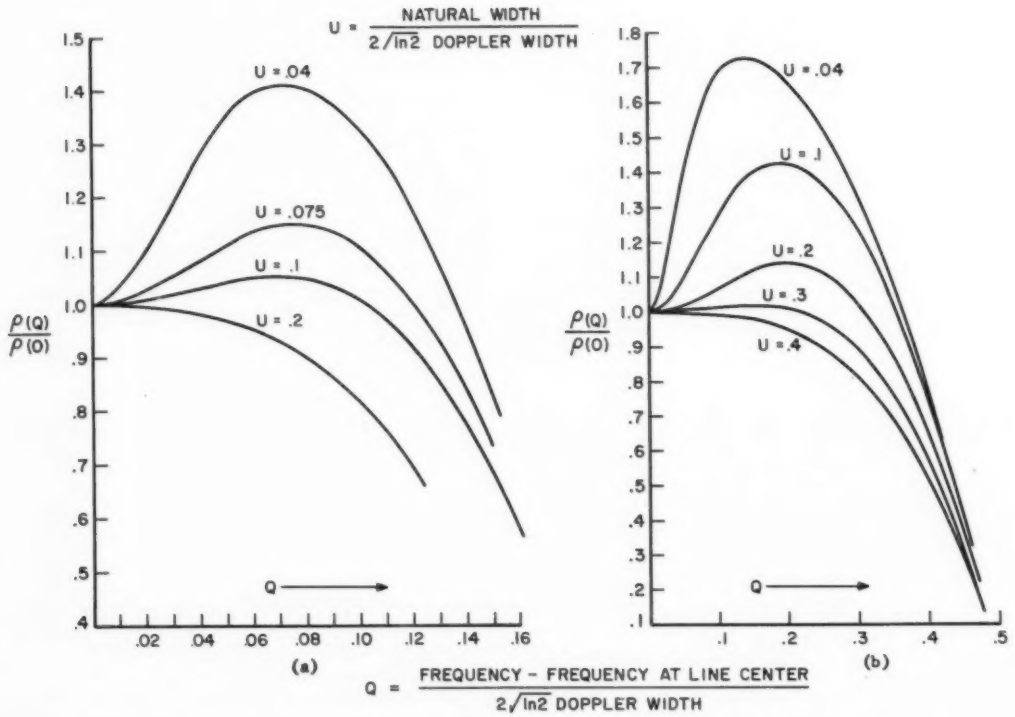

Fig. 1. Normalized power output vs normalized frequency for various line-widths. (a) Threshold adjusted to occur at 0.2 $(2\sqrt{\ln 2}) \times$ Doppler width. ($Q_{TH} = 0.2$); (b) Threshold adjusted to occur at 0.5 $(2\sqrt{\ln 2}) \times$ Doppler width. ($Q_{TH} = 0.5$).

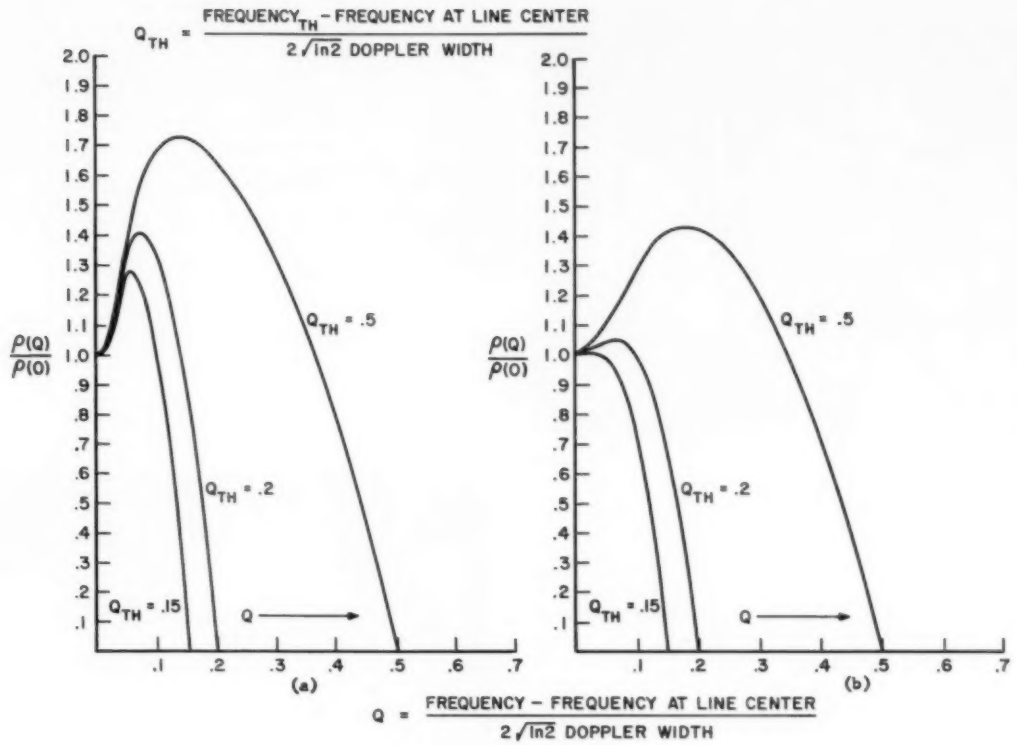
Q_{TH} = FREQUENCY$_{TH}$ − FREQUENCY AT LINE CENTER / $2\sqrt{\ln 2}$ DOPPLER WIDTH
$\frac{\rho(Q)}{\rho(0)}$
Q_{TH} = .5
Q_{TH} = .2
Q_{TH} = .15
Q
(a)
(b)
Q = FREQUENCY − FREQUENCY AT LINE CENTER / $2\sqrt{\ln 2}$ DOPPLER WIDTH

Fig. 2. Normalized power output vs normalized frequency for various thresholds.

(a) $U = \dfrac{\text{natural width}}{2\sqrt{\ln 2}\ \text{Doppler width}} \approx 0.04;$

(b) $U = \dfrac{\text{natural width}}{2\sqrt{\ln 2}\ \text{Doppler width}} \approx 0.1$

We have made the assumption that the pumping power is sufficiently close to threshold so that when oscillation occurs at the center of the Doppler line the depth of the hole "burned" in the line is small compared to the height of the unperturbed line. This implies $Q_{TH} \leq 1/2$.

In Figs. 1 and 2 we present curves of $\rho(Q)/\rho(0)$ for various values of the parameters Q and U consistent with our assumption of oscillation close to threshold.

We are indebted to M. C. Newstein for many valuable discussions in connection with this problem.

References

1. R. A. McFarlane, W. R. Bennett, Jr., and W. E. Lamb, Jr., Appl. Phys. Letters **2**, 189 (1963).
2. A. Javan, 3rd Internatl. Symp. on Quantum Electronics, Paris, France, Feb. 1963.
3. P. Rabinowitz and S. Jacobs, 3rd Internatl. Symp. on Quantum Electronics, Paris, France, Feb. 1963.
4. W. E. Lamb, Jr., 3rd Internatl. Symp. on Quantum Electronics, Paris, France, Feb. 1963.
5. W. R. Bennett, Jr., Appl. Opt. Suppl. on Optical Masers (1962), p. 24.
6. W. R. Bennett, Jr., 3rd Internatl. Symp. on Quantum Electronics, Paris, France, Feb. 1963.

Richard Tousey *Naval Research Laboratory* (left), Sheldon Phillips *Eastman Kodak*, Fred W. Clarke *Rogers and Clarke*, and Paul Fenlon *Borg-Warner*.

photo D. L. MacAdam

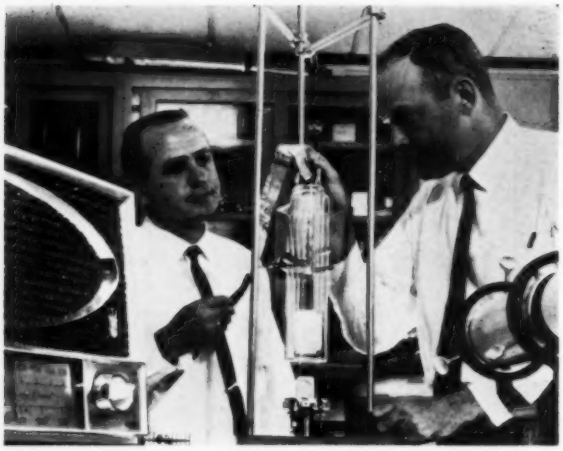

IBM Engineers Kenneth E. Niebuhr (left) and Robert C. Green are shown preparing apparatus for an experiment in the transmission of audio signals over an injection laser beam. They are inserting the laser in a dewar of liquid nitrogen which is used to cool the laser during operation; voice signals from a microphone are processed by special electronic circuitry and transmitted to the laser at the end of the foil strip. The laser emits light pulses which carry the audio signals to the phototube (lower right-hand corner). There, the light pulses are converted back into electrical signals which are used to power the speaker system (left foreground).

General Telephone and Electronics Laboratory have recently developed a liquid laser based on a europium chelate [benzoylacetonate—see Phys. Rev. Letters **4**, 133(1963)]. The laser emits at 6130 Å. The solvent for the Eu chelate is a mixture of alcohols operated at about −150°C at which temperature it is a viscous fluid. The photograph shows Alexander Lempicki (left) and Harold Samelson, both members of the Optical Society of America, who developed the laser filling the Fabry-Perot cavity with the solution. In the background is the flash excitation apparatus.

IBM scientists Kurt Weiser (left) and Ralph S. Levitt examine one of the new indium phosphide injection lasers as they prepare to set up an experiment. Achievement of the indium phosphide laser marks the first time scientists have been able to make an injection laser from a semiconductor material other than gallium arsenide and its alloys.

ANNUAL SUBSCRIPTIONS

OSA members	$ 6.00
Other AIP societies' members	$ 8.00
Non-members and libraries	$10.00
Single copies	$ 2.00

Subscriptions should be addressed to APPLIED OPTICS Subscription Handling, American Institute of Physics, 335 East Forty-Fifth Street, New York 17, New York. **Eight weeks should be allowed for order processing.**

ADVERTISING

Advertising inquiries, orders, plates, and correspondence should be addressed to the APPLIED OPTICS Advertising Office, 1155 Sixteenth Street, N.W., Washington 6, D.C. 202-DI 7-4131. Mrs. Boraks.

RUSSIAN MASERS

Typical examples of Russian masers papers published in recent issues of OPTICS AND SPECTROSCOPY, OSA's monthly translation journal:

Transmission and Reflection of a Plane-Parallel Layer in the Conditions of Amplification and Generation Stepanov and Khapalyuk

Detection of the Isotope K^{40} by Means of Optical Pumping Alexandrov and Chodovoy

Deformation Splitting of Lines in the Spectra of Alkali Fluoride Crystals Activated by Sm and Eu Divalent Ions Kaplyanskii and Przhevuskii

Zeeman Effect in the Absorption and Luminescence Spectrum of CaF_2-Sm^{++} and SrF_2-Sm^{++} Zakharchenya and Ryskin

Microwave Spectrum of the HDNCN and D_2NCN Molecules Shipulo

Spectroscopic Sum Rules Taking into Account the Induced Emission Rebane and Sild

Determination of the Mean Lifetime of Excited States by a Polarimetric Method Agarbiceanu, Kukurezianu, Popesku, and Vasilu

Some Problems of the Nonlinear Theory of the Optical Properties of Plane-Parallel Layers Samson and Stepanov

Calculation of the Maser Power of a System of Particles with Three Energy Levels Stepanov and Samson

Amplification Properties of a Dielectric Filament Prokhurov

Emission Pulsations from a Ruby Laser Galanin, Leontovich, Sviridenkov, Smorchkov, and Chizhikova

Absorption, Luminescence and Stimulated Emission of Neodymium in SrF_2 Crystals Kariss and Feofilov

Order your subscription to the 1963 issues now (Feb. '63 issue published in English translation in May)

OPTICS AND SPECTROSCOPY
ROOM 101, OSA
1155 16th St. N.W.
Washington 20036, D.C.

ORDER FORM

Please enter my/our subscription to the 1963 issues of OPTICS AND SPECTROSCOPY (Vols. XIV and XV):

- ☐ OSA member rate $7.50 monthly
- ☐ OiS club member rate $11.00 monthly
- ☐ Nonmember rate $15.00 monthly

Name _____ OSA Membership No. _____

OiS Club Cooperating Society _____

Address _____

_____

_____

_____ **cash with order preferred**

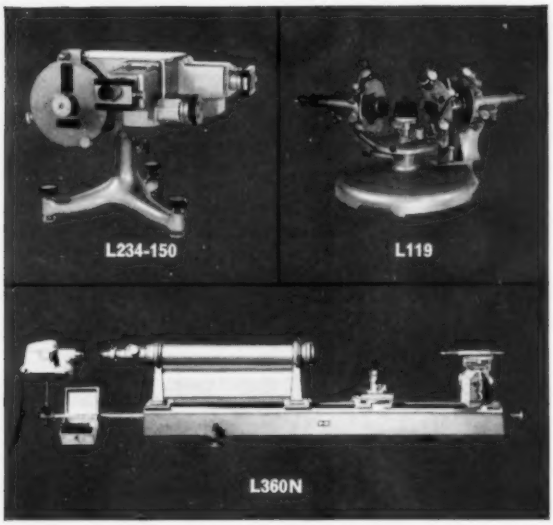

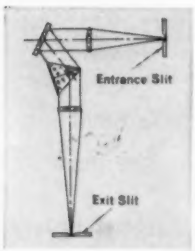

Optical Diagram of
L234-150 Monochromator

DEPENDABLE ACCURACY

Gaertner Scientific thrives on solving difficult measuring problems . . . with precision unexcelled—reputation unsurpassed. Instruments shown represent a few of the many optical measuring systems available that can be applied or modified to your requirements.

L234-150 QUARTZ MONOCHROMATOR—High speed enables studies of absorption spectra, photosensitive materials, phosphorescence, and energy distribution. With camera attachment, unit converts to high aperature spectrograph. **Request Bulletin 158-61**

L119 ELLIPSOMETER—Accurate measurement of extremely thin film down to 2 or 3 Angstroms. Also adaptable to birefringence and surface studies with elliptically polarized light. **Request Bulletin 203-61**

L360N OPTICAL-INSTRUMENT BENCH—For checking optics, experimental and mock-up arrangements requiring alignment, unique positioning, linear or rotational movement of test pieces or components. **Request Bulletin 156-59**

Your inquiry for existing or proposed instrumentations will be answered immediately. GSC-3-219

Gaertner
SCIENTIFIC CORPORATION
1294 Wrightwood Ave., Chicago 14, Ill.
Area Code 312, BUckingham 1-5335

Use **THIN FILM (8μ) BEAM SPLITTERS**

NO GHOSTS!
NO REFRACTIVE ERRORS!

- Flatness to 1/8" wave and parallelism to less than 1 fringe per inch; on special order.
- Sizes: Up to 24" (and still growing).
- Large coating selection, including dichroics.

SEND FOR FREE BOOKLET
"Application and Specification of Pellicles"

Important reading for manufacturers, designers and users of glass beam splitters, mirrors, filters and prisms.

NPC National Photocolor Corp.
225 East 44th Street, New York 17, N. Y.
MU 7-0267-8

RARE EARTH CHELATES

These interesting compounds are particularly suited for studies in:

ENERGY TRANSFER
and
OPTICAL PUMPING

Several complete series, derived from spectroscopic grade rare earths, are now commercially available.

Benzoylacetonates
Dibenzoylmethides
o-hydroxo-acetophenones
o-hydroxo-benzophenones

Inquiries concerning these compounds are invited.

M & W MATERIALS RESEARCH, INC.
925 Truman N. E.
Albuquerque, New Mexico

KORAD CORPORATION • 2520 COLORADO AVENUE • SANTA MONICA 4, CALIFORNIA • AREA CODE 213 • 393-6737

KORAD UNION CARBIDE

A SUBSIDIARY OF UNION CARBIDE CORPORATION

LASER LEADERSHIP...in research, products and applications

HIGH-ENERGY LASERS

HIGH PEAK-POWER LASERS

FAST-RISE PHOTODETECTORS

ADVANCED LASER POWER SUPPLIES

ELECTRON INJECTION LASER DIODES

LASER APPLICATIONS ENGINEERING

Korad LASER products are the results of comprehensive research, development and engineering programs in lasering materials, laser pumping, super-power LASER devices and application investigation.

For more detailed information concerning Korad products or research and engineering services phone or write our headquarters in Santa Monica, California, or call our offices in New York or Washington, D.C.

DEVICES • SYSTEMS • APPLICATIONS

NEW YORK, AREA 212 • 551-2345 • SANTA MONICA, AREA 213 • 393-6737 • WASHINGTON, AREA 202 • 393-7755

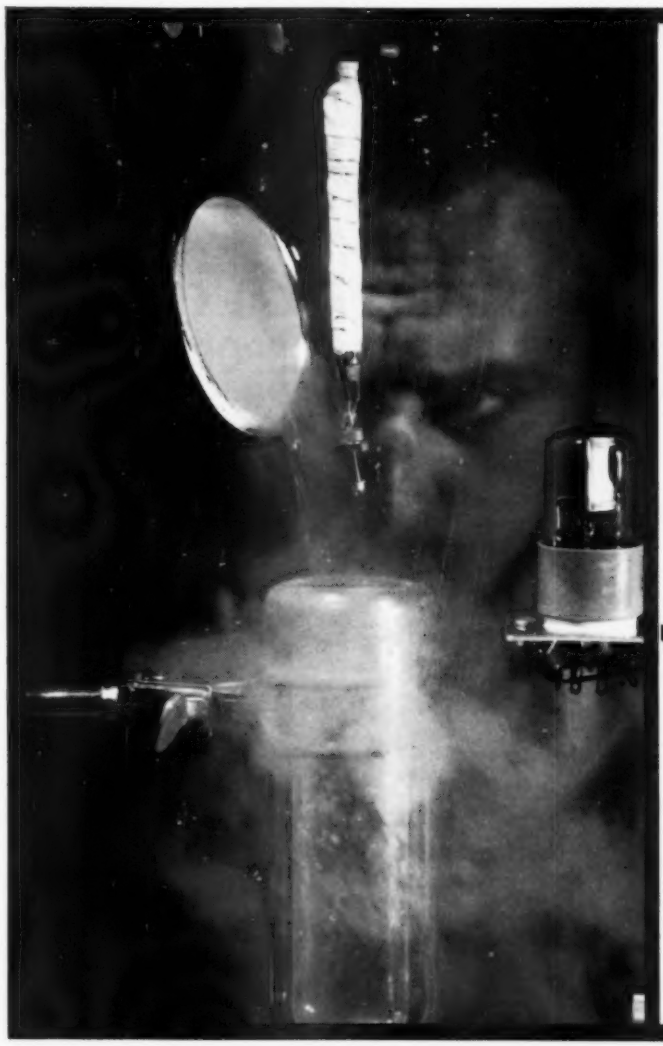

K-1 COMPLETE LASER SYSTEM

K-D1 PHOTODETECTOR

INTEGRATED KERR CELL MODULATORS
FOR

e o INSTRUMENTS

• GIANT LASER PULSING
• ULTRAHIGH-SPEED PHOTOGRAPHY

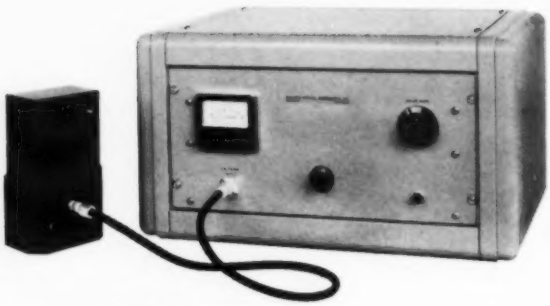

MODEL ILM-70

Laser Modulators Feature
- Multi-megawatt "Q" spoiling
- Complete H.V. protection
- Flexible coupling
- Ultra-clean Kerr cells

Camera Systems Feature
- Nanosecond range exposures and triggering
- Interchangeable PFN's to 20 microseconds
- High quality optics

Low Cost
- System prices from below $2,500*

*Prices subject to change without notice.

FOR DETAILED SPECIFICATIONS, PRICE AND DELIVERY INFORMATION TO...
ELECTRO-OPTICAL INSTRUMENTS INC.
922 SOUTH MYRTLE AVENUE MONROVIA, CALIFORNIA
ELLIOTT 9-9391

OPPORTUNITY FOR INDIVIDUAL CONTRIBUTION

Our clients are seeking both theoretical and experimental physicists who are capable of making significant individual contributions in the field of modern optics. If your interest and experience encompass any of the following areas, you are invited to investigate growth opportunities offering remuneration up to $25,000.

Electro-optical imaging systems. . .interferometric techniques. . .spatial filtering. . . diffraction theory. . .modern image theory . . .geometric lens design . . .laser research and investigation.

For further information, you are invited to direct your resume to:

Mr. Vincent A. Nickerson
Department B-8

ABBOTT'S of Boston
"EMPLOYMENT SPECIALISTS"
150 Tremont Street
Boston 11, Massachusetts
HAncock 6-8400

AMERICAN OPTICAL COMPANY LASER INCORPORATED

PHYSICISTS ***SCIENTISTS***

MS and PhD

Our new research facility in suburban Westchester County has recently been completed and is now being staffed.

Professional opportunities available for Physicists experienced and interested in Laser Technology and Optical Phenomena.

Please send resume or contact:

LASER, INC.

Dr. Eugene T. Booth
Scientific Director
914 Wilson 1-6500

Laser, Incorporated
320 Old Briarcliff Road
Briarcliff Manor, New York

WILEY BOOKS

DITCHBURN

revises and updates his treatise . . .

LIGHT

SECOND EDITION. *By* R. W. DITCHBURN, *F.R.S., University of Reading.* Recent, important developments added, original text retained as much as possible. THEORETICAL: coherence and concept of a lens system as transmitter of information on spatial frequencies. PRACTICAL: more on physical receptors, stressing continuity among instruments for ultraviolet, visible, infra-red regions of the spectrum—theory of their performance and limitations introduced by material on geometrical optics, photometry, colorimetry. Theory of stimulated emission applied to masers. *An Interscience Book. 1963. 833 pages. $12.00*

PROGRESS IN OPTICS

A NEW SERIES. *Edited by* EMIL WOLF, *University of Rochester.* International review articles on theoretical, applied optics, and related fields. All articles printed in English. *A North-Holland (Interscience) Book. Vol. I, 1961. 336 pages. $12.00. Vols. II and III, 1963. 298 pages. $11.50*

Send now for on-approval copies

INTERSCIENCE PUBLISHERS

A Division of John Wiley & Sons, Inc.

605 Third Avenue New York, N. Y. 10016

MODEL L-35

INTERFEROMETER

for
PRECISE EVALUATION OF
LASER CRYSTALS
PRISMS & FLATS
LENS SYSTEMS

A General Purpose Twyman-Green Interferometer
Vibration Isolated, Versatile, & Compact

Specifications: 3.5cm Aperture, Pinhole Turret,
with Prefocused Reflex Camera—$1950.00

Cadmium Source, Housing & Power Supply— $160.00

TROPEL, INC., 52 WEST AVE., FAIRPORT, N.Y.

CONSULTANTS AND DESIGNERS OF OPTICAL SYSTEMS
MANUFACTURERS OF PROTOTYPE LENSES AND INSTRUMENTS

A NEW Catalog

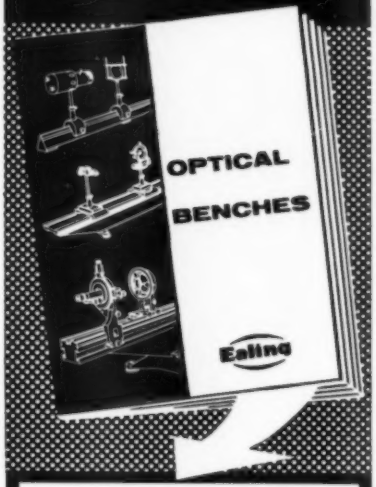

Introduction page

" This, we believe, is the most comprehensive range of Optical Benches and Accessories offered.

There are five basic benches for different applications with varying accuracies, each with its appropriate carriers. There are sixty different accessories.

This range meets every requirement from simple alignment to the precise investigation of any optical system.

A unique feature of this range of Optical Benches is its flexibility.

The first three benches all take accessories mounted on 13·5 mm. stems and therefore all 40 accessories listed — can be used interchangeably on these three benches.

The last three benches take the research accessories listed.

The middle bench, that is the Precision Lathe Bed Optical Bench — has the special advantage of taking both the standard accessories — and the research accessories listed."

WANT TO READ FURTHER?
This Catalog is FREE
on request from

THE Ealing CORPORATION

2239 Massachusetts Ave.
Cambridge 40, Massachusetts
Telephone: (617) 491-1515

EC/44

CLOSED-CYCLE

maser COOLING

This cryostat is part of an Air Products closed-cycle 2.5°K maser refrigerator supplied to the Bell Telephone Laboratories under its contract with the Army Ordnance Missile Command.

A completely self-contained refrigerator, it does not require an external source of cryogenic liquids. Other features:

- Reaches 2.5°K in 2½ hours
- Operates through all antenna orientations
- Cools down automatically
- Designed for field operation
- Light-weight, oil-free compressors

Air Products provides a complete line of cryogenic refrigeration systems operating as "warm" as 80°K. Today, these systems are helping industry and government customers solve a wide range of problems requiring cryogenic temperatures.

Let Air Products put this experience and proved capability to work on your problem. For further information write:

CRYOGENIC REFRIGERATION SYSTEMS
DEFENSE AND SPACE DIVISION

Air Products and Chemicals INC.
ALLENTOWN, PENNSYLVANIA

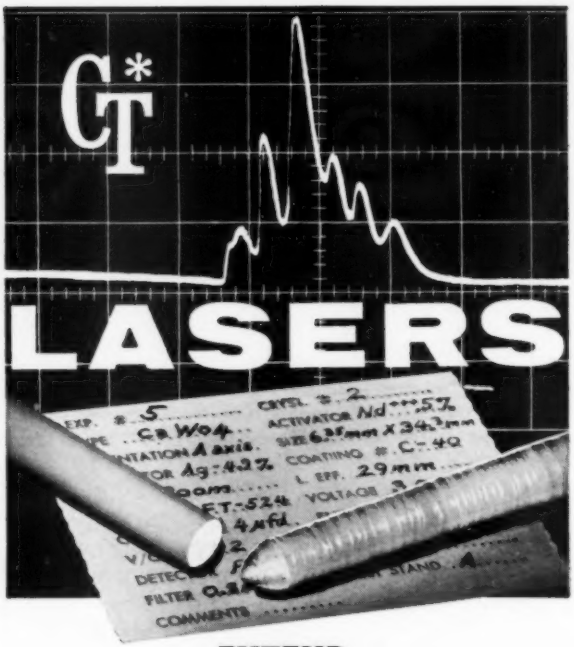

EXTEND YOUR LASER INVESTIGATION CAPABILITIES

ISOMET has the nation's most extensive facilities for high quality Laser Crystal growth, fabrication, finishing, and quantity production.

TESTED LOW THRESHOLD

✱ ***Certified Threshold*** Each ISOMET laser rod is accompanied by an actual oscilloscope photograph of its output performance at threshold and complete data on the experimental conditions of the test.

BOULES OR FABRICATED RODS ends polished optically flat and parallel, confocal, spherical or faceted to meet your requirements.

STOCKED FOR IMMEDIATE DELIVERY

$CaWO_4$, $SrMoO_4$, $PbMoO_4$ doped with Nd^{3+}
Chromium doped Ruby, 0° or 90° orientation
Nd^{3+} doped glass
CaF_2 and BaF_2 doped with Sm^{2+}, U^{3+}, Nd^{3+}

GROWN TO ORDER

$CaWO_4$, $SrMoO_4$, $PbMoO_4$, CaF_2, CdF_2, BaF_2 or other hosts doped with any of the rare earths or transition elements.

REFLECTIVE SURFACES Evaporated metallic or multiple dielectric coatings.

NEW LARGE SIZE LASERS

ISOMET has perfected a method of growing Calcium Tungstate doped crystals in sizes never before possible. As a result, we stock $CaWO_4$ boules capable of being fabricated into laser rods up to ¼" diameter x 5" long and ½" x 4" long. On special order, we can supply ¼" rods up to 10" long, ½" rods up to 6".

Write for new technical bulletin AO1000

ISOMET
CORPORATION
PALISADES PARK, NEW JERSEY

LASER CAPABILITY

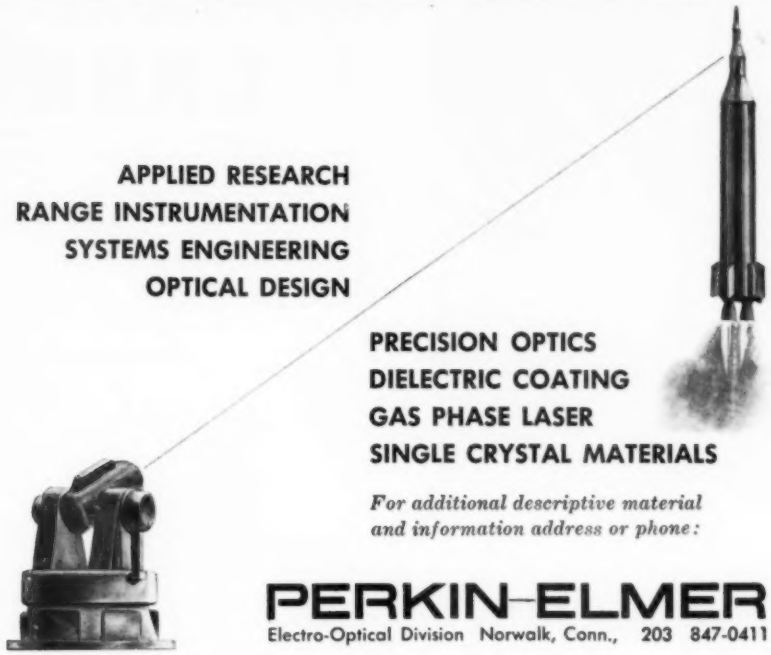

APPLIED RESEARCH
RANGE INSTRUMENTATION
SYSTEMS ENGINEERING
OPTICAL DESIGN

PRECISION OPTICS
DIELECTRIC COATING
GAS PHASE LASER
SINGLE CRYSTAL MATERIALS

For additional descriptive material and information address or phone:

PERKIN-ELMER
Electro-Optical Division Norwalk, Conn., 203 847-0411

SENIOR OPTICS PHYSICISTS

Join Advanced Optics Research for Space Applications

with IIT Research Institute

Senior Optics Physicists are required for advanced space-oriented research in I I T Research Institute's Physics Division. Qualifications include a sound background, gained through several years experience, in one or more of these areas: astronomical spectroscopy, astronomy, advanced optics instrumentation, reconnaissance and surveillance, the optics of planetary atmospheres.

These new opportunities emphasize our growing involvement in the nation's space effort. Further indication of this is the opening in April of the Institute's new Astro Sciences Center which is concerned with developing new approaches to technical problems of large, complex space missions.

As a staff member of the Physics Division, you will be supported by the extensive resources of the entire Institute, including the space-oriented physicists of the Astro Sciences Center and the high level staff from various disciplines within the Physics Division itself.

Please address your inquiry to Mr. Ron C. Seipp.

IIT RESEARCH INSTITUTE

formerly Armour Research Foundation of Illinois Institute of Technology

10 West 35th St., Chicago 16, Illinois

An Equal Opportunity Employer

LASER

GIANT PULSE SYSTEM

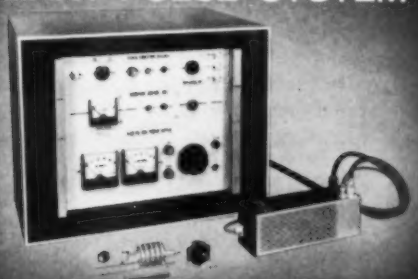

ACHIEVES LASER OUTPUT IN THE 100 MEGAWATT RANGE—AND UP.

Kappa Scientific's Kerr Cell LASER Control System is a precision apparatus for controlling the pulse shape, timing and amplitude of a LASER to achieve a single intense pulse output in the multi-megawatt range.

This system is part of a growing line of LASER products and accessories covered in our new catalog. Write for your copy today.

KAPPA SCIENTIFIC CORPORATION

49 South Baldwin Ave. / Sierra Madre, Calif. / EL 6-1614

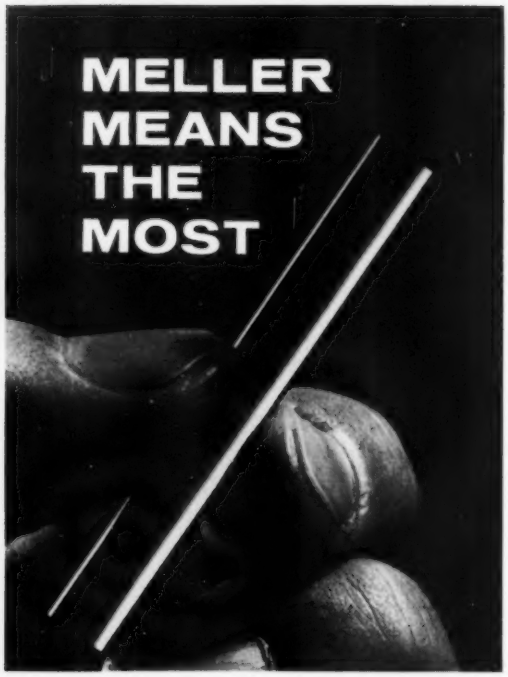

Crystals of all types and sizes, guaranteed to laser!

In stock, hundreds of single crystals. All configurations (plain flat and parallel ends, TIR configuration, Brewster's angle). Optically corrected for lowest threshold, narrowest beam divergence. Extra slow grown and annealed for minimum strain. **Guaranteed to laser!**

- NEW glass crystals w/neodymium^{3+} 2.0% — finest quality, no bubbles, straie, strains.
- New NPS1 super-uniform ruby crystals.
- Ruby rods up to 12"
- Calcium tungstate crystals w/neodymium^{3+} 0.5% up to 5" long.
- Strontium fluoride crystals w/samarium^{2+} 0.1%, neodymium^{3+} 0.5%.
- Barium fluoride crystals w/neodymium^{3+} 0.5%, uranium^{3+} 0.1%.
- Calcium fluoride crystals w/neodymium^{3+} 0.5%, samarium^{2+} 0.1% dysprosium^{2+} .05%, or uranium^{3+} 0.1%.

For full specifications and prices, write or call Adolf Meller Company, Box 6001, Providence 1, R. I. Telephone: DExter 1-3717 (Area Code 401).

MELLER SAPPHIRE PRODUCTS

Synthetic Sapphires • Ruby Lasers & Masers
Alumina Powder

POWER SUPPLIES
AND
LIGHT PUMPS
FOR
LASERS

Standard model Power Supplies, Light Pumps and Special Devices are available for prompt delivery. They are designed and built to be readily adaptable to the requirements of almost every type of solid state laser material. New equipments with enlarged capabilities and new features are under development. The models listed below merely indicate the variety of units now in production.

POWER SUPPLIES

All models with continuously variable voltages from 0 to maximum rating. Fast recycling.

Console Models

325 – 5,000 volt with output to 20,000 joules.
330 – 10,000 volt with output to 20,000 joules.

Modular Units

Model 265 – 5,000 volt with output to 20,000 joules.

Model 320 – 10,000 volt with output to 20,000 joules.

PORTABLE LASER POWER SUPPLY

with self-contained energy storage.

Model 322–Complete, self-contained Power Supply and Energy Storage. Voltage continuously variable 0 to 3,000. Output to 800 joules.

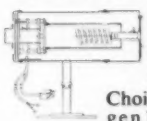

SOLID STATE LASER MOUNTS

6 models available. Choice of air or liquid (nitrogen) cooling for helix or straight arc flash tubes. Maximum powers, 2,000 to 20,000 joules.

ENERGY STORAGE BANKS...

available in units of 1,000 joules for use with the Power Supplies listed above.

SPECIAL DEVICES...

Model 3C-4039 External Reflector

Model 3C-4040 Rotary Disc and Prism Assembly for "Q" spoiling or "Q" dumping.

Write for further information

ELECTRO POWERPACS, INC.

A subsidiary of Hydra-Power Corp.

6 Hadley Street
Cambridge 40, Mass.

SENIOR INFRARED PHYSICIST

Manager Infrared Systems

To perform experimental and theoretical research in infrared backgrounds, atmospheric transmission and infrared properties of gases. Will be responsible for the theoretical aspects of the program as well as data acquisition and handling. Requirements include a demonstrated capability in infrared studies and a familiarity with the state of the art in infrared detectors, radiometers and measurement techniques.

SENIOR INFRARED SYSTEMS ENGINEER

To join a group of instrumentation physicists and engineers who are developing advanced infrared systems. Requirements include a demonstrated capability in infrared systems design and a working knowledge of detectors, electronics, optical systems and specialized infrared techniques.

For further details, write in strictest confidence to:
John A. Haverfield, Manager—Professional Placement

MELPAR INC

A SUBSIDIARY OF WESTINGHOUSE AIR BRAKE COMPANY
3396 Arlington Boulevard / Falls Church, Virginia
(a suburb of Washington, D. C.)
an equal opportunity employer

BALZERS

- Multilayer high-reflectivity coating
- Excellent mechanical and thermal resistance
- Centered on wavelength according to your specifications
- Coatings to be applied on your own rubies or flats
- Short delivery time by air mail
- Moderate prices

A GREAT NUMBER OF *WORKING* SYSTEMS ARE EQUIPPED WITH BALZERS' TOP PERFORMANCE COATINGS

Balzers Aktiengesellschaft
Balzers
Princ. of Liechtenstein

BALZERS

1923 FS 1963

40th ANNIVERSARY

Steady growth during the past 40 years, finds us today with an extremely wide variety of essentials that meet the exacting requirements of modern technology.

Our plant, which covers over 20,000 square feet, is producing an ever increasing number of products for both science and industry. It includes an optical division with unsurpassed facilities for grinding, polishing and surfacing, an instrument shop with modern machinery, a high-vacuum coating laboratory as well as a section for the manufacture of diamond-impregnated tools using a sintering process for metal matrix only for working of quartz, glass, ceramics or other hard, brittle material. We also import and distribute the finest optical glass. We'll be glad to study your requirements and give you our recommendations.

MULTI-LAYER INTERFERENCE FILMS

Made in our New Rochelle High Vacuum Coating Laboratory

For dichroic and achromatic beam splitters and filters. High efficiency. . .Relatively wide band

Our coatings were used in the first TELSTAR color TV transmission

For lasers and masers

Over 99% reflectivity

#530–630	reflects 530 mμ to 660 mμ
#N-6343	reflects 610 mμ to 710 mμ
#N-680	reflects 670 mμ to 750 mμ
#N-1064	reflects 980 mμ to 1120 mμ
#N-1150	reflects 1120 mμ to 1220 mμ

Coatings are also available with peak reflectivity at any other desired wavelength.

Unaffected by immersion in liquid nitrogen. Can easily be cleaned with Acetone, Alcohol, or normal detergents.

ABSORPTION TYPE COLORED OPTICAL FILTER GLASS

Processed in our New Rochelle Optical Shop in about 100 types for the ultra-violet (from 250 mμ), visible, and infrared (to 3000 mμ) spectral regions. Available in flat or as solid bars for the manufacture of tubing for liquid laser excitation.

Also Anti-Laser Eye-Protection Filter Glass BG-18

•

NEODYMIUM DOPED GLASSES FOR SOLID STATE LASERS

Type	LG-2	LG-4
Basic Glass	Borosilicate glass	Lanthanum-Borosilicate glass
Doping	2 weight % Nd_2O_3	2 weight % Nd_2O_3

Emission wavelength: 1.06 μ

FISH-SCHURMAN CORPORATION
90 Portman Road, New Rochelle, N. Y.

OSA Around-the-World Group Flight 1964

Revised Information

The International Commission for Optics Symposium on Photographic and Spectrographic Optics will be held in Tokyo 1–8 September 1964, preceded by a Conference on Interference and Coherence convened under the auspices of the ICO and the Australian Academy of Science in Sydney, 23–29 August 1964. The airlines have recently approved an around-the-world group flight fare for 15 persons or more, and OSA, even at this early date, is interested in learning the number of members who are potentially interested in attending these two meetings and participating in this group flight. It is also hoped to have an informal gathering in Israel (say 13–17 August), and perhaps something similar in India (say 18–19 August). It appears better for our purpose to finish this around the world trip in the Orient (rather than to start it there as had been our original intent), so our revised—but still tentative—schedule now looks like:

		From	To	Purpose
Aug. 8	lv. 10:00 pm	NYC	London	**This part will probably be dropped and we shall fly directly from N.Y.C. to Tel Aviv on 8 August**
9	arr. 9:35 am		London	
11	lv. 11:55 am	London	Athens	
	arr. 4:20 pm		Athens	
13	lv. 7:20 pm	Athens	Tel Aviv	informal colloquium?
	arr. 9:20 pm		Tel Aviv	
17	lv. 9:25 pm	Tel Aviv	New Delhi	
18	arr. 9:10 am		New Delhi	
19	lv. 12:15 pm	New Delhi	Bangkok	
	arr. 5:15 pm		Bangkok	
21	lv. 6:05 pm	Bangkok	Singapore	
	arr. 8:40 pm		Singapore	
22	lv. 9:30 pm	Singapore	Sydney	
23	arr. 9:35 am		Sydney	ICO Interference and Coherence Meeting—(Sessions 24–25, visits to lab. 26–27, visits outside Sydney 28–30)
31	lv. 10:05 am	Sydney	Tokyo	
31	arr. 11:40 pm		Tokyo	ICO Mtg. Tokyo & Kyoto on Photographic and Spectroscopic Optics
Sept. 1–8				
10	lv. 11:15 pm	Tokyo	Honolulu	
10	arr. 11:40 am		Honolulu	
11	lv. 11:30 pm	Honolulu	San Francisco	
12	arr. 7:15 am		San Francisco	
12	lv. 8:30 am	San Francisco	New York	

The group fare would be approximately $1150 economy class round trip. Only OSA members and their immediate relatives may participate. Would members who are potentially interested (there is no commitment) fill in and return this form. The interest of those who have already written in is recorded.

Assistant Secretary, OSA
Room 101
1155 Sixteenth Street, N.W.
Washington 36, D.C.

REPLY

I am interested in principle in participating in the OSA 1964 AROUND-THE-WORLD GROUP FLIGHT, and I wish to have information as it becomes available.

☐ I would travel alone ☐ accompanied by my wife ☐ my children (state how many)

Name..... OSA Membership Number.....

Address.....

.....

.....

HIGH QUALITY STANDARDS

. . . in Optical Crystal Blanks

Calcium Fluoride	Sodium Chloride
Barium Fluoride	Potassium Chloride
Lithium Fluoride	Potassium Bromide

• *Prompt Delivery* • *Large Size Availability*
• *Precision Cutting* • *Scattering Free*
• *Impurity Absorption Free* • *Strain Free*

. . . in Optical Maser Crystals

$U^{+3} \cdot CaF_2$	$Dy^{+2} \cdot CaF_2$	$Nd^{+3} \cdot CaF_2$
$U^{+3} \cdot BaF_2$	$Sm^{+2} \cdot CaF_2$	$Nd^{+3} \cdot BaF_2$
$U^{+3} \cdot SrF_2$	$Sm^{+2} \cdot SrF_2$	$Nd^{+3} \cdot SrF_2$
$Tm^{+3} \cdot SrF_2$	$Tm^{+2} \cdot CaF_2$	$Ho^{+3} \cdot CaF_2$

Also, all other trivalent rare earths in CaF_2, BaF_2 and SrF_2.

Indicative of our quality, most of the above were first mased in Optovac grown crystals.

OPTOVAC, INC.

NORTH BROOKFIELD, MASSACHUSETTS

Avco-Everett Research Laboratory

The Avco-Everett Research Laboratory's re-entry experiments operations program has five specially adapted aircraft carrying Avco's monitoring team leaders and technicians that fly the Atlantic and Pacific missile ranges to make optical measurements of re-entering vehicles with both photographic and radiometric instruments. The results are significantly important to the Army Nike-Zeus missile program and the development of advanced type air force re-entry vehicles.

Senior Openings exist for individuals to work on instruments both photographic and radiometric for re-entry monitoring. Must be able to conceive, design, specify and supervise procurement and/or fabrication of components, assembly, check out of data gathering equipment in accordance with data needs.

Other Senior Openings encompass mechanical design of airborne instruments including lens mounts, timing lights, and altazimuth mounts; design and evaluation of methods of vibration, isolation of airborne cameras; evaluation of motors, actuated solenoids, clutches, etc. being used in photographic and radiometric devices; design of laboratory equipment for testing optical instruments.

These positions are at the Everett Laboratory where significant contributions are continually being made in re-entry physics.

If you qualify, this is an invitation to join this outstanding group of scientists and engineers. Please write or send resume to:

R. E. McDonald, *Personnel Manager*

AVCO EVERETT RESEARCH LABORATORY

A Division of Avco Corporation
2385 Revere Beach Parkway
Everett 49, Massachusetts

An equal opportunity employer

new dual-axis autocollimator

Kollmorgen Model K222 combines 0.1 second of arc sensitivity ... ease of use ... freedom from eye strain.

Demonstrably superior! No other manual autocollimator on the market today ... imported or domestic ... offers you so many operating advantages.

Simultaneous measurement of vertical and horizontal angles eliminates errors or delays inherent in 90° rotation of instrument or eyepiece. Both measurements in the same plane ... no parallax! Each axis has its independent micrometer ... no compromise with accuracy.

Largest objective lens aperture (1.8 in.) available on an NAS barrel and full correction of lens for spherical and chromatic aberration permit accurate measurements over a field of view of 26 minutes of arc. Maximum working distance is 150 feet.

Illuminated fine adjustment scale utilizes eyepiece readout to eliminate constant refocusing of the viewing eye and resultant eye fatigue. This illumination also permits instrument use in total darkness. Since readouts are located outside the instrument's field of view, micrometer adjustments are always 'honest' ... not influenced by any observer's natural tendency to resolve fractional splits in his favor. Micrometer scale divisions are seconds and tenths of seconds; one minute per revolution.

A demonstration will convince you that the Kollmorgen Model K222 Dual-Axis Autocollimator provides the quickest, easiest way to align, square, erect or position structures, machinery and their components to the highest order of accuracy available in a standard commercial instrument.

Informative 12-page bulletin contains complete data on Model K222 and other new Kollmorgen optical tooling instruments: Single-Axis Manual and Dual-Axis Automatic Autocollimators, Dual-Axis and Line-of-Sight Alignment Telescopes, Pointing Interferometer and all required accessories. Write for this bulletin today ... 347 King Street, Northampton, Mass.

K C **KOLLMORGEN**
CORPORATION
NORTHAMPTON, MASSACHUSETTS

INJECTION LASERS

NOW AVAILABLE ON
RAPID DELIVERY SCHEDULES

GaAs Injection Lasers . . . 8400 Å

GaAsP Injection Lasers . . . 6200 Å-8400 Å

GaP Injection Sub-Lasers . . . 6400 Å

GaAs Injection Sub-Lasers . . . 9100 Å

GaAsP Injection Sub-Lasers . . . 6600 Å-9100 Å

GaSb Injection Sub-Lasers . . . 16000 Å

Tiny p-n junction diodes emit coherent radiation by direct application of electric current. Standard configurations now available. Consultation and design services on custom configurations offered.

Diodes operated beneath the laser threshold emit non-coherent light retaining the general spectral characteristic and fast time-constant of the Injection Laser. Sub-Lasers listed above are available, in standard configurations, on rapid delivery schedules. Other III-V sources available on special order.

For illustrated brochure, write to:

ELECTRO-NUCLEAR LABORATORIES, INC.

2437 LEGHORN STREET, MOUNTAIN VIEW, CALIFORNIA

OPTICS FOR LASERS
FROM
PERKIN-ELMER

Perkin-Elmer is a convenient, reliable source of precision optics for lasers, in quantities for research or production programs. All are of unexcelled quality. All reflect Perkin-Elmer's years of experience in the design and development of precision optics and optical instrumentation.

INTERFEROMETER FLATS
1.0", 1.5" and 2.0" diameter
Surface: $\frac{\lambda}{10}$ to $\frac{\lambda}{200}$
BK-7 and Quartz

SPHERICAL MIRRORS
1.0", 1.5" and 2.0" diameter
1M, 2M, 3M, 10M, 25M, 50M
radius of curvature
BK-7 and Quartz

WINDOWS
1.0", 1.5" and 2.0" diameter
Standard or Brewster's angle
BK-7 and Quartz

DIELECTRIC COATINGS
Durable, minimum loss,
specified reflectivities
for the full spectrum of laser
research and development

SINGLE CRYSTALS
Tungstate, Molybdate, Sapphire,
Garnet, Emerald

SPECIAL OPTICS
Trihedral and 90° prisms with
deviation within 2 seconds

Perkin-Elmer—a single-source, total capability in optical maser technologies including research, design, material development, fabrication and performance testing, plus development engineering of optical maser systems and applications.

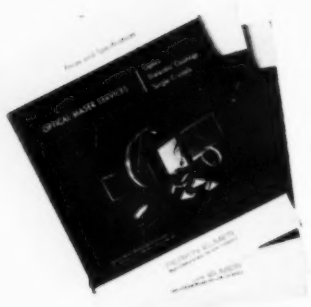

Send today for "Prices and Specifications—Optical Maser Services". Write or phone Perkin-Elmer, Optical Maser Marketing, Norwalk, Conn. Area Code 203-847-0411.

PERKIN-ELMER